

# Novel Processes for Modular Integration of Silicon-Germanium MEMS with CMOS Electronics

*Carrie Wing-Zin Low*



Electrical Engineering and Computer Sciences  
University of California at Berkeley

Technical Report No. UCB/EECS-2007-31

<http://www.eecs.berkeley.edu/Pubs/TechRpts/2007/EECS-2007-31.html>

February 28, 2007

Copyright © 2007, by the author(s).  
All rights reserved.

Permission to make digital or hard copies of all or part of this work for personal or classroom use is granted without fee provided that copies are not made or distributed for profit or commercial advantage and that copies bear this notice and the full citation on the first page. To copy otherwise, to republish, to post on servers or to redistribute to lists, requires prior specific permission.

Novel Processes for Modular Integration of Silicon-Germanium MEMS  
with CMOS Electronics

By

Carrie Wing-Zin Low

B.S. (University of California, Berkeley) 2001

M.S. (University of California, Berkeley) 2004

A dissertation submitted in partial satisfaction of the

requirements for the degree of

Doctor of Philosophy

in

Engineering - Electrical Engineering and Computer Sciences

in the

Graduate Division

of the

University of California, Berkeley

Committee in charge:

Professor Tsu-Jae King Liu, Co-chair

Professor Roger T. Howe, Co-chair

Professor Richard M. White

Professor Oscar D. Dubón, Jr.

Spring 2007

The dissertation of Carrie Wing-Zin Low is approved:

Co-chair \_\_\_\_\_ Date \_\_\_\_\_

Co-chair \_\_\_\_\_ Date \_\_\_\_\_

\_\_\_\_\_ Date \_\_\_\_\_

\_\_\_\_\_ Date \_\_\_\_\_

University of California, Berkeley

Spring 2007

Novel Processes for Modular Integration of Silicon-Germanium MEMS  
with CMOS Electronics

Copyright © 2007

by

Carrie Wing-Zin Low

## **Abstract**

Novel Processes for Modular Integration of Silicon-Germanium MEMS  
with CMOS Electronics

By

Carrie Wing-Zin Low

Doctor of Philosophy in Engineering - Electrical Engineering and Computer Sciences

University of California, Berkeley

Professor Tsu-Jae King Liu, Co-chair

Professor Roger T. Howe, Co-chair

Equipment control, process development and materials characterization for LPCVD poly-SiGe for MEMS applications are investigated in this work. In order to develop a repeatable process in an academic laboratory, equipment monitoring methods are implemented and new process gases are explored. With the dopant gas  $\text{BCl}_3$ , the design-of-experiments technique is used to study the dependencies of deposition rate, resistivity, average residual stress, strain gradient and wet etch rate in hydrogen-peroxide. Structural layer requirements for general MEMS applications are met within the process temperature constraint imposed by CMOS electronics. However, the strain gradient required for inertial sensor applications is difficult to achieve with as-deposited films.

Approaches to reduce the strain gradient of LPCVD poly-SiGe are investigated. Correlation between the strain gradient and film microstructure is found using stress-depth profiling and cross-sectional TEM analysis. The effects of film deposition

conditions on film microstructure are also determined. Boron-doped poly-SiGe films generally have vertically oriented grains -- either conical or columnar in shape. Films with conical grain structure have large strain gradient due to highly compressive stress in the lower (initially deposited) region of the film. Films with small strain gradient usually have columnar grain structure with low defect density. It is also found that the uniformity of films deposited in a batch LPCVD reactor can be improved by increasing the deposited film thickness, using a proper seeding layer, and/or depositing the film in multiple layers. The best strain gradient achieved in our academic research laboratory is  $1.1 \times 10^{-6} \mu\text{m}^{-1}$  for a  $\sim 3.5 \mu\text{m}$  thick film deposited at  $410^\circ\text{C}$  in 8 hours, with a worst-case variation across a 150 mm-diameter wafer of  $1.6 \times 10^{-5} \mu\text{m}^{-1}$  and a worse-case variation across a load of twenty-five wafers of  $7 \times 10^{-5} \mu\text{m}^{-1}$ . The effects of post-deposition annealing and argon implantation on mechanical properties are also studied. While the as-deposited film can achieve the desired mechanical properties, post-deposition processing at elevated temperatures can degrade the strain gradient.

---

Professor Tsu-Jae King Liu, Co-chair

Date

---

Professor Roger T. Howe, Co-chair

Date

To Mom and Dad

# Table of Contents

<b>List of Figures</b> .....	v
<b>List of Tables</b> .....	ix
<b>Acknowledgements</b> .....	xi
<b>Chapter 1: Introduction</b> .....	1
1.1 Process strategies for MEMS and CMOS integration .....	1
1.2 SiGe research in IC and MEMS .....	5
1.3 Desired MEMS properties for poly-SiGe .....	6
1.4 Overview of dissertation .....	7
References .....	9
<b>Chapter 2: LPCVD Poly-SiGe Technology</b> .....	14
2.1 LPCVD reactor overview .....	14
2.2 Process gases .....	15
2.3 Process recipes .....	17
2.4 Wafer placement .....	18
2.5 Quartz tube .....	20
2.6 Process control .....	22
2.6.1 Pressure control .....	22
2.6.2 Temperature control .....	22
2.6.3 Gas flow rate control .....	24
2.7 Process monitor .....	26
2.7.1 Automatic process condition monitor .....	26
2.7.2 Process logbook .....	26
2.7.3 Injector condition monitor .....	26
2.7.4 MFC monitor .....	31
2.8 Summary .....	38
References .....	39
<b>Chapter 3: Investigation of Advanced Process Gases</b> .....	40
3.1 Boron trichloride (BCl <sub>3</sub> ) as the boron dopant gas .....	40
3.1.1 BCl <sub>3</sub> mixture concentration .....	41
3.1.2 Experimental details .....	46
3.1.3 Results and discussion .....	48
3.1.3.1 Deposition rate .....	50
3.1.3.2 Crystallinity .....	51
3.1.3.3 Dopant incorporation .....	52
3.1.3.4 Stress .....	55
3.1.3.5 Strain gradient .....	57
3.1.3.6 Process uniformity .....	57
3.1.3.7 Furnace configuration optimization .....	60
3.1.4 Comparison of the two boron dopant gases .....	63

3.2 Disilane ( $\text{Si}_2\text{H}_6$ ) as the silicon precursor .....	64
3.2.1 Literature review .....	64
3.2.2 Experimental results and discussion .....	66
3.3 Germynl silanes ( $(\text{H}_3\text{Ge})_x\text{SiH}_{4-x}$ ) as the silicon germanium precursors .....	67
3.3.1 Literature review .....	67
3.3.2 Experimental plan .....	69
3.4 Summary .....	71
References .....	73
<b>Chapter 4: LPCVD Poly-SiGe Process Optimization .....</b>	<b>75</b>
4.1 Experimental details .....	75
4.2 Characterization methods .....	76
4.2.1 Transmission electron microcopy .....	76
4.2.2 X-ray diffraction .....	78
4.2.3 Strain gradient measurement .....	80
4.3 Overall experimental data .....	82
4.4 1st design of experiments .....	86
4.4.1 Experimental design .....	86
4.4.2 Results and interpretation .....	87
4.4.3 Mechanical properties study .....	90
4.4.4 Summary .....	106
4.5 Ramping experiments .....	106
4.5.1 Experimental setup .....	106
4.5.2 Results and interpretation .....	109
4.5.3 Summary .....	112
4.6 2nd design of experiments .....	112
4.6.1 Experimental setup .....	112
4.6.2 Results and interpretation .....	113
4.6.3 Summary .....	123
4.7 Thick deposition .....	124
4.8 Multiple-layered film deposition .....	127
4.9 Seeding layer experiments .....	128
4.10 Structural properties study .....	133
4.10.1 Strain gradient and film microstructure .....	134
4.10.2 Film microstructure and deposition conditions .....	138
4.10.3 Uniformity .....	141
4.11 Summary .....	144
References .....	146
<b>Chapter 5: Post-Deposition Processing of Poly-SiGe Films .....</b>	<b>149</b>
5.1 Furnace annealing .....	149
5.2 Rapid thermal annealing .....	154
5.3 Flash lamp annealing .....	157
5.4 Excimer laser annealing .....	162
5.5 Argon implantation .....	165
5.6 CMOS thermal budget limitations .....	168

5.6.1 Processing of the MEMS layers .....	168
5.6.2 Metal contact damage .....	170
5.6.3 Film delamination after RTA .....	173
5.6.4 Electrical measurement .....	175
5.7 Summary .....	183
References .....	184
<b>Chapter 6: Conclusion .....</b>	<b>187</b>
6.1 Contributions of this work .....	187
6.2 Recommendations for future work .....	189
References .....	191
<b>Appendix A: SAM coating of poly-SiGe for stiction reduction .....</b>	<b>192</b>
A.1 SAM overview .....	192
A.2 Experimental details .....	193
A.3 Results and discussion .....	195
A.3.1 Film characterization .....	195
A.3.2 Thermal stability .....	197
A.4 Summary .....	200
References .....	202
<b>Appendix B: Stress stability of LPCVD poly-SiGe and SiO<sub>2</sub> films .....</b>	<b>204</b>
B.1 Experimental details .....	204
B.2 Results and discussions .....	205
B.3 Modeling thin film stress .....	209
B.4 Summary .....	212
References .....	214
<b>Appendix C: Tystar20 logbook .....</b>	<b>215</b>

## List of Figures

1.1 Schematic of wafer-scale encapsulation for MEMS-first integration [1.5] .....	3
1.2 Schematic of modular integration of MEMS and CMOS with poly-SiGe (courtesy of R. T. Howe and B. L. Bircumshaw) .....	4
2.1 LPCVD reactor schematic .....	15
2.2 a) Open boat; b) Caged boat [2.3] .....	19
2.3 Temperature and power profiles of a 425 °C deposition .....	24
2.4 Mass flow controller schematic [2.4] .....	25
2.5 Pressure reading for a new injector and a clogged injector .....	30
2.6 Historical data for injector pressure .....	31
2.7 SiH <sub>4</sub> MFC monitoring data .....	35
2.8 GeH <sub>4</sub> MFC monitoring data .....	36
2.9 Si <sub>2</sub> H <sub>6</sub> MFC monitoring data .....	36
2.10 BCl <sub>3</sub> MFC monitoring data .....	37
2.11 N <sub>2</sub> Dope and N <sub>2</sub> BKFL MFCs monitoring data .....	37
3.1 Arrhenius plot of deposition rate .....	51
3.2 Cross-sectional TEM images: a) Run T6 - 0.5 um film; b) Run T12 - 1.5 um film .....	52
3.3 Boron concentration vs. dopant gas partial pressure .....	53
3.4 Resistivity vs. boron concentration .....	54
3.5 a) Resistivity and b) Stress vs. Film thickness .....	55
3.6 Average stress vs. doping .....	56
3.7 Strain gradient vs. thickness .....	57
3.8 Deposition rate and resistivity across load.....	59
3.9 Cross-load uniformity of sheet resistance with gas ring and injector .....	61
3.10 Cross wafer uniformity of sheet resistance with low BCl <sub>3</sub> flow rate .....	62
3.11 Cross wafer uniformity of sheet resistance with high BCl <sub>3</sub> flow rate .....	62
3.12 Structures of the germlyl-silanes [3.13] .....	69
3.13 Temperature dependence of the first epitaxial layer growth rates for various precursors on Si (100) [3.14] .....	69
4.1 Cross-sectional TEM sample preparation method .....	78
4.2 Strain gradient measurement: a) cross-sectional schematic of a released cantilever beam; b) stress depth profile before release; c) stress depth profile after release, but before bending .....	81
4.3 1 <sup>st</sup> design of experiments input parameter values .....	87
4.4 Values and confidence intervals for various responses .....	90
4.5 Stress profiles and TEM images for DOE1 recipes .....	92-96
4.6 Average residual stress vs. film thickness for films deposited at various temperatures: a) 410°C; b) 425°C; c) 440°C .....	98
4.7 Strain gradient vs. film thickness for films deposited at various temperatures: a) 410°C; b) 425°C; c) 440°C .....	99
4.8 Strain gradient vs. resistivity for 2-µm thick films deposited at various	

temperatures: a) 410°C; b) 425°C; c) 440°C .....	101
4.9 Strain gradient vs. resistivity for films deposited at 410 °C, showing:	
a) linear correlation; b) non-linear correlation; c) minimum strain gradient .....	105
4.10 Process conditions of the reference deposition (Ramp-ref) .....	108
4.11 Process conditions of the SiH <sub>4</sub> flow ramp-up deposition (Ramp-SiH <sub>4</sub> ) .....	108
4.12 Process conditions of the temperature ramp-down deposition (Ramp-temp) .....	109
4.13 Stress profiles and cross-sectional TEM images for the ramping experiments .....	111
4.14 Strain gradient vs. resistivity for DOE2: a) 600 mTorr depositions (DOE2-1, DOE2-2 and DOE2-3); b) 350 mTorr depositions (DOE2-4, DOE2-5 and DOE2-6) .....	115
4.15 Strain gradient vs. film thickness for DOE2: a) 600 mTorr depositions (DOE2-1, DOE2-2 and DOE2-3); b) 350 mTorr depositions (DOE2-4, DOE2-5 and DOE2-6) .....	117
4.16 Stress profiles and cross-sectional TEM images for DOE2 .....	120
4.17 TEM images for recipe 410 °C, 600 mTorr, 140 sccm SiH <sub>4</sub> , 60 sccm GeH <sub>4</sub> and 35 sccm BCl <sub>3</sub> : a) film deposited for 60 minutes at wafer slot #15; b) film deposited for 60 minutes at wafer slot #3; c) film deposited for 230 minutes at wafer slot #9 .....	122
4.18 Top view TEM images for film deposited with recipe DOE2-2 at various depths (Courtesy of Dr. Erdmann Spiecker) .....	123
4.19 SEM image of released cantilever beam array for Recipe ThickDepo. ....	125
4.20 Strain gradient vs. film thickness plot .....	125
4.21 Stress profile and cross sectional TEM image for recipe ThickDepo .....	126
4.22 Stress profile and cross sectional TEM image for Recipe LayerStack .....	128
4.23 Cross sectional TEM image for film deposited with recipe SiGeSeed-t1 .....	130
4.24 Stress profile and cross sectional TEM image for recipe SiGeSeed-1 .....	131
4.25 Stress profile and cross sectional TEM image for recipe SiGeSeed-2 .....	132
4.26 Strain gradient vs. film thickness for various recipes .....	133
4.27 X-TEM images of as-deposited poly-SiGe films with strain gradient $>4.5 \times 10^{-4} \mu\text{m}^{-1}$ , deposited with: a) Recipe Ramp-ref; b) Recipe DOE2-5; c) Recipe SiGeSeed-1. (ref. Table 4.2) .....	134
4.28 X-TEM images of as-deposited poly-SiGe films with positive strain gradient $<1 \times 10^{-5} \mu\text{m}^{-1}$ , deposited with: a) Recipe DOE2-2; b) Recipe Thick-depo; c) Recipe SiGeSeed-2. (ref. Table 4.2) .....	135
4.29 Stress-vs.-depth profiles: a) film with large strain gradient, shown in Figure 2.27(b); b) film with small strain gradient, shown in Figure 4.28(b) .....	136
4.30 XRD data for films shown in Figure 4.27 and Figure 4.28 .....	137
4.31 Relationship between strain gradient and resistivity, and film microstructure for films deposited near to the amorphous-to-polycrystalline transition temperature. ....	140
4.32 Variation in strain gradient vs. the average strain gradient. ....	143
5.1 Stress profile and cross-sectional TEM image for the as-deposited film (film deposited by Recipe ThickDepo) .....	152
5.2 Stress profile and cross-sectional TEM image for FA-a (film deposited	

by Recipe ThickDepo) .....	152
5.3 Cross-sectional TEM image for FA-b (film deposited by Recipe ThickDepo) .....	153
5.4 Stress profile and cross-sectional TEM image for FA-c (film deposited by Recipe ThickDepo) .....	153
5.5 Stress profile and cross-sectional TEM image for RTA-b (film deposited by Recipe ThickDepo) .....	156
5.6 Cross-sectional TEM image for RTA-e (film deposited by Recipe ThickDepo) .....	156
5.7 Stress profile and cross-sectional TEM image for the as-deposited film (film deposited by Recipe DOE1-3) .....	160
5.8 Cross-sectional TEM image for FLA-b (film deposited by Recipe DOE1-3) .....	160
5.9 Cross-sectional TEM image for FLA-c (film deposited by Recipe DOE1-3) .....	161
5.10 Stress profile and cross-sectional TEM image for the as-deposited film (film deposited by Recipe DOE1-13) .....	161
5.11 Cross-sectional TEM image for FLA-f (film deposited by Recipe DOE1-13) .....	162
5.12 Cross-sectional TEM image for the as-deposited film in the ELA experiment .....	164
5.13 Cross-sectional TEM image for ELA-c .....	164
5.14 Stress profile and cross-sectional TEM image for the as-deposited film (film deposited by Recipe LayerStack) .....	166
5.15 Stress profile and cross-sectional TEM image for AI-f (film deposited by Recipe LayerStack) .....	166
5.16 Correlation of strain gradient with post-deposition argon implantation conditions. ....	167
5.17 Schematic of MEMS layers processing on foundry CMOS .....	169
5.18 CMOS metal contacts: a) after all depositions; b) after SiGe film removal; c) after oxide film removal; d) after Ge film removal .....	171
5.19 CMOS metal contacts: a) after all depositions and rapid thermal annealed at 430°C; b) after SiGe film removal; c) after oxide film removal; d) after Ge film removal .....	172
5.20 CMOS metal contacts: a) without depositions and etched in 30% H <sub>2</sub> O <sub>2</sub> solution at 80°C for 5 minutes; b) without depositions and etched in HF solution (50 ml 49% HF + 200 ml DI water) at room temperature for 10 minutes .....	173
5.21 0.13 μm technology transistor performance before and after post-processing. ....	179
5.22 0.13 μm technology Kelvin via resistance before and after post-processing. ....	180
5.23 0.13 μm technology metal electromigration test structure resistance before and after post-processing. ....	181
5.24 0.25 μm technology transistor performance before and after post-processing. ....	182
A.1 Images of water droplet on various surfaces .....	196
A.2 Water contact angle measurements on OTS SAM-coated Si, SiGe and Ge to assess thermal stability in N <sub>2</sub> ambient. ....	198
A.3 Water contact angle measurements on 1-octadecene SAM-coated Si, SiGe and Ge to assess thermal stability in N <sub>2</sub> ambient. ....	198
B.1 Layer stacks for stress monitoring .....	205
B.2 Stress stability of poly-Si, SiGe and Ge on various substrates. ....	206
B.3 Stress stability of poly-SiGe on LPCVD oxide .....	207

B.4 Stress stability of LPCVD oxide .....	208
B.5 Stress stability of various oxides .....	209
B.6 Cross-sectional views of a substrate with thin films on both sides for $n = 2$ and $m = 2$ : a) before release; b) after release. ....	210

## List of Tables

2.1 Summary of process gases (Hazards information from MSDS of Matheson Tri-Gas, Inc.) .....	16
2.2 Full factorial design to identify critical parameter for injector condition monitoring .....	28
2.3 Effect tests of parameter for injector pressure gauge reading .....	28
2.4 Parameter estimates for injector pressure gauge reading .....	29
2.5 N <sub>2</sub> equivalent correction factor (data from Unit Instruments application note) .....	33
3.1 Summary of the BCl <sub>3</sub> doped epi-SiGe process [3.1, 3.2] .....	41
3.2 Summary of the BCl <sub>3</sub> doped poly-SiGe process with 0.1% concentration bottle .....	43
3.3 Summary of the B <sub>2</sub> H <sub>6</sub> doped epi-SiGe process [3.5] .....	44
3.4 Summary of the B <sub>2</sub> H <sub>6</sub> doped poly-SiGe process .....	44
3.5 Results summary for BCl <sub>3</sub> doped poly-SiGe process verification .....	49
3.6 Comparison of BCl <sub>3</sub> and B <sub>2</sub> H <sub>6</sub> as dopant gases for poly-SiGe process .....	64
3.7 SiGe deposition with Si <sub>2</sub> H <sub>6</sub> as the silicon precursor with 100 mm-diameter wafers, caged boat [3.12] .....	65
3.8 SiGe deposition with Si <sub>2</sub> H <sub>6</sub> as the silicon precursor with 150 mm-diameter wafers, open boat .....	66
3.9 Adjustable process parameters with H <sub>3</sub> GeSiH <sub>3</sub> in the Berkeley Microlab's LPCVD poly-SiGe reactor (Tystar20) .....	71
4.1 XRD 2θ angle calculation .....	80
4.2 Experimental data for all runs .....	84, 85
5.1 Summary of post-deposition furnace annealing (FA) .....	150
5.2 Summary of post-deposition rapid thermal annealing (RTA) .....	155
5.3a Summary of post-deposition flash lamp annealing (FLA) for deposition DOE1-3. ....	158
5.3b Summary of post-deposition flash lamp annealing (FLA) for deposition DOE1-13. ....	158
5.4 Summary of post-deposition excimer laser annealing (ELA) .....	163
5.5 Summary of post-deposition argon implantation (AI) for deposition LayerStack. ....	165
5.6 Stress of individual thin film after each thermal process step .....	174
5.7 Adhesion of various thin film stacks after RTA at 430 °C for 1 minute .....	174
5.8 CMOS test summary .....	176-177
6.1 Summary of materials development of poly-SiGe (as-deposited films) .....	188
A.1 OTS coating procedure .....	194
A.2 1-octadecene coating procedure .....	194
A.3 Water contact angle data for poly-Si, poly-SiGe and poly-Ge surfaces .....	196
B.1 Deposition and removal conditions of the various thin films .....	205

B.2 Material and geometric constants .....	210
C.1 Tystar20 logbook .....	216-247

## Acknowledgement

I would first like to thank my research advisor, Professor Roger Howe, for encouraging me to go to graduate school and introducing me to the world of MEMS. His broad knowledge and endless enthusiasm about the MEMS field provided a tremendous amount of energy throughout the course of my graduate work. Professor Tsu-Jae King Liu has been providing insightful technical advice at all stages of my research. I am especially thankful to have Professor Liu as my official co-advisor after Professor Howe's departure to Stanford University; the last chapter of my research would have been impossible without her support. In addition, Professor Oscar Dubón's input on materials science was a great supplement to this work. I would also like to thank Professor Richard White for serving in my qualifying exam and thesis committee.

The work presented here is a collaborative effort with many individuals and groups. UC Berkeley Microfabrication Laboratory staff, including Patrick Wehrly, Jimmy Chang, Danny Pestal Bob Hamilton, Bill Flounders and Katalin Voros, provided tremendous support in maintaining the SiGe furnace and making custom modifications for my research. Dr. Andrea Franke provided professional guidance and shared her friendship during the first phase of my poly-SiGe study. Prof. Sherif Sedky of the American University in Cairo provided insight on the excimer laser annealing work. Dr. Yasuo Kunii of Hitachi Kokusai Electric, Inc. shared his experience in the  $\text{BCl}_3$  development work. Dr. Uthara Srinivasan and Brian Bush provided valuable discussions on anti-stiction coating. Xin Sun's assistance on CMOS testing during the weekend was greatly appreciated. In addition, the TEM analysis was conducted at the National Center

of Electron Microscopy at the Lawrence Berkeley National Laboratory. Dr. Erdman Spiecker spent many hours preparing my samples using the double-wedge technique, not to mention it was a few days before his departure back to Germany with his family.

My research work was also supported by industrial partners. On-going technical support in many areas of this research was provided by Analog Devices, Inc.. Kieran Nunan helped me to get up on the LPCVD learning curve with his experience in the poly-Si process and gave me an industrial perspective of process development. Hundreds of long emails were exchanged with Kieran on strain gradient optimization and manufacturing requirements for poly-SiGe. SIMS analysis was provided by Cascade Scientific Ltd and Materials Analytical Services. Flash lamp annealing was demonstrated by Mattson Technology. Discussions on  $\text{BCl}_3$  bottle were held with Scott Specialty Gases. In-line thickness measurement for thick poly-SiGe film development was collaborated with Sopra, Inc.. Foundry CMOS test chips were provided by Taiwan Semiconductor Manufacturing Company. The feasibility of using germyl silance was discussed with Voltaix, Inc..

It is my good fortune to have many friends in the Berkeley Sensor & Actuator Center and the Device Group, thanks for your helping hands and attentive ears. Noel Arellano, Dr. Sunil Bhave, Dr. Brian Bircumshaw, Dr. Wesley Chang, Peter Chen, Rishi Kant, Joanna Lai, Donovan Lee, Dr. Marie Eyoum, Dr. Karen Lemay, Blake Lin, Dr. Emmanuel Quévy, Christopher Roper, Xin Sun, Hideki Takeuchi, Varadarajan Vidya, Frank Zendejas, and Maryam Zieie-Moayyed – these wonderful individuals have made my time in Cory Hall very enjoyable. Noel, Wes and Frank, thanks for the company in the cubicle, sharing the “Devil’s Drink” and giving me a ride home every night.

Ruth Gjerde in the Graduate Office was a great source of support and information. The administrative support from Tom Parsons, Lindy Manly, John Huggins, Jukka-Pekka Vainio and other BSAC staff were deeply appreciated.

Last but not least, I would like to thank my family, especially my husband Andy Mai, for their love and support through the years.

This work was supported by the Defense Advanced Research Projects Agency MEMS Program under Contract N66001-01-1-8967 and by Analog Devices, Inc.

# Chapter 1: Introduction

## 1.1 Process strategies for MEMS and CMOS integration

The ability to integrate MEMS and IC technology is highly desirable for high performance MEMS devices. There are two main challenges in integration: standard metallization of electronic circuits limits the post process temperature to be below 450°C, and the large topography after the MEMS process limits the compatibility with further lithography steps. Using silicon as the MEMS structural material, most of the integration processes have mixed fabrication of both MEMS and CMOS steps to overcome the temperature limit of the CMOS and the topography problem created by the MEMS structures. Some examples include Analog Devices' *iMEMS*<sup>®</sup> process [1.1], Sandia National Laboratory's embedded MEMS process [1.2] and UC Berkeley's SOI process [1.3]. All these mixed fabrication processes are specialized and foundry services are limited.

To take advantage of the low manufacturing cost of foundry services, modular integration of MEMS and CMOS electronics has received substantial interest. In addition, modular integration allows separate development and optimization of the MEMS and the CMOS modules. Modular integration can have the MEMS steps first or the CMOS steps first.

For MEMS-first modular integration, single crystal or epitaxial silicon surface is required for the CMOS module. Stanford's and Bosch's wafer-scale encapsulation process using epitaxial silicon has the potential for MEMS-first modular integration [1.4], [1.5]. The schematic of the wafer-scale encapsulation process is shown in Figure 1.1. The

starting material is an SOI wafer. The buried oxide serves as the sacrificial material, and the MEMS structures are defined by lithography and deep reactive ion etching. A layer of gasket oxide is deposited as the sacrificial material between the MEMS structures and the capping layer. The gasket oxide is patterned and removed from the MEMS anchor regions and the circuit areas. Then 10  $\mu\text{m}$  of silicon is grown in an epitaxial reactor at 1000°C. Polycrystalline silicon is deposited over the oxide, serving as the capping layer; single crystal silicon is grown where the gasket oxide is removed. Etch holes are defined and the structure is released with vapor HF. The etch holes are then sealed with thermal oxide. The thermal oxide is removed from the metal contact area and the single crystal silicon area. CMOS process can be potentially done on the single crystal silicon area after the MEMS process. In this approach, the MEMS structures are made out of the single crystal silicon device layer of the SOI wafer, and high-quality inertial sensors and RF resonators can be built. Also, the 10  $\mu\text{m}$  thick encapsulation layer can withstand conventional back-end packaging process, such as dicing and injection molding. However, for the CMOS module, the electronic circuits cannot be placed directly on top of the MEMS area due to the selective epitaxial growth. Also, controlling the quality of the epitaxial silicon is very challenging for the circuitry areas.

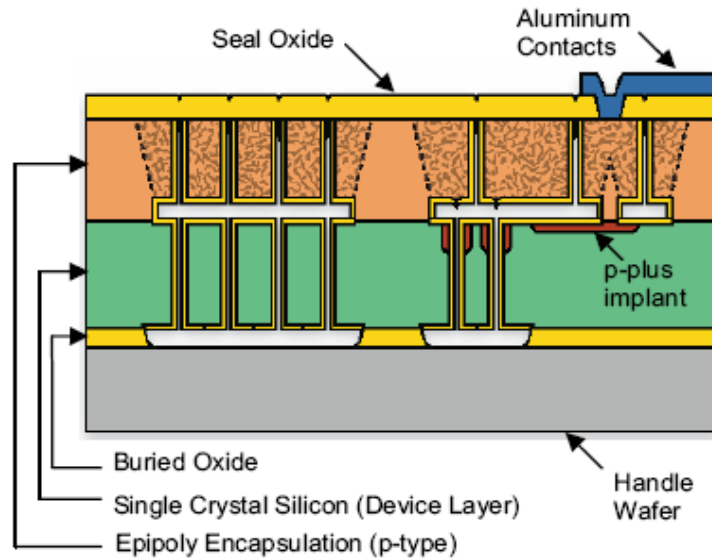


**Figure 1.1** Schematic of wafer-scale encapsulation for MEMS-first integration [1.5]

For CMOS-first modular integration, low process temperature materials are used for the MEMS steps to overcome the temperature limit imposed by the foundry CMOS. For example, Texas Instruments has a commercially successful process to make digital micromirror displays using a Ti-Al alloy [1.6]. IBM is developing a copper-based MEMS process for RF switches and resonators [1.7]. Aluminum nitride (AlN) is being explored as the structural material for RF filters and resonators at UC Berkeley [1.8]. Amorphous silicon (a-Si:H) has been demonstrated for bimorph thermal actuator application by University of Waterloo[1.9]. Polycrystalline-silicon-germanium (poly-SiGe) is another low-temperature surface micromachining material. Compared to Ti-Al, Cu, AlN and a-Si:H films, poly-SiGe has similar properties and process as the conventional surface micromachining material polycrystalline-silicon (poly-Si). Also, poly-SiGe can be used for adaptive optics [1.10], RF resonators [1.11] and inertial

sensors applications [1.12]. Figure 1.2 is a schematic of a SiGe MEMS resonator built on top of foundry CMOS electronics. After the completion of the CMOS steps, contacts are opened and vias to the electronics are first made. Sacrificial material can be either silicon dioxide or pure germanium. Poly-SiGe is used as the structural material. In this approach, MEMS devices are built directly on top of the circuitry, reducing interconnect resistance and saving valuable die area. Since there is a temperature constraint on the MEMS process, the mechanical properties of poly-SiGe are not as good as the single crystal silicon used in the wafer-scale encapsulation process discussed above. The Young's modulus and quality factor of poly-SiGe are slightly lower than those of single crystal silicon or poly-Si. With the temperature limitation, achieving the specifications of the low residual stress and strain gradient for inertial sensor applications are the main challenges for poly-SiGe. This work studies the control of the desired poly-SiGe materials properties with the temperature constraint.

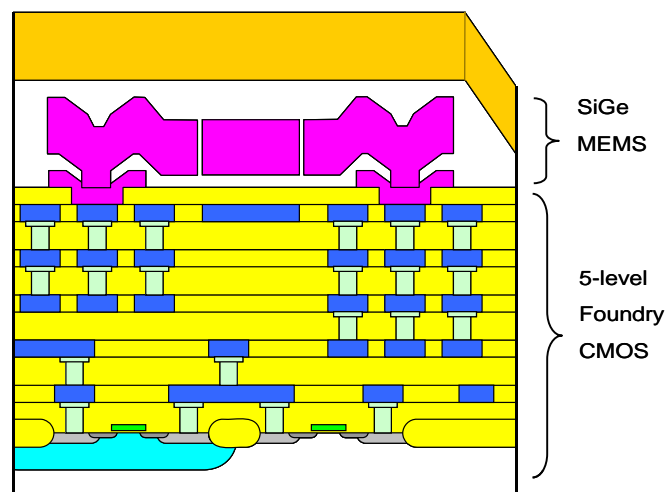


**Figure 1.2** Schematic of modular integration of MEMS and CMOS with poly-SiGe (courtesy of R. T. Howe and B. L. Bircumshaw)

## 1.2 SiGe research in IC and MEMS

Silicon-germanium has been studied extensively as the base material for heterojunction bipolar junction transistors [1.13], [1.14]; as the gate, source/drain or channel material for CMOS devices [1.15]-[1.17]; and as the absorption material for optical or thermal electronics [1.18]-[1.20]. Recently, poly-SiGe has been investigated as an alternative structural material for surface micromachining. Poly-SiGe has materials properties that are similar to those of poly-Si. In contrast to poly-Si, poly-SiGe can be deposited and crystallized at very low temperatures with good stability, which makes it promising for post-CMOS integration of MEMS [1.12], [1.21], [1.22]. This modular approach to MEMS integration is an attractive route to higher-performance and lower-cost microsystems.

Several approaches to depositing poly-SiGe for MEMS applications have been investigated by various research groups: atmospheric- or reduced-pressure chemical vapor deposition (APCVD or RPCVD) [1.23], low-pressure chemical vapor deposition (LPCVD) [1.21], [1.24], [1.25], plasma enhanced chemical vapor deposition (PECVD) [1.24], [1.26], [1.27] and pulsed laser deposition (PLD) [1.28]. The deposition rate for the APCVD or RPCVD processes is about 4 nm/min at 520°C, which is too low to be economical at CMOS compatible temperatures. Films deposited by PLD have high particle density and require additional annealing for crystallization. Poly-SiGe LPCVD and PECVD processes are well established and most promising for use in manufacturing. The deposition rate for the PECVD process is about 100 nm/min at 450°C, which is about 6× higher than that of the LPCVD process at the same temperature. On the other hand,

PECVD films typically have very high hydrogen content. The hydrogen evolves with excimer laser annealing and leaves small pores in the film [1.29]. While the LPCVD process has lower deposition rate, it usually has a large batch size for higher throughput and lower cost. Also, excimer laser annealing does not result in pores in LPCVD film [1.30]. Another major advantage of LPCVD process is its conformal coverage of all surfaces, which can also be used for planarization and gap filling. While PECVD and LPCVD poly-SiGe processes are both promising for post-CMOS integration, recent research has focused on pushing down the thermal budget, fine tuning the materials properties and developing a robust process for large volume production.

### **1.3 Desired MEMS properties for poly-SiGe**

The desired SiGe properties for MEMS applications are very different from those of electronic device applications. In general, a film thicker than 2  $\mu\text{m}$  is needed for lateral capacitive sensing. For post CMOS processing, the deposition temperature of poly-SiGe is limited to below 450°C. Deposition rate and crystallinity of the film can be improved with higher germanium content. However, the etch selectivity of a pure germanium sacrificial layer to a poly-SiGe structural layer for  $\text{H}_2\text{O}_2$  etching decreases with increasing germanium content in the poly-SiGe film. A germanium content of 60% is desired for reasonable deposition rate and crystallinity with adequate resistance to  $\text{H}_2\text{O}_2$  etching. In order to have good electrical connection to the electronics, the desired resistivity is below 10  $\text{m}\Omega\text{-cm}$  for RF MEMS applications. For inertial sensor applications with long suspension length, low residual stress and strain gradient are required. To avoid buckling of a clamped-clamped beam, a small tensile residual stress is desired. However, with

special design, films with compressive stress can also be used. Low strain gradient is the most critical requirement for inertial sensor applications. The typical strain gradient specification for inertial sensors is less than  $1 \times 10^{-5} \mu\text{m}^{-1}$ , which results in less than 5  $\mu\text{m}$  tip deflection for a 1 mm long beam. In addition to the above materials requirements, developing a high throughput, high yield and repeatable process is critical for large volume production.

#### **1.4 Overview of dissertation**

This work presents the materials and the process development of LPCVD poly-SiGe. This dissertation is organized in the following chapters:

Chapter 2 reviews the LPCVD poly-SiGe reactor. The deposited thin-film materials properties and the robustness of the process heavily depend on the condition of the reactor. The configuration, the design, the operation and the process monitoring of the reactor are discussed.

In Chapter 3, the development and the challenges of using new process gases are described. Boron trichloride ( $\text{BCl}_3$ ) has been successfully developed as a better p-type dopant gas to replace diborane ( $\text{B}_2\text{H}_6$ ); disilane ( $\text{Si}_2\text{H}_6$ ) is investigated as a silicon precursor; germyl silanes ( $(\text{H}_3\text{Ge})_x\text{SiH}_{4-x}$ ) are reviewed as the potential single-source silicon and germanium precursors.

Chapter 4 describes the process development to achieve the desired materials properties for RF MEMS and inertial sensor applications. The focus is on optimizing the strain gradient of the film, which is the most challenging materials property for inertial sensor applications. Uniformity and repeatability of the process are also discussed.

In Chapter 5, the effects of post-deposition processing on the materials properties are investigated. Also, a study of the CMOS thermal budget limits is presented.

Chapter 6 summarizes the main contributions of this work and suggests future directions.

## References

- [1.1] T. A. Core, W. K. Tsang and S. J. Sherman, "Fabrication technology for an integrated surface-micromachined sensor," *Solid State Technology*, Oct. 1993, pp. 39-47
- [1.2] J. H. Smith, S. Montague, J. J. Sniegowski, J. R. Murray, R. P. Manginell and P. J. McWhorter, "Characterization of the embedded micromechanical device approach to the monolithic integration of MEMS with CMOS," *SPIE*, vol. 2879, pp. 306-314, 1996
- [1.3] T. J. Brosnihan, "An SOI based, fully integrated fabrication process for high-aspect ratio microelectromechanical systems," Ph.D. Thesis, Dept. of ME, University of California at Berkeley, 1998
- [1.4] R. N. Candler, W.-T. Park, H. Li, G. Yama, A. Partridge, M. Lutz and T. W. Kenny, "Single wafer encapsulation of MEMS Devices," *IEEE Transactions of Advanced Packaging*, vol. 26, no. 3, 2003, pp. 227-232
- [1.5] W.-T. Park, R. N. Candler, S. Kromnueller, M. Lutz, A. Partridge, G. Yama and T. W. Kenny. "Wafer-scale film encapsulation of micromachined accelerometers," in *Proc. 12<sup>th</sup> International Conference on Solid-State Sensors, Actuators and Microsystems (Transducers 03)*, June 2003, pp. 1903-1906
- [1.6] P. F. Van Kessel, L. J. Hornbeck, R. E. Meier and M. R. Douglass, "A MEMS-based projection display," *Proc. of IEEE*, vol. 86, no. 8, 1998, pp. 1687-1704
- [1.7] C. V. Jahnes, J. Cotte, J. L. Lund, H. Deligianni, A. Chinthakindi, L. P. Buchwalter, P. Fryer, J. A. Tornello, N. Hoivik, J. H. Magerlein and D. Seeger, "Simultaneous fabrication of RF MEMS switches and resonators using copper-based CMOS

- interconnect manufacturing methods,” *17<sup>th</sup> IEEE Micro Electro Mechanical Systems Conference (MEMS-04)*, Maastricht, The Netherlands, Jan. 25-29, 2004
- [1.8] G. Piazza, “Piezoelectric aluminum nitride vibrating RF MEMS for radio front-end technology,” Ph.D. Thesis, Dept. of EECS, University of California at Berkeley, 2005
- [1.9] S. Chang and S. Sivoththaman, “Development of a low temperature MEMS process with a PECVD amorphous silicon structural layer,” *J. Micromech. Microeng.* vol. 16, 2006, pp. 1307-1313
- [1.10] B. C.-Y. Lin, T.-J. King and R. S. Muller, “Poly-SiGe MEMS actuators for adaptive optics,” *Photonics WEST*, sponsored by SPIE, The International Society for Optical Engineering, Conference 6113, Paper 6113-28, San Jose, CA, January 25, 2006
- [1.11] E. P. Quévy, A. San Paulo, E. Basol, R. T. Howe, T.-J. King, and J. Bokor, “Back-end-of-line Poly-SiGe disk resonators,” *19<sup>th</sup> IEEE Micro Electro Mechanical Systems Conference (MEMS-06)*, Istanbul, Turkey, Jan. 2006
- [1.12] A. Witvrouw, A. Mehta, A. Verbist, B. Du Bois, S. Van Aerde, J. Ramos-Martos, J. Ceballos, A. Ragel, J. M. Mora, M. A. Lagos, A. Arias, J. M. Hinojosa, J. Spengler, C. Leinenbach, T. Fuchs and S. Kronmüller, “Processing of MEMS gyroscopes on top of CMOS ICs,” in *Proc. 52nd IEEE International Solid-State Circuits Conference*, San Francisco, CA, February 6-10, 2005, pp. 88-89
- [1.13] S. S. Iyer, G. L. Patton, S. S. Delage, S. Tiwari, J. M. C. Stork, “Silicon-germanium base heterojunction bipolar transistors by molecular beam epitaxy,” in *Proc. International Electron Devices Meeting*, New York, 1987, pp. 874-876

- [1.14] J. D. Cressler and G. Niu, *Silicon-Germanium Heterojunction Bipolar Transistors*, Artech House, 2003
- [1.15] N. Kistler and J. Woo, "Symmetric CMOS in fully-depleted silicon-on-insulator using P<sup>+</sup>-polycrystalline SiGe gate electrodes," in *Proc. International Electron Devices Meeting*, 1993, pp. 727-730
- [1.16] H. Takeuchi, W.-C. Lee, P. Ranade, and T.-J. King, "Improved PMOSFET short-channel performance using ultra-shallow Si<sub>0.8</sub>Ge<sub>0.2</sub> source/drain extensions," in *Proc. International Electron Devices Meeting*, 1999, pp. 501-504
- [1.17] T.-J. King and K. C. Saraswat, "Polycrystalline silicon-germanium thin-film transistors," *IEEE Transactions on Electron Devices*, vol 41, no. 9, 1994, pp. 1581-1591
- [1.18] S. Sedky, P. Fiorini, K. Baert, L. Hermans and R. Mertens, "Characterization and optimization of infrared poly SiGe bolometers," *IEEE Transactions on Electron Devices*, vol 46, no. 4, 1999, pp. 675-682
- [1.19] M. Strasser, R. Aigner, M. Franosch and G. Wachutka, "Miniaturized thermoelectric generators based on poly-Si and poly-SiGe surface micromachining," *Sensors and Actuators A*, vol 97-98, 2002, pp. 535-542
- [1.20] P. Van Gerwen, T. Slater, J. B. Chévrier, K. Baert and R. Mertens, "Thin film boron-doped poly-crystalline silicon<sub>70%</sub>-germanium<sub>30%</sub> for thermopiles," *Sensors and Actuators A*, vol. 53, 1996, pp. 325-329
- [1.21] A. E. Franke, J. M. Heck, T.-J. King and R. T. Howe, "Polycrystalline silicon germanium films for integrated microsystems," *IEEE/ASME Journal of Microelectromechanical Systems*, vol. 12, pp. 160-171, Apr. 2003

- [1.22] C. W. Low, B. L. Bircumshaw, T. Dorofeeva, G. Solomon, T. -J. King and R. T. Howe, "Stress stability of poly-SiGe and various oxide films in humid environments," in *Proc. Stability of Thin Films and Nanostructures Symposium, Materials Research Society Meeting*, Boston, MA, Nov. 29 - Dec. 3, 2004
- [1.23] S. Sedky, P. Fiorini, M. Caymax, S. Loreti, K. Baert, L. Hermans and R. Mertens, "Structure and mechanical properties of polycrystalline silicon germanium for micromachining applications," *IEEE/ASME Journal of Micro-electromechanical Systems*, vol. 7, no. 4, pp. 365-372, Dec. 1998
- [1.24] T. Fuchs, C. Leinenbach, S. Kronmueller, f. Laermer, T. Thomas, K. Robb, H. Seidel and W. Frey, "Industrial applications of poly-silicon-germanium as functional MEMS material," in *Proc. Electrochemical Society SiGe Materials, Processing, and Devices Symposium*, Honolulu, HI, Oct. 3-8, 2004, pp. 1001-1013
- [1.25] C. W. Low, M. L. Wasilik, H. Takeuchi, T.-J. King and R. T. Howe, "In-situ doped poly-SiGe LPCVD process using BCl<sub>3</sub> for post-CMOS integration of MEMS devices," in *Proc. Electrochemical Society SiGe Materials, Processing, and Devices Symposium*, Honolulu, HI, Oct. 3-8, 2004, pp. 1021-1032
- [1.26] T. Van der Donck, J. Proost, C. Rusu, K. Baert, C. Van Hoof, J.-P. Celis and A. Witvrouw, "Effect of deposition parameters on the stress gradient of CVD and PECVD poly-SiGe for MEMS applications," in *Proc. SPIE Conference*, San Jose, CA, USA, Jan. 28-29, 2004, pp. 8-18
- [1.27] A. Mehta, M. Gromova, P. Czarnecki, K. Baert and A. Witvrouw, "Optimization of PECVD poly-SiGe layers for MEMS post-processing on top of CMOS," in *Proc.*

*13th International Conference on Solid-State Sensors, Actuators and Microsystems (Transducers 05)*, Seoul, Korea, June 5-9, 2005, pp. 1326-1329

- [1.28] S. Sedky, I. El Defrar and O. Mortagy, "Pulsed laser deposition of boron doped  $\text{Si}_{70}\text{Ge}_{30}$ ," in *Proc. Materials Research Society Meeting*, San Francisco, CA, 2006
- [1.29] S. Sedky, M. Gromova, T. Van der Donck, J.-P. Celis, A. Witrouw, "Characterization of KrF excimer laser annealed PECVD  $\text{Si}_x\text{Ge}_{1-x}$  for MEMS post-processing," *Sensors and Actuators A*, vol. 127, 2006, pp. 316-323
- [1.30] S. Sedky, R. T. Howe and T.-J. King, "Pulsed Laser Annealing, a Low Thermal Budget Technique for Eliminating Stress Gradient in Poly-SiGe MEMS Structures," *IEEE/ASME Journal of Micro-electromechanical Systems*, vol. 13, no.4, pp.669-675, Aug. 2004

## Chapter 2: LPCVD Poly-SiGe Technology

Low pressure chemical vapor deposition (LPCVD) is an industry standard deposition technique commonly used to form poly-Si, silicon dioxide and silicon nitride films. Chemical vapor deposition involves the thermal decomposition of source gases to form a solid thin film directly on the wafer substrate. LPCVD has the advantage of high throughput, conformal step coverage and good uniformity. In this section, the configuration, the design, the operation and the process monitoring of the LPCVD poly-SiGe reactor are presented.

### 2.1 LPCVD Reactor Overview

*In-situ* doped poly-SiGe films were deposited in a Tystar hot-wall horizontal LPCVD reactor, approximately 125 cm in length and 23 cm in diameter (Figure 2.1). This reactor is configured to accommodate various process conditions and hardware modifications in an academic research environment. The operating pressure range of the furnace is 100 mTorr – 2000 mTorr and the operating temperature range is 300°C – 450°C. There are four channels for precursor gases and two channels for dopant gases with various flow ranges. Process gases can be introduced into the tube via the gas ring or the injector. Unreacted gases are pumped out to the exhaust. This furnace is capable of processing both 100 mm-diameter and 150 mm-diameter wafers. Wafers are placed vertically in wafer boats at the center of the reactor. There is a computer connected to the reactor for process control and recipe management. The furnace normally runs in an automatic mode. It can also be operated manually for setup verification or trouble

shooting. Since hazardous chemicals are used, there are multiple safety interlocks implemented in the software and the hardware.

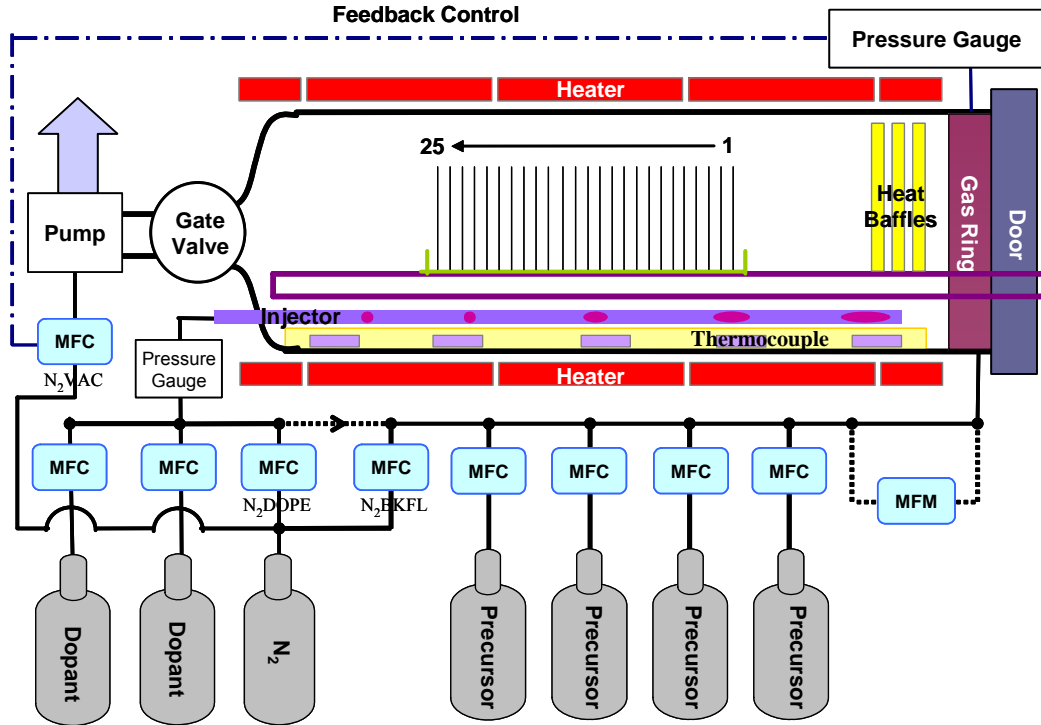


**Figure 2.1:** LPCVD reactor schematic

## 2.2 Process gases

The details of all the process gases are listed in Table 2.1 below. Pure silane ( $\text{SiH}_4$ ) or disilane ( $\text{Si}_2\text{H}_6$ ) and germane ( $\text{GeH}_4$ ) are available as the gaseous silicon and germanium precursor gases, respectively. Boron trichloride ( $\text{BCl}_3$ ), diborane ( $\text{B}_2\text{H}_6$ ) and phosphine ( $\text{PH}_3$ ) can be used as the dopant gases. The dopant gases are diluted to target the desired doping concentration in the film. Most of the precursor and dopant gases are reactive and are health or fire hazards. Toxic and flammable gases are stored in exhausted gas cabinets, each with a sprinkler and a gas leak detector. The  $\text{N}_2$  bottle is hooked up to

three lines since it has three roles in the furnace: N<sub>2</sub>Dope – to monitor the injector condition and to prevent deposition in the injector for undoped film processes; N<sub>2</sub>Vac – to reduce the pumping efficiency for pressure control; N<sub>2</sub>BKFL – to flush out toxic gases and bring the tube to atmospheric pressure.

**TABLE 2.1** Summary of process gases (Hazards information from MSDS of Matheson Tri-Gas, Inc.)

Gas	Conc.	Range (sccm)	Function	Route	Hazards (NFPA rating)			Status
					Health	Fire	Reactivity	
SiH <sub>4</sub>	100%	200	Silicon precursor	Gas ring	2	4	3	Active
Si <sub>2</sub> H <sub>6</sub>	100%	200	Silicon precursor	Gas ring	1	4	2	Active
GeH <sub>4</sub>	100%	200	Germanium precursor	Gas ring	3	4	2	Active
BCl <sub>3</sub>	1% in He	50	Boron dopant	Injector/gas ring	3	0	2	Active
B <sub>2</sub> H <sub>6</sub>	10% in H <sub>2</sub>	100	Boron dopant	Injector/gas ring	4	4	3	Inactive
PH <sub>3</sub>	50% in H <sub>2</sub>	10	Phosphorous dopant	Injector/gas ring	4	4	2	Inactive
N <sub>2</sub>	100%	100	Injector maintenance	Injector/gas ring	1	0	0	Active
N <sub>2</sub>	100%	2000	Pressure control	Pump	1	0	0	Active
N <sub>2</sub>	100%	5000	Flush and backfill	Gas Ring	1	0	0	Active

As shown in Figure 2.1, process gases can be introduced into the reactor either through the gas ring located at the door (load) end of the tube or through the multi-pore injector located beneath the wafer boats. Silicon and germanium precursor gases are introduced from the door end through the gas ring; the dopant gases are introduced from the pump side via the injector. Introducing the dopant gases via the gas ring is also feasible. During deposition, reaction gases are consumed faster at the gas inlet and their partial pressures are depleted down the stream. The depletion effect across the load is more pronounced for gases introduced via the gas ring. The multi-pore injector helps to reduce the cross-load depletion effect by injecting gas at multiple pores along the load. The pores have increasing diameter along the line of gas flow to compensate the pressure loss along the stream. Since the injector pores are small, the pressure inside the injector is fairly high. Silicon and germanium precursor gases should not be introduced through the injector because the injector is at the deposition temperature and the injector pores will

quickly clog due to the high SiGe deposition rate inside the injector. On the other hand, the pores in the gas ring do not clog readily because they have large orifices and the gas manifold temperature is lower than the deposition chamber temperature.

The dopant gas can also clog up the injector but by a different mechanism.  $B_2H_6$  can easily decompose into a solid polymer  $B_xH_y$  in the furnace operating temperature range [2.1]. The polymer slowly builds up inside the injector. After a certain threshold, the dopant gas flow can no longer be approximated as uniform, and the deposition results in cloudy film having high resistivity. An injector change is required at this point. The  $B_2H_6$  doping process was terminated after the alternative boron dopant gas  $BCl_3$  was successfully demonstrated.

The gas line for phosphine ( $PH_3$ ) is also inactive. For post-CMOS SiGe deposition, low thermal budget is the essential requirement. Phosphine retards the deposition rate and extra annealing is required to activate the dopant [2.2]. With the precursor gases  $SiH_4$ ,  $Si_2H_6$  and  $GeH_4$  introduced via the gas ring and  $BCl_3$  introduced via the injector, there remain one precursor gas channel and one dopant gas channel available in the reactor for advanced process experiments.

### **2.3 Process recipes**

Process recipes are stored in the control computer. Process temperature, process pressure, gas flow rates and deposition time are the variables in the recipe. The recipe has a pre-programmed process sequence. A typical deposition recipe consists of the following steps: pump/purge cycles after wafer loading, leak check, process parameters (temperature, gas flow rate and pressure) stabilization, deposition, and finally

pump/purge cycles to flush out the unreacted process gases and bring the pressure up to atmospheric pressure. Multiple depositions with different process parameters can be programmed into one recipe. If the process parameters are out of tolerance, the recipe will go to an abort sequence, which shuts off all the toxic gases and flushes the tube with nitrogen. The process can be re-directed to normal mode manually after trouble-shooting.

A standby recipe is loaded if the furnace is not running a deposition. The standby recipe consists of a 5-minute  $\text{Si}_2\text{H}_6$  coating step at  $450^\circ\text{C}$  for conditioning purpose. After the coating step, the tube is flushed and held in  $\text{N}_2$  ambient.

## **2.4 Wafer placement**

About 50 wafers can be loaded vertically in the SiGe reactor. Wafers can be placed in either open wafer boats or caged wafer boats. Figure 2.2 shows both wafer boat configurations. Boats with different length and wafer spacing are readily available. Process gases can reach the wafers in open boat from all directions, whereas the gases can only enter through the slots of the caged boat. For mass transport-limited deposition, the deposition rate tends to be higher towards the wafer edge for open boat configuration due to diffusion effects. In such a case, caged boat can improve the cross-wafer uniformity significantly. If the deposition is surface reaction-limited, the uniformity is about the same for both wafer boat configurations. In this case, the deposition rate is significantly lower for wafers sitting inside the caged boat due to the loading effect of the wafer boat surface. The surface area of the caged boat is about the same as that of the wafers sitting inside. Process gases are consumed by the deposition on the wafer boat surface.

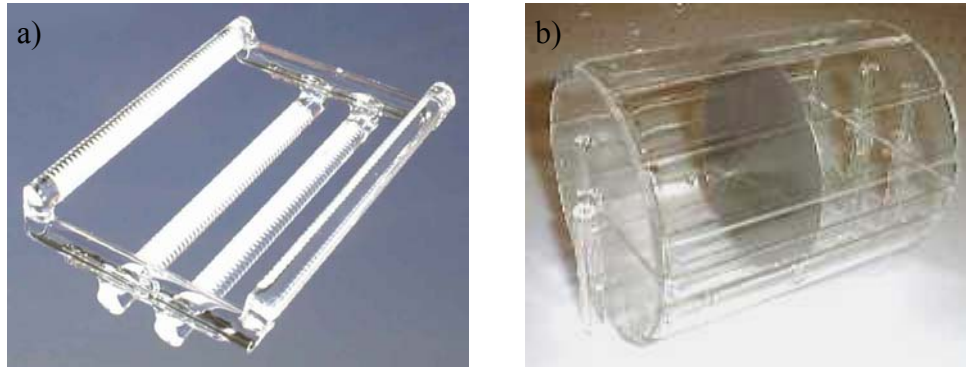


**Figure. 2.2** a) Open boat; b) Caged boat [2.3]

Since an LPCVD system is a batch reactor, the throughput can be increased by using the maximum number of process wafers. However, there are tradeoffs between throughput and uniformity. The number of wafers in the reactor is limited by the length of the temperature flat zone and by gas transport. Process temperature has less fluctuation at the center of the tube. The process gases are consumed as they travel down the tube, resulting in a higher deposition rate for wafers sitting near the gas inlet. There is also a limit on wafer spacing. If wafers are placed too close to each other, diffusion transport limitations could result in higher deposition rate at wafer edges.

Both 100 mm-diameter and 150 mm-diameter wafers can be placed on wafer boats sitting on the cantilevers. However, the 100 mm-diameter wafers are placed below the center axis in the 230 mm-diameter reactor and there is more open space for gas flow on the top of the wafer. By comparison, 150 mm-diameter wafers are nearly centered in the reactor, resulting in better cross-wafer deposition uniformity.

The placement of the wafers in the boat and the placement of the boat on the cantilevers both affect the characteristics of the deposited film. In order to achieve

reproducible results, consistency in wafer placement is necessary. Wafers sitting at the leading and trailing edges of the load usually have worse uniformity due to vortexes. Therefore, dummy wafers should be placed at the edges.

## **2.5 Quartz tube**

The process tube is made of quartz. Since the reactor is a hot-wall system, deposition occurs on the quartz wall as well as on the wafers. The deposited SiGe film has good adhesion to the quartz wall. The film is compressive and the stress applied on the quartz wall increases as the film gets thicker. Also, poly-SiGe and quartz have different thermal expansion coefficients. The quartz tube will eventually crack due to stress and thermal cycling. In industry, the quartz tube is pulled out and cleaned regularly because it is very expensive to ruin a full load of wafers that have gone through many process steps. In an academic research laboratory, the cost of changing the quartz-ware is lower compared to that of regular cleaning. In this case, the quartz tube stays in the furnace until it cracks. Tube cracking is not a safety hazard, since the tube operates at low pressure during deposition, the toxic and flammable process gases cannot leak out unless the pump fails at the same time. Also the reactor is enclosed in an exhausted gas cabinet. In addition, the tube usually cracks during loading and unloading when temperature and pressure change significantly.

The quartz tube usually cracks near the door where there is a greater temperature gradient and the deposited film is thicker. A liner can be used to increase the lifetime of the tube. The liner is an extra piece of quartz cylinder inserted inside the tube that can significantly reduce the deposition on the tube. Since the vacuum is held by the tube,

process does not go down with small cracks on the liner wall unless it collapses. Recent year's process record shows that the lifetime of the quartz tube is about 200 hours of deposition, which corresponds to roughly 100  $\mu\text{m}$  of film thickness.

A 5 minute leak monitor step is set up in all recipes to monitor the rate of the pressure rise in the tube. The furnace is hard-pumped in the previous step. The pump is then turned off for 5 minutes and pressure rise is measured. The initial intention for this monitor step was to correlate the rate of pressure rise and the quartz tube lifetime. No strong correlation between the rate of pressure rise and the quartz tube lifetime was found, but the origin of the pressure rise was determined.

The leak monitor step is set up in two different ways. In the standby recipe, the leak monitor was done quite early in the process sequence, before the temperature stabilization. For the deposition recipe, the leak monitor was done after the temperature stabilization. It turns out that the leak rate for the standby recipe is usually about 10 mTorr/min and always  $<1$  mTorr/min for the deposition recipe. The standby recipe is usually loaded after users remove their wafers. The rising pressure is caused by moisture outgasing after loading. For the deposition recipe, the leak monitor was done after the quartz ware was baked out for more than an hour. If the standby recipe is run after the door is closed for a few hours, the rate of rise goes down significantly.

The pressure sensor is not good enough to measure the rate of pressure rise due to the real leaking since it is designed to measure the deposition pressure in the 100 mTorr range. The small leak rate results in an oxygen content in the poly-SiGe film in the order of  $1 \times 10^{19} \text{ cm}^{-3}$ , compared to  $1 \times 10^{18} \text{ cm}^{-3}$  in an industrial reactor with a  $\text{N}_2$  load-lock chamber.

## **2.6 Operation control**

### **2.6.1 Pressure control**

The pressure in the furnace is controlled by the pump, the pressure gauge and the N<sub>2</sub>Vac line using feedback. The base pressure can reach <1 mTorr while the pump is running at its full power and there is no gas flowing in the furnace. Typical rate of rise is 4 mTorr/min when the pump is turned off and the quartz tube is in good condition. Flowing process gases increase the pressure, yet the pressure is still typically below the desired process pressure. The process pressure is measured by the pressure gauge located near the door. To adjust the pressure, a controlled amount of nitrogen (N<sub>2</sub>Vac line) is introduced to the pump to reduce its efficiency. For a particular amount of process gas flow, the minimum achievable process pressure is set by the pumping efficiency; the maximum achievable process pressure is set by the upper limit of N<sub>2</sub>Vac flow used to reduce the pumping speed. A particular feedback setting can accommodate a range of pressure with a fixed total gas flow rate. With proper feedback setting, the usual settling time for the pressure is about 1 minute and the process is capable of pressure change during deposition.

### **2.6.2 Temperature control**

The temperature control system includes a five-zone resistor coil heater and two sets of thermocouple tubes mounted inside and outside of the reactor. The two outer zones of the heater are called the guard zones. Since heat is lost faster at the door end and the pump end of the tube, the two guard-zone heaters run at higher powers than those in

the center flat zone. The center flat zone has three heaters, which makes temperature gradient control possible. The manufacturer's nominal operating temperature of this particular furnace is 600°C for the best temperature control. However, the desired deposition temperature for poly-SiGe is in the range of 400°C – 450°C and even lower for pure poly-Ge. For the low temperature range, the heater is only running at 20 – 30% of its full power. The feedback control between the heater and the thermocouple is digitized, and small changes can vary the temperature significantly at the low temperature range. As a result, the temperature profile during deposition is approximately a sinusoidal function with a peak-to-peak amplitude of 6°C and a period of 25 minutes. A typical temperature profile of a 425 °C deposition is shown in Figure 2.3. The temperature profiles recorded by the five thermocouples are labeled in the plot. The pump side and the door side temperatures have the most fluctuations. It usually takes an hour for the temperature to settle within  $\pm 5^\circ\text{C}$  of the set point.

Temperature calibration can help to stabilize the temperature faster. During the calibration session, the heater power for a particular temperature is stored in memory for future reference. This can significantly reduce the adjustment time during temperature stabilization. Since the heater condition changes over time, temperature calibration should be done regularly, especially after a power shutdown.

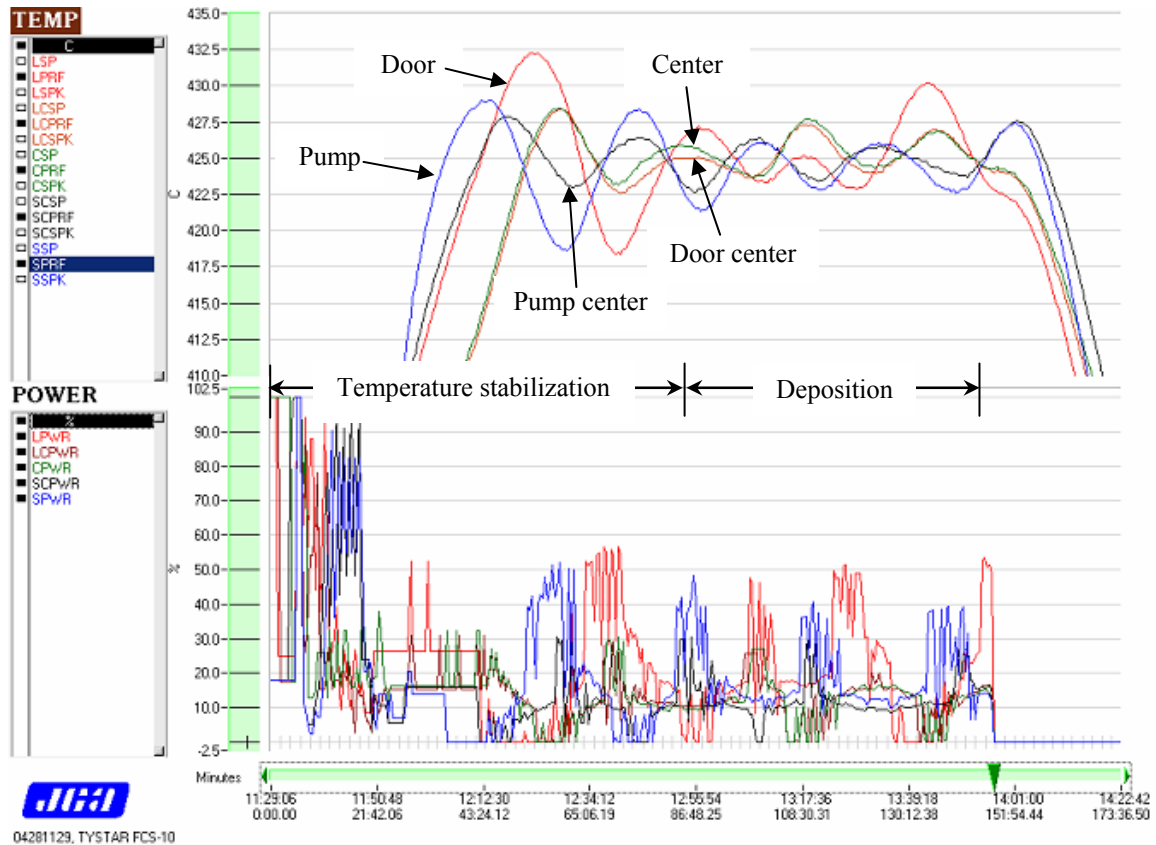


**Fig. 2.3** Temperature and power profiles of a 425 °C deposition

### 2.6.3 Gas flow rate control

The flow rate of each gas is controlled by individual mass flow controllers (MFC). The MFC range for each gas is showed in Table 2.1 in sccm. The manufacture’s specification is  $\pm 1\%$  output error the for gas flow within 5% to 95% of the full range.

Figure 2.4 shows the schematic of a mass flow controller. It can be separated into two main components: a mass flow meter (MFM) and a proportional controller. The mass flow meter divides the flow between a heated sensing tube, where the mass flow is actually measured, and a flow bypass, where the majority of flow passes. Mass flow meters use the thermal properties of a gas to directly measure the mass flow rate. The

resistors wrapped around the sensing tube serve as both the heating and sensing elements. As the gas flow through the heated sensing tube, it absorbs some heat, and creates a temperature difference along the stream. The temperature difference between the two resistors is measured by a Wheatstone bridge so that mass flow in the sensor tube can be determined. Since each gas molecule has a specific ability to pick up heat, each MFC is calibrated to a particular gas or gas mixture. The other main component, the proportional controller, consists of a variable displacement solenoid valve and the control electronics. The controller drives the valve to the correct position so that the measured flow equals the desired flow set point.

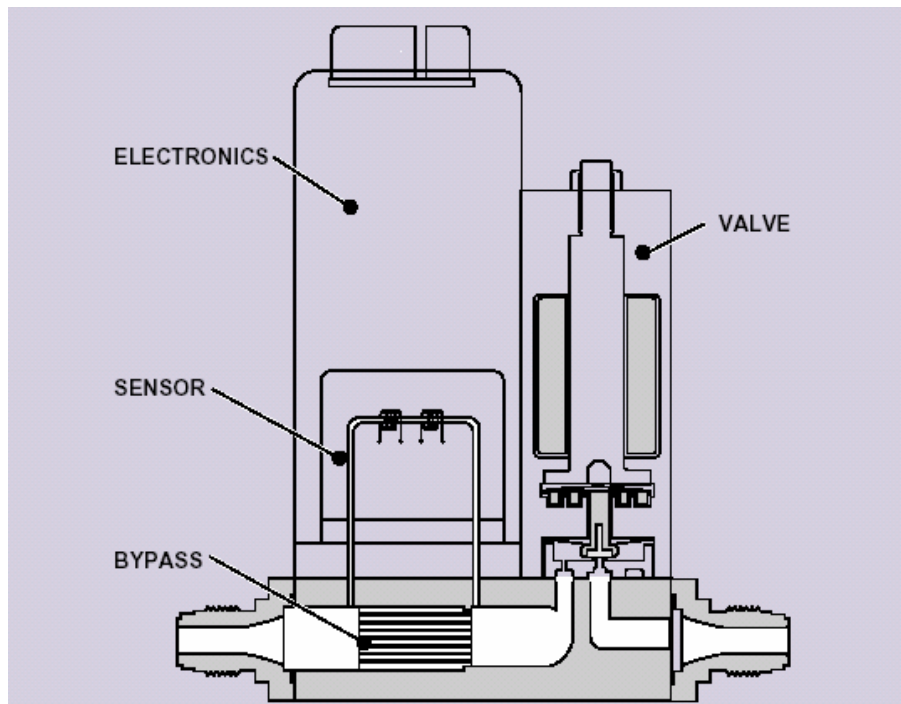


**Fig. 2.4** Mass flow controller schematic [2.4]

## **2.7 Process monitor**

### **2.7.1 Automatic process condition monitor**

The furnace control computer has the capability to monitor the real-time process condition. The computer acquires data from the reactor every 30 seconds. Temperature, pressure, gas flow rates, gas valve conditions are recorded and archived in the computer. Figure 2.3 is a typical example of temperature and heater power for a deposition. The data acquisition runs 24 hours a day. This archival data is very useful for trouble shooting aborted depositions and maintaining statistical process control.

### **2.7.2 Process logbook**

In addition to the automatic process monitoring, a process logbook (Appendix C) has been manually maintained since 2002 to better sustain the process. The process logbook contains the process condition for all depositions, problem reports and maintenance notes. Historical information of the reactor has been studied for failure analysis, design improvement and new process qualification.

### **2.7.3 Injector condition monitor**

As discussed in Section 2.2, injector clogging caused by dopant gas  $B_2H_6$  is a main challenge for uniformity and repeatability control. As shown in Figure 2.1, the injector is hooked up to the dopant gases and  $N_2Dope$  line. Dopant gas is used during deposition and  $N_2Dope$  is used during standby. A pressure gauge is mounted at the upstream of the injector to monitor the clogging condition. When there is some gas flowing through the injector, pressure will build up and it can be measured by the

pressure gauge. As the injector clogs, the pressure reading will go up. The reading of the pressure gauge depends on several factors:

- The gas flow rate through the injector
- The temperature of the tube
- The pressure of the tube
- The clogging condition of the injector

For injector monitoring purposes, the pressure gauge reading vs. the clogging condition is of highest interest. The simplest approach is to keep all other factors constant and make the clogging condition the only dependence of the pressure gauge reading. However, it is important to know how small fluctuations of other factors could affect the pressure gauge reading before taking the simplified approach. A monitor recipe can be chosen after identifying critical parameters in injector pressure gauge reading. The control limit for injector change can be determined by comparing a good injector and a clogged injector. To identify critical parameters in injector pressure gauge output, full factorial design is used because the experiment is neither time consuming nor expensive.

Flowing either  $B_2H_6/H_2$  mixture or  $N_2$ dope generates a pressure inside the injector; therefore the injector condition monitoring could be done during either deposition or standby. For the interest of reducing  $B_2H_6$  usage,  $N_2$  is chosen as the monitoring gas. Since the  $N_2$ Dope MFC has full range of 100 sccm, outputting 10 – 90 sccm of  $N_2$  will be accurate. If 10 – 90 sccm of  $N_2$  is the only gas flow in the furnace, the pressure of the tube can be controlled between 100 to 900 mTorr. The pressure of the tube acts as an external load to the injector and therefore affects the injector pressure gauge reading. The operating temperature of the furnace is in the range of 300 – 450 °C.

Since the gas flow in the injector is heated up inside the furnace, the temperature of the tube influences the pressure of the injector.

Based on the hardware limits, low, medium and high values are chosen for the gas flow rate, the tube pressure and the temperature. For the clogging condition, a new injector and a clogged injector are used in the experiment for comparison. The  $3^3 \times 2$  full factorial design is summarized in Table 2.2. For each clogging condition, four replications were done at the center point where N<sub>2</sub>Dope flow rate = 45 sccm, tube pressure = 500 mTorr and temperature = 400 °C.

**TABLE 2.2** Full factorial design to identify critical parameter for injector condition monitoring

Variables		Settings	
N <sub>2</sub> Dope flow rate (sccm)	10	45	90
Tube pressure (mTorr)	100	500	900
Temperature (°C)	350	400	450
Injector condition	New		Clogged

Multivariate analysis of variance (MANOVA) [2.5] in Table 2.3 shows that the N<sub>2</sub>Dope flow rate and the clogging condition are the most statistically significant factors with large F ratio and small p-value. The interaction term of N<sub>2</sub>Dope flow and the clogging condition is also very significant. The tube pressure does not matter, and the temperature term has a small contribution.

**TABLE 2.3** Effect tests of parameter for injector pressure gauge reading

source	DF	Sum of Squares	Mean Square	F Ratio	Prob. > F
N <sub>2</sub> Dope flow rate (sccm)	1	261.83	261.83	2552.7	< 0.0001
Tube pressure (mTorr)	1	0.2341	0.2341	2.2823	0.1373
Temperature (°C)	1	0.8639	0.8638	8.4220	0.0055
Injector condition	1	58.115	58.115	566.59	< 0.0001
N <sub>2</sub> Dope (sccm) × Tube pressure (mTorr)	1	0.0027	0.0027	0.0266	0.8711
N <sub>2</sub> Dope (sccm) × Temperature (°C)	1	0.1432	0.1431	1.3956	0.2432
Tube pressure (mTorr) × Temperature (°C)	1	0.0043	0.0043	0.0416	0.8392
N <sub>2</sub> Dope (sccm) × Injector condition	1	7.5486	7.5486	73.594	< 0.0001
Tube pressure (mTorr) × Injector condition	1	0.00004	0.00004	0.0004	0.9835
Temperature (°C) × Injector condition	1	0.0659	0.0659	0.6423	0.4268

Parameter estimations in Table 2.4 show that the pressure gauge output increases with the N<sub>2</sub>Dope flow rate and the clogging condition. The parameter of the interaction term of the N<sub>2</sub>Dope flow rate and the clogging condition are also positive. Therefore, for the same clogging condition, high N<sub>2</sub>Dope flow rate gives better sensitivity of the pressure gauge reading.

**TABLE 2.4** Parameter estimates for injector pressure gauge reading

Term	Estimate	Std. Error	t Ratio	Prob. >  t
Intercept	0.7442	0.4389	1.70	0.0963
N <sub>2</sub> Dope flow rate (sccm)	0.0672	0.0013	50.5	< 0.0001
Tube pressure (mTorr)	0.0002	0.0001	1.51	0.1373
Temperature (°C)	0.0031	0.0011	2.90	0.0055
Injector condition	0.9842	0.0413	23.8	< 0.0001
(N <sub>2</sub> Dope (sccm) - 45) × (Tube pressure (mTorr) - 500)	-6.649e-7	0.0000	-0.16	0.8711
(N <sub>2</sub> Dope (sccm) - 45) × (Temperature (°C) - 400)	0.0000	0.0000	1.18	0.2432
(Tube pressure (mTorr) - 500) × (Temperature (°C) - 400)	-6.667e-7	0.0000	-0.20	0.8392
(N <sub>2</sub> Dope (sccm) - 45) × Injector condition	0.0114	0.0013	8.58	< 0.0001
(Tube pressure (mTorr) - 500) × Injector condition	-0.0000	0.0001	-0.02	0.9835
(Temperature (°C) - 400) × Injector condition	-0.0009	0.0011	-0.80	0.4268

Knowing the parameter dependence of the pressure gauge reading, the regular monitoring of the injector condition can be simplified. A standby step is chosen for run-to-run monitoring. In this particular step:

- N<sub>2</sub>Dope flow rate = 90 sccm
- Tube pressure ≈ 110 mTorr
- Temperature = 350 – 450°C

This is the standby condition the furnace should be in before the user loads the deposition recipe. All users are required to record injector condition data for every run. The nitrogen flow rate in this step is controlled by a mass flow controller, which is relatively reliable. The tube pressure has a small fluctuation due to variations in pumping efficiency. However, the tube pressure is the least significant factor for the injector pressure reading. Although the temperature set point is 350°C for this step, actual

temperature can vary from 350°C to 450°C because a 450°C coating is the prior step and it takes sometime for the tube to cool down. To make the regular monitoring user friendly, waiting for the temperature to stabilize to 350°C is not required. To choose the threshold for injector change, a new injector and a clogged injector are compared at various temperatures with 90 sccm of N<sub>2</sub> flow and 110 mTorr of tube pressure.

Comparing a new and a clogged injector in Figure 2.5 for the simplified monitoring condition, the control limit for an injector change is chosen as 9 Torr. This control limit is rather conservative and adds to the workload of the maintenance staff, but it is desirable for process stability.

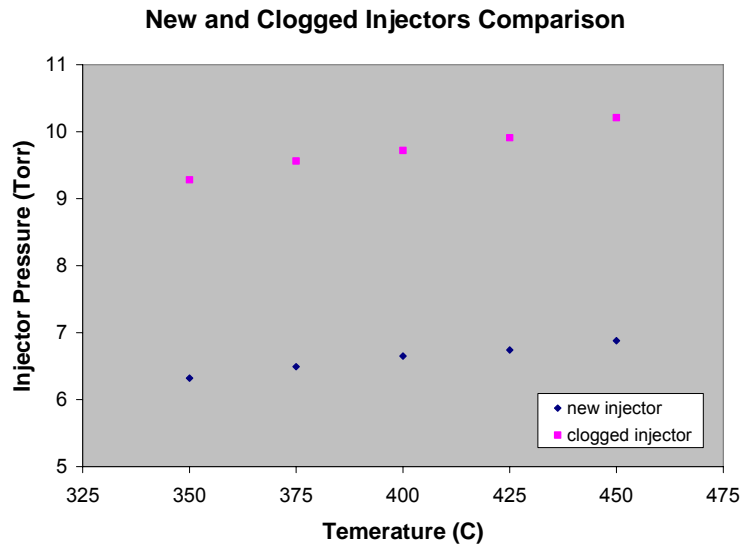


**Figure 2.5:** Pressure reading for a new injector and a clogged injector

Historical data of injector pressure since the injector monitoring was set up are shown in Figure 2.6. Before February 2004, B<sub>2</sub>H<sub>6</sub> was the only boron dopant gas available. The data have a periodical pattern: injector pressure rises with B<sub>2</sub>H<sub>6</sub> doped process usage and drops after the injector change. On average, injector change was done after ~ 20 hours of deposition. In some cases, when the deposition is not critical and some

users could not wait for the injector change, they used the injector above the control limit.

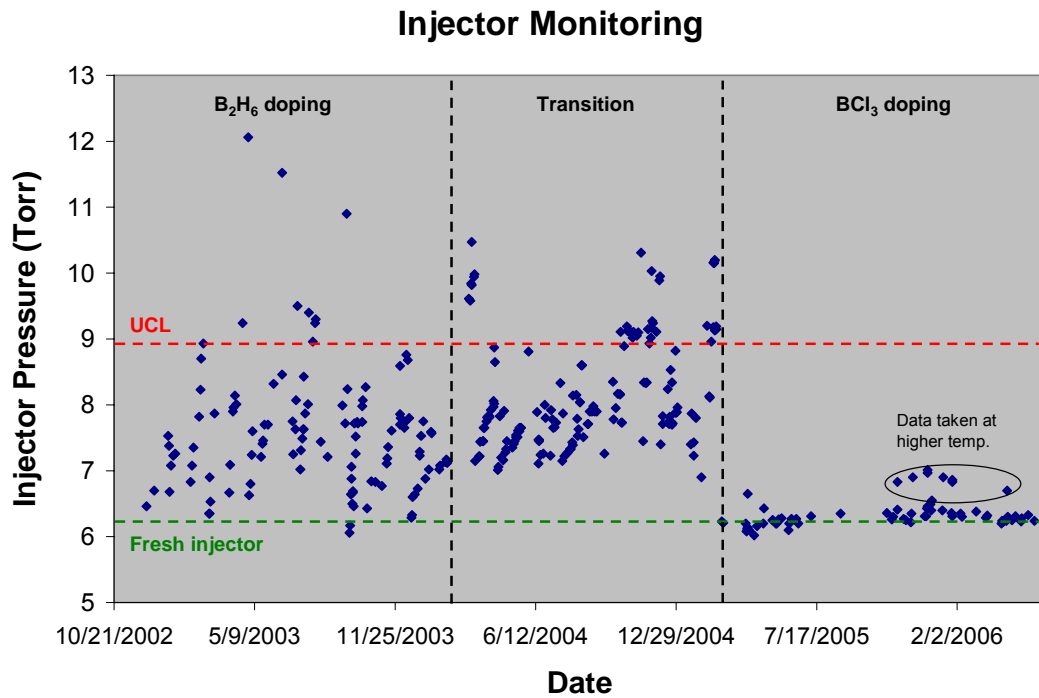


**Figure 2.6** Historical data for injector pressure

Single-use quartz injector is not conducive for frequent changes due to the high risk of cracking. Stainless steel injectors have been used for a few years. Since a stainless steel injector is more expensive than a quartz injector, stainless steel injectors have been cleaned and reused over and over. The clogged injector can be drilled out in the machine shop and re-installed in the furnace. This cleaning method is not very satisfactory, as there is always some residue left after the drilling. It can be seen that the initial pressure of a “freshly clean” injector rises over time.

Pulling out the injector so frequently is a maintenance issue and process repeatability is still not guaranteed, due to the small drift of the injector condition over time. Also, contamination is always a concern for injectors coming back from the

machine shop.

$\text{BCl}_3$  doping was investigated since February 2004 [2.6]. Details of the  $\text{BCl}_3$  doping process development will be presented in Chapter 3. The same technique has been used to monitor the injector pressure over time. Since  $\text{BCl}_3$  is more thermally stable compared to  $\text{B}_2\text{H}_6$  and it does not form a solid polymer inside the injector, injector clogging does not seem to be an issue (see Fig. 2.6). The  $\text{B}_2\text{H}_6$  bottle was removed permanently from the reactor in March 2005 and a quartz injector was installed for the  $\text{BCl}_3$  line. The injector pressure has been very stable and the injector lifetime is the same as other quartz-ware in the furnace.

#### **2.7.4 MFC monitor**

The SiGe film is deposited using  $\text{SiH}_4$  and  $\text{GeH}_4$ . The deposition rate and the thin-film's mechanical properties depend strongly on the germanium content, which in turn depend on the outputs of the  $\text{SiH}_4$  and  $\text{GeH}_4$  mass flow controllers. The output gas flow rate could drift throughout the lifetime of the MFC. The most important attribute of an MFC for achieving run-to-run repeatability is not the accuracy, but the consistency. It is necessary to monitor the performance of the MFCs for process control.

If the MFC is taken out of the reactor, its output can be tested with nitrogen instead of the actual gas the MFC is calibrated to, such as  $\text{SiH}_4$  or  $\text{GeH}_4$ . With the electronic set point entered and the input line hooked up to the nitrogen bottle, the nitrogen output will be regulated by the MFC, which can then be quantified with a trusted mass flow meter (MFM) calibrated to nitrogen. As discussed before, the mass flow measurement depends on the specific heat of the gas. Since nitrogen has a different

specific heat than the gas that the MFC is calibrated to, a correction factor (CF) should be used to convert the actual nitrogen output from the MFC being tested:

$$N_2 \text{ flow through a MFC calibrated to gas A} = \frac{\text{set point}}{CF} \quad (2.1)$$

Correction factor for the gases used in the SiGe reactor are listed in Table 2.5 below.

**TABLE 2.5** N<sub>2</sub> equivalent correction factor (data from Unit Instruments application note)

Gas	Correction factor (CF)
SiH <sub>4</sub>	0.603
Si <sub>2</sub> H <sub>6</sub>	0.321
GeH <sub>4</sub>	0.591
1% BCl <sub>3</sub> in He ≈ pure He	1.399
N <sub>2</sub>	1

Measuring the MFC with the external MFM is not a convenient way to monitor the performance of the MFC regularly. Pulling out the MFC from the gas line involves running a few pump/purge cycles and switching some valves in order to prevent contamination and to ensure safety. To track the MFC performance easier, an *in-situ* mass flow verification system is implemented with a mass flow meter installed at the downstream of all the MFCs in the reactor, as shown in Figure 2.1. The black dashed line shows the connection of the MFM loop. The MFM is bypassed during regular deposition to minimize its usage and it is activated only for the MFC monitoring purpose by some valve switching. All of the dopant gases are re-routed so that they can go through the MFM and enter the tube via the gas ring. Individual gas coming out from the MFC can flow through the MFM for calibration. The mass flow meter is calibrated to primary standard with N<sub>2</sub>. In this case, the correction factor is used again to convert the actual gas flow:

$$\text{gas } X \text{ flow through a MFM calibrated to } N_2 = \text{MFM output} \times CF \quad (2.2)$$

For the monitoring recipe, all gases are directed to flow through the MFM individually. Three set points are chosen for each gas to check linearity. The range of the MFM is chosen to be 500 sccm of  $N_2$ , which accommodates most of the ranges of  $SiH_4$ ,  $Si_2H_6$ ,  $GeH_4$  and  $N_2Dope$  and  $N_2BKFL$  as listed in Table 2.1. The  $BCl_3/He$  MFC range is too small for the MFM to resolve. To get around this problem, 90 sccm of  $N_2Dope$  is flowing together with the  $BCl_3/He$  mixture so that the total gas flow rate falls into the measurable range of the MFM. After the gas flow rate quantification, the MFM is flushed and cleaned with nitrogen flow.

MFC monitoring data using the internal MFM loop since November 2005 are presented in Figures 2.7 – 2.11. Both the  $SiH_4$  and  $GeH_4$  MFCs were pulled out of the reactor and measured with an external MFM in February 2005. The external MFM and the internal MFM give similar reading for the  $GeH_4$  output. During the subsequent 9-month period, the  $SiH_4$  MFC experienced a downward drift in gas output for some unknown reason, but the  $SiH_4$  MFC output has stayed roughly constant since November 2005. Since consistency is more important than accuracy, the  $SiH_4$  MFC was not changed out. It can be seen that the output of the  $Si_2H_6$  MFC is slowly drifting higher. The  $Si_2H_6$  flow rate is not very critical for process control because it is mainly used for standby coating and amorphous-Si seeding layer. The  $BCl_3/He$  mixture and  $N_2$  MFCs are fairly constant. It can be seen that most of the data do not match the number calculated with Equation 2.2. The MFCs or the MFM might not be perfectly accurate, but consistency is more critical.

With the regular monitoring, it is possible to achieve run-to-run repeatability with drifting MFCs. The gas flow rate in the deposition recipe could be corrected to accommodate the change in the MFC output. For a more sophisticated system, feedback could be implemented for self-correction.

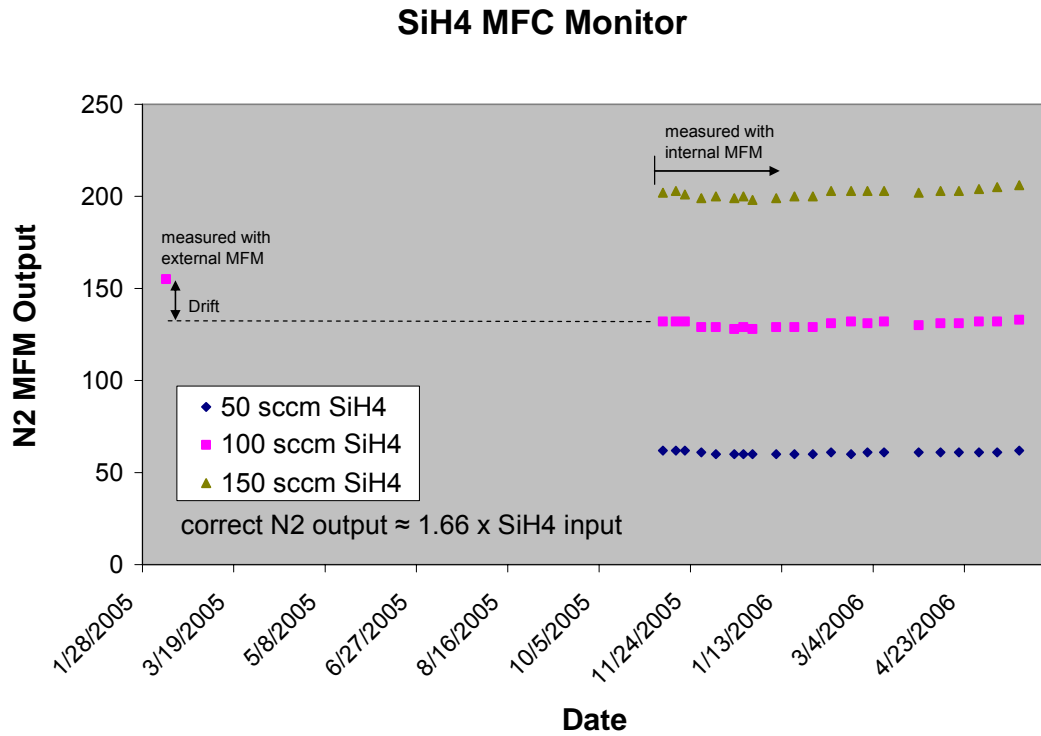


**Figure 2.7** SiH<sub>4</sub> MFC monitoring data

### GeH<sub>4</sub> MFC Monitor

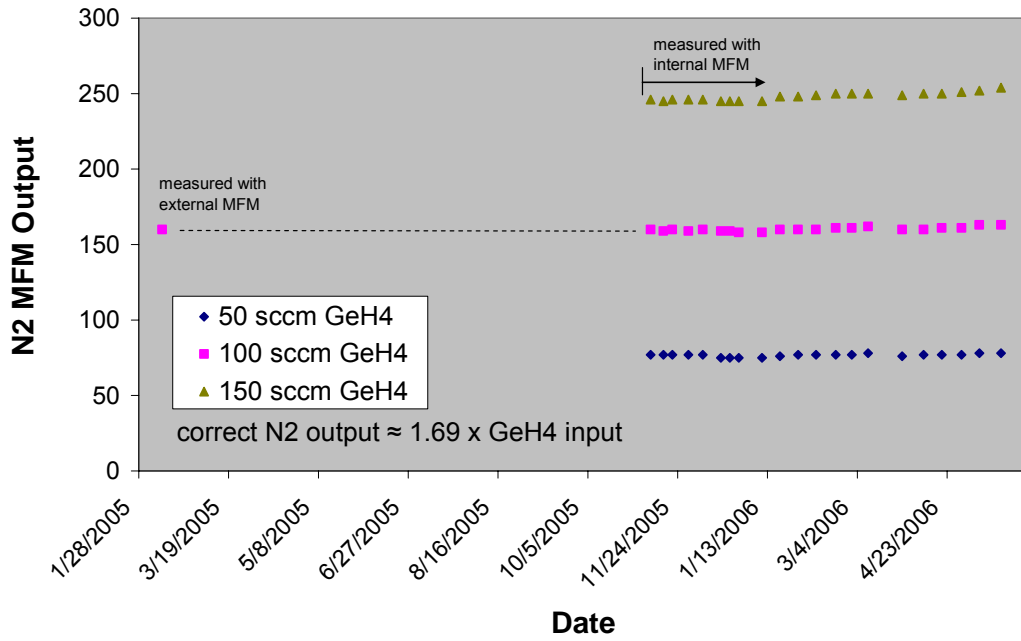


Figure 2.8 GeH<sub>4</sub> MFC monitoring data

### Si<sub>2</sub>H<sub>6</sub> MFC Monitor

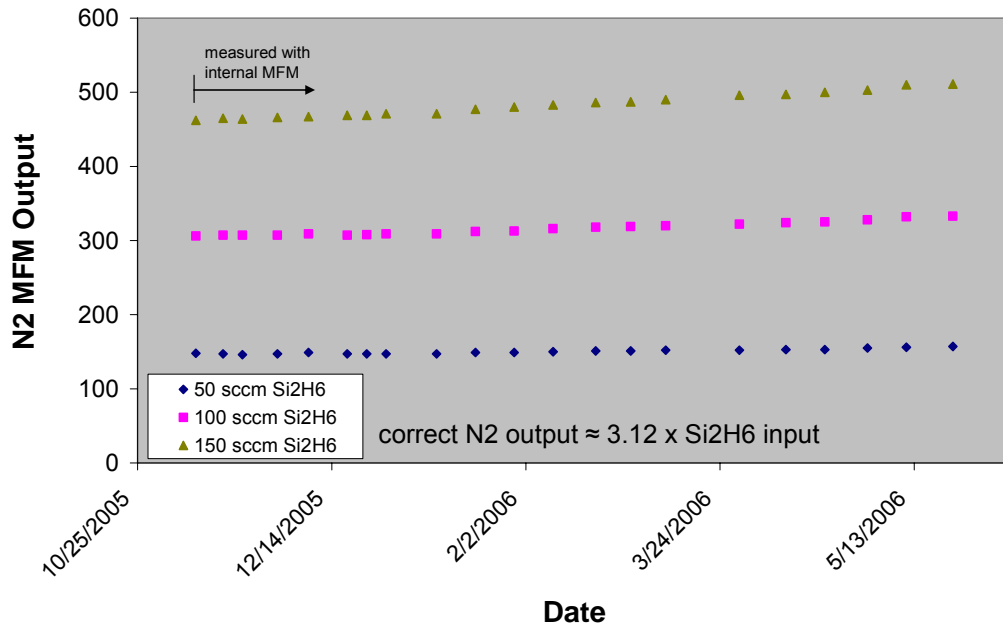
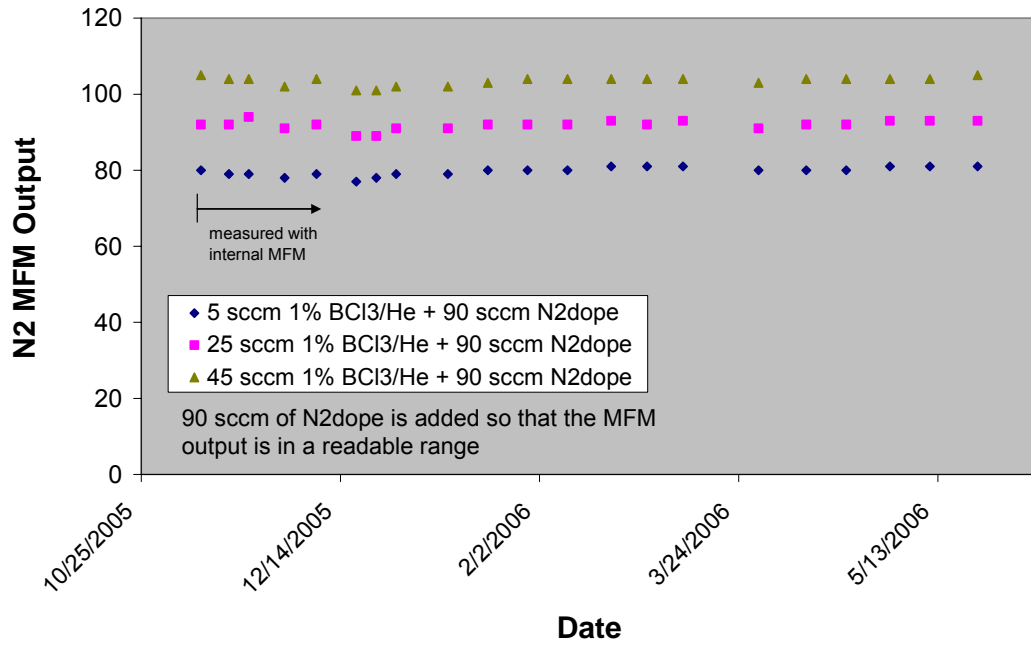


Figure 2.9 Si<sub>2</sub>H<sub>6</sub> MFC monitoring data

### BCI3 MFC Monitor



**Figure 2.10** BCl<sub>3</sub> MFC monitoring data

### N2 MFCs Monitor

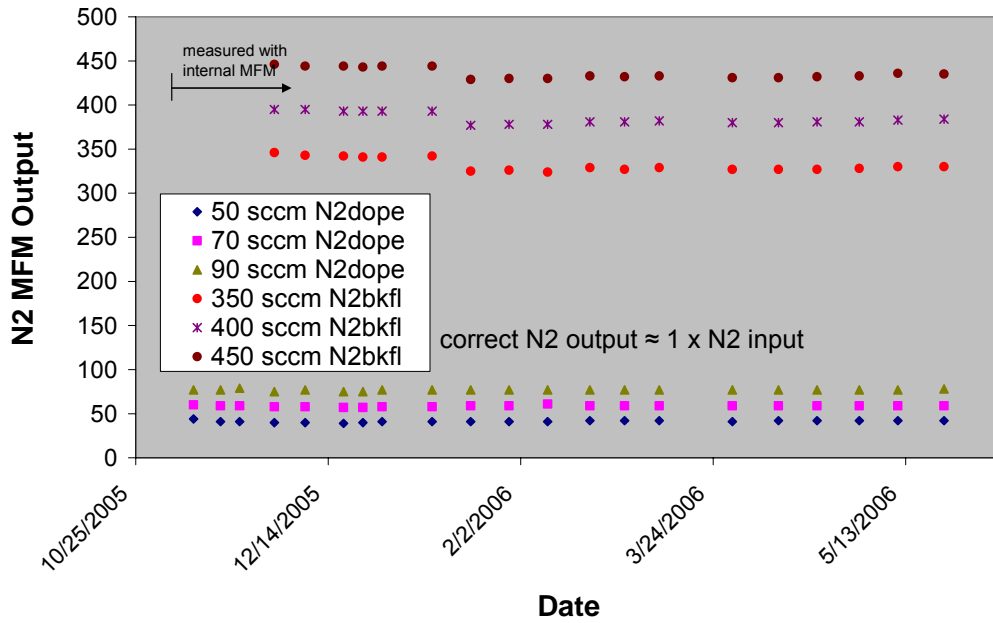


**Figure 2.11** N<sub>2</sub>Dope and N<sub>2</sub>BKFL MFCs monitoring data

## **2.8 Summary**

The initial design of the LPCVD poly-SiGe reactor was very similar to that of an LPCVD poly-Si reactor. Some special modifications were implemented for the poly-SiGe reactor because of the usage of multiple precursor gases and different dopant sources. With appropriate maintenance and regular process monitoring, the poly-SiGe reactor has fairly good performance in process uniformity and repeatability for academic research purposes.

## References

- [2.1] L. H. Long, "The mechanisms of thermal decomposition of diborane and of interconversion of the boranes, a reinterpretation of the evidence", *J. Inorg. Nucl. Chem*, vol. 32, 1970, pp. 1097-1115
- [2.2] Y.-C. Jeon, T.-J. King and R. T. Howe, "Properties of phosphorous-doped poly-SiGe films for microelectromechanical system applications", *J. Electrochemical Society*, vol. 150(1), 2003, pp. H1-H6
- [2.3] <http://www.amquartz.com/waferscarriers.htm>
- [2.4] [http://www.celerity.net/support/technical\\_data/technical\\_articles/2000\\_june.pdf](http://www.celerity.net/support/technical_data/technical_articles/2000_june.pdf), "MFC Mass Flow Controller", *European Semiconductor Magazine*, pp. 3 (2000)
- [2.5] D. C. Montgomery, *Introduction to Statistical Quality Control*, 4<sup>th</sup> edition, John Wiley & Sons, Inc., 2001, pp. 571-672
- [2.6] C. W. Low, M. L. Wasilik, H. Takeuchi, T.-J. King and R. T. Howe, "In-situ doped poly-SiGe LPCVD process using BCl<sub>3</sub> for post-CMOS integration of MEMS devices," in *Proc. Electrochemical Society SiGe Materials, Processing, and Devices Symposium*, Honolulu, HI, Oct. 3-8, 2004, pp. 1021-1032

## Chapter 3: Investigation of Advanced Process Gases

Silane ( $\text{SiH}_4$ ), germane ( $\text{GeH}_4$ ), diborane ( $\text{B}_2\text{H}_6$ ) and phosphine ( $\text{PH}_3$ ) are the conventional precursor and dopant gases for SiGe deposition with LPCVD, PECVD and UHV-CVD processes. LPCVD poly-SiGe MEMS technology has unique challenges in achieving good process control with large batch sizes and limiting the thermal budget for post-CMOS processing. In an effort to improve the process control and deposition rate, advanced process gases have been investigated. This chapter discusses the developments and challenges of using boron trichloride ( $\text{BCl}_3$ ) as a dopant gas, disilane ( $\text{Si}_2\text{H}_6$ ) as a silicon precursor and germyl silanes ( $(\text{H}_3\text{Ge})_x\text{SiH}_{4-x}$ ) as single-source silicon and germanium precursors.

### 3.1 Boron trichloride ( $\text{BCl}_3$ ) as the boron dopant gas

For MEMS applications, low resistivity is one of the requirements for the poly-SiGe structural layer. Ion implantation is not an attractive option since dopant activation with high temperature annealing increases the thermal budget for the post-CMOS process. Also, the mechanical properties would be hard to control with the non-uniform dopant distribution. *In-situ* doping does not have these disadvantages, but there are other process challenges.  $\text{B}_2\text{H}_6$  and  $\text{PH}_3$  are the conventional boron and phosphorous sources for *in-situ* doping. As mentioned in Section 2.2, dopant gas  $\text{B}_2\text{H}_6$  clogs up the injector and makes the process difficult to control;  $\text{PH}_3$  doping retards the deposition rate and requires post-deposition annealing to improve dopant activation. Recently, a high-throughput LPCVD process was developed using  $\text{BCl}_3$  as the dopant source for epitaxial

SiGe growth [3.1, 3.2]. Also, BCl<sub>3</sub> is being studied for *in-situ* doping of poly-Si [3.3]. These results initiated the development of the BCl<sub>3</sub> doping process for poly-SiGe [3.4].

### 3.1.1 BCl<sub>3</sub> mixture concentration

To investigate the feasibility of using BCl<sub>3</sub> for the poly-SiGe process, the BCl<sub>3</sub> doped epi-SiGe process was studied [3.1, 3.2]. The epi-SiGe system is a vertical LPCVD furnace, capable of processing fifty 200 mm-diameter wafers. A summary of the epitaxial process conditions and data are listed in Table 3.1 below. Pure gas partial pressure is shown instead of flow rate to normalize the difference in system size and pumping. Hydrogen is used as the carrier gas in the epi-SiGe system.

**TABLE 3.1** Summary of the BCl<sub>3</sub> doped epi-SiGe process [3.1, 3.2]

Temp. (°C)	Pressure (mTorr)	SiH <sub>4</sub> (mTorr)	GeH <sub>4</sub> (mTorr)	BCl <sub>3</sub> (mTorr)	Doping (cm <sup>-3</sup> )	Resistivity (mΩ-cm)	Ge content	Dep. Rate (nm/min)
500	228	45.6	0.912	0	NA	NA	10%	0.5
500	228	45.6	2.28	0	NA	NA	20%	1.5
500	228	45.6	4.1	0	NA	NA	30%	3
470	228	39.5	2.7	1.5 × 10 <sup>-4</sup>	4 × 10 <sup>18</sup>	NA	26.7%	NA
470	228	39.5	2.7	1.7 × 10 <sup>-3</sup>	8 × 10 <sup>19</sup>	1	26.7%	0.6
470	228	39.5	2.7	4.6 × 10 <sup>-3</sup>	1 × 10 <sup>20</sup>	NA	26.7%	NA

Although there are significant differences between the reactors and the processes, the target doping concentration for the poly-SiGe film is in the same order of magnitude as that of the epi-SiGe film. To install a BCl<sub>3</sub> bottle to the poly-SiGe reactor, the gas concentration and the MFC range need to be specified. To roughly match the doping level of 8 × 10<sup>19</sup> cm<sup>-3</sup>, the gas flow rate of pure BCl<sub>3</sub> can be calculated as:

$$\begin{aligned}
& BCl_3 \text{ flow rate in the poly reactor} \\
&= \frac{BCl_3 \text{ pressure in the epi reactor}}{SiH_4 \text{ pressure in the epi reactor}} \times SiH_4 \text{ flow rate in the poly reactor} \quad (3.1) \\
&= \frac{1.7 \times 10^{-3} \text{ mTorr}}{39.5 \text{ mTorr}} \times 100 \text{ sccm} \\
&= 0.0043 \text{ sccm}
\end{aligned}$$

The volume of epi-SiGe reactor is about 6× greater than the volume of the poly-SiGe reactor. Also, 1000 sccm of pure SiH<sub>4</sub> and 42 sccm of 0.1% BCl<sub>3</sub> are used for the epitaxial deposition. Assuming 100 sccm of SiH<sub>4</sub> flow in the poly-SiGe reactor, the calculation in Equation 3.1 is in good agreement with the epi-SiGe reactor's BCl<sub>3</sub> flow rate. The pure BCl<sub>3</sub> flow rate of 0.0043 sccm is very difficult to control with a mass flow controller. If the dopant gas is diluted, a larger flow rate can be used. In this case, flowing 4.3 sccm of 0.1% BCl<sub>3</sub> would be reasonable to control with a 10 sccm range MFC.

As a comparison, 5% of BCl<sub>3</sub> diluted in He is used in the epi-SiGe reactor. The gas is further diluted down to 0.1% in H<sub>2</sub> in the system before getting into the deposition chamber. Since the poly-SiGe reactor does not have the capability to dilute the dopant gas in the system, using a 0.1% concentration gas bottle would be more convenient. However, this simplified approach limits the flexibility of adjusting the dopant concentration if the doping level does not come out as expected. To keep the cost of installation low, 0.1% BCl<sub>3</sub> diluted in He was first used as the dopant gas. Preliminary results of the BCl<sub>3</sub> doped process using the 0.1% concentration bottle are summarized in Table 3.2.

**TABLE 3.2** Summary of the BCl<sub>3</sub> doped poly-SiGe process with 0.1% concentration bottle

Temp. (°C)	Pressure (mTorr)	SiH <sub>4</sub> (mTorr)	GeH <sub>4</sub> (mTorr)	BCl <sub>3</sub> (mTorr)	Doping (cm <sup>-3</sup> )	Resistivity (mΩ-cm)	Ge content	Dep. Rate (nm/min)
425	400	247	148	$5.0 \times 10^{-3}$	$1.4 \times 10^{17}$	790	70%	8.6
425	400	236	141	$2.3 \times 10^{-2}$	$5.6 \times 10^{17}$	264	70%	8.9
425	400	227	136	$4.1 \times 10^{-2}$	$5.4 \times 10^{18}$	93.6	70%	8.8
425	400	225	136	$4.1 \times 10^{-2}$	$5.2 \times 10^{18}$	100	70%	8.9
425	400	165	99	$1.4 \times 10^{-1}$	$2.2 \times 10^{19}$	32	70%	3.1

The resistivity of the poly-SiGe films deposited using the 0.1% concentration BCl<sub>3</sub> bottle is much higher than desired. The last run listed in Table 3.2 has a dopant concentration closer to the desired range, but the deposition rate is significantly lower than in other runs. In this case, the SiH<sub>4</sub> and GeH<sub>4</sub> flow rates are scaled down by 5× so that the BCl<sub>3</sub> partial pressure is increased. Comparing results in Table 3.1 and Table 3.2, the offset in boron incorporation between the epi-SiGe and poly-SiGe films is about two orders of magnitude. These results show that neglecting the mismatches between the epi-SiGe and the poly-SiGe processes in Equation 3.1 is not a valid assumption. The difference in dopant incorporation of the two systems comes from several sources: the deposition temperature of the poly-SiGe film is much lower; the oxygen contamination level of the poly-SiGe system is an order of magnitude higher; the poly-SiGe film is deposited on an oxide surface, whereas the epi-SiGe film is deposited on an ultra-clean Si surface; the germanium content of the poly-SiGe film is much higher, and the deposition rate of the poly-SiGe film is more than 10× faster than that of the epi-SiGe.

Since the BCl<sub>3</sub> doped epi-SiGe process was developed for the same reason that dopant gas B<sub>2</sub>H<sub>6</sub> does not yield satisfactory process stability, a comparison of the results for both dopant gases in the epi-SiGe process and then scaling with the B<sub>2</sub>H<sub>6</sub>-doped poly-SiGe process can lead to a more accurate calculation of the appropriate BCl<sub>3</sub> bottle

concentration for the poly-SiGe process. Table 3.3 and Table 3.4 show the results of the B<sub>2</sub>H<sub>6</sub> doped epi-SiGe and poly-SiGe processes, respectively.

**TABLE 3.3** Summary of the B<sub>2</sub>H<sub>6</sub> doped epi-SiGe process [3.5]

Temp. (°C)	Pressure (mTorr)	SiH <sub>4</sub> (mTorr)	GeH <sub>4</sub> (mTorr)	B <sub>2</sub> H <sub>6</sub> (mTorr)	Doping (cm <sup>-3</sup> )	Resistivity (mΩ-cm)	Ge content	Dep. Rate (nm/min)
550	228	45.6	1.52	3.8 × 10 <sup>-2</sup>	8.0 × 10 <sup>19</sup>	2	22%	7
550	228	45.6	15.2	2.0 × 10 <sup>-3</sup>	1.5 × 10 <sup>19</sup>	7	60%	60

**TABLE 3.4** Summary of the B<sub>2</sub>H<sub>6</sub> doped poly-SiGe process

Temp. (°C)	Pressure (mTorr)	SiH <sub>4</sub> (mTorr)	GeH <sub>4</sub> (mTorr)	B <sub>2</sub> H <sub>6</sub> (mTorr)	Doping (cm <sup>-3</sup> )	Resistivity (mΩ-cm)	Ge content	Dep. Rate (nm/min)
450	600	275	160	16.4	1.2 × 10 <sup>19</sup>	37	65%	15

Comparing the results of the B<sub>2</sub>H<sub>6</sub> doped epi-SiGe and poly-SiGe processes, there is also an offset in dopant incorporation for the two processes. To recalculate the appropriate BCl<sub>3</sub> bottle concentration for the poly-SiGe process, one approach is to take the ratio of the BCl<sub>3</sub> and B<sub>2</sub>H<sub>6</sub> doped processes with the same boron concentration:

$$\begin{aligned}
 & \text{BCl}_3 \text{ pressure in the poly reactor} \\
 &= \frac{\text{BCl}_3 \text{ pressure in the epi reactor}}{\text{B}_2\text{H}_6 \text{ pressure in the epi reactor}} \times \text{B}_2\text{H}_6 \text{ pressure in the poly reactor} \\
 &= \frac{1.7 \times 10^{-3} \text{ mTorr}}{3.8 \times 10^{-2} \text{ mTorr}} \times 16.4 \text{ mTorr} \tag{3.2} \\
 &= 0.73 \text{ mTorr} \quad (\text{assume } 600 \text{ mTorr process pressure, } 1.2 \times 10^{19} \text{ cm}^{-3} \text{ boron conc.)} \\
 &\text{or } 0.49 \text{ mTorr} \quad (\text{assume } 400 \text{ mTorr process pressure, } 1.2 \times 10^{19} \text{ cm}^{-3} \text{ boron conc.)}
 \end{aligned}$$

Assuming that the process pressure is 400 mTorr and the gas flow rates of SiH<sub>4</sub>, GeH<sub>4</sub> and BCl<sub>3</sub> are 100 sccm, 60 sccm and 10 sccm, respectively; the BCl<sub>3</sub> concentration can be calculated as:

$$\begin{aligned}
 & \frac{10 \text{ sccm BCl}_3 \text{ mixture} \times \text{BCl}_3 \text{ concentration}}{100 \text{ sccm SiH}_4 + 60 \text{ sccm GeH}_4 + 10 \text{ sccm BCl}_3 \text{ mixture}} \times 400 \text{ mTorr} = 0.49 \text{ mTorr} \tag{3.3} \\
 & \Rightarrow \text{BCl}_3 \text{ concentration} = 2\% \quad (\text{for } 1.2 \times 10^{19} \text{ cm}^{-3} \text{ boron concentration})
 \end{aligned}$$

The calculations in Equations 3.2 and 3.3 neglect the effects of temperature and deposition rate on boron incorporation in the film.

The other approach to estimate the appropriate BCl<sub>3</sub> bottle concentration is to extrapolate information from Table 3.2, where all the data are for the BCl<sub>3</sub> doped poly-SiGe process. A curve fitting for data in Table 3.2 yields the relationship:

$$\begin{aligned} \text{boron concentration} &= 5 \times 10^{17} e^{34.1 \times \text{BCl}_3 \text{ pressure}} \\ \Rightarrow 0.099 \text{ mTorr BCl}_3 \text{ pressure yields } 1.2 \times 10^{19} \text{ cm}^{-3} \text{ boron concentration} & \quad (3.4) \\ \text{or } 0.165 \text{ mTorr BCl}_3 \text{ pressure yields } 1.0 \times 10^{20} \text{ cm}^{-3} \text{ boron concentration} & \end{aligned}$$

Again, assuming 400 mTorr process pressure and the gas flow rates of SiH<sub>4</sub>, GeH<sub>4</sub> and BCl<sub>3</sub> mixture are 100 sccm, 60 sccm and 10 sccm, respectively, the BCl<sub>3</sub> concentration can be calculated as:

$$\begin{aligned} \frac{10 \text{ sccm BCl}_3 \text{ mixture} \times \text{BCl}_3 \text{ concentration}}{100 \text{ sccm SiH}_4 + 60 \text{ sccm GeH}_4 + 10 \text{ sccm BCl}_3 \text{ mixture}} \times 400 \text{ mTorr} &= 0.099 \text{ mTorr} \\ \Rightarrow \text{BCl}_3 \text{ concentration} &= 0.42\% \quad (\text{for } 1.2 \times 10^{19} \text{ cm}^{-3} \text{ boron concentration}) \\ \text{or BCl}_3 \text{ concentration} &= 0.7\% \quad (\text{for } 1.0 \times 10^{20} \text{ cm}^{-3} \text{ boron concentration}) \end{aligned} \quad (3.5)$$

The two approaches above both yield numbers larger than 0.1% BCl<sub>3</sub> concentration for the desired doping level although calculation with Equations 3.4 and 3.5 is more reliable. Since the target resistivity for poly-SiGe film is less than 10 mΩ-cm, the boron doping concentration should be in the range of  $1.0 \times 10^{20} \text{ cm}^{-3}$ . According to Equation 3.5, a 1% concentration would be appropriate. If the boron doping level is slightly off target with the 1% concentration BCl<sub>3</sub> mixture, the gas flow rate can be adjusted to accommodate. Further experiments justified that the 1% concentration is appropriate for LPCVD poly-SiGe deposition.

It should be noted that pure BCl<sub>3</sub> is a liquid at room temperature with a vapor pressure of 988 Torr. Pumping the gas into the reactor was once a concern. However, when BCl<sub>3</sub> is diluted with a gas that liquifies at much higher pressure, the overall liquification pressure of the mixture is higher than that of pure BCl<sub>3</sub>. With lower BCl<sub>3</sub>

concentration in the mixture, liquification pressure of the overall mix is higher. The inert gas helium is used to dilute  $\text{BCl}_3$ . The mixture of 0.1% or 1%  $\text{BCl}_3$  balanced in He is in gas phase at the maximum pressure limit of the tank. The gas mixture was made with gravimetric blending for which each individual gas is weighted while pouring them into cylinder.

### **3.1.2 Experimental details**

The epi-SiGe reactor that first demonstrated the  $\text{BCl}_3$  doped process is a vertical LPCVD system with all the process gases introduced via one gas inlet and an open boat for automatic loading [3.2]. The epi-SiGe reactor is capable of processing fifty 200 mm-diameter wafers and across-load uniformity is within  $\pm 5\%$  for resistivity and  $\pm 2\%$  for film thickness.

The initial test of the  $\text{BCl}_3$  doped poly-SiGe process used a similar configuration as the epi-SiGe reactor.  $\text{SiH}_4$  and  $\text{GeH}_4$  were introduced at the gas ring located at the load side of the tube. The  $\text{BCl}_3/\text{He}$  mixture was also introduced through the gas ring for these experiments, even though introducing  $\text{BCl}_3$  via a multi-pore injector located at the bottom of the wafer boats is another option. Twenty-five 4"-diameter and twenty-five 6"-diameter wafers placed in open boats at the center of the reactor were used per load. To investigate the feasibility of the process, the deposition rate, crystallinity, dopant incorporation, resistivity, residual stress, strain gradient, as well as effects of thickness on electrical and mechanical properties were characterized [3.4].

The process conditions of various depositions are summarized in Table 3.5. Poly-SiGe films were deposited onto Si wafers coated with  $\sim 2 \mu\text{m}$  thick low-temperature

(450°C) LPCVD SiO<sub>2</sub>. A ~5 nm thick undoped amorphous Si (a-Si) seeding layer was deposited first using 100 sccm of Si<sub>2</sub>H<sub>6</sub> to promote adhesion of SiGe to SiO<sub>2</sub>. The a-Si layer was deposited at 300 mTorr for 15 minutes at various temperatures. For the poly-SiGe deposition, the process pressure was held constant at 400 mTorr. Temperature, BCl<sub>3</sub> partial pressure, and deposition time were varied. The SiH<sub>4</sub> to GeH<sub>4</sub> gas flow ratio was held constant in order to target a 70% Ge content. The flow rates of the two gases however were reduced in some cases to increase the partial pressure of BCl<sub>3</sub>. The high Ge content was chosen to ensure crystallinity for consistent resistivity measurement with boron doping. It should be noted that the selectivity of pure Ge to Si<sub>30</sub>Ge<sub>70</sub> for H<sub>2</sub>O<sub>2</sub> etching is degraded to 10:1 [3.6]. High peroxide etching selectivity is desired for integrated MEMS applications because the use of pure Ge as the conformal sacrificial layer eliminates the need to passivate the underlying CMOS.

Experimental data was collected with five 4"-diameter wafers that were placed in slots 3, 8, 13, 18, and 23 of the wafer boats, counting from the gas inlet side. A four-point probe instrument was used to measure the sheet resistance. The films were patterned and etched for the thickness measurement using a stylus-based profiler. Wafer curvature was measured before and after SiGe deposition (backside SiGe film removed) to determine the average residual stress of the film. A cantilever beam array was patterned and released for strain gradient measurement. The strain gradient was calculated as the reciprocal of the radius of curvature of the cantilevers with various lengths. Resistivity, thickness, and strain gradient were measured at various points on each wafer, and average numbers are reported here. Ge content, B and Cl concentrations were determined by secondary ion mass spectroscopy (SIMS) with wafers at the gas inlet side of the load. The

crystallinity of selected films was determined by transmission electron microscopy.

### **3.1.3 Results and discussion**

Overall results of average deposition rate, resistivity, residual stress, Ge content, and B doping level, along with uniformity of the  $\text{BCl}_3$  and  $\text{B}_2\text{H}_6$  doped poly-SiGe processes are summarized in Table 3.5. Both  $\text{B}_2\text{H}_6$  and  $\text{BCl}_3$  doped SiGe films have similar Cl concentration, all below  $2 \times 10^{16} \text{ cm}^{-3}$ , which indicates Cl incorporation is not a problem for the  $\text{BCl}_3$  doping process.

**Table 3.5** Results summary for BCl<sub>3</sub> doped poly-SiGe process verification

Run #	Deposition Recipe										Results									
	a-Si		SiGe layer								Entire Load					Gas Inlet Side (near door)				
	Temp (°C)	Temp (°C)	SiH <sub>4</sub> (sccm)	GeH <sub>4</sub> (sccm)	BCl <sub>3</sub> /He conc. (sccm)	BCl <sub>3</sub> conc.	Time (min)	Avg. DR (nm/min)	DR XL unif.	DR XL unif.	DR XL unif.	Avg. Res. (mΩ-cm)	Res. XW unif.	Res. XL unif.	Avg. stress (MPa)	Stress stdev	Ge cont.	B. conc. (cm <sup>-3</sup> )	Res. (mΩ-cm)	
T22	450	350	0	100	16.5	0.1%	60	7	2%	3%	70	7%	12%	-240	26	100%	8.0×10 <sup>18</sup>	65		
T2	400	400	100	60	9.2	0.1%	60	4.4	3%	5%	673	32%	68%	-268	21	74%	3.4×10 <sup>18</sup>	180		
T4	400	400	100	60	16.5	0.1%	60	4.5	2%	2%	175	21%	60%	-301	13	74%	1.0×10 <sup>19</sup>	58		
T5	425	425	100	60	1.8	0.1%	60	8.6	3%	8%	893	4%	10%	-74	16	70%	1.4×10 <sup>17</sup>	790		
T1	425	425	100	60	9.2	0.1%	60	8.9	2%	6%	412	7%	25%	-61	16	70%	5.6×10 <sup>17</sup>	264		
T6	425	425	100	60	16.5	0.1%	60	8.8	2%	6%	199	10%	41%	-100	17	70%	5.8×10 <sup>18</sup>	93.6		
T11	425	425	100	60	16.5	0.1%	60	8.9	2%	6%	221	12%	41%	-94	26	70%	5.2×10 <sup>18</sup>	100		
T14	425	425	100	60	16.5	0.1%	120	8.7	1%	6%	131	13%	46%	-70	18	70%	6.2×10 <sup>18</sup>	54		
T12	425	425	100	60	16.5	0.1%	180	8.8	2%	7%	110	13%	48%	-34	9	70%	6.0×10 <sup>18</sup>	46		
T17	425	425	80	48	16.5	0.1%	90	7.6	2%	8%	180	12%	46%	-70	11	70%	6.9×10 <sup>18</sup>	77		
T18	425	425	50	30	16.5	0.1%	120	5.7	2%	9%	142	13%	50%	-139	19	68%	9.3×10 <sup>18</sup>	58		
T9	425	425	20	12	16.5	0.1%	180	3.1	NA	NA	45	NA	NA	-99	8	64%	2.2×10 <sup>19</sup>	32		
T3	450	450	100	60	9.2	0.1%	60	13.4	2%	8%	655	5%	20%	-15	9	67%	3.3×10 <sup>17</sup>	472		
T19	425	425	100	60	3.6	1%	60	8.5	3%	8%	69	17%	64%	-130	18	73%	2.8×10 <sup>19</sup>	21		
T20	425	425	100	60	9.2	1%	60	8.4	3%	9%	9.3	15%	60%	NA	NA	73%	1.5×10 <sup>20</sup>	3.6		
T23	425	425	100	60	9.2	1%	60	8.4	3%	10%	9.2	16%	63%	-157	13	NA	NA	3.5		
T21	425	425	100	60	16.5	1%	60	8.5	3%	12%	2.7	9%	40%	-163	14	73%	3.1×10 <sup>20</sup>	1.6		
R3*	400	400	100	60	60 B <sub>2</sub> H <sub>6</sub>	10%	60	7.9	2%	3%	0.87	2%	3%	-240	28	NA	NA	0.90		
R1*	425	425	100	60	60 B <sub>2</sub> H <sub>6</sub>	10%	60	9.2	2%	9%	7.2	7%	86%	-108	34	72%	4.0×10 <sup>19</sup>	16		
R2*	450	450	100	60	60 B <sub>2</sub> H <sub>6</sub>	10%	60	13.1	2%	13%	65.7	6%	66%	-36	16	NA	NA	119		

\*B<sub>2</sub>H<sub>6</sub> was introduced from the pump side through a multi-pore injector. Caged boats were used. Thirty 4"-diameter and fifteen 6"-diameter wafers were used per load.

### 3.1.3.1 Deposition rate

Comparison of Runs T5, T1, T6, T19, T20, and T21 with  $\text{BCl}_3$  partial pressure as the only difference, the deposition rate does not depend strongly on the  $\text{BCl}_3$  flow rate for the doping range studied here. Also, depositions with identical parameters but various deposition times (Runs T11, T14, and T12) show the same deposition rate, which suggests that there is no incubation period at the beginning of the deposition.

An Arrhenius plot of deposition rate is shown in Figure 3.1 for 100 sccm  $\text{SiH}_4$ , 60 sccm  $\text{GeH}_4$  depositions at 400 mTorr for both  $\text{BCl}_3$  and  $\text{B}_2\text{H}_6$  processes. The deposition temperatures of these runs are rather low and the processes are believed to be operating in the surface reaction-limited regime. The activation energies of the  $\text{BCl}_3$  and the  $\text{B}_2\text{H}_6$  doped processes are extracted to be 0.94 eV and 0.42 eV, respectively. They are of the same order of magnitude as the undoped poly-SiGe process reported before [3.7]. For the 425°C and 450°C depositions, the deposition rates are similar for both dopant gases.  $\text{B}_2\text{H}_6$  process has a much higher deposition rate at 400 °C. The resistivity of the 400 °C  $\text{B}_2\text{H}_6$  recipe is very low, and boron incorporation for this film is estimated to be on the order of  $1 \times 10^{21} \text{ cm}^{-3}$ .  $\text{B}_2\text{H}_6$  is known to enhance deposition for poly-Si, but the temperature effect and the doping effect cannot be distinguished in Figure 3.1.

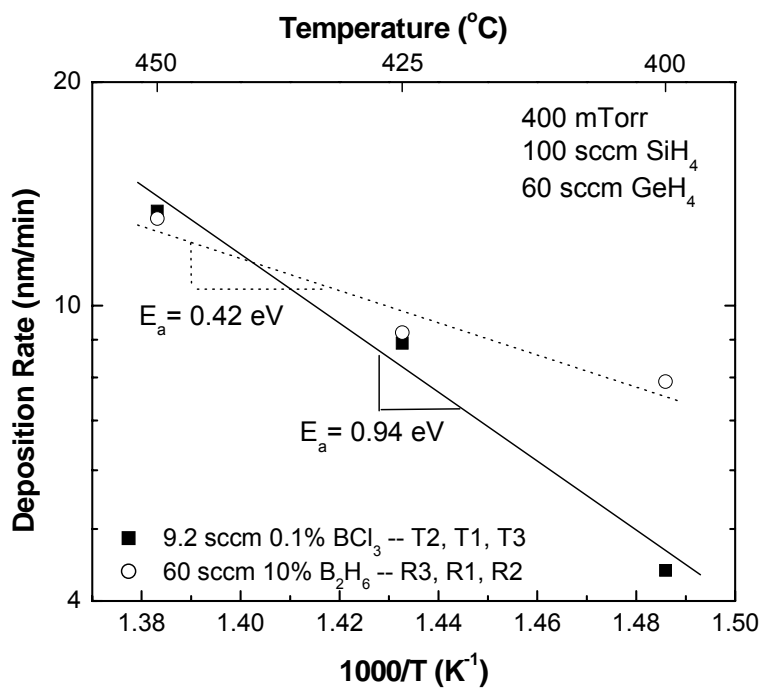


**Figure 3.1** Arrhenius plot of deposition rate

### 3.1.3.2 Crystallinity

Cross-sectional TEM images for films of different thicknesses are shown in Figure 3.2. These two films have exactly the same recipe except the deposition times are 1 hour and 3 hours for the thin film and the thick film, respectively. Both films have vertically-oriented grain structure with finer grains at the bottom. The two TEM images are shown on the same scale. As the film gets thicker, the grains grow significantly larger.

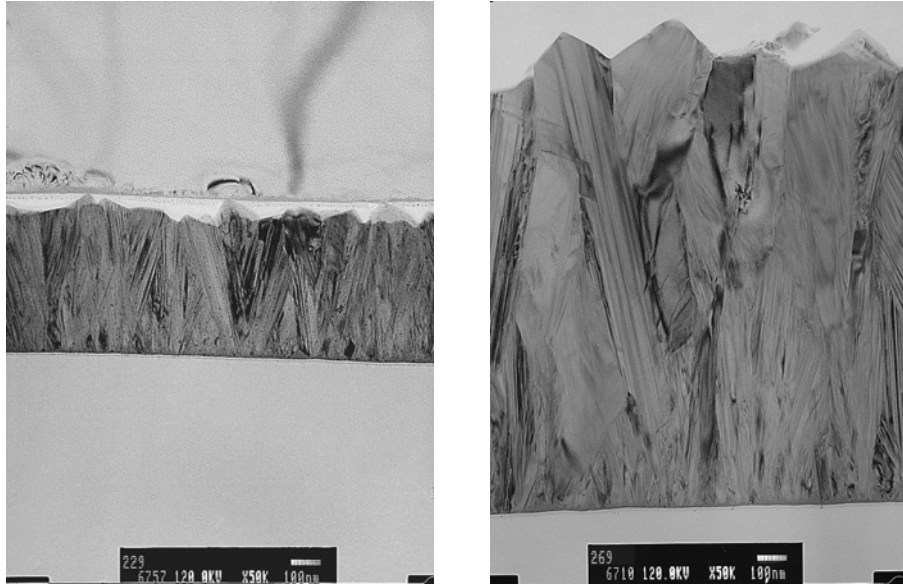


**Figure 3.2** Cross-sectional TEM images: a) Run T6 - 0.5  $\mu\text{m}$  film; b) Run T12 - 1.5  $\mu\text{m}$  film

### 3.1.3.3 Dopant incorporation

Figure 3.3 plots boron concentration *vs.* partial pressure for all 425°C poly-SiGe depositions. As a comparison, data for epi-SiGe deposited at 470°C [C.1, C.2] is also shown. As discussed previously, the difference in dopant incorporation of the two systems comes from several sources: the deposition temperature, the oxygen contamination level, the deposition substrate, the germanium content and the deposition rate. All of the above differences result in more than two orders of magnitude offset in boron incorporation between the films.

A data point from the  $\text{B}_2\text{H}_6$  process is also shown in Figure 3.3. A high  $\text{B}_2\text{H}_6$  partial pressure is required to achieve similar doping levels in the film while other deposition conditions are identical. The consumption of  $\text{B}_2\text{H}_6$  is mainly due to the

decomposition inside injector rather than the disassociation on the wafer surface. Comparing the three  $B_2H_6$  depositions (R3, R1 and R2) at various temperatures provides further evidence of the temperature instability of  $B_2H_6$ . Resistivity is found to be an order of magnitude higher for an increment in temperature of  $25^\circ C$  with the same  $B_2H_6$  flow rate.

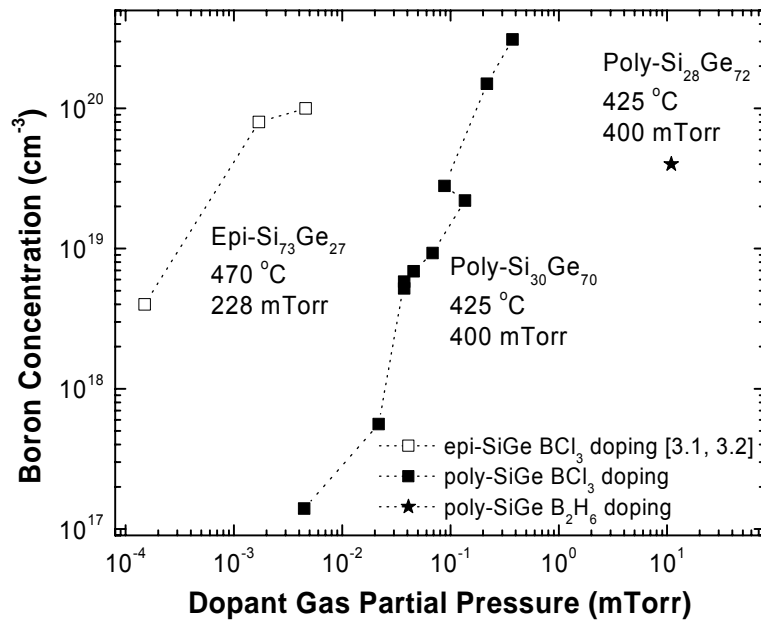


**Figure 3.3** Boron concentration vs. dopant gas partial pressure

Resistivity vs. boron concentration for the  $BCl_3$  doped process is plotted in Figure 3.4 for  $\sim 70\%$  germanium content films deposited at  $425^\circ C$  with similar thicknesses. As expected, resistivity decreases linearly with boron doping. The resistivity of poly-SiGe is more than  $10\times$  higher than that of single crystalline films due to carrier trapping at the grain boundaries.

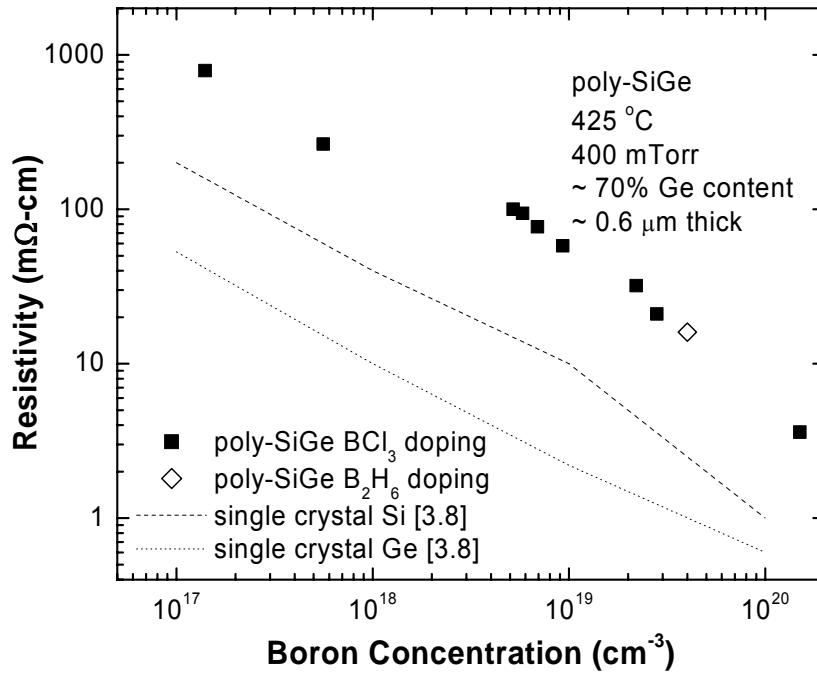


**Figure 3.4** Resistivity vs. boron concentration

A comparison of BCl<sub>3</sub> runs (T1, T2, and T3) with same deposition conditions except for temperatures shows that higher temperature gives lower doping level and higher resistivity. This phenomenon could be explained by less efficient boron incorporation as the deposition rate goes up with temperature.

Resistivity vs. film thickness is plotted in Figure 3.5(a) for runs having the same deposition conditions but different deposition times. Wafer positions are also labeled on the graph. For wafers from the same run, higher resistivity and lower deposition rate are observed at the gas outlet due to the gas depletion effect. Comparing wafers at the same position from different runs, thicker films are found to have lower resistivity. This might be a result of furnace annealing and/or crystal growth during deposition. A two-hour 425°C anneal in N<sub>2</sub> ambient was done for several 1-hour deposition films to discriminate

the two effects. There is no change in resistivity after the annealing stage. As shown in Figure 3.2 earlier, thicker films have larger grains, which is consistent with this lower resistivity observation since carrier trapping is more significant with higher grain boundary density [3.9].

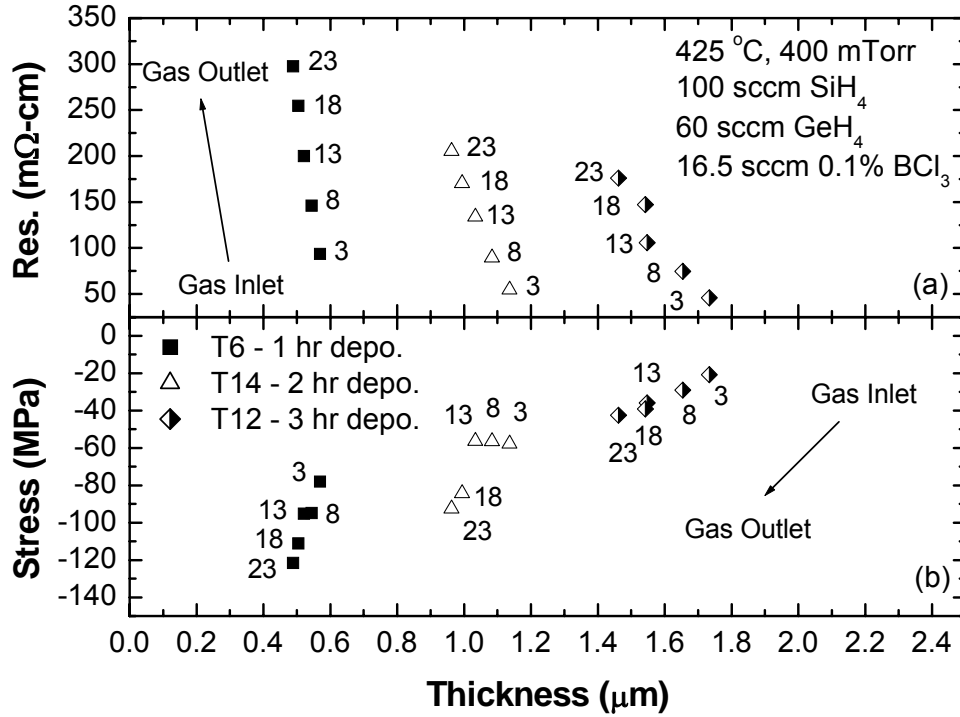


Figure 3.5 a) Resistivity and b) Stress vs. Film thickness

### 3.1.3.4 Stress

Figure 3.5(b) shows the average residual stress vs. film thickness. Thicker films have less compressive stress. Furnace annealing at 425 °C for 2 hours does not cause significant change in residual stress. This reduction in residual stress magnitude with thickness allows the growth of thick films without peeling off. However, the origins of

the residual stress and the reasons for its decrease with film thickness are not completely understood.

Comparing films with similar thickness and boron doping as the only process variable, we can see that the average residual stress is more compressive as boron doping increases, as shown in Figure 3.6. This possibly indicates the boron atoms are not residing in substitutional lattice sites, but interstitial lattice sites or grain boundaries. A data point from the  $B_2H_6$  process shows that the average stress for  $B_2H_6$  doped film is less compressive for the same level of doping. Further investigation on crystallinity might be able to explain this phenomenon. However,  $0.6\ \mu\text{m}$  films are too thin for most MEMS applications, and the  $1.7\ \mu\text{m}$  thick  $BCl_3$  doped film with  $6.0 \times 10^{18}\ \text{cm}^{-3}$  doping yields reasonably low residual stress of  $-21\ \text{MPa}$ .

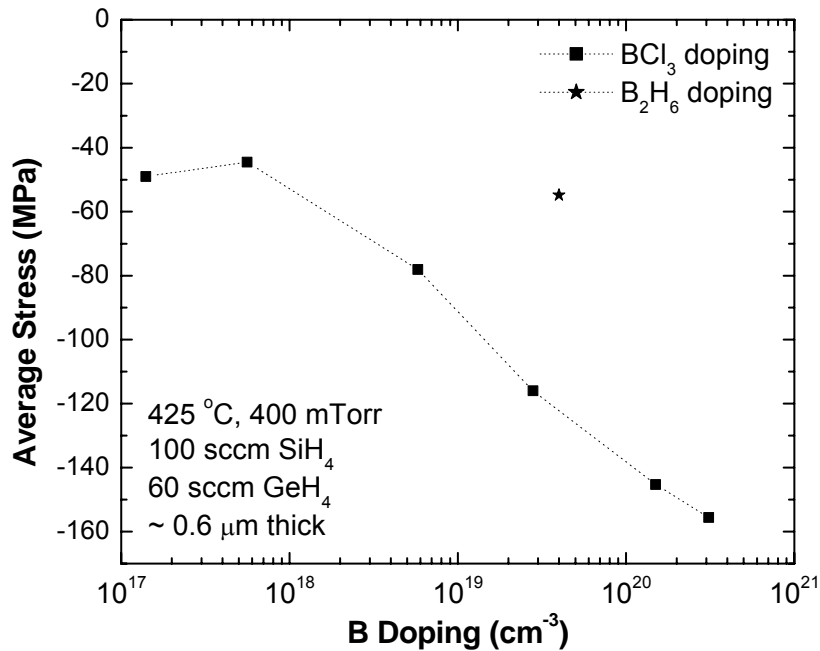


Figure 3.6 Average stress vs. doping

### 3.1.3.5 Strain gradient

Cantilever beam arrays from the thicker films were released for strain gradient measurement. Films with thickness less than 1  $\mu\text{m}$  are too thin for reliable strain gradient measurements. As shown in Figure 3.7, the error increases as the film gets thinner and strain gradient is smaller for thicker film.

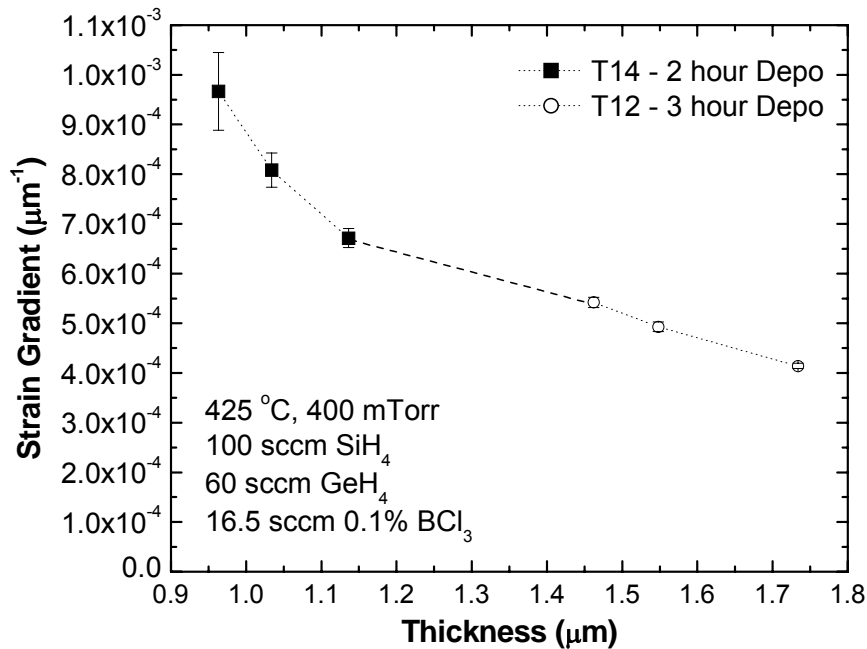


Figure 3.7 Strain gradient vs. thickness

### 3.1.3.6 Process uniformity

Process uniformity summarized in Table 3.5 is defined as the normalized standard deviation across the wafer and across the load. A few  $\text{B}_2\text{H}_6$  doped depositions done in the same LPCVD reactor are listed at the bottom of Table 3.5 for comparison. The dopant gas  $\text{B}_2\text{H}_6$  is introduced from the pump side via a multi-pore injector located underneath the wafer boats to minimize the depletion effect. Caged boats were used in the  $\text{B}_2\text{H}_6$  doped process. As a comparison, the  $\text{BCl}_3$  process provides similar uniformity within a

wafer and better cross load uniformity in most cases with open boats and without using a gas injector.

The wafer flat region has lower resistivity for the  $\text{BCl}_3$  process, which is due to the fact that the 100 mm-diameter wafers are placed below the center axis in the 230 mm-diameter reactor and there is more open space for gas flow on the top of the wafer flat. As a comparison, 150 mm-diameter wafers, which are nearly centered in the reactor, have better cross-wafer uniformity in resistivity.

Deposition rate and resistivity of selected  $425^\circ\text{C}$  runs are plotted vs. wafer position in Figure 3.8 to demonstrate the cross load uniformity of the  $\text{BCl}_3$  process. Wafers at the gas inlet side have higher deposition rate and lower resistivity, which suggests a gas depletion effect. Increasing the gas flow rate together with using an injector to introduce  $\text{BCl}_3$  could result in better cross-load uniformity. A  $425^\circ\text{C}$   $\text{B}_2\text{H}_6$  deposition is also shown in Figure 3.8 as a reference. Cross-load variation in deposition rate and resistivity is similar to the  $\text{BCl}_3$  process, despite the fact that  $\text{B}_2\text{H}_6$  is introduced via a multi-pore injector. Cross-load resistivity of the  $\text{B}_2\text{H}_6$  shows the opposite trend compared to the  $\text{BCl}_3$  process, because  $\text{B}_2\text{H}_6$  was introduced from the pump side.

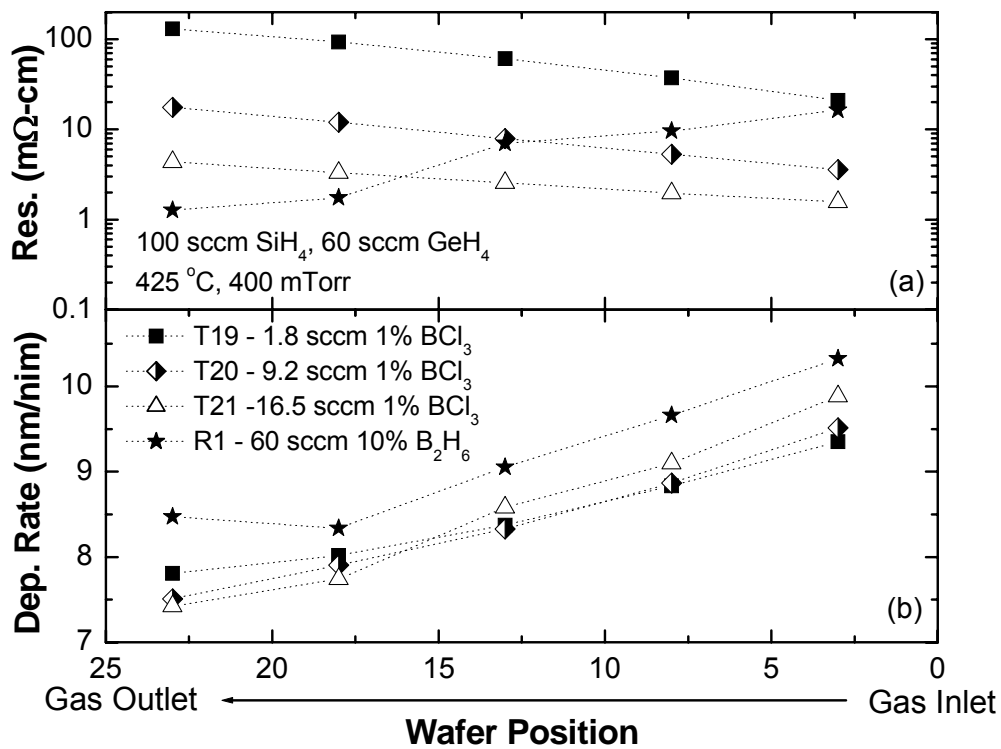


Figure 3.8 Deposition rate and resistivity across load

Runs T6 and T11, as well as Runs T20 and T23 have exactly the same deposition parameters, but they were separated by a few other depositions. The results show that the BCl<sub>3</sub> process is reproducible. Moreover, results of other similar depositions are reasonably consistent, which indicates that the process is operating in a relatively stable manner. In comparison, the decomposition of B<sub>2</sub>H<sub>6</sub> causes periodic clogging of the injector, which results in large run-to-run variation unless the injector is changed approximately every 20 hours of deposition. Decomposition of BCl<sub>3</sub> is rather slow compared to B<sub>2</sub>H<sub>6</sub>, and injector clogging is not anticipated to be a problem. On the other hand, introducing B<sub>2</sub>H<sub>6</sub> through the gas ring to avoid injector clogging is not an option

since large across load variation in film thickness and resistivity [3.11] resulted from its tendency to decompose at low temperature.

### **3.1.3.7 Furnace configuration optimization**

All of the above experiments had the  $\text{BCl}_3$  mixture introduced via the gas ring together with  $\text{SiH}_4$  and  $\text{GeH}_4$  in order to match the configuration of the epi-SiGe system and to minimize conflict with the existing  $\text{B}_2\text{H}_6$  process for initial test. As discussed in Chapter 2, the poly-SiGe reactor is fairly flexible to accommodate new processes. To further improve the resistivity uniformity, different hardware configurations have been investigated.

As mentioned before, the cross-load resistivity uniformity of the  $\text{BCl}_3$  doped poly-SiGe process could be further improved using an injector. A few  $\text{BCl}_3$ -doped depositions were done to study the improvement in uniformity with the injector. Since  $\text{B}_2\text{H}_6$  is known to clog up the injector, a second injector was installed in the furnace to isolate the clogging problem. The second injector can be installed parallel to the  $\text{B}_2\text{H}_6$  injector from the rear (pump) side or opposite to the  $\text{B}_2\text{H}_6$  injector from the front (door) side. The two-injector configuration was setup temporarily with a few additional hand valves for manually switching between the lines. The rear injector configuration is identical to the existing  $\text{B}_2\text{H}_6$  injector. The front injector is easier to install and remove, but it was later found out that the dopant gas leaked out near the door, making the front injector configuration very similar to the gas ring configuration. Sheet resistance data across the load of 50 wafers are shown in Figure 3.9. With the rear injector, the cross-load uniformity is improved by an order of magnitude.

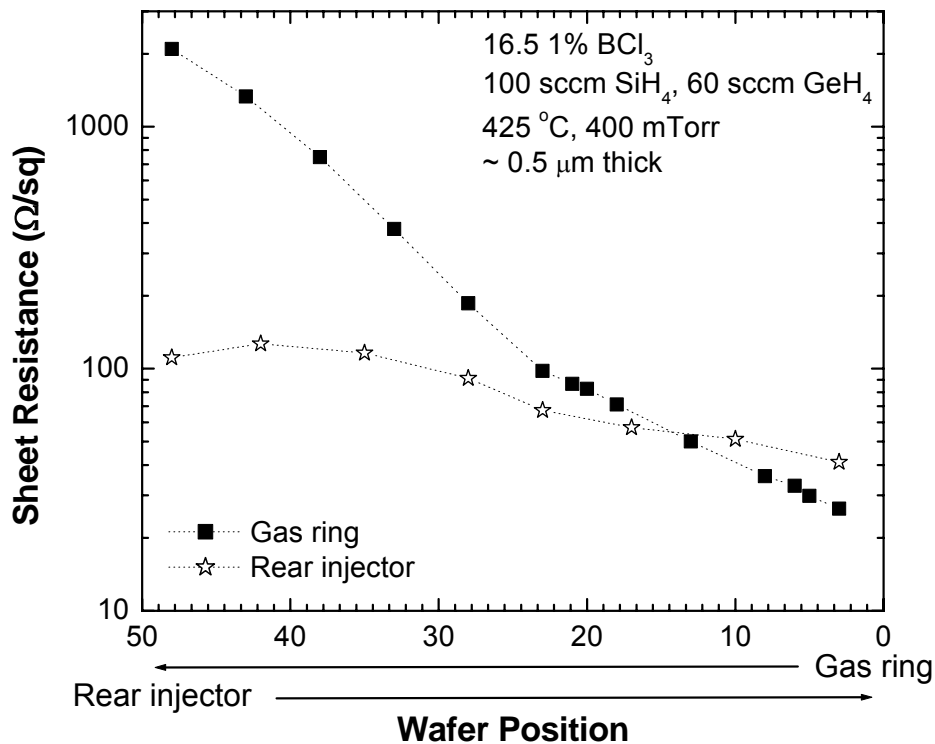


**Figure 3.9** Cross-load uniformity of sheet resistance with gas ring and injector

When the BCl<sub>3</sub>/He mixture is introduced via the gas ring, it comes out through multiple orifices along the circumference of the ring so cross wafer uniformity is not a problem. When the BCl<sub>3</sub>/He mixture is injected from the bottom of the furnace using the injector, the cross load uniformity is improved whereas the cross wafer uniformity is sacrificed due to gas depletion. The depletion effect is more pronounced when the dopant gas flow rate is small. Figure 3.10 shows the variation in sheet resistance for both 100 mm-diameter and 150 mm-diameter wafers with 3.6 sccm of BCl<sub>3</sub> flow rate. The cross wafer uniformity of sheet resistance is not terribly bad for the 100 mm-diameter wafers at slots 1-25, but there is about 3× variation across the 150 mm-diameter wafers at slots 26-50. Increasing the BCl<sub>3</sub> flow rate can minimize the depletion effect and improve the cross

wafer uniformity. Figure 3.11 shows data for a deposition with 16.5 sccm of  $\text{BCl}_3$  flow rate and cross wafer uniformity in sheet resistance is significantly improved.

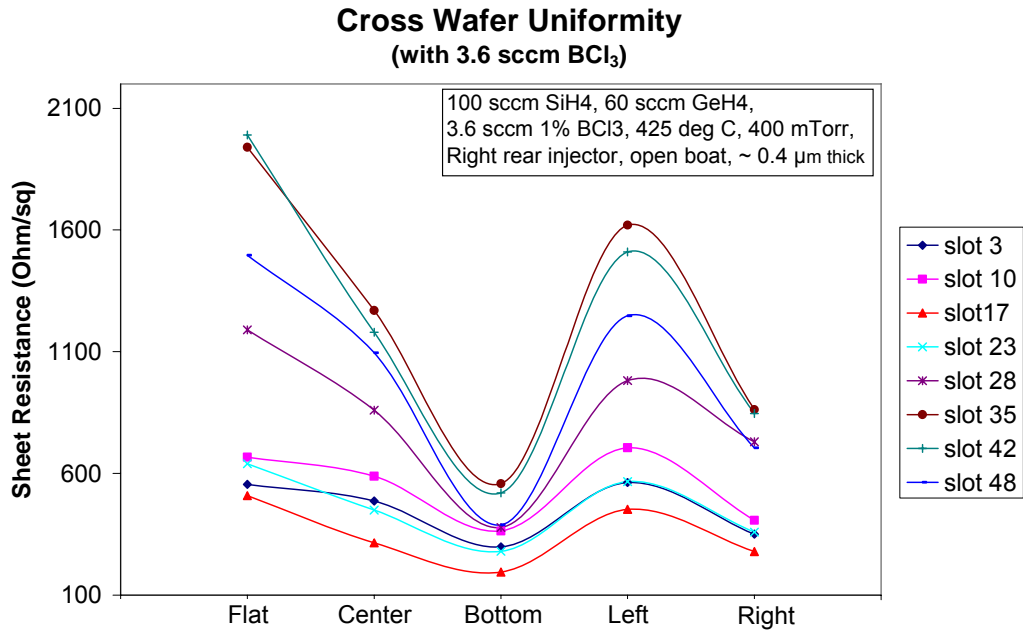


**Figure 3.10** Cross wafer uniformity of sheet resistance with low  $\text{BCl}_3$  flow rate

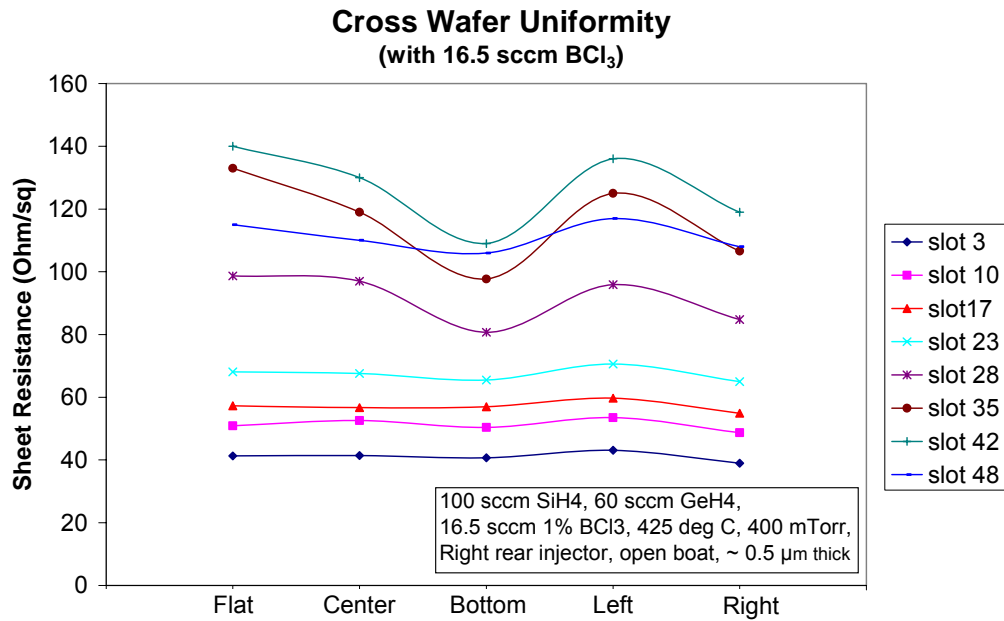


**Figure 3.11** Cross wafer uniformity of sheet resistance with high  $\text{BCl}_3$  flow rate

The experiments above show that using the rear injector with large dopant gas flow rate would be the optimal configuration to yield the best uniformity in resistivity. It is also confirmed that the injector does not get clogged up with the  $\text{BCl}_3$  doping process. However, it is a concern if both  $\text{B}_2\text{H}_6$  and  $\text{BCl}_3$  are available in a reactor with two injectors. During the deposition with one dopant line, the injector for the other dopant line is at standby with no gas flow. Deposition on the standby injector will build up material at the small pores and eventually clog them up. Flowing a small amount of  $\text{N}_2$  at the standby injector could prevent deposition on the pores, but this approach would involve significant hardware modification.

#### **3.1.4 Comparison of the two boron dopant gases**

To conclude the investigation of  $\text{BCl}_3$  as a new dopant gas, a comparison with  $\text{B}_2\text{H}_6$  is made in Table 3.6 for the study of the deposition and properties of LPCVD poly- $\text{Si}_{30}\text{Ge}_{70}$ . The desired doping level for poly- $\text{Si}_{30}\text{Ge}_{70}$  is achieved with 1%  $\text{BCl}_3$  concentration. The better uniformity and higher doping efficiency for the  $\text{BCl}_3$  process is clearly advantageous over the  $\text{B}_2\text{H}_6$  process for poly-SiGe films, but the small degradation in deposition rate and increase in residual stress are drawbacks. Tradeoffs between residual stress and resistivity are also involved in optimizing boron concentration for the  $\text{BCl}_3$  doped process studied here. Both residual stress and resistivity can be improved by increasing the film thickness. Thicker films also have advantages in strain gradient and grain crystallinity, and thicker films are desired for better electro-mechanical performance in electrostatically driven MEMS applications. The initial  $\text{BCl}_3$  doped process shows better process uniformity and repeatability than the more mature

B<sub>2</sub>H<sub>6</sub> doped process. Based on these results, the B<sub>2</sub>H<sub>6</sub> process was abandoned. Further development with the BCl<sub>3</sub> doped poly-SiGe process with the desired properties for MEMS applications will be discussed in Chapter 4.

**TABLE 3.6** Comparison of BCl<sub>3</sub> and B<sub>2</sub>H<sub>6</sub> as dopant gases for poly-SiGe process

Comparison	BCl <sub>3</sub> doping	B <sub>2</sub> H <sub>6</sub> doping
Deposition rate	Similar	Similar
Crystallinity	Similar	similar
Dopant incorporation	+++	---
Residual stress	-	-
Strain gradient	Similar	similar
Uniformity	++	--
repeatability	++	--
Safety	Toxic and corrosive	Toxic and flammable
Shelf life	24 months	6 months
Cost	Negligible compared to GeH <sub>4</sub>	Negligible compared to GeH <sub>4</sub>

### 3.2 Disilane (Si<sub>2</sub>H<sub>6</sub>) as the silicon precursor

#### 3.2.1 Literature review

Disilane (Si<sub>2</sub>H<sub>6</sub>) has been used as the silicon source for low temperature poly-silicon deposition due to its higher reactivity compared to silane (SiH<sub>4</sub>) [3.11]. Disilane fragments into SiH<sub>4</sub>, SiH<sub>3</sub> and SiH<sub>2</sub> in the gas phase. SiH<sub>3</sub> and SiH<sub>2</sub> decompose readily to form silicon at lower temperatures than SiH<sub>4</sub>. Disilane has also been previously used as the silicon source for poly-SiGe deposition [3.10, 3.12], but the higher cost of using disilane was a concern.

Since lowering the thermal budget is an important consideration for SiGe post foundry-CMOS integration, anything that helps to increase the deposition rate other than temperature would be worth considering for this goal. The benefit of Si<sub>2</sub>H<sub>6</sub> over SiH<sub>4</sub> is re-investigated to understand how much improvement can be gained with Si<sub>2</sub>H<sub>6</sub> in reducing the thermal budget and how this change impacts the physical properties of the film. The cost of using disilane should not be a significant factor if there is a large

improvement in the process. LPCVD systems have large batch sizes so the additional cost is spread over many wafers and might become insignificant.

Data from previous poly-SiGe depositions using  $\text{Si}_2\text{H}_6$  as the silicon source are summarized in Table 3.7 [3.12]. The poly-SiGe deposition was done in the same reactor in 2002. At that time, 100 mm-diameter wafers and caged boats were used.

**TABLE 3.7** SiGe deposition with  $\text{Si}_2\text{H}_6$  as the silicon precursor with 100 mm-diameter wafers, caged boat [3.12]

Temp. (°C)	Press. (mTorr)	$\text{Si}_2\text{H}_6$ (sccm)	$\text{GeH}_4$ (sccm)	$\text{PH}_3$ (sccm)	$\text{B}_2\text{H}_6$ (sccm)	Dep. Rate (nm/min)	Resistivity ( $\text{m}\Omega\text{-cm}$ )	Stress (MPa)	% Ge by RBS
350	300	25	175	0	0	1.2	NA	NA	NA
400	300	25	175	0	0	1.8	NA	NA	66
450	300	25	175	0	0	4.0	NA	NA	NA
450	300	10	190	5	0	6.6	1300	-180	79
450	300	15	185	5	0	7.0	50000	-270	72
500	300	15	185	5	0	9.0	130	-170	74
500	300	25	175	5	0	9.4	120	-170	68
550	300	15	185	5	0	10.0	180	NA	80
550	300	25	175	5	0	9.6	170	-100	78
550	300	35	165	5	0	8.2	200	-50	75
550	300	50	150	5	0	10.5	50	-180	65
350	300	25	175	0	40	10.5	7800	NA	58
400	300	25	175	0	40	13.0	5400	NA	54
450	300	25	175	0	40	22.0	5.5	NA	50

In the interest of lowering the thermal budget or increasing the deposition rate, the numbers in Table 3.7 are encouraging. The deposition rate with  $\text{Si}_2\text{H}_6$  and  $\text{GeH}_4$  is about  $2\times$  higher than with  $\text{SiH}_4$  and  $\text{GeH}_4$  for the same total gas flow rate. The resistivity with  $\text{PH}_3$  doping is a lot higher than desired, but there is room for improvement in the  $\text{B}_2\text{H}_6$  doped process. The average residual stress is in a reasonable range. There is no information on process uniformity. Since  $\text{Si}_2\text{H}_6$  is more reactive, more  $\text{GeH}_4$  flow is needed to achieve a similar germanium content as compared against the  $\text{SiH}_4$  and  $\text{GeH}_4$  process. To obtain similar film thickness, the cost of using  $\text{Si}_2\text{H}_6$  as the silicon source is slightly higher, mainly because more  $\text{GeH}_4$  is used.

### 3.2.2 Experimental results and discussion

Based on the results above, a few depositions were done to explore the Si<sub>2</sub>H<sub>6</sub> process by finding out the deposition rate and basic material properties. The experiments were done during the development of the BCl<sub>3</sub> doped poly-SiGe process using SiH<sub>4</sub> and GeH<sub>4</sub> (Chapter 4). To make the comparison easier, the same furnace geometry was used with Si<sub>2</sub>H<sub>6</sub> replacing SiH<sub>4</sub> for the deposition. There are twenty-five 150 mm-diameter wafers sitting in an open boat per load. The process conditions and the results are summarized in Table 3.8.

**TABLE 3.8** SiGe deposition with Si<sub>2</sub>H<sub>6</sub> as the silicon precursor with 150 mm-diameter wafers, open boat

Temp. (°C)	Press. (mTorr)	Si <sub>2</sub> H <sub>6</sub> (sccm)	GeH <sub>4</sub> (sccm)	BCl <sub>3</sub> (sccm)	Dep. Rate (nm/min)	Resistivity (mΩ-cm)	Stress (MPa)	% Ge by SIMS	B conc. (cm <sup>-3</sup> )
425	600	25	175	12	12.7	Not uniform	NA	NA	NA
375	600	25	175	12	7.7	Amorphous	-386	58	2.8×10 <sup>19</sup>
400	600	25	175	12	NA	Not uniform	NA	58	2.5×10 <sup>19</sup>
400	300	15	185	18	9.4	Amorphous	-248	63	3.9×10 <sup>19</sup>
425	300	15	185	18	11.2	3.1	-163	62	4.9×10 <sup>19</sup>
425	350	25	175	18	NA	Not uniform	NA	55	3.1×10 <sup>19</sup>
425	350	15	150	18	NA	Amorphous	NA	59	3.9×10 <sup>19</sup>

Data in Table 3.8 show there is indeed an improvement in deposition rate with Si<sub>2</sub>H<sub>6</sub> compared to data shown in Table 4.2 with SiH<sub>4</sub> at similar temperatures, but there are tradeoffs between uniformity and crystallinity. High deposition temperature and high deposition pressure result in poor uniformity – the film at the center of the wafer is thinner with very high resistivity. In this case, the reaction is in the mass transportation limited regime since disilane is very reactive. The gas reacts on the wafer edge before it diffuses to the wafer center. In the extreme case, the wafer looks darker than usual, especially at the edge. Gas-phase nucleation happens here. Silicon particles form in the gas phase and reach the wafer surface, creating a porous film with high particle density. Lowering the deposition temperature, the deposition pressure, and the disilane/germane

gas flow ratio can push the deposition into the surface-reaction limited regime. However, with lower temperature and lower germanium content, the film is amorphous. Although the boron concentration is quite high, the film is not conductive. This set of experiment shows that the process window with disilane is narrow. The deposition condition has to be carefully chosen to get a uniform and conductive film. Reducing the total gas flow rate, increasing the wafer spacing or use of a caged boat could increase the process window.

The benefits of changing the source gas from  $\text{SiH}_4$  to  $\text{Si}_2\text{H}_6$  are not being maximized due to the effect on Ge content in the film. The  $\text{Si}_2\text{H}_6$  partial pressure needs to be reduced to keep the same Ge content, which reduces the deposition rate and makes the net gain in deposition rate small. Also, the increase in deposition rate using  $\text{Si}_2\text{H}_6$  is not worth the negative impact on process control. Other variables such as tube pressure and total gas flow may offer better means to achieve higher deposition rates with the  $\text{SiH}_4$  and  $\text{GeH}_4$  process.

### **3.3 Germlyl silanes ( $(\text{H}_3\text{Ge})_x \text{SiH}_{4-x}$ ) as the silicon germanium precursors**

#### **3.3.1 Literature review**

As a promising material for modular CMOS and MEMS integration, the major challenges for LPCVD poly-SiGe in manufacturing are achieving good control of mechanical properties and lowering the SiGe deposition thermal budget.

The thin-film mechanical properties and the deposition rate depend strongly on germanium content. However, there are difficulties in controlling the germanium content in a LPCVD reactor using  $\text{SiH}_4$  and  $\text{GeH}_4$ . As discussed in Chapter 2, mass flow

controllers are used to control the SiH<sub>4</sub> and GeH<sub>4</sub> gas flow rates. MFC drift has been an issue and it is a concern for run-to-run repeatability. Also, since SiH<sub>4</sub> and GeH<sub>4</sub> have different consumption rates, the wafers closer to the gas inlet have higher germanium content. This in combination with the loading effect results in a deposition rate that is higher at the gas inlet side than at the exhaust side of the furnace.

While the above difficulties could be overcome with sophisticated engineering solutions like MFC recalibration and precursor injection, the new family of precursor germynyl silanes ((H<sub>3</sub>Ge)<sub>x</sub>SiH<sub>4-x</sub>) for SiGe deposition that has been developed recently can potentially be a simpler approach to solve these issues [3.13, 3.14]. As shown in Figure 3.12, this family of germynyl silanes has direct Si-Ge bonds. The SiGe film compositional control is defined by the Si:Ge ratio of the precursor molecule rather than the precision of the gas delivery system with the binary precursor gases such as SiH<sub>4</sub> and GeH<sub>4</sub>. Because the optimal germanium content for MEMS applications is between 50% and 70%, H<sub>3</sub>GeSiH<sub>3</sub> and (H<sub>3</sub>Ge)<sub>2</sub>SiH<sub>2</sub> are of particular interest. Figure 3.13 shows the Arrhenius plot of the epitaxial deposition rate for various precursor gases [3.14]. The germynyl silane molecules provide high deposition rates at low temperatures relative to disilane. The SiGe deposition rate achieved with the germynyl silane precursors is expected to be greater than that achieved with SiH<sub>4</sub> and GeH<sub>4</sub>. Therefore, germynyl silane precursors could facilitate further reductions in the thermal budget for fabrication of MEMS on CMOS, to minimize any detrimental impact on CMOS reliability.

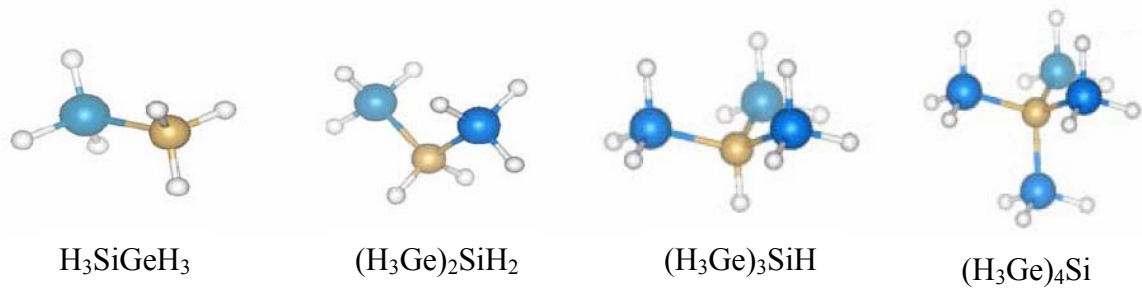


**Figure 3.12** Structures of the germeryl-silanes [3.13]

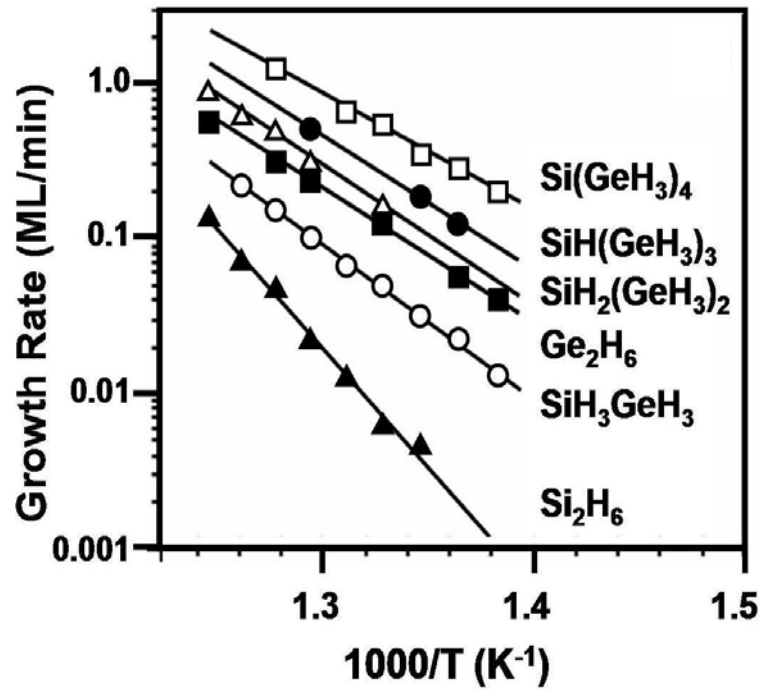


**Figure 3.13** Temperature dependence of the first epitaxial layer growth rates for various precursors on Si (100) [3.14]

### 3.3.2 Experimental plan

The germeryl silane precursors are being developed commercially [3.15] and collaborations are underway to test the deposition with these precursors with the LPCVD

system. While the germynyl silane precursors have the potential benefits of precise germanium content control, run-to-run reproducibility, higher deposition rate and lower deposition temperature, there are also some unknowns. Since the germynyl silane molecules have large molecular weight with high reactivity, the process should be carefully designed so that the deposition is in the surface reaction limited regime. There will be tradeoffs between uniformity and deposition rate like that seen for  $\text{Si}_2\text{H}_6$  deposition.

Most of the germynyl silane precursors are liquids at room temperature, except that  $\text{H}_3\text{GeSiH}_3$  is in gas phase. The vapor pressures at  $22^\circ\text{C}$  for  $(\text{H}_3\text{Ge})_2\text{SiH}_2$ ,  $(\text{H}_3\text{Ge})_3\text{SiH}$  and  $(\text{H}_3\text{Ge})_4\text{Si}$  are 55 Torr, 10 Torr and 1 Torr, respectively. If these liquid phase precursors are used, heating of the gas bottle and the delivery line will likely be needed to ensure sufficient gas is being pumped into the reaction chamber. To find out if heating would be needed for the LPCVD system, the gas flow and pressure stability can be verified manually once the precursor is hooked up to the reactor. Diluting the liquid with another gas or using a bubbler might be alternatives to heating, if lower concentration is necessary for better uniformity control.

To simplify the installation, the gas-phase precursor pure  $\text{H}_3\text{GeSiH}_3$  will be tested first. Initial depositions should be targeted to understand the basic process and material properties. Cross wafer and cross load process uniformity, deposition rate, germanium content, resistivity, crystallinity and average residual stress should be characterized. Based on the results of the initial depositions, the process can be fine tuned to once the tradeoffs among deposition rate, uniformity and crystallinity are understood. For the LPCVD reactor in the UC Berkeley Microlab, the adjustable process parameters and their range are listed in Table 3.9.

**TABLE 3.9** Adjustable process parameters with  $\text{H}_3\text{GeSiH}_3$  in the Berkeley Microlab's LPCVD poly-SiGe reactor (Tystar20)

Parameters	Process space
Gas flow rates	10 – 90% MFC range of $\text{H}_3\text{GeSiH}_3$ 10 – 4500 sccm of $\text{N}_2$ dilution
Temperature	300 – 450°C Temperature ramping across the load
Tube pressure	200 – 800 mTorr
Wafer placement	Wafers can be placed at every slot or further apart from each other Open boat or caged boat can be used

Since the deposition will result in 50% germanium content SiGe film with relatively high deposition rate, an amorphous film might result from deposition temperatures below 425°C. A thin crystalline seeding layer generated with  $\text{SiH}_4$  and  $\text{GeH}_4$  can be used to help to form a fully crystalline seed for the  $\text{H}_3\text{GeSiH}_3$  main deposition.

### 3.4 Summary

The investigation of new process gases discussed in this chapter involves a good amount of background study, hardware modification and process verification. Boron trichloride ( $\text{BCl}_3$ ) has been proven to be a better boron dopant source compared to diborane ( $\text{B}_2\text{H}_6$ ), resulting in a more stable and better controlled process. Further development and characterization with the  $\text{BCl}_3$  doped process will be discussed in the next Chapter. As a silicon precursor, disilane ( $\text{Si}_2\text{H}_6$ ) can improve the deposition rate and lower the thermal budget of the process; however there is significant drawback in the process control due to its high reactivity. The process space with  $\text{Si}_2\text{H}_6$  is narrow and the cost of using disilane will be higher since more germane will be needed to get the desired germanium content. As single-source silicon and germanium precursors, germynil silanes ( $(\text{H}_3\text{Ge})_x\text{SiH}_{4-x}$ ) have the potential of providing higher deposition rate and producing

uniform germanium content film across a large batch. Experiments beyond the scope of this thesis are needed to understand germly silanes' pros and cons in LPCVD applications once these gases are available for laboratory experiments.

## References

- [3.1] Y. Kunii, Y. Inokuchi, A. Moriya, H. Kurokawa and J. Murota, "In situ B doping of SiGe(C) using BCl<sub>3</sub> in ultraclean hot-wall LPCVD", *Appl. Surface Sci.*, vol. 224, pp. 68-72, 2004
- [3.2] Y. Kunii *et al.*, private communication, 2004
- [3.3] B. Caussat, E. Scheid, B. de Mauduit and R. Berjoan, "Influence of dopant concentration and type of substrate on the local organization of low-pressure chemical vapour deposition in situ boron doped silicon films from silane and boron trichloride", *Thin Solid Films*, vol. 446, pp. 218-226, 2004
- [3.4] C. W. Low, M. L. Wasilik, H. Takeuchi, T.-J. King and R. T. Howe, "In-situ doped poly-SiGe LPCVD process using BCl<sub>3</sub> for post-CMOS integration of MEMS devices," in *Proc. Electrochemical Society SiGe Materials, Processing, and Devices Symposium*, Honolulu, HI, Oct. 3-8, 2004, pp. 1021-1032
- [3.5] A. Moriya, M. Sakuraba, T. Matsuura and J. Murota, "Doping and electrical characteristics of in situ heavily B-doped Si<sub>1-x</sub>Ge<sub>x</sub> films epitaxially grown using ultraclean LPCVD", *Thin Solid Film*, vol. 343-344, pp. 541-544, 1999
- [3.6] B. L. Bircumshaw, M. L. Wasilik, E. B. Kim, Y. R. Su, H. Takeuchi, C. W. Low, A. P. Pisano, T.-J. King and R. T. Howe, "Hydrogen peroxide etching and stability of p-type poly-SiGe films," *17<sup>th</sup> IEEE Micro Electro Mechanical Systems Conference (MEMS-04)*, Maastricht, The Netherlands, Jan. 25-29, 2004, pp. 514-519
- [3.7] M. Cao, A. Wang and K. C. Saraswat, "Low pressure chemical vapor deposition of Si<sub>1-x</sub>Ge<sub>x</sub> films on SiO<sub>2</sub>, characterization and modeling", *J. Electrochem. Soc.*, vol. 142(5), pp. 1566-1572, 1995

- [3.8] S. M. Sze, *Physics of Semiconductor Devices*, 2<sup>nd</sup> ed., p. 32-33, John Wiley & Sons, New York, 1981
- [3.9] N. C. C. Lu, C. Y. Lu, M. K. Lee, C. C. Shin, C. S. Wang, W. Reuter and T. T. Sheng, “The effect of film thickness on electrical properties of LPCVD polysilicon films”, *J. Electrochem. Soc.*, vol. 131(4), pp. 897-902, 1984
- [3.10] A. E. Franke, “Polycrystalline Silicon-Germanium Films for Integrated Microsystems,” Ph.D. Thesis, Dept. of EECS, University of California at Berkeley, pp. 118-119, 2000
- [3.11] T. Kamins, *Polycrystalline silicon for integrated circuits and displays*, 2<sup>nd</sup> edition, Kluwer Academic Publishers, pp. 44, 48 and 52, 1998
- [3.12] Y-C. Jeon, T.-J. King, R. T. Howe, “Properties of phosphorus-doped poly-SiGe films for microelectromechanical systems”, *J. Electrochem. Soc.*, vol. 150(1), pp. H1-H6, 2003
- [3.13] C. J. Ritter, C.-W. Hu, A. V. G. Chizmeshya, J. Tolle, d. Kelewer, I. S. T. Tsong and J. Kouvetakis, “Synthesis and fundamental studies of  $(\text{H}_3\text{Ge})_x\text{SiH}_{4-x}$  molecules: precursors to semiconductor hetero- and nanostructures on Si”, *J. Am. Chem. Soc.*, vol. 127(27), pp. 9855-9864, 2005
- [3.14] C.-W. Hu, J. Tolle, A.V.G. Chizmeshya, J. Menéndez, I. S. T. Tsong, C. Ritter and J. Kouvetakis, “Low-temperature pathways to Ge-rich  $\text{Si}_{1-x}\text{Ge}_x$  alloys via single-source hydride chemistry”, *Appl. Phys. Lett.*, vol. 87, pp. 181903, 2005
- [3.15] M. D. Stephens, C. J. Ritter and M. A. Pikulin, “The utility of novel single-source germyl silanes”, in Proc. *Proc. Electrochemical Society SiGe & Ge Materials, Processing, and Devices Symposium*, Cancun, Mexico, Oct. 29 – Nov. 3, 2006

## Chapter 4: LPCVD Poly-SiGe Process Optimization

For MEMS applications, poly-SiGe's low resistivity, low wet-etch rate in heated hydrogen peroxide ( $\text{H}_2\text{O}_2$ ) solution, low tensile stress and low strain gradient are the desirable properties. The electrical and mechanical properties of poly-SiGe films depend strongly on the deposition process conditions. This chapter describes the process development to achieve the optimal poly-SiGe film for RF MEMS devices and inertial sensors.

The experimental details and thin film characterization methods are presented first. The results of all the depositions are summarized in section 4.3. Each set of experiments is described individually in the follow sections. Then the results of all experiments are reviewed together for microstructural properties study, and the characteristic microstructure for achieving low strain gradient film is elucidated.

### 4.1 Experimental details

Boron-doped poly-SiGe films were deposited in a Tystar hot-wall horizontal LPCVD reactor as described in Chapter 2. Pure  $\text{SiH}_4$  and  $\text{GeH}_4$  were used as the silicon and germanium precursor gases, respectively. 1%  $\text{BCl}_3$  diluted in He was used as the dopant gas.  $\text{SiH}_4$  and  $\text{GeH}_4$  were introduced through a gas ring located at the load side of the tube. The  $\text{BCl}_3/\text{He}$  mixture was introduced from the pump side through a multi-hole injector located beneath the wafer boats. Twenty-five 150 mm-diameter wafers were placed in open boats at the center of the reactor per load. Poly-SiGe films were deposited onto silicon substrates coated with a 2  $\mu\text{m}$ -thick LPCVD  $\text{SiO}_2$ . A very thin (<5 nm)

amorphous-silicon seed layer was deposited first using  $\text{Si}_2\text{H}_6$  to promote the adhesion of poly-SiGe to the oxide.

Experimental data were collected with five 4"-diameter wafers that were placed in slots 3, 9, 15, and 21 of the wafer boats, counting from the gas inlet side. A four-point probe instrument was used to measure the sheet resistance. The films were patterned and etched for the thickness measurement using a stylus-based profiler. Wafer curvature was measured before and after SiGe deposition (with backside SiGe film removed) to determine the average residual stress of the film. A cantilever beam array was patterned and released for strain gradient measurement. Resistivity, thickness, and strain gradient were measured at various points on each wafer, and average numbers are reported here. The crystal orientation of selected films was studied by X-ray diffraction. Transmission electron microscopy (TEM) analysis was used extensively to understand the film's microstructure and its correlation with the deposition condition and mechanical properties.

## **4.2 Characterization methods**

### **4.2.1 Transmission electron microscopy**

Transmission electron microscopy analysis is commonly used to obtain crystallographic information from specimens that are thin enough to transmit electrons [4.1]. A stream of electrons produced by the electron gun is focused to a small and coherent beam by a set of condenser lenses and aperture. The beam then strikes the specimen and part of it is transmitted. The transmitted part is focused by a set of

objective lenses and the image of the specimen is passed onto the image plane for the user to see.

While the theory and operation of the transmission electron microscope are fairly simple, the challenge of TEM analysis is in the sample preparation. The thickness of the specimen should be less than a few thousand angstroms for the electron beam to penetrate through. The sample preparation is time consuming and requires patience. Cross-sectional TEM analysis is mainly used for this dissertation. Figure 4.1 illustrates the general procedure for cross-sectional TEM specimen preparation. First, the wafer with the thin film is cleaved into a few 3 mm by 3 mm pieces. Two pieces are glued together with the thin films facing each other using epoxy (M-bond 610). Two dummy pieces are glued on the sides as mechanical supports. The sandwich is then cut into a few slides approximately 500  $\mu\text{m}$  thick using a diamond saw. The slide is chopped into a disk using a slurry disk cutter. The sample then goes to the dimpler for mechanical grinding and polishing. Once the center region of the sample is thinned down to about 20  $\mu\text{m}$ , the disk is mounted in an ion-milling machine where the specimen is further sputter thinned by ion bombardment until a hole appears. The edge near the hole is thin enough for imaging under the electron microscope.

Top view TEM specimen can be prepared using similar techniques with the bonding and slicing steps skipped. A disk can be cut from the wafer and the sample is mechanically polished and ion milled to final thickness from the backside.

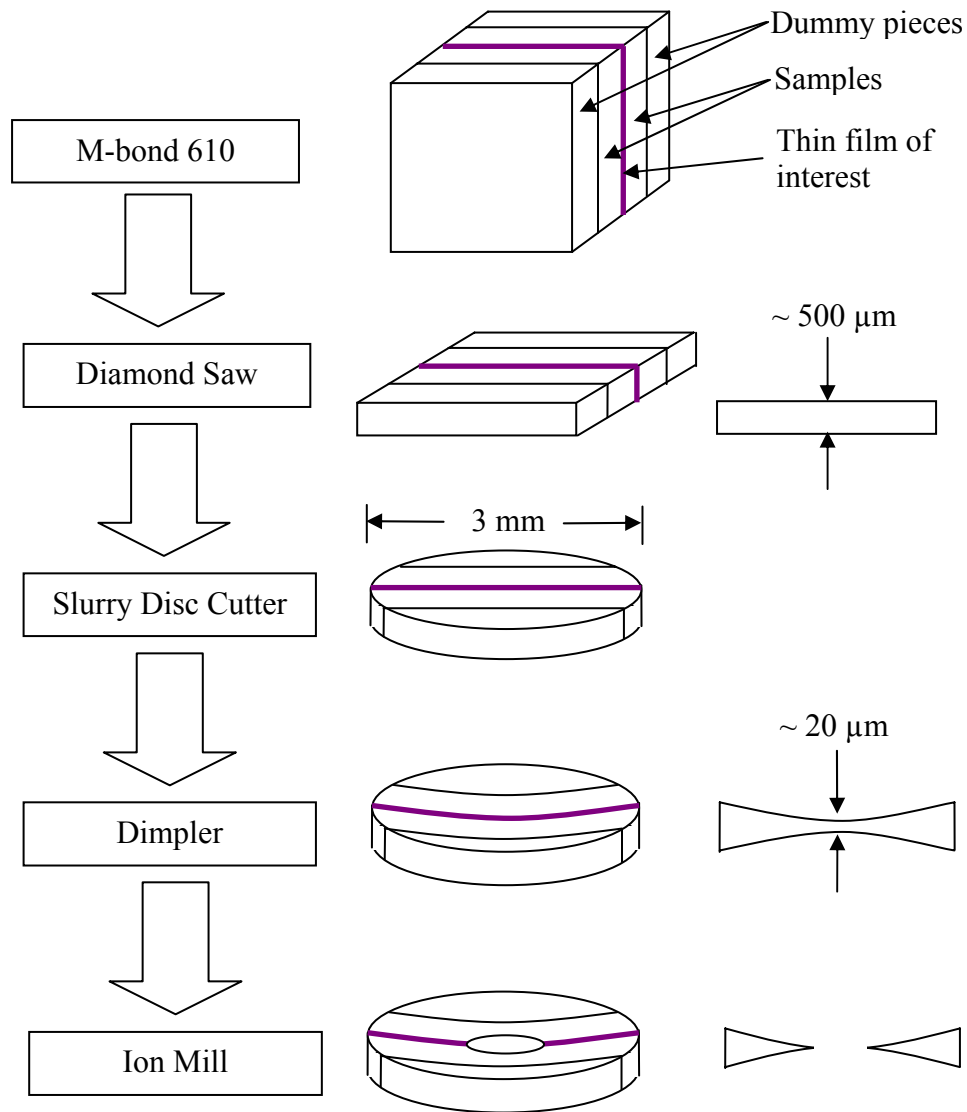


**Figure 4.1** Cross-sectional TEM sample preparation method

#### 4.2.2 X-ray diffraction

X-ray diffraction (XRD) measurement is a non-destructive method that provides information on crystallinity and texture of bulk solids and thin films. Monochromatic X-ray is used to determine the inter-planar spacing of the material. Material composition

and crystal orientation can be obtained from the X-ray spectra. When the Bragg condition for constructive interference is obtained, a diffraction peak is produced and the relative peak height is proportional to the number of grains in a preferred orientation.

For a poly-SiGe thin film on a single-crystal silicon substrate, the X-ray spectra contain diffraction peaks for both the thin film and the substrate. The diffraction peak positions can be calculated with Bragg's Law [4.2]:

$$\lambda = 2d \sin \theta \quad (4.1)$$

$$d = \frac{a}{\sqrt{h^2 + k^2 + l^2}} \quad (4.2)$$

where h, k and l are the Miller indices for the direction and a is the lattice constant for a cubic material. The lattice constant of Si, Ge and Si<sub>1-x</sub>Ge<sub>x</sub> are listed below:

$$\text{Si: } a = 5.43 \text{ \AA} \quad (4.3)$$

$$\text{Ge: } a = 5.66 \text{ \AA} \quad (4.4)$$

$$\text{Si}_{1-x}\text{Ge}_x: a(x) = (5.43 + 0.20x + 0.027x^2) \text{ (\AA)} \quad [4.3] \quad (4.5)$$

$$\text{Si}_{40}\text{Ge}_{60}: a = 5.56 \text{ \AA} \quad (4.6)$$

The peak position shifts with different germanium content. However, it is difficult to calculate the germanium content from the peak position since peak shift can also be induced by stresses in the film. The diffraction peaks of the poly-SiGe sample are listed in Table 4.1.

**TABLE 4.1** XRD 2 $\theta$  angle calculation

Material	Direction	d (Å)	2 $\theta$ (°)
Si	<200>	2.72	33.96
Si	<400>	1.36	69.14
Ge	<200>	2.83	31.59
Ge	<400>	1.42	65.96
Si <sub>40</sub> Ge <sub>60</sub>	<111>	3.21	27.77
Si <sub>40</sub> Ge <sub>60</sub>	<220>	1.97	46.14
Si <sub>40</sub> Ge <sub>60</sub>	<311>	1.68	54.71
Si <sub>40</sub> Ge <sub>60</sub>	<222>	1.61	57.36
Si <sub>40</sub> Ge <sub>60</sub>	<400>	1.39	67.31
Si <sub>40</sub> Ge <sub>60</sub>	<331>	1.28	74.30

### 4.2.3 Strain gradient measurement

Minimization of the strain gradient, or the out-of-plane curvature of a released beam, is a critical requirement for inertial sensor applications in which the lateral dimensions of mechanical structures are in the range of hundreds of microns. A typical target value of strain gradient is  $1 \times 10^{-5} \mu\text{m}^{-1}$  for inertial sensor applications, which would yield 1.25  $\mu\text{m}$  tip deflection of a 500  $\mu\text{m}$  long cantilever beam. The dependence of stress and strain gradient on film microstructure and deposition conditions is well-understood for poly-Si films [4.1], [4.4]. The mechanical properties of poly-SiGe can be studied with similar techniques used for poly-Si.

The released cantilever beam shown in Figure 4.2(a) is commonly used for strain gradient measurement. Strain gradient is calculated as [4.5]:

$$\frac{1}{\rho} = \frac{2\Delta z}{L^2} \quad (4.7)$$

where  $\rho$  is the radius of curvature of the beam,  $\Delta z$  is the out-of-plane deflection of the tip and  $L$  is the length of the cantilever beam.

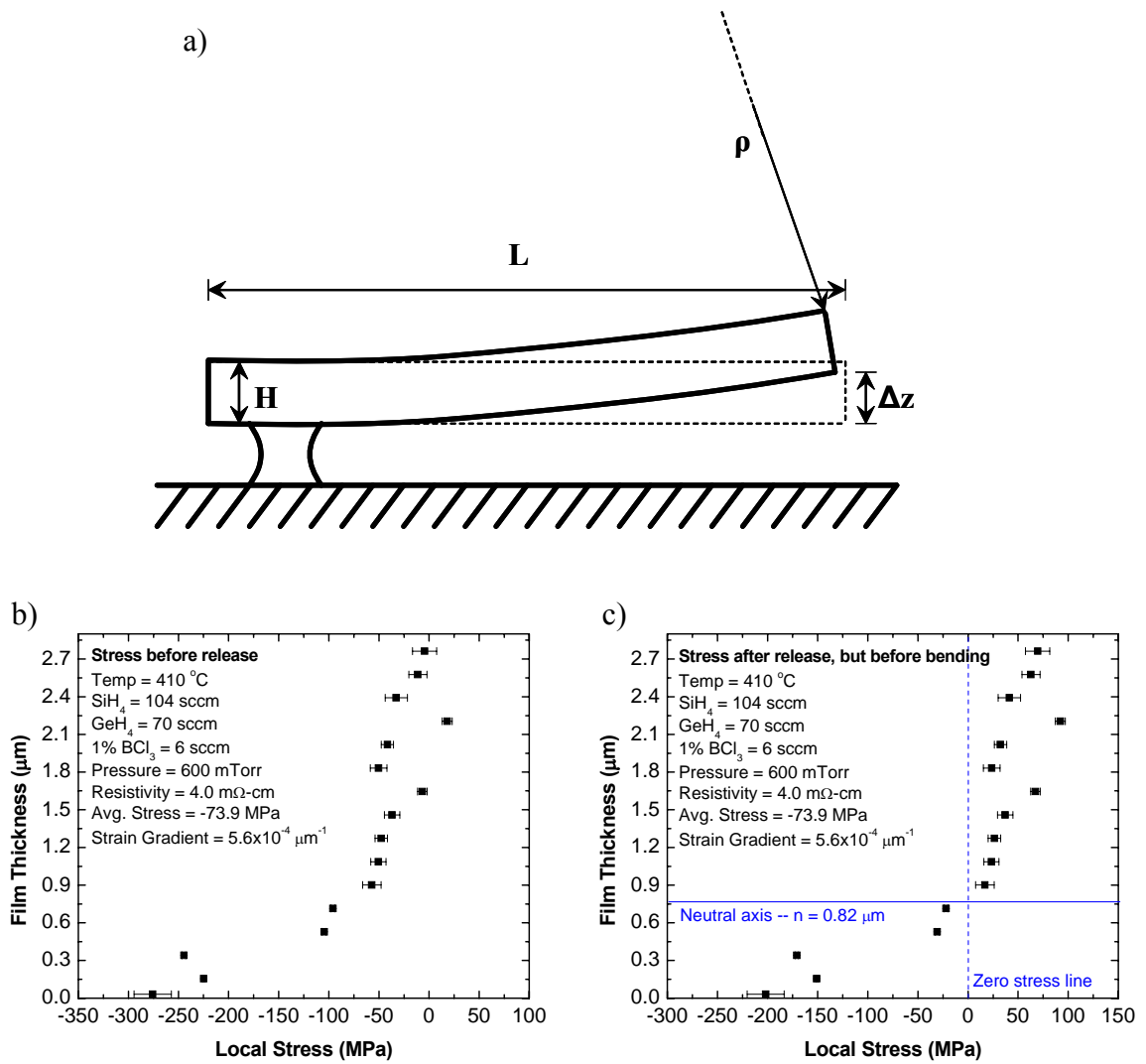


**Figure 4.2** Strain gradient measurement: a) cross-sectional schematic of a released cantilever beam; b) stress depth profile before release; c) stress depth profile after release, but before bending

The strain gradient of the film can also be calculated as [4.5]:

$$\frac{1}{\rho} = \frac{12M}{EWH^3} = \frac{12}{EH^3} \int_{-n}^{H-n} \sigma(z) z dz \quad (4.8)$$

where  $M$  is the bending moment,  $E$  is the Young's Modulus,  $W$  is the width of the cantilever beam,  $H$  is the film thickness,  $n$  is the position of the neutral axis,  $\sigma(z)$  is the stress depth profile in the film and  $z$  is the distance from the neutral axis. Strain gradient

is related to stress gradient with the Young's Modulus as a proportionality factor, assumed to be 140 GPa for poly-SiGe.

Stress vs. depth profiles  $\sigma(z)$  for Equation (4.8) were generated by incrementally etching (thinning) an unpatterned poly-SiGe film on the front side of the wafer and then measuring the change in wafer curvature, in an iterative manner [4.1]. Initial wafer curvature was measured prior to any etching of the poly-SiGe film using a reactive ion etcher. After every 0.16  $\mu\text{m}$  of etching, the wafer was taken out from the etcher for wafer curvature measurement. The stress of the thin etched layer was determined from the change in wafer curvature. This process was repeated until the poly-SiGe film was completely etched away. A typical stress profile of a film before release is shown in Figure 4.2(b). To find the neutral axis in Equation (4.8), the stress profile is shifted by the amount of average residual stress and the position of the neutral axis is at the intersection of the zero stress line and the shifted stress profile, as shown in Figure 4.2(c). Error bars displayed on the stress curve indicate the measurement uncertainty. Note that the systematic error is significantly larger at the bottom of the film because of the cumulative effect of cross-wafer etch-rate non-uniformity, which reduces the validity of the assumption of uniform film thickness for the stress measurement toward the bottom of the film. Nonetheless, the general shape of the stress profile is still valid and the two methods of strain gradient measurement yield similar results with  $\sim 20\%$  discrepancy.

### **4.3 Overall experimental data**

The average deposition rate, resistivity, average residual stress and strain gradient, along with cross-wafer (XW) and cross-load (XL) deposition uniformity, are summarized

in Table 4.2. Uniformity is reported as normalized standard deviation for deposition rate and resistivity. Standard deviation is reported for average residual stress since its value can be both positive and negative. Average strain gradient and its best value within each run are reported in Table 4.2. Further statistical analysis of the strain gradient is discussed later in the chapter.

The experimental study was done in a series of design-of-experiments (DOE) runs. The 1<sup>st</sup> DOE was performed to understand the process space and characterize the deposition rate, resistivity, average residual stress, strain gradient and wet etch rate in hydrogen-peroxide solution. The results of the 1<sup>st</sup> DOE showed that the structural layer requirements for general MEMS applications can be met within the process temperature constraint imposed by CMOS electronics, but the strain gradient requirements for inertial sensor applications remain a major challenge. The rest of the experiments were all designed to achieve low strain gradient with good uniformity. The ramping experiment explores the option of ramping down the temperature and germanium content during deposition for grain control. The 2<sup>nd</sup> DOE looked into the effect of varying the dopant gas flow rate and the process pressure. In addition, the effects of film thickness and the initial seed layer were studied with the best recipe from the 2<sup>nd</sup> DOE. Also, multiple layer deposition was used to create fine-grain microstructure. Low strain gradient can be achieved with several of the approaches described above. All recipes which yield films with absolute strain gradient  $\leq 1 \times 10^{-4} \mu\text{m}^{-1}$  are highlighted in Table 4.2. Strain gradient uniformity study has focused on these highlighted recipes.

Run #		SiGe seed							SiGe Deposition							Results										
		Si <sub>2</sub> H <sub>6</sub> seed	Temp. (°C)	Press. (mT)	SiH <sub>4</sub> (sccm)	GeH <sub>4</sub> (sccm)	*BCl <sub>3</sub> (sccm)	Time (min)	Temp. (°C)	Press. (mT)	SiH <sub>4</sub> (sccm)	GeH <sub>4</sub> (sccm)	*BCl <sub>3</sub> (sccm)	Time (min)	Avg. film thk. (μm)	Avg. DR (nm/min)	DR XL unif. (%)	DR XW unif. (%)	Avg. Res. (nm)	Res. XL unif. (%)	Res. XW unif. (%)	Avg. stress (MPa)	Stress XL stdev (MPa)	Avg. strain gradient (μm <sup>-1</sup> )	Best Strain gradient (μm <sup>-1</sup> )	H <sub>2</sub> O <sub>2</sub> ER. (nm/μm)
DOE1-1	Yes	None	410	600	120	50	6	381	410	600	120	50	6	381	1.8	4.7	3%	9%	6.9	67%	37%	-228	24	6.60e-4	4.09e-4	1.3
DOE1-2	Yes	None	410	600	104	70	6	335	410	600	104	70	6	335	2.6	7.8	1%	11%	5.2	24%	31%	-92	16	6.74e-4	5.13e-4	18
DOE1-3	Yes	None	410	600	112	60	12	318	410	600	112	60	12	318	2.1	6.5	2%	12%	2.4	18%	18%	-168	8	5.88e-4	1.84e-4	2.2
DOE1-4	Yes	None	410	600	120	50	18	421	410	600	120	50	18	421	2.6	6.2	2%	14%	0.96	13%	11%	-161	26	-5.22e-6	-9.05e-6	0.78
DOE1-5	Yes	None	410	600	104	70	18	250	410	600	104	70	18	250	2.0	7.9	2%	14%	1.8	15%	14%	-155	17	6.06e-4	2.66e-4	4.9
DOE1-6	Yes	None	425	600	112	60	6	302	425	600	112	60	6	302	2.2	7.2	2%	12%	7.3	23%	38%	-120	26	8.24e-4	5.87e-4	0.33
DOE1-7	Yes	None	425	600	120	50	12	290	425	600	120	50	12	290	1.8	6.1	2%	13%	3.1	19%	17%	-171	27	9.74e-4	6.37e-4	0.39
DOE1-8	Yes	None	425	600	112	60	12	302	425	600	112	60	12	302	2.2	7.4	1%	14%	3.2	22%	21%	-119	21	7.95e-4	6.03e-4	1.1
DOE1-9	Yes	None	425	600	104	70	12	230	425	600	104	70	12	230	2.4	9.9	1%	14%	3.8	25%	28%	-73	19	5.10e-4	3.26e-4	4.6
DOE1-10	Yes	None	425	600	112	60	18	256	425	600	112	60	18	256	2.5	8.2	2%	15%	2.1	17%	14%	-97	21	5.38e-4	3.89e-4	1.6
DOE1-11	Yes	None	440	600	120	50	6	185	440	600	120	50	6	185	1.9	7.6	1%	12%	9.8	43%	21%	-126	25	5.09e-4	3.41e-4	1.1
DOE1-12	Yes	None	440	600	104	70	6	135	440	600	104	70	6	135	1.7	12.5	2%	14%	19	59%	31%	-53	21	4.68e-4	4.05e-4	8.2
DOE1-13	Yes	None	440	600	112	60	12	218	440	600	112	60	12	218	2.0	9.3	1%	15%	5.5	34%	26%	-104	24	4.42e-4	3.67e-4	0.78
DOE1-14	Yes	None	440	600	120	50	18	265	440	600	120	50	18	265	2.0	7.6	2%	14%	2.6	17%	17%	-131	27	5.30e-4	3.52e-4	0.056
DOE1-15	Yes	None	440	600	104	70	18	182	440	600	104	70	18	182	1.9	10.8	1%	15%	3.3	27%	23%	-70	18	4.87e-4	4.07e-4	2.33
Ramp-ref	Yes	None	430	600	140	60	30	230	430	600	140	60	30	230	1.9	8.4	2%	14%	1.4	7%	7%	-135	21	6.40e-4	4.86e-4	NA
Ramp-SiH <sub>4</sub>	Yes	None	430	600	140-190	60	30	30*11	430	600	140-190	60	30	30*11	2.6	7.9	2%	14%	1.3	10%	7%	-126	14	3.80e-4	2.74e04	NA
Ramp-temp	Yes	None	430-380	600	140	60	30	30*11	430-380	600	140	60	30	30*11	2.5	7.6	2%	12%	1.0	5%	6%	-164	25	3.87e-4	2.86e04	NA
DOE2-t1	Yes	None	410	1200	150	50	30	60	410	1200	150	50	30	60	0.61	10.2	NA	NA	NA	NA	NA	NA	NA	NA	NA	NA
DOE2-t2	Yes	None	410	900	150	50	30	60	410	900	150	50	30	60	0.58	9.7	NA	NA	NA	NA	NA	NA	NA	NA	NA	NA
DOE2-t3	Yes	None	410	700	150	50	30	60	410	700	150	50	30	60	0.55	9.2	NA	NA	NA	NA	NA	NA	NA	NA	NA	NA
DOE2-t4	Yes	None	410	600	140	60	30	60	410	600	140	60	30	60	0.52	8.7	NA	NA	NA	NA	NA	NA	NA	NA	NA	NA
DOE2-t5	Yes	None	410	350	140	60	30	60	410	350	140	60	30	60	0.38	6.4	NA	NA	1.3	NA	NA	NA	NA	NA	NA	NA



## 4.4 1<sup>st</sup> design-of-experiments

### 4.4.1 Experimental design

For the LPCVD process, the process variables include temperature, pressure, silane-to-germane gas flow ratio, dopant gas flow rate, and load size. In this section, the LPCVD poly-SiGe process parameter space is explored with a 15-run DOE [4.6]. SiH<sub>4</sub>-to-GeH<sub>4</sub> gas flow ratio, BCl<sub>3</sub> gas flow rate, and temperature are the input variables; deposition rate, resistivity, average residual stress, strain gradient and H<sub>2</sub>O<sub>2</sub> etch rate are functions of the input variables.

All depositions targeted a poly-SiGe film thickness of 2 μm. For the design of experiments, a face-centered central composite design was used. Deposition temperature (410°C, 425°C, or 440°C), SiH<sub>4</sub> to GeH<sub>4</sub> ratio (104/70, 112/60 or 120/50 sccm/sccm), and BCl<sub>3</sub> flow rate (6, 12 or 18 sccm) were chosen as input variables. It should be noted that initial design intended to have the summation of SiH<sub>4</sub> and GeH<sub>4</sub> flow rates as a constant – 200 sccm. However, the SiH<sub>4</sub> MFC experienced an electronic drift prior to this experiment, so that the actual SiH<sub>4</sub> gas flow rate was later found out to be ~80% of the design value. The process pressure was kept constant at 600 mTorr in each recipe. The process details for each deposition run are summarized in Figure 4.3. The lower value of temperature was set by the amorphous-to-polycrystalline transition temperature, and the upper value was set by thermal budget limits imposed by foundry CMOS electronics. The upper and lower values of SiH<sub>4</sub>/GeH<sub>4</sub> flow ratio were set by the crystallinity requirement and hydrogen-peroxide etch rate, respectively. High-germanium-content films have lower amorphous-to-polycrystalline transition temperature. However, the wet etch rate is higher for germanium-rich films, which is not desirable for micro-machining processes using

pure germanium as the sacrificial material [4.7]. The lower value of  $\text{BCl}_3$  flow rate was set by resistivity considerations, while the upper value was set by the maximum flow rate of the mass flow controller (MFC).

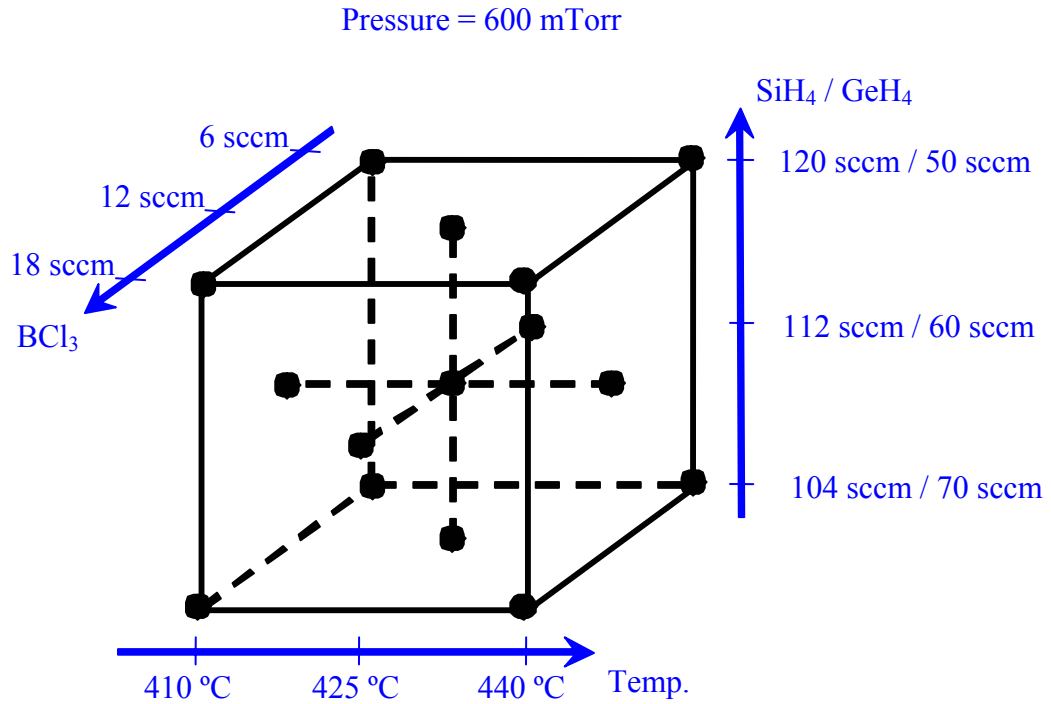


**Figure 4.3** 1<sup>st</sup> design of experiments input parameter values

#### 4.4.2 Results and interpretation

The experimental data for the 1<sup>st</sup> design of experiment can be found in Table 4.2. The deposition rate, resistivity, and wet etch rate fall within reasonable ranges. Depending on the application, a recipe can be chosen to meet specific requirements. The average residual stress is compressive for each of the recipes although a small tensile stress is desired for some applications. The strain gradient is higher than desired for inertial sensor applications.

Since a LPCVD system is a batch reactor, cross-load uniformity is an important manufacturing consideration. The wafer-to-wafer uniformity and within-wafer uniformity reported here are for the Tystar reactor in an academic research laboratory; it is not surprising that they do not meet specifications for high volume production. However, uniformity is expected to be significantly better for the sophisticated LPCVD systems used within production environments. In our research tool, the cross-wafer uniformity of deposition rate is better than 3%. Due to the different consumption rates of  $\text{SiH}_4$  and  $\text{GeH}_4$ , the germanium content in films deposited onto wafers closest to the gas inlet is about 3 atomic percent higher than for films deposited onto the wafers closest to the exhaust [4.7]. This gradient in germanium content, in combination with the loading effect, results in a deposition rate that is higher at the gas inlet side than at the exhaust side. To improve the cross-load uniformity, an injector can be used for the precursor gases. The dopant gas is introduced via an injector located at the bottom of the reactor. Thus, the film resistivity is lower in the regions of the wafers closer to the injector. Due to gas depletion effects, recipes utilizing low  $\text{BCl}_3$  flow rate tend to have worse cross-wafer uniformity in resistivity. Since the injector design was not optimal, cross-load uniformity of resistivity depends on the wafer position relative to location of the injector holes. Improved injector design, higher  $\text{BCl}_3$  flow rate, and *in-situ* wafer rotation as in a vertical furnace should all enhance the uniformity of film resistivity.

To deduce general trends, the average values for deposition rate, resistivity, residual stress, strain gradient, and wet etch rate were analyzed using the JMP<sup>TM</sup> statistical software package [4.8]. Confidence intervals for the output observables *vs.* input factors are shown in Figure 4.4. The deposition rate increases with temperature, but

decreases with  $\text{SiH}_4/\text{GeH}_4$  ratio and shows no dependence on dopant gas flow rate. The film resistivity mainly depends on  $\text{BCl}_3$  flow rate. The average residual stress becomes less compressive with increasing temperature and decreasing  $\text{SiH}_4/\text{GeH}_4$  ratio. Average residual stress was previously reported to become more compressive when boron doping is increased by orders of magnitude in Chapter 3. In this experiment, the boron doping variation range is small, and no significant trend is found for the average residual stress vs. dopant concentration. For the strain gradient data, the error bar is larger than the slope of the trend in Figure 4.4. Further investigation of the strain gradient will be discussed in the next section. Wet etch rate mainly depends on the germanium content in the film and thus increases inversely with  $\text{SiH}_4/\text{GeH}_4$  ratio as expected.

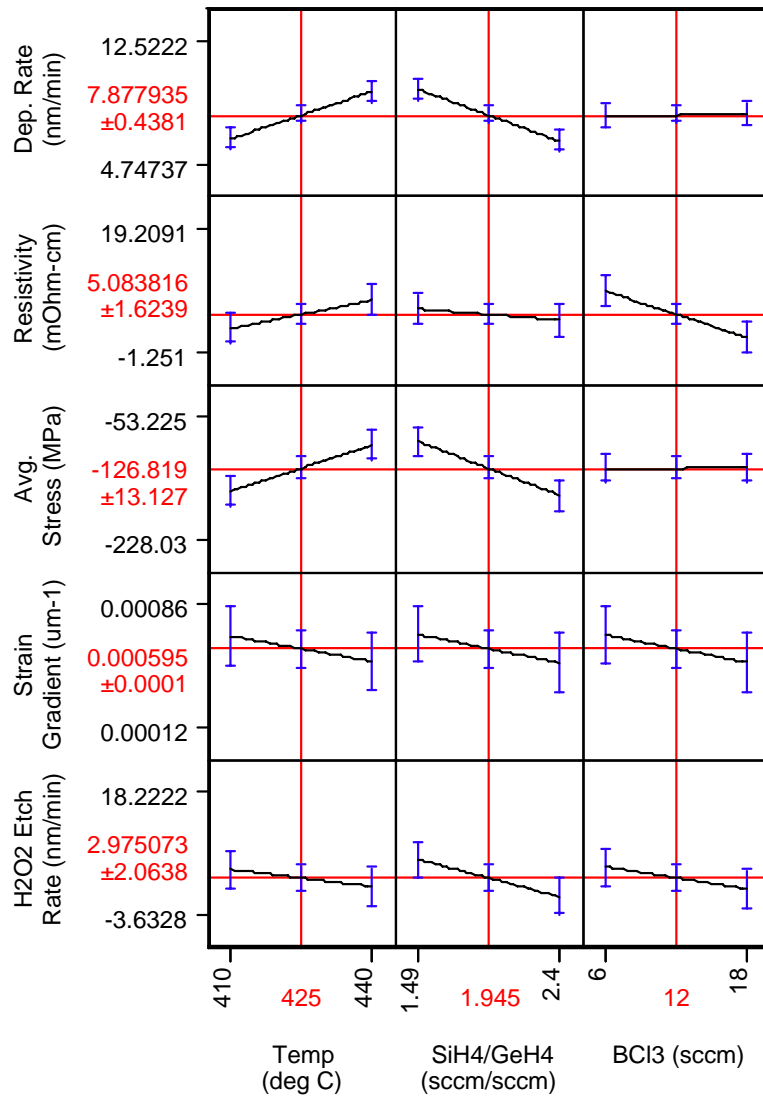
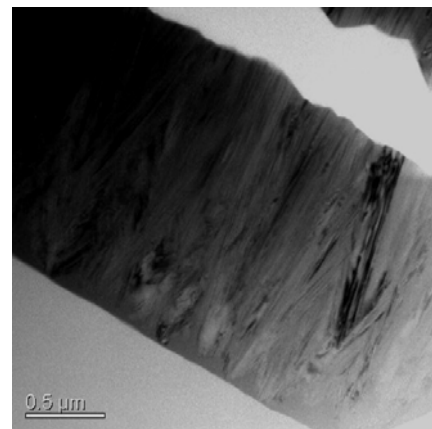
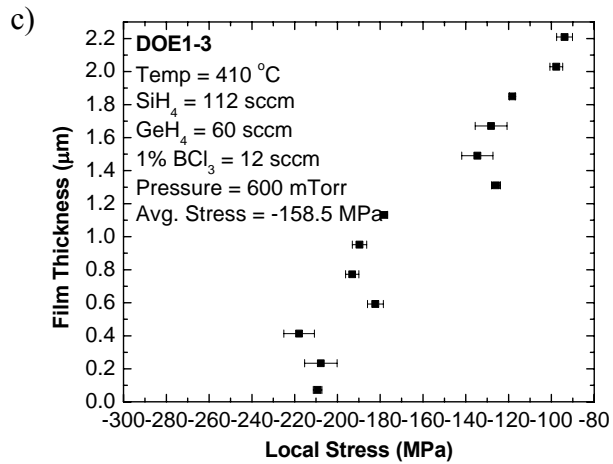
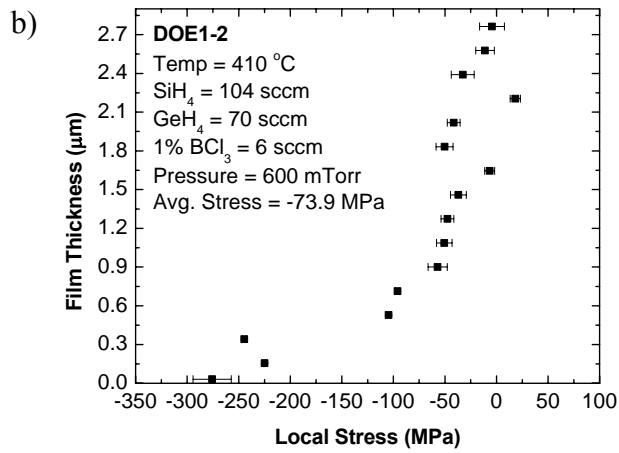
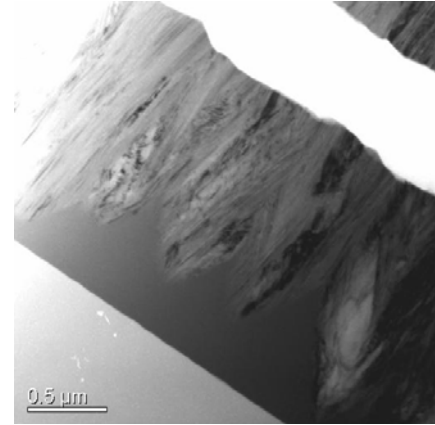
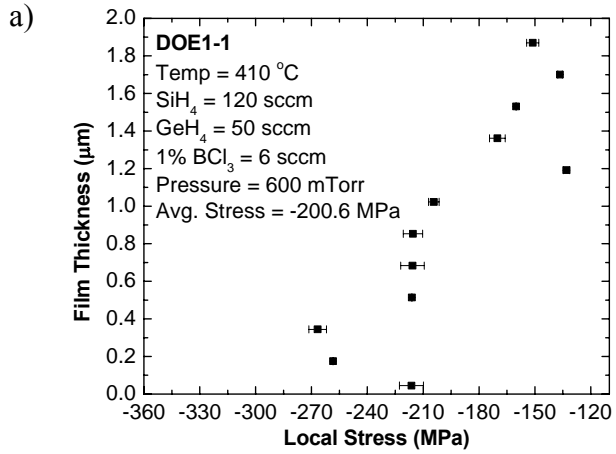


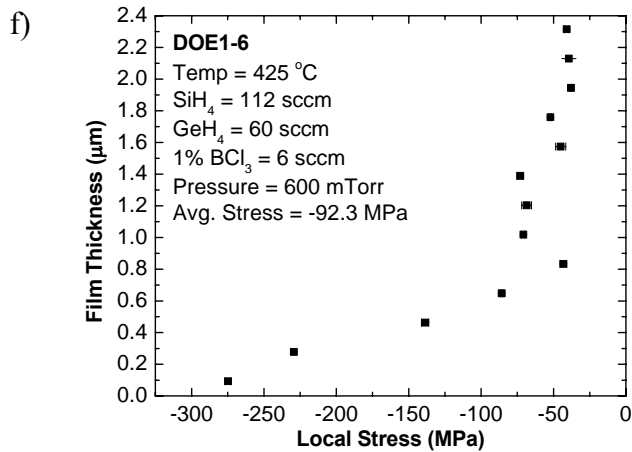
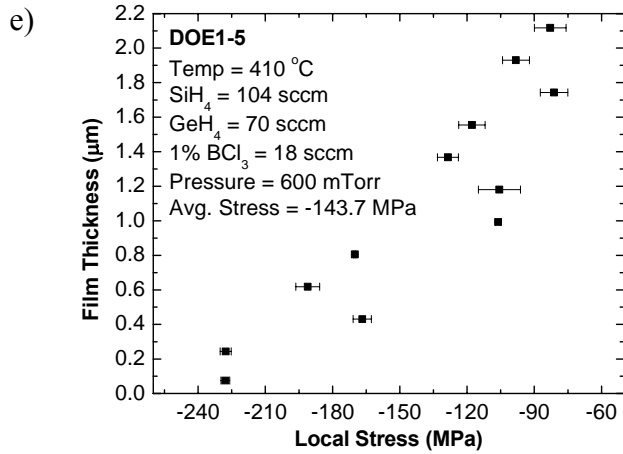
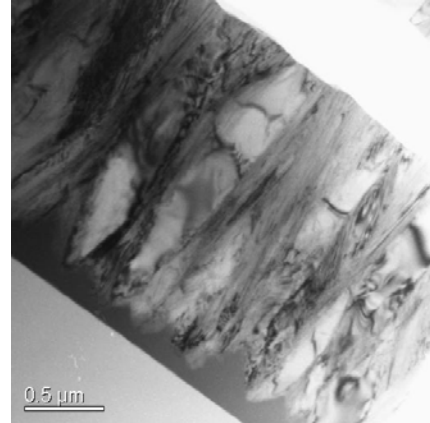
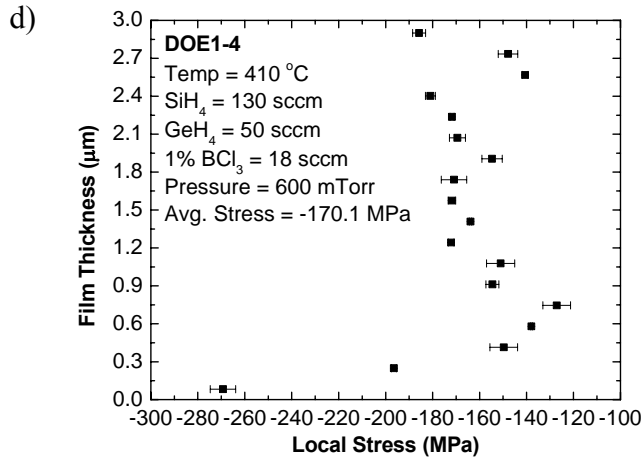
**Figure 4.4:** Values and confidence intervals for various responses

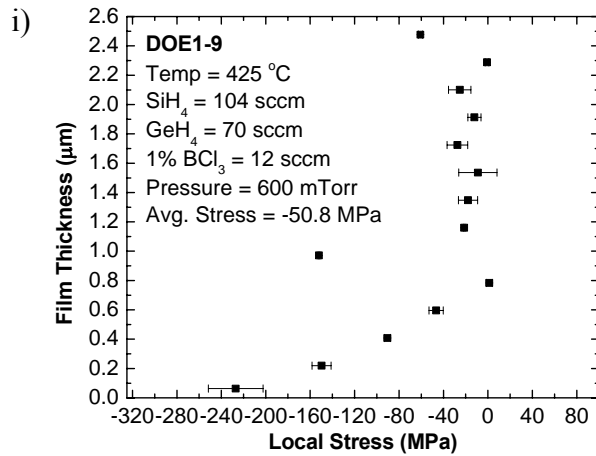
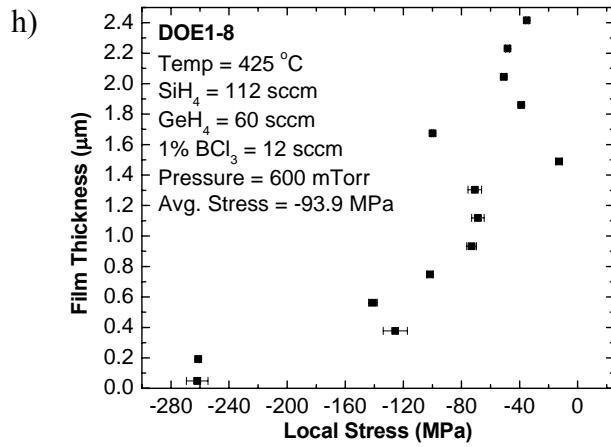
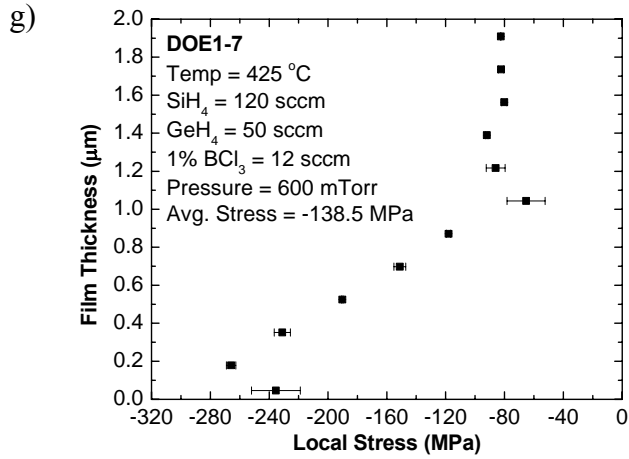
#### 4.4.3 Mechanical properties study

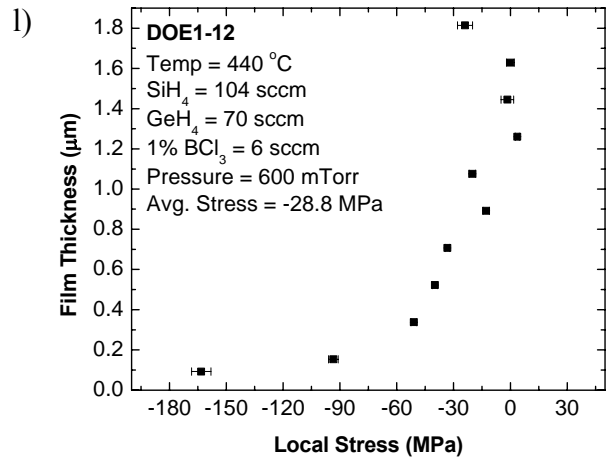
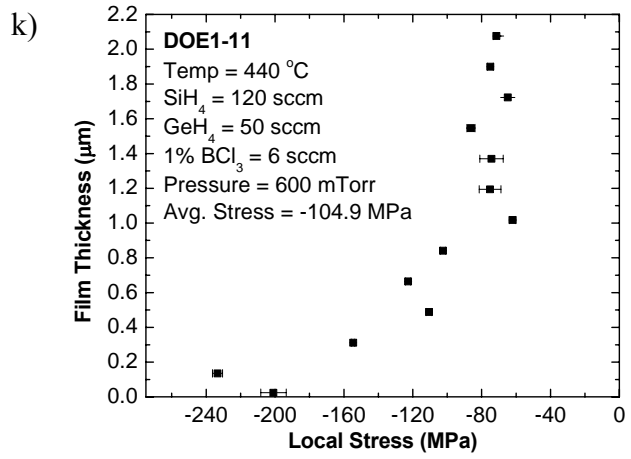
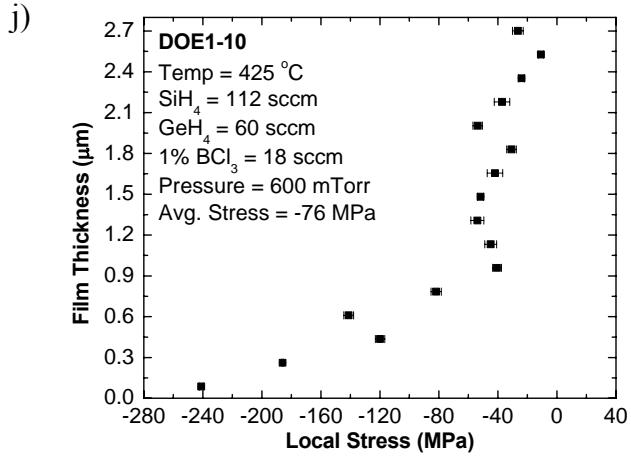
The stress profiles of all the deposition conditions along with some TEM images are presented in Figure 4.5 over the next few pages. The majority of the deposited films have upward curvature upon release, because the compressive stress at the bottom of the film is usually significantly higher than in the rest of the film. The slope of the stress

profile (hence the strain gradient) depends on the film deposition conditions. Similar results have been found for APCVD and PECVD poly-SiGe films [4.9], [4.10].









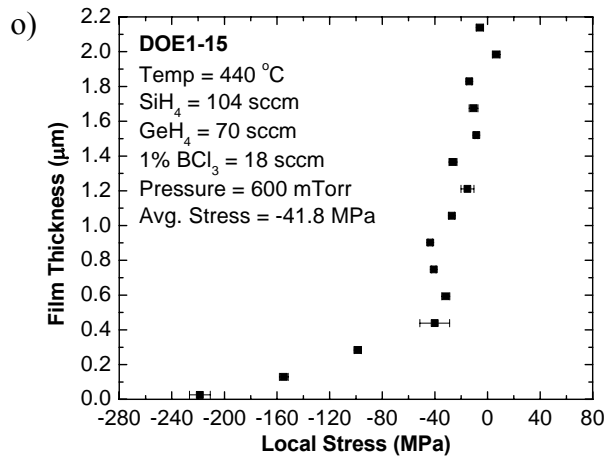
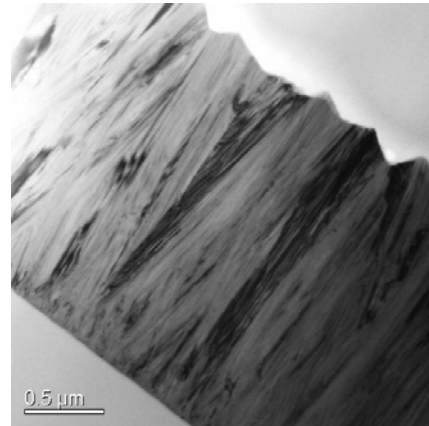
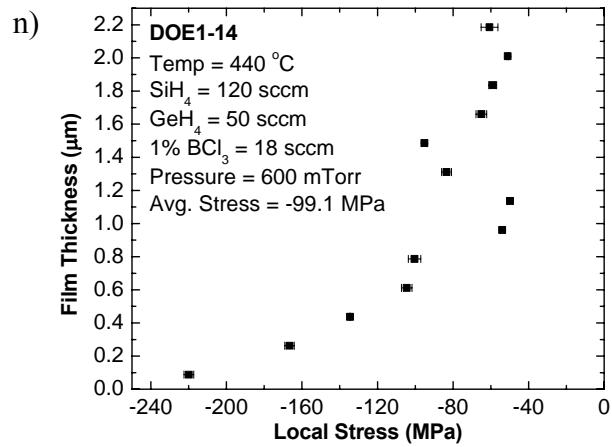
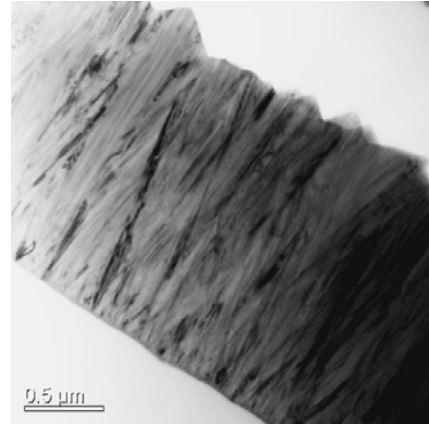
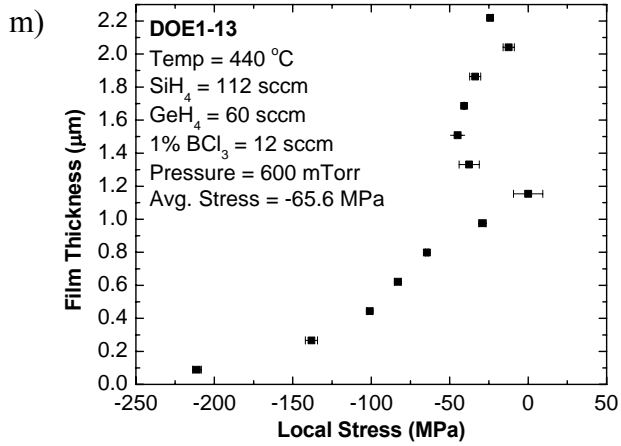


**Figure 4.5** Stress profiles and TEM images for DOE1 recipes.

Based on the stress profiles shown above, the average residual stress is expected to decrease (become less compressive) with increasing film thickness since the compressive stress gradually releases along the film thickness. The average strain gradient is also expected to decrease with increasing film thickness. As discussed previously, there is a thickness variation across the load for each deposition run. Figure 4.6 shows that the average residual stress becomes less compressive with increasing film thickness. Figure 4.7 shows that the strain gradient decreases with increasing film thickness, as expected. From Figure 4.4 it can be seen that the average residual stress and the strain gradient each varies with germanium content. The small variation (3 atomic percent) in germanium content across the load is a secondary effect for the observed dramatic changes in average residual stress and strain gradient.

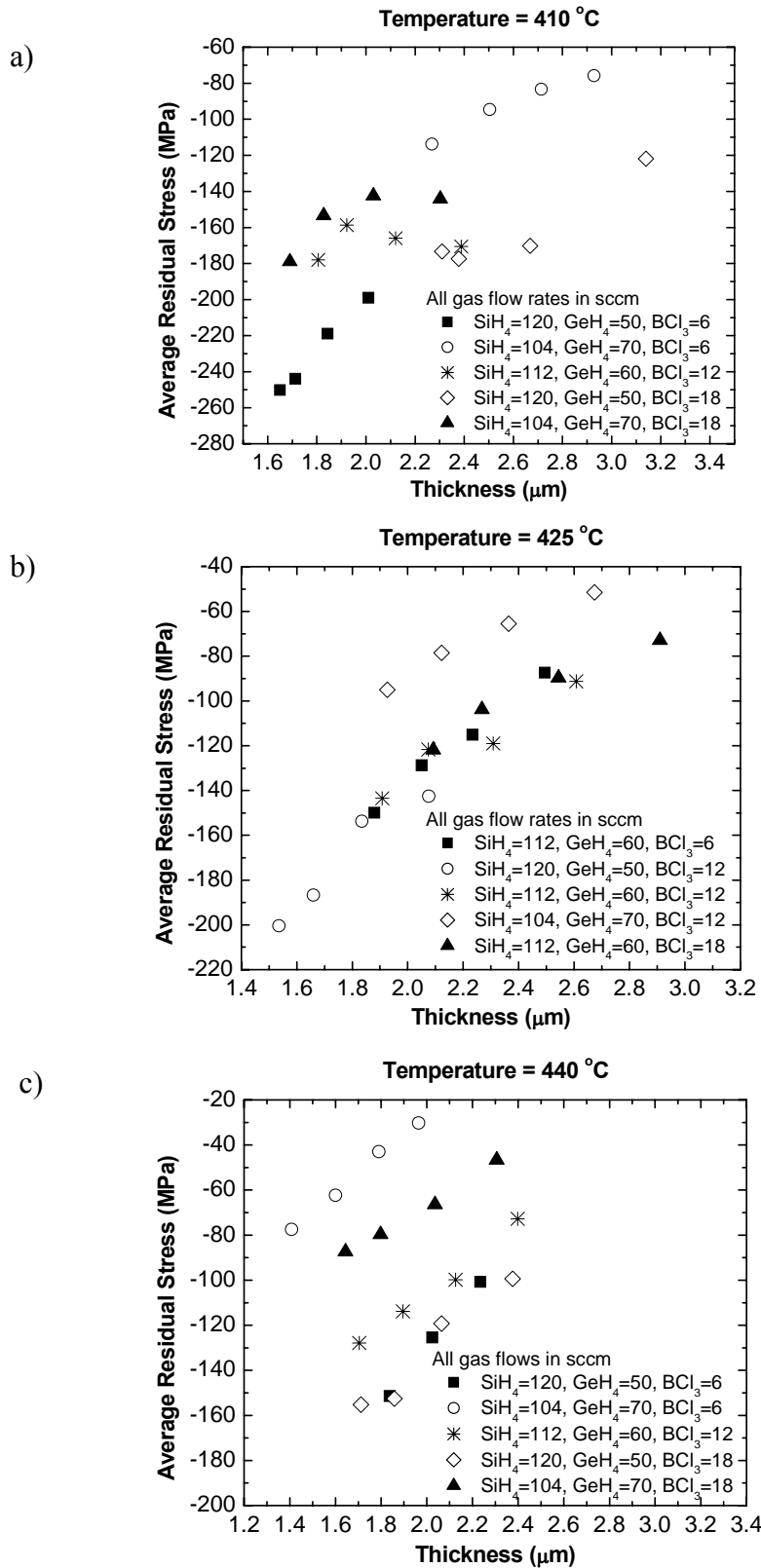


**Figure 4.6** Average residual stress vs. film thickness for films deposited at various temperatures: a) 410°C; b) 425°C; c) 440°C

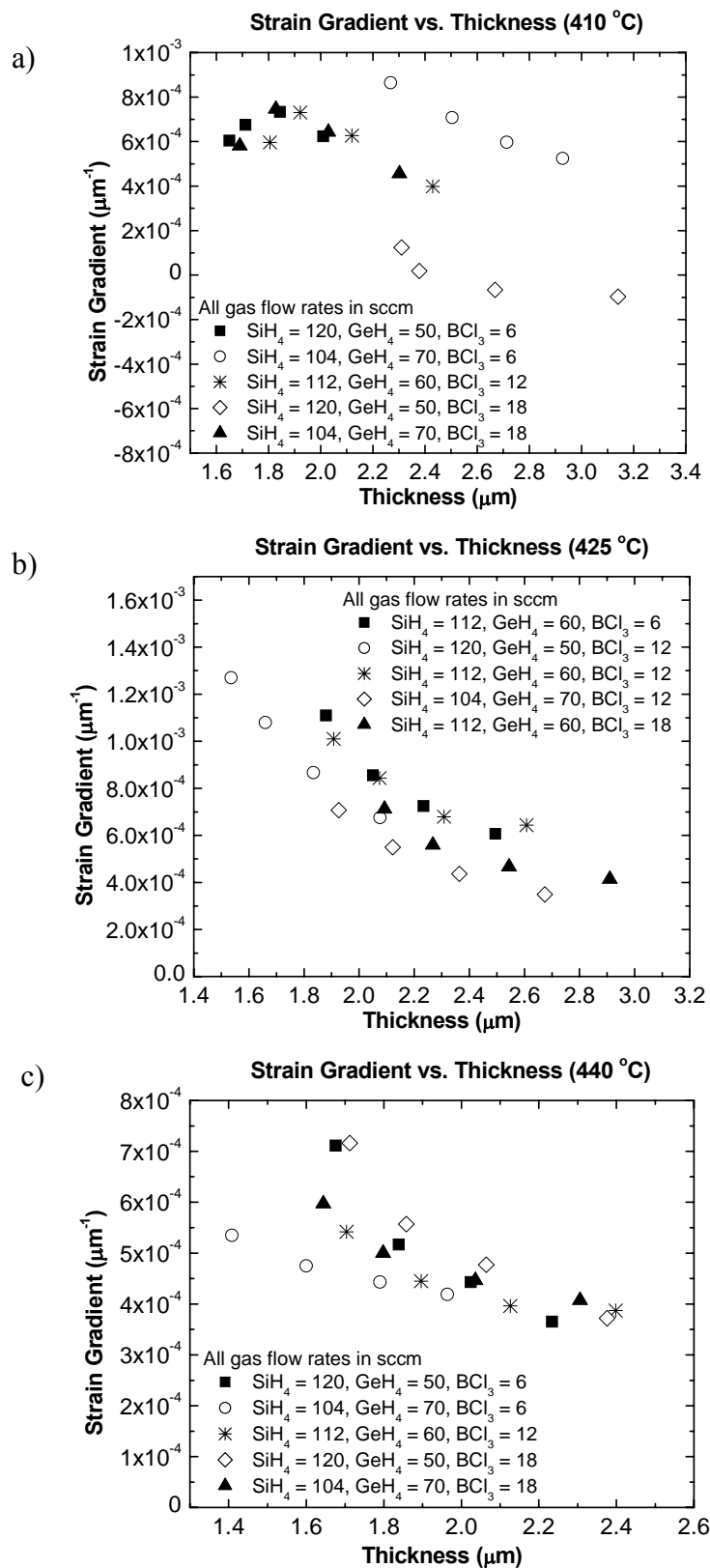


**Figure 4.7** Strain gradient vs. film thickness for films deposited at various temperatures: a) 410°C; b) 425°C; c) 440°C

Figure 4.8 shows the correlation of strain gradient with resistivity, for 2- $\mu\text{m}$ -thick films. Five measurements were taken from each wafer. It should be noted that the dopant injector is not well-optimized for uniformity; so there is variation in film resistivity across the wafer. Since the deposition rate does not depend on dopant concentration, the film thickness is fairly uniform across the wafer. For films deposited at 410°C, the strain gradient increases with resistivity, but there is no significant correlation seen for films deposited at 425°C or 440°C.

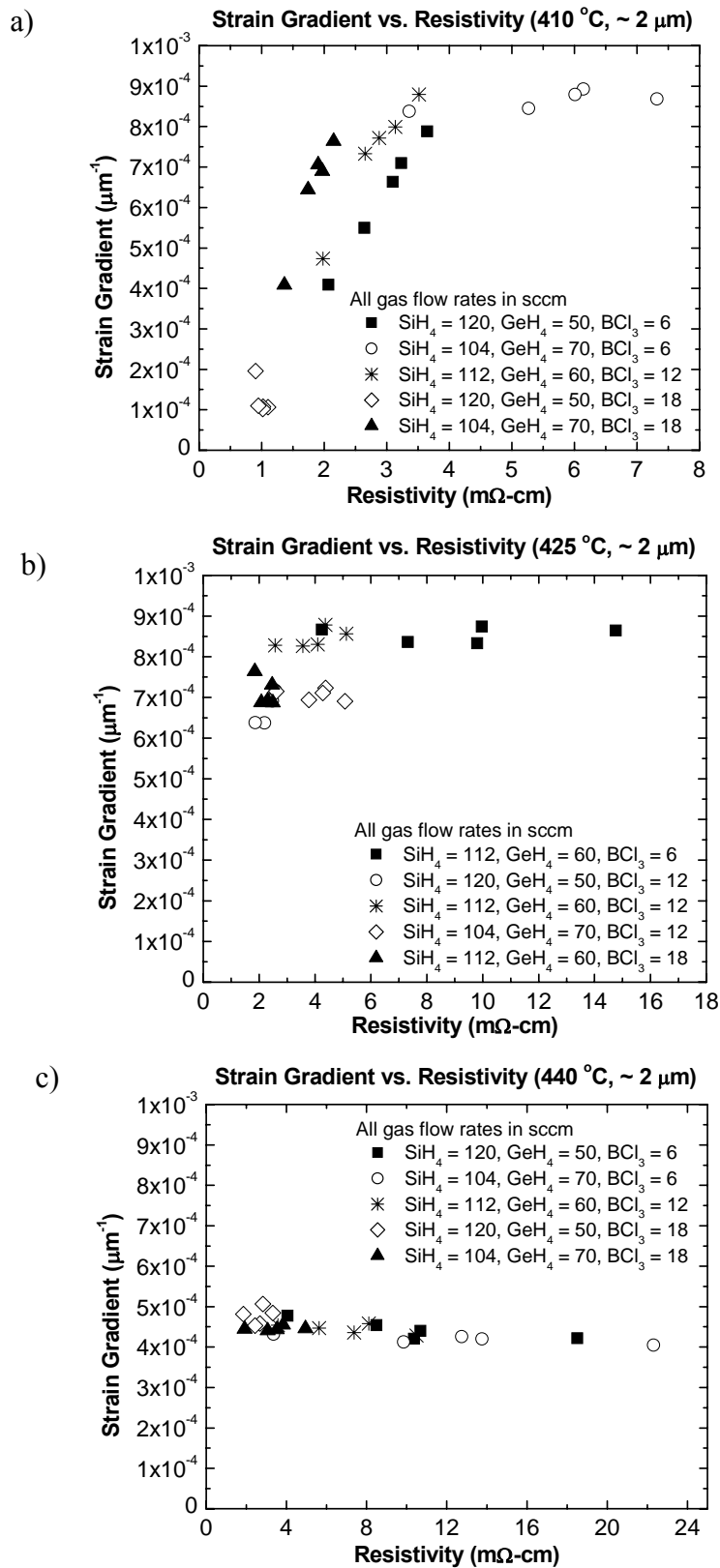


**Figure 4.8** Strain gradient vs. resistivity for 2- $\mu\text{m}$  thick films deposited at various temperatures: a) 410°C; b) 425°C; c) 440°C

The microstructure of selected films was studied by transmission electron microscopy (TEM). The images are shown next to the stress profile in Figure 4.5. Comparing the films deposited with Recipes DOE1-1 and DOE1-4, they are both deposited at 410°C but with different BCl<sub>3</sub> flow rates. The more heavily doped film has a thinner amorphous layer at the bottom of the film. This is consistent with previous reports that *in-situ* boron doping enhances the crystallinity of poly-SiGe [4.11]. In addition, the more heavily doped film has a vertically uniform grain structure through its thickness. The microstructure depth profiles correlate well with the stress depth profile measurements shown to the left. At the oxide-substrate interface, the film is amorphous and hence has highly compressive stress. Furthermore, the film with lower boron concentration has a conical grain structure and the variation in grain size along the film thickness results in a larger stress gradient.

The cross-sectional TEM image of films deposited at 440°C (Recipe DOE1-13 and DOE1-14) are also shown in Figure 4.5(m) and Figure 4.5(n). There is no significant difference in the microstructures for these two films although they have different doping level and germanium content. Due to the higher deposition temperature, the film is polycrystalline at the oxide substrate interface. As the film grew, the average grain size increased, so that the grains are conical. The stress profile shown to the left indicates that the highest compressive stress is located at the bottom of the film where the average grain size is smallest, which results in an upward curvature of the released film. As seen in Figure 4.8(b) and Figure 4.8(c), the strain gradients of the films deposited at 425°C and 440°C do not depend on the boron concentration. Thus it is very likely that the thermal effect is more significant for crystallinity compared to the boron doping effect. The

440°C recipes yield films with lower strain gradient compared to the 425°C recipes, possibly because the stress is relieved by *in-situ* annealing during the higher temperature deposition.

Comparing the TEM images of DOE1-3 and DOE1-13 in Figure 4.5(c) and Figure 4.5(l), the only difference in deposition condition is the temperature. Since higher temperature enhances crystallization, the crystal seeding of DOE1-13 starts earlier and has a higher density. The growth rate of the crystals also increases with temperature and the film in DOE1-13 is rougher at the surface. The microstructures of both recipes are conical in shape and have high strain gradient.

Revisiting Figure 4.8(a), it seems very promising to reduce the strain gradient by increasing the boron doping for films deposited at low temperature (near the amorphous-to-polycrystalline transition temperature). For a closer examination of the strain gradient vs. resistivity trend, all of the data for films deposited at 410°C are plotted in Figure 4.9. Figure 4.9(a) shows the data for two recipes yielding a linear correlation between strain gradient and resistivity. The improvement in strain gradient with decreasing resistivity is mainly due to crystallinity enhancement by boron doping. Figure 4.9(b) shows the data for two recipes that do not yield a linear correlation between strain gradient and resistivity. Since these recipes yield films with relatively high resistivity, this suggests that there exists a threshold of minimum boron doping required for crystallinity enhancement. Moreover, this threshold doping level depends on the germanium content: films with higher germanium content have better crystallinity for a given deposition temperature, and the boron doping effect is not as pronounced. Figure 4.9(c) shows the data for the recipe that yields the lowest strain gradient; the released films can have either

positive or negative out-of-plane curvature. The significant cross-load variation makes it difficult to control strain gradient via doping. The variation from wafer to wafer is due to cross-load variations in film thickness and germanium content. The smaller variation in strain gradient across a wafer is a result of microstructure non-uniformity. Since the deposited film consists of a single columnar-grain layer, local variations [4.12], [4.13] in microstructure makes strain-gradient control challenging in the range of  $1 \times 10^{-5} \mu\text{m}^{-1}$  and lower.

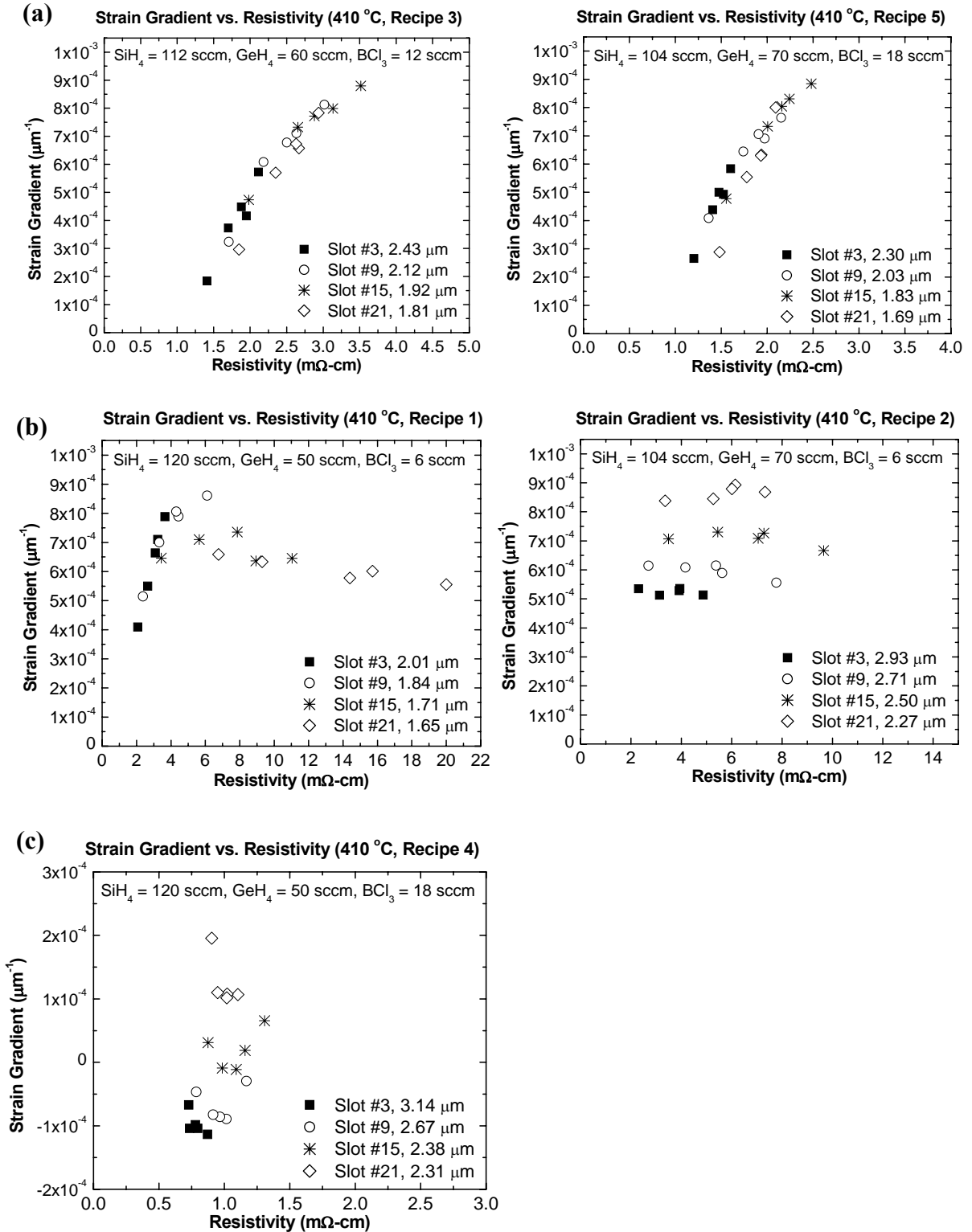


**Figure 4.9** Strain gradient vs. resistivity for films deposited at 410 °C, showing: a) linear correlation; b) non-linear correlation; c) minimum strain gradient

#### 4.4.4 Summary

The design of experiments method has been used to investigate deposition of *in-situ*-boron-doped poly-SiGe films by LPCVD. Films with low resistivity and slow wet-etch rate (in heated H<sub>2</sub>O<sub>2</sub> solution) can be achieved at reasonable rates at low temperatures suitable for post-CMOS MEMS integration. Within the process space explored, all of the films have compressive residual stress; so designers must be aware of the potential for buckling of released clamped-clamped poly-SiGe beams. The minimum achievable strain gradient for a ~2 μm thick single layer of poly-SiGe is at least an order of magnitude higher than desired for inertial sensor applications. The large stress gradient is due to highly compressive stress in the lower portion of the film formed at the beginning of the deposition process. For films deposited at low temperature (near the amorphous-to-polycrystalline transition temperature), crystallinity can be enhanced by *in-situ* boron doping. As a result, films with higher boron doping develop a more columnar microstructure and hence a lower strain gradient. Strain gradient control in the range of  $1 \times 10^{-5} \mu\text{m}^{-1}$  remains a challenge for single step deposition that is ~2 μm thick due to local variations in single-layer columnar microstructures.

#### 4.5 Ramping experiment

##### 4.5.1 Experimental setup

The results of DOE1 show that the initially deposited amorphous region has higher compressive stress compared to the crystalline region, resulting in a positive stress profile within the film thickness. Also, films with conical microstructures have large strain gradients due to variations in grain size. Starting the deposition at high temperature

and high Ge content can enhance initial crystallization and the amorphous region at the oxide surface can be reduced.

To understand how the germanium content and temperature variation could affect the microstructure, a set of ramping experiment was performed. This set of experiment consists of a reference recipe (Ramp-ref), a SiH<sub>4</sub> flow ramp-up recipe (Ramp-SiH<sub>4</sub>) and temperature ramp-down recipe (Ramp-temp) as listed in Table 4.2. The SiH<sub>4</sub>-to-GeH<sub>4</sub> ratio is increased or the process temperature is decreased during the deposition in this experiment. All recipes have constant pressure, GeH<sub>4</sub> and BCl<sub>3</sub> flow rates. Higher BCl<sub>3</sub> flow rate 30 sccm was used to improve the resistivity uniformity. The reference recipe has constant temperature at 430°C and constant SiH<sub>4</sub> flow rate at 140 sccm. The SiH<sub>4</sub> flow ramp-up recipe has a constant temperature at 430°C. It has a step time of 30 minutes and the SiH<sub>4</sub> flow rate is ramped up from 140 sccm by +5 sccm at each step until reaching 190 sccm. The temperature ramp-down recipe has a constant SiH<sub>4</sub> flow rate at 140 sccm. It has a step time of 30 minutes and the temperature is ramp down from 430°C by -5°C at each step till 380°C. For both ramping recipes, the vacuum was not broken between steps to ensure continuous grain growth.

The process conditions of all three depositions are shown in Figure 4.10-12. As discussed in Chapter 2, the process temperature has sinusoidal fluctuations at constant set point and this phenomenon can be seen again in Figure 4.10 for the reference recipe. The process pressure and the gas flow rates are very stable. For the SiH<sub>4</sub> flow ramp-up deposition shown in Figure 4.11, the SiH<sub>4</sub> MFC can quickly follow the input value and has a step response. The temperature ramp-down deposition has the process temperature following the set point with some oscillation, as shown in Figure 4.12.

### Reference Run

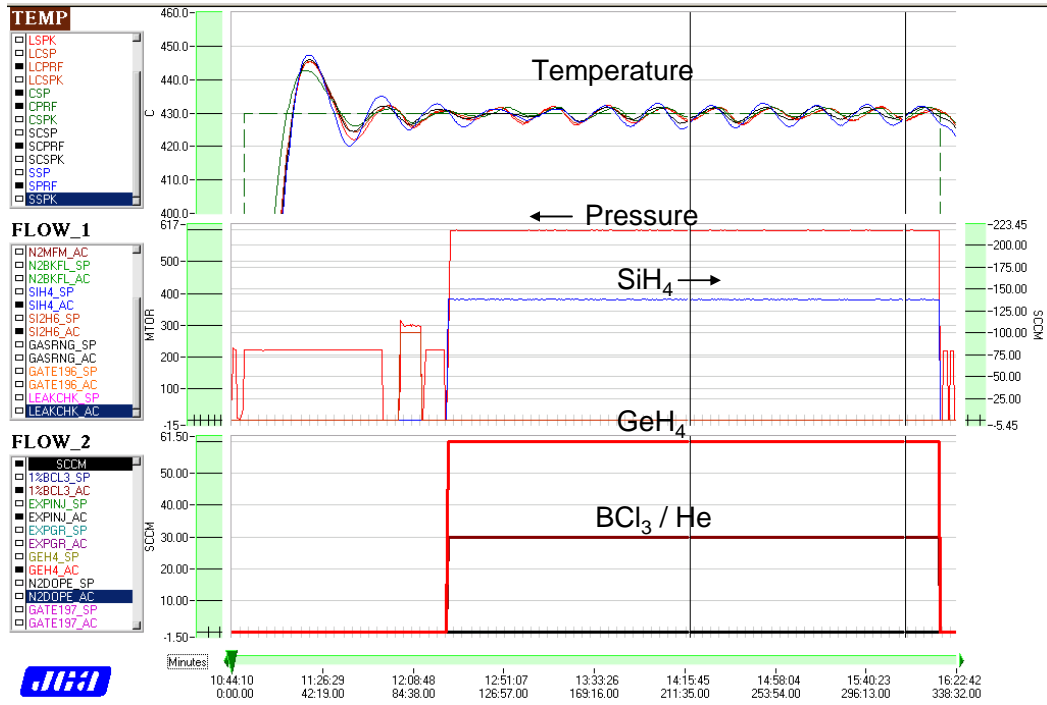


Figure 4.10 Process conditions of the reference deposition (Ramp-ref)

### SiH<sub>4</sub> Ramp Up

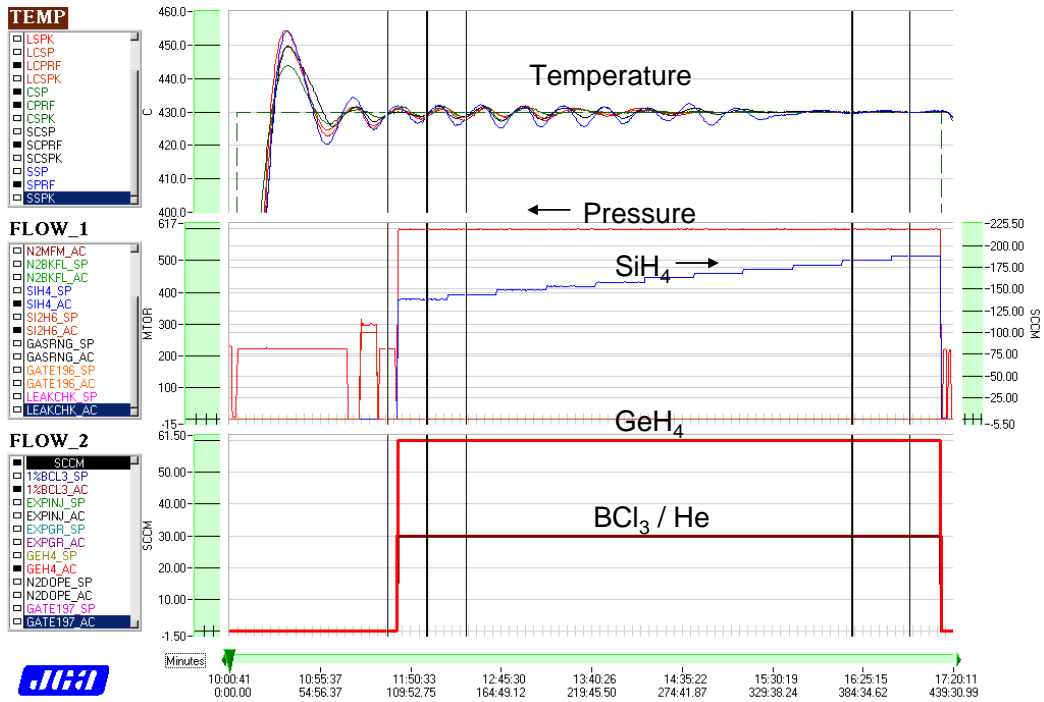
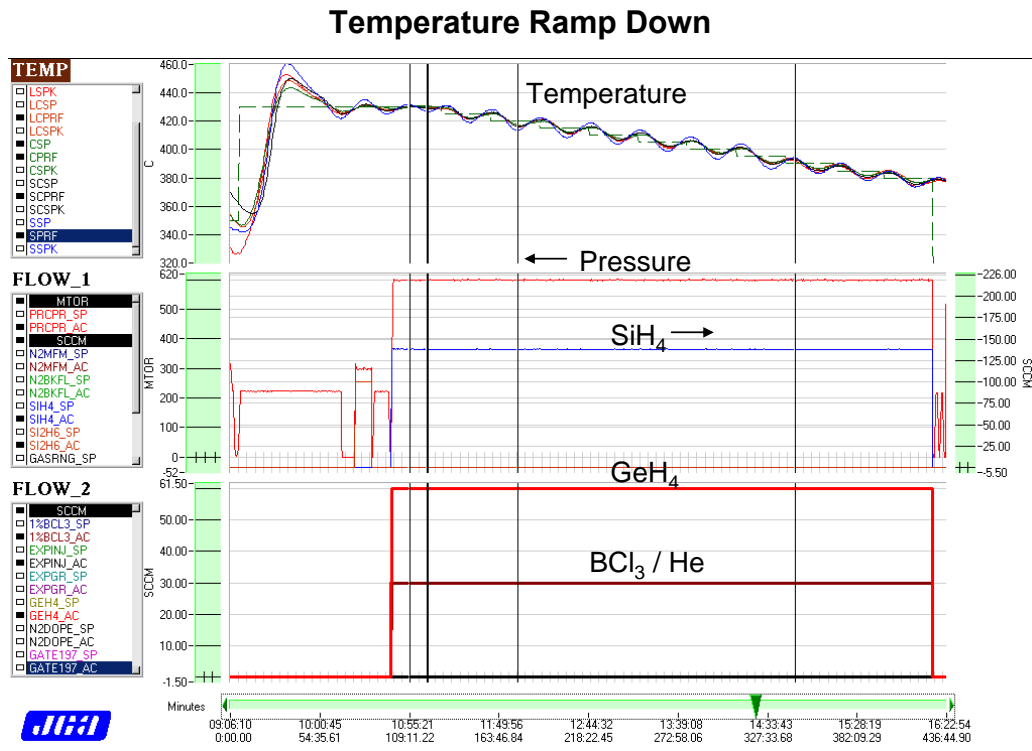


Figure 4.11 Process conditions of the SiH<sub>4</sub> flow ramp-up deposition (Ramp-SiH<sub>4</sub>)



**Figure 4.12** Process conditions of the temperature ramp-down deposition (Ramp-temp)

#### 4.5.2 Results and interpretation

The data of the ramping experiments are listed in Table 4.2. All of the depositions targeted film thickness of 2  $\mu\text{m}$ . The deposition rate for the two ramping recipes was underestimated and films are thicker than expected. Comparing to DOE1, resistivity uniformity is improved with high  $\text{BCl}_3/\text{He}$  flow rate. Since the stress and strain gradient vary with film thickness, wafers with 2.3  $\mu\text{m}$  thick film from these three runs are being compared for mechanical properties. The reference run (Ramp-ref), the  $\text{SiH}_4$  flow ramp-up run (Ramp- $\text{SiH}_4$ ) and the temperature ramp-down run (Ramp-temp) have average residual stress of -109 MPa, -140 MPa and -183 MPa. The result for average residual stress is as expected. Low germanium content and low temperature films have higher

compressive stress. Since all recipes have the same starting layer, the larger compressive stress is from the low germanium content or low temperature top layers.

The strain gradients for the 2.3  $\mu\text{m}$  thick film from each recipe have no significant differences; all are around  $4.5 \times 10^{-4} \mu\text{m}^{-1}$ . The stress profile and the cross-sectional TEM images are shown in Figure 4.13. Considering the measurement errors, the stress profiles of the three recipes do not show a significant difference. Also, the microstructures of the three recipes have similar conical texture.

It should be noted that the last few layers of the  $\text{SiH}_4$  flow ramp-up run and the temperature ramp-down run would give amorphous films if they were deposited directly on oxide. Since the grain growth is continuous, the low Ge content or low temperature layers follow the “footprint” of the existing polycrystalline grain structure and continue to be polycrystalline. The surface roughness of the temperature ramp-down recipe is significantly lower than the reference recipe due to the low processing temperature later in the deposition.

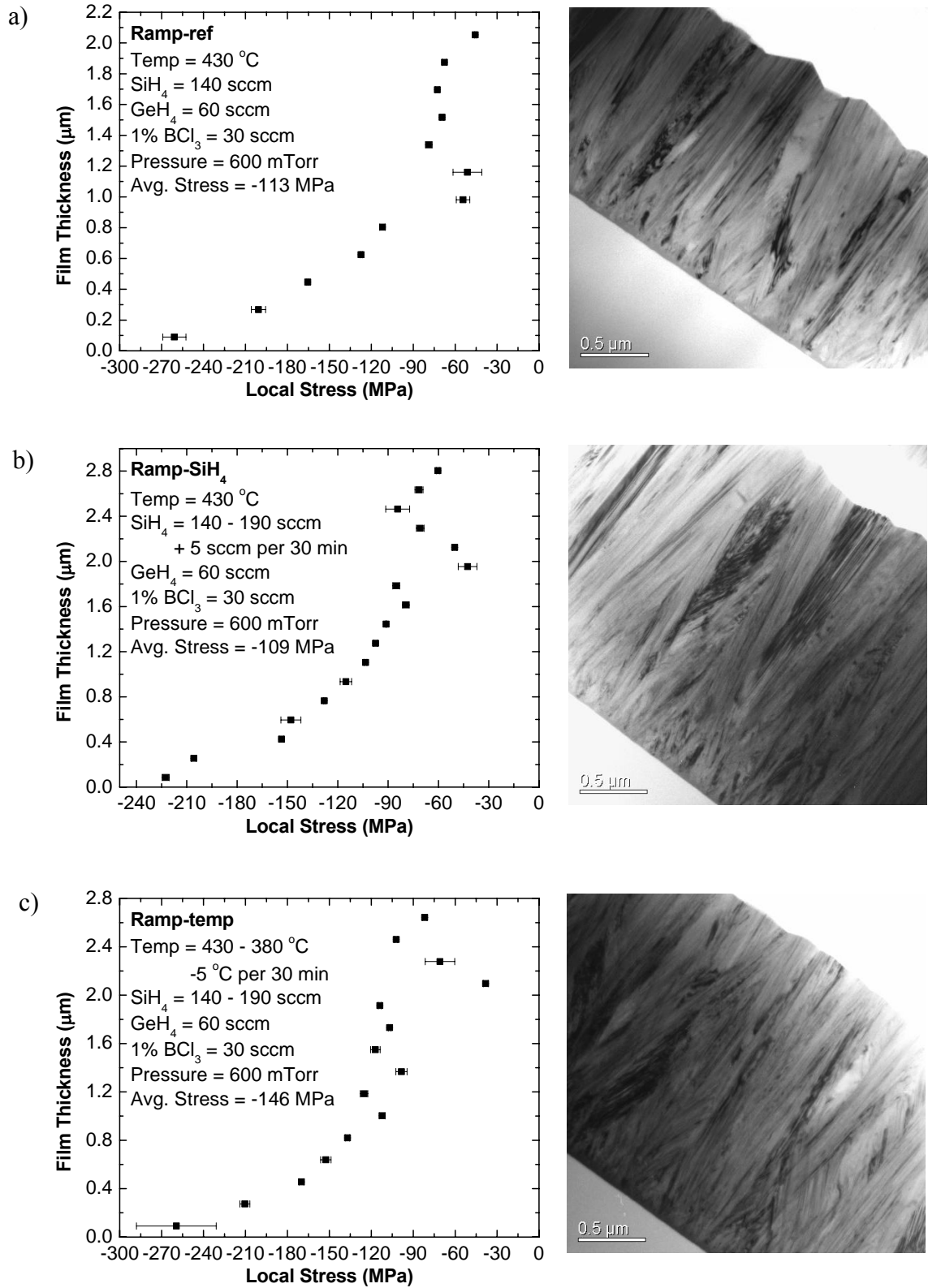


Figure 4.13 Stress profiles and cross-sectional TEM images for the ramping experiments

### 4.5.3 Summary

The set of ramping experiments show that ramping up the  $\text{SiH}_4$  flow rate or ramping down the process temperature during the deposition increases the average compressive stress in the film and does not improve strain gradient. The lower germanium content or lower temperature deposition slows down the deposition rate and lateral diffusion rate becomes significant. All films in this experiment have conical microstructures with high strain gradient. The temperature ramp down recipe is desired for reducing thermal budget without sacrificing the deposition rate or resistivity, but temperature control is problematic with the Tystar furnace at low deposition temperatures.

## 4.6 2<sup>nd</sup> design-of-experiments

### 4.6.1 Experimental setup

The 1<sup>st</sup> DOE shows that recipes utilizing low  $\text{BCl}_3$  flow rate tend to have worse cross-wafer uniformity in resistivity due to gas depletion effects. Also, at low deposition temperature ( $410^\circ\text{C}$ ), strain gradient decreases with resistivity. The  $\text{BCl}_3$  mass flow controller was re-calibrated from 20 sccm range to 50 sccm range after DOE1. Higher  $\text{BCl}_3$  gas flow rate of 15 sccm, 30 sccm and 45 sccm were used in DOE2, in order to look into improvement in resistivity uniformity and strain gradient with higher doping levels.

Variation in pressure is also explored in DOE2. Higher process pressure enhances deposition rate, but film thickness uniformity will be sacrificed if the deposition is so fast that it is no longer limited by the surface reaction rate. DOE1 used 600 mTorr process pressure. This process pressure results in reasonable deposition rate with good film

thickness uniformity. A few short test runs (DOE2-t1 through DOE2-t5 listed in Table 4.2) were performed to understand the process pressure range for DOE2. The test runs show that the deposition rate increases with process pressure, but films deposited at pressure above 700 mTorr are very rough with significant color variation across the wafer. Gas phase nucleation happened in these cases. With high process pressure, some nucleation happens before the gas molecules reach the wafer surface [4.14]. The clusters formed in gas-phase nucleation coat the wafer surface later. Diffusion is limited on the wafer surface for these clusters and the film on the wafer is porous and has poor uniformity. The process pressures for DOE2 were chosen as 350 mTorr and 600 mTorr.

The six depositions of the 2<sup>nd</sup> DOE with BCl<sub>3</sub> flow rate and process pressure as variables are listed in Table 4.2. A deposition temperature of 410°C and germanium content of ~60% were chosen based on the results from DOE1. All depositions targeted film thickness of 2 μm. Reducing the strain gradient is the main goal for this set of experiments.

#### **4.6.2 Results and interpretation**

The results are also summarized in Table 4.2. Higher BCl<sub>3</sub> flow rate enhances the deposition rate. Higher BCl<sub>3</sub> flow rate also reduces the gas depletion effects and improves the cross wafer resistivity uniformity. Lower process pressure decreases the deposition rate, but improves the cross wafer resistivity uniformity.

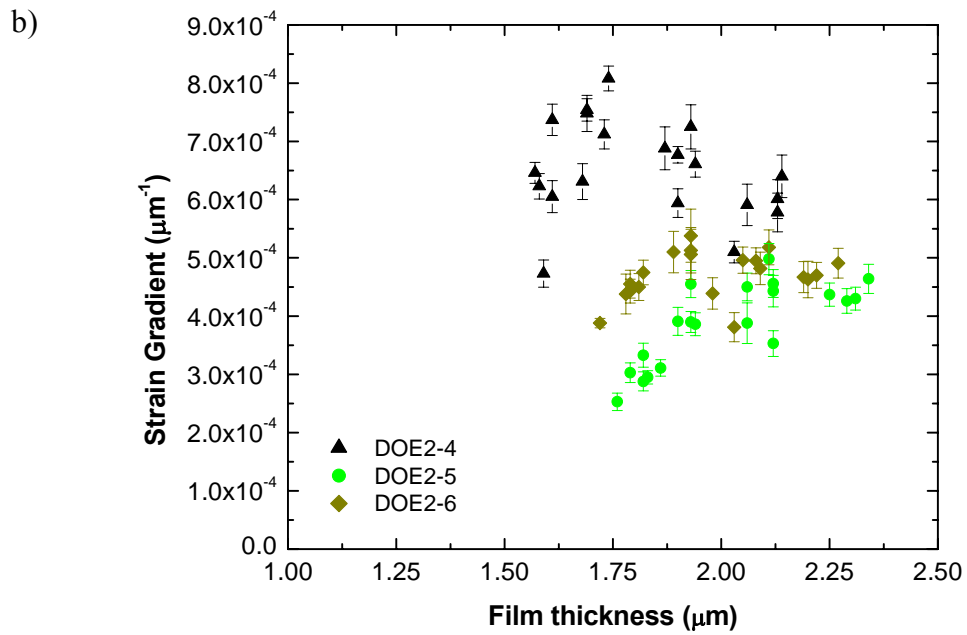
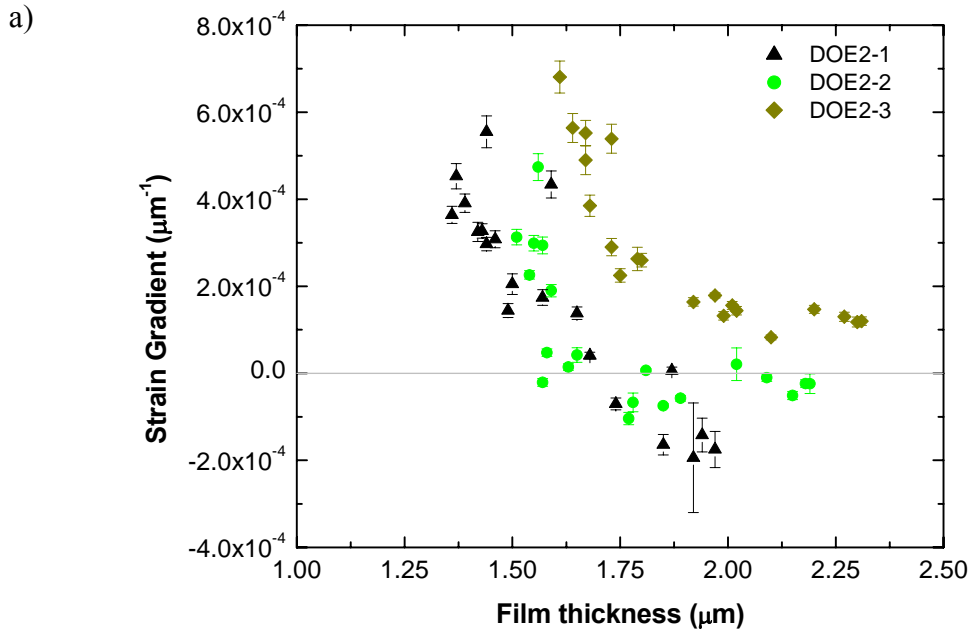
The strain gradient for the films deposited at 600 mTorr (DOE2-1, DOE2-2, DOE2-3) is relatively low, which is consistent with the results from DOE1. Figure 4.14(a) plots the strain gradient against the resistivity for the 600 mTorr runs. For recipe

DOE2-1 with 15 sccm of  $\text{BCl}_3$  flow, the strain gradient decreases with resistivity and this follows the trend from Figure 4.8(a). However, strain gradient becomes independent of doping after resistivity  $< 1 \text{ m}\Omega\text{-cm}$ . Recipe DOE2-2 gives the lowest strain gradient, but there is a significant amount of variation.

Films deposited at 350 mTorr (DOE2-4, DOE2-5, DOE2-6) have relatively high strain gradient. The relationship between strain gradient and resistivity is plotted in Figure 4.14(b). For the 350 mTorr depositions, doping does not help reduce the strain gradient as much as for the 600 mTorr depositions. Lower pressure gives lower deposition rate; so crystallinity enhancement by boron doping is less significant.



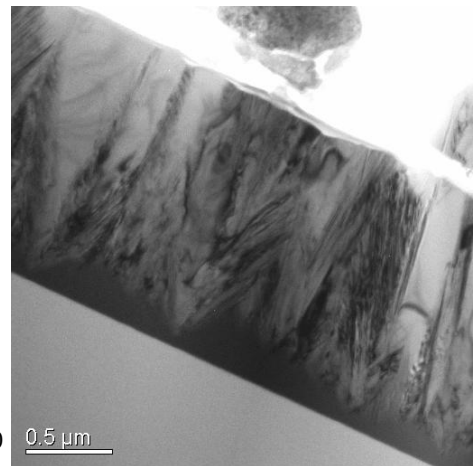
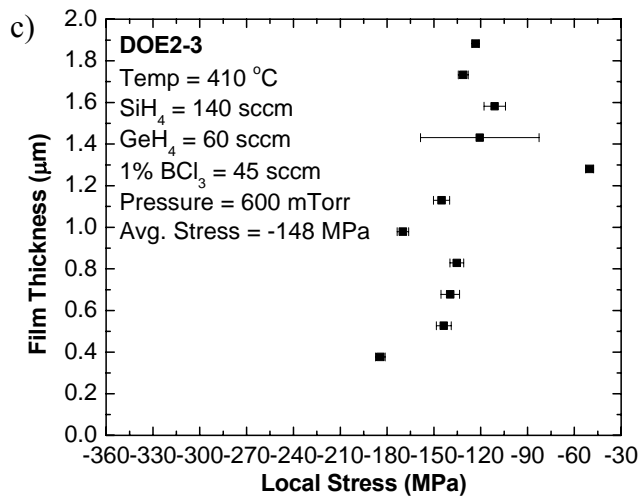
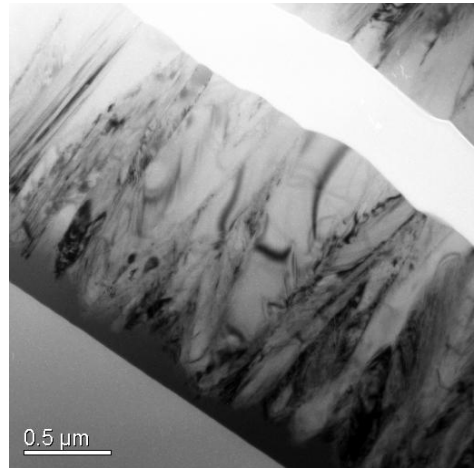
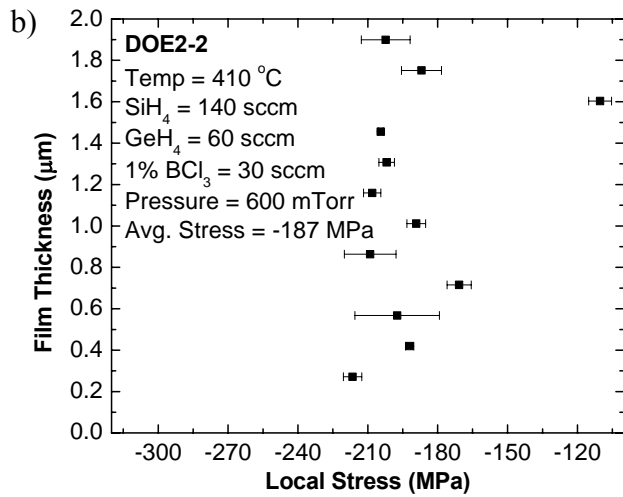
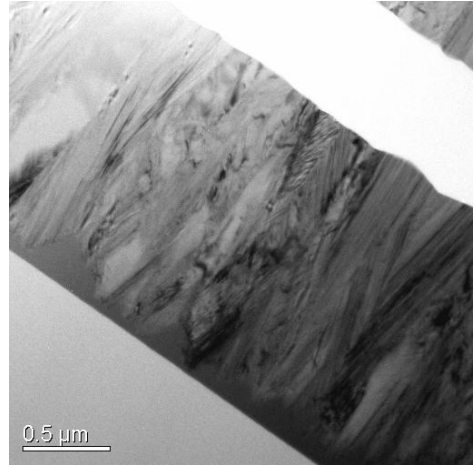
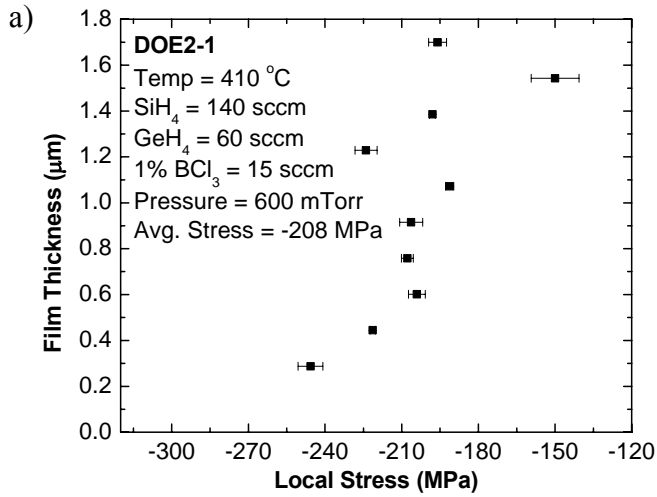
As discussed before, from the same run, there is film thickness variation across the load due to the gas depletion effect with wafers closer to gas inlet having a thicker film. Strain gradient vs. film thickness are plotted in Figure 4.15. For the 600 mTorr depositions, strain gradient decreases with increasing film thickness, but the slope of the trend becomes smaller after a certain thickness for recipes DOE2-2 and DOE2-3. As discussed in the 1<sup>st</sup> DOE, films with strain gradient below  $1 \times 10^{-4} \mu\text{m}^{-1}$  have significant variation across the wafer due to local variation in microstructure. For the 350 mTorr depositions, strain gradient is almost independent of film thickness.



**Figure 4.15** Strain gradient vs. film thickness for DOE2: a) 600 mTorr depositions (DOE2-1, DOE2-2 and DOE2-3); b) 350 mTorr depositions (DOE2-4, DOE2-5 and DOE2-6)

Stress profile and TEM images for each recipe are shown in Figure 4.16. The 600 mTorr depositions have uniform stress profiles along the film thickness, whereas the 350 mTorr depositions have positive stress profiles, corresponding to large strain gradients. Comparing the TEM images of DOE2-1, DOE2-2 and DOE2-3, there are no significant differences in their microstructures. They all have ~200 nm amorphous layers at the bottom. In each film, there are a few grains with very low defect density and others have twinning defects. Recipe DOE2-2 has the lowest strain gradient in this set of experiment and its microstructures have the lowest defect densities. Figure 4.15(a) shows that strain gradient decreases with film thickness for the 600 mTorr depositions. The amorphous portion of the film has higher compressive stress compared to the columnar portion and this contributes to a positive strain gradient. Thicker films consist of a large columnar portion; so the effect of the amorphous portion is reduced.

The film deposited at 350 mTorr (DOE2-5) has a much thinner amorphous region. Also, the low pressure film has a conical texture with twinning defects in all grains. The slope of the stress is roughly constant and the strain gradient does not have a strong dependence on film thickness. In this case, the strain gradient is related to the variation in grain size in the film.



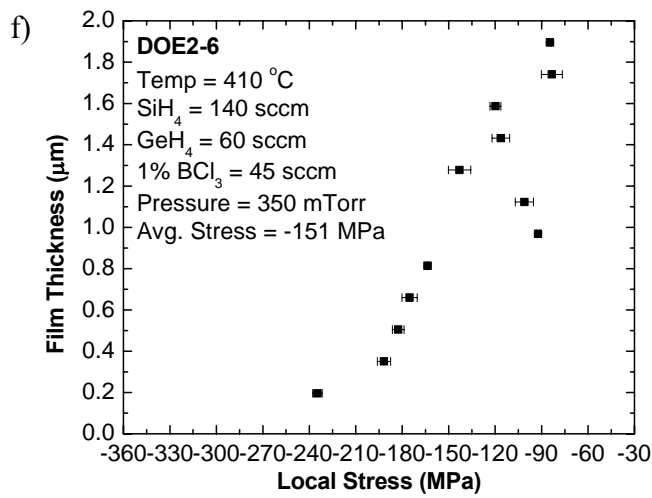
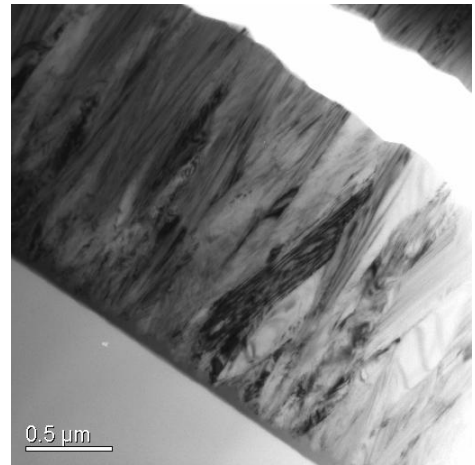
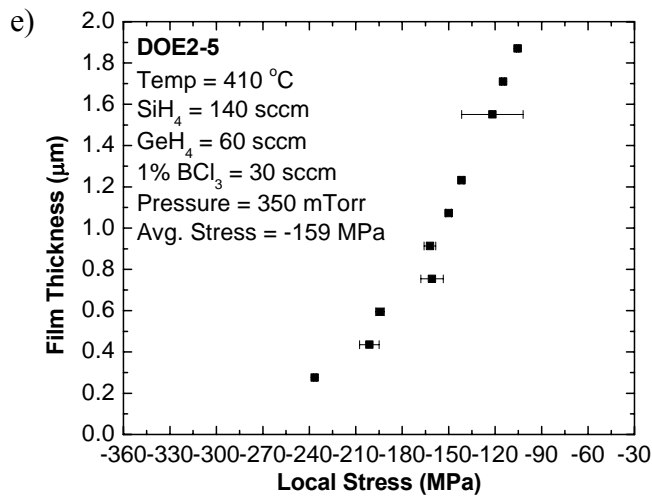
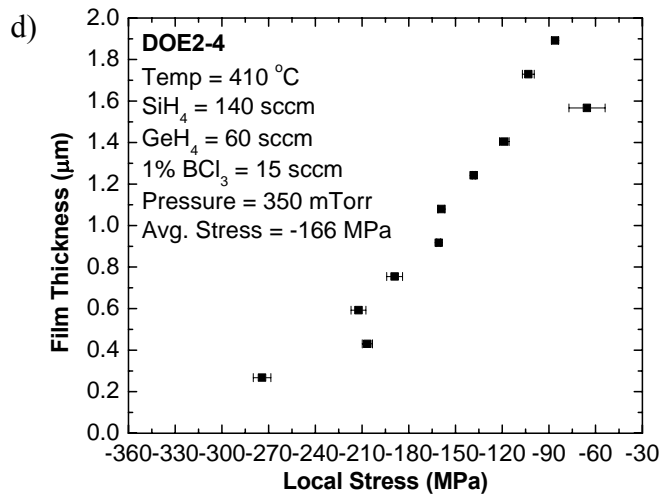


**Figure 4.16** Stress profiles and cross-sectional TEM images for DOE2

Test run DOE2-t4 has similar parameters as run DOE2-2, except for a shorter deposition time. The TEM images from these two runs are put together for comparison in Figure 4.17. Two samples from different boat locations are being studied for the initial grain growth process from run DOE2-t4 with 60 minutes of deposition time. Figure 4.17(a) is a sample from a wafer closer to the gas outlet (slot #15) and Figure 4.17(b) is a sample from a wafer closer to the gas inlet (slot #3). The wafer at the gas outlet has a thinner film and there is still some amorphous region being exposed at the top surface. The wafer closer to gas inlet has a thicker film and the top surface is completely crystallized. The crystal seeds are spaced out about 100 nm apart. The crystals grow vertically and expand laterally. Once the neighboring crystals meet, the amorphous region is covered up. Figure 4.17(c) is a sample from DOE2-2 with 230 minutes of deposition time. We can see that the thickness of the amorphous region for DOE2-t4 and DOE2-2 is about the same. Longer deposition time or *in-situ* annealing at the deposition temperature does not crystallize the amorphous region.

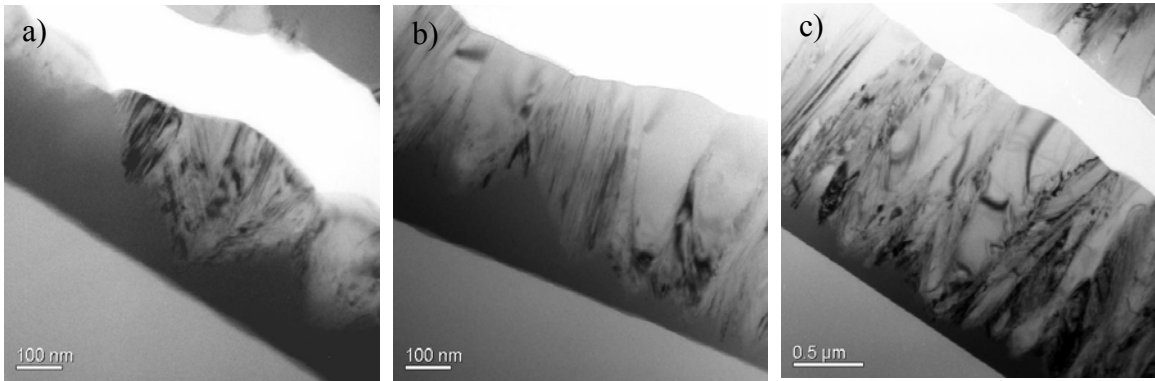


**Figure 4.17** TEM images for recipe 410 °C, 600 mTorr, 140 sccm SiH<sub>4</sub>, 60 sccm GeH<sub>4</sub> and 35 sccm BCl<sub>3</sub>: a) film deposited for 60 minutes at wafer slot #15; b) film deposited for 60 minutes at wafer slot #3; c) film deposited for 230 minutes at wafer slot #9

To further understand the formation of the film deposited by DOE2-2, a special TEM sample was prepared by double-wedge technique for top view imaging at various depths. The double-wedge TEM analysis is courtesy of Dr. Erdmann Spiecker of the National Center for Electron Microscopy at Lawrence Berkeley National Laboratory. Depth profile quantification is still being studied. Images in Figure 4.18 are taken at the same magnification from the bottom to the top of the film. More pictures are taken at the lower portion (the first 0.5 μm) of the film where the grain evolution occurs. These images clearly show the grain growth process during the deposition. Near the sacrificial oxide layer, the SiGe film has a transition zone from amorphous to polycrystalline. The sparse crystalline seeds start among the amorphous region. As the deposition goes along, the seeding density and crystal size increase. Eventually, the film becomes fully crystalline and the grains reach their final lateral size once the film reaches 0.4 μm in thickness.

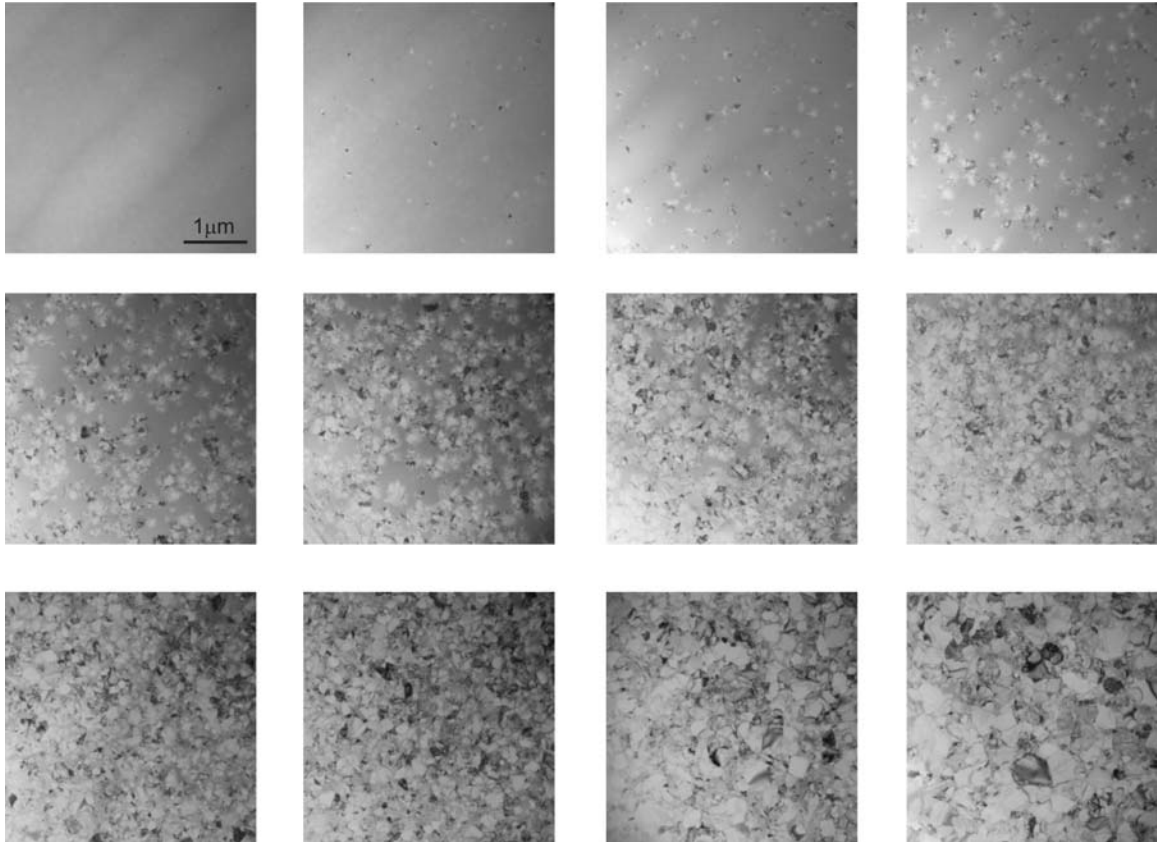


**Figure 4.18** Top view TEM images for film deposited with recipe DOE2-2 at various depths (Courtesy of Dr. Erdmann Spiecker)

#### 4.6.3 Summary

The 2<sup>nd</sup> DOE confirms the low strain gradient result from the 1<sup>st</sup> DOE. The optimal recipe for low strain gradient film is found to be: 410 °C, 600 mTorr, 140 sccm SiH<sub>4</sub>, 60 sccm GeH<sub>4</sub> and 35 sccm BCl<sub>3</sub>. The low strain gradient film consists of a thin amorphous region at the oxide interface and columnar crystalline microstructure with very few defects. The films consist of a single layer microstructure and low range strain gradient  $< 1 \times 10^{-4} \mu\text{m}^{-1}$  is very sensitive to small variation in microstructure. The thickness variation of the amorphous region results in large variation in strain gradient.

Increasing the overall film thickness will increase the polycrystalline portion of the film and the effect of the bottom amorphous layer will be minimized. Also, thicker films result in beams that are stiffer for out-of-plane bending, which reduces the impact of the strain gradient. Multilayer depositions with separate  $\text{Si}_2\text{H}_6$  nucleation might create several layers of microstructures. The randomness of microstructure could be averaged out, resulting in better strain gradient uniformity. The thick film deposition and the layer stack experiments will be discussed in the following sections.

#### **4.7 Thick deposition**

Using the optimal recipe from DOE2 with a longer deposition time, thicker films are being studied. This experiment targets film thickness of 4  $\mu\text{m}$ , whereas all previous experiments targeted film thickness of 2  $\mu\text{m}$ . The results of the thick deposition (ThickDepo) are summarized in Table 4.2. Figure 4.19 shows a SEM image of a released cantilever beam array. The strain gradient of this film is very small and the tip deflection of the cantilever beam is hardly visible. The strain gradient vs. thickness for the thick deposition is plotted together with results from DOE2 in Figure 4.20. As expected, the strain gradient and its uniformity are improved as the film thickness increases. The strain gradient reaches the range of  $1 \times 10^{-5} \mu\text{m}^{-1}$ . The variations across the load and across the wafer are also significantly smaller.

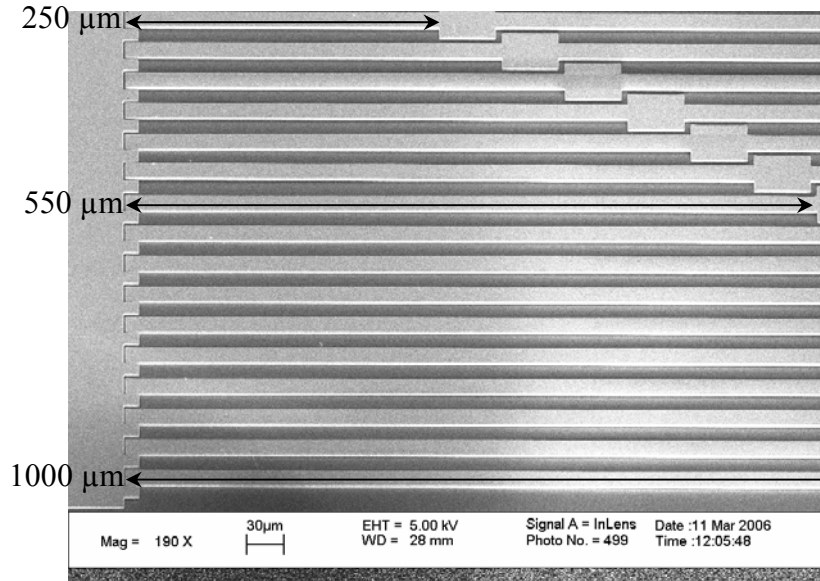


**Figure 4.19** SEM image of released cantilever beam array for Recipe ThickDepo.

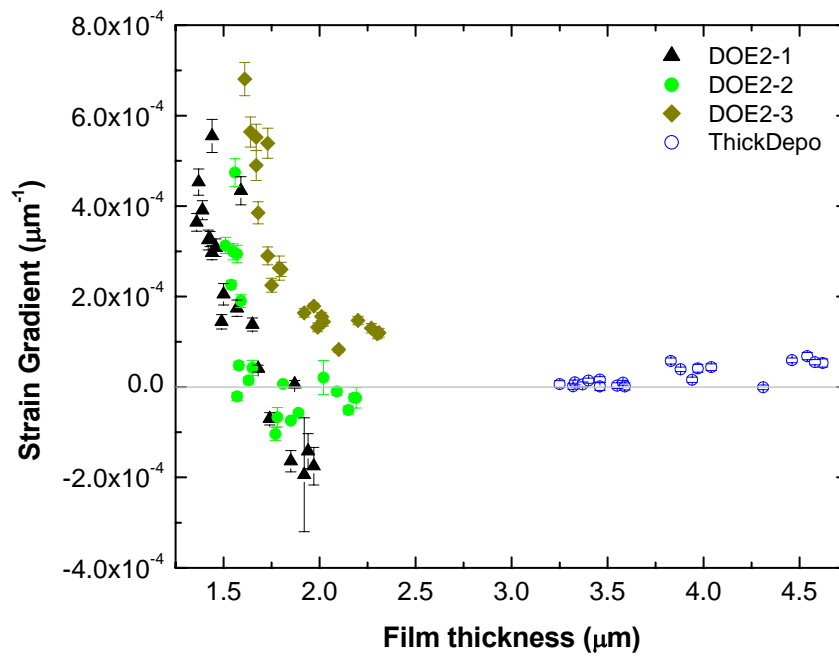


**Figure 4.20** Strain gradient vs. film thickness plot

The stress profile and the cross sectional TEM image for the thick deposition are shown in Figure 4.21. The stress profile through the film thickness is relatively uniform. The film consists of a large portion of columnar microstructure and the defect density within each grain is very low. This thick film has similar deposition condition as DOE2-2, except for slightly higher  $\text{BCl}_3$  flow rate and longer deposition time. Comparison of the stress profile and the microstructure of this thick film with DOE2-2 shown in Figure 4.16(b) can be made. The thicker film has slightly lower (less compressive) stress, especially for the stress in the lower portion of the film. Some of the stress might be released due to *in-situ* annealing during the long deposition. In both cases, the thickness of the amorphous region is similar, but the thicker film has taller columnar grains. Thus, a larger portion of the thicker film consists of columnar crystalline structures.

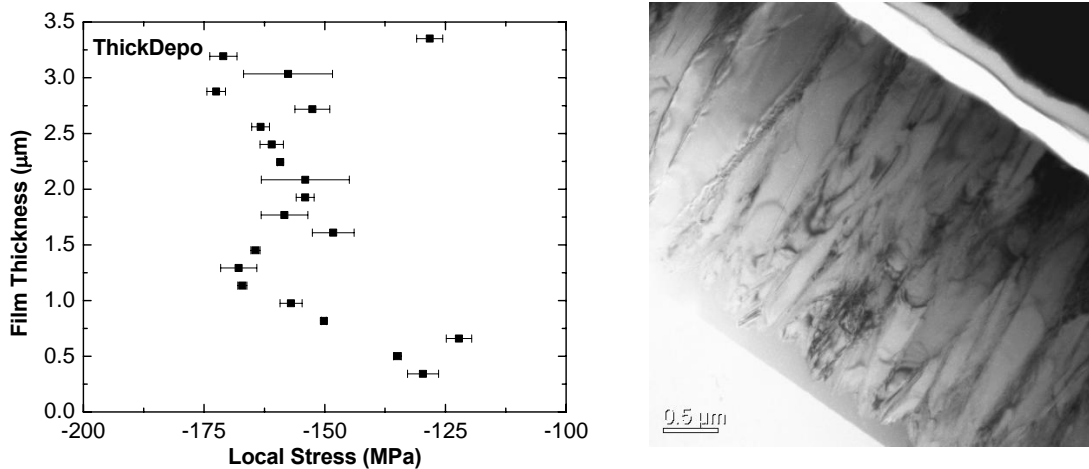


**Figure 4.21** Stress profile and cross sectional TEM image for recipe ThickDepo

#### 4. 8 Multiple-layered film deposition

Fine-grained poly-Si films with low strain gradient have been demonstrated to be sufficiently reproducible for high-volume production [4.4]. If the average grain size in a poly-SiGe film is comparable to its thickness, there can be considerable variation in mechanical properties from beam to beam, which is not acceptable for high-volume manufacturing processes. The average grain size can be limited by depositing the film in multiple steps to create a layered stack, to average out random variations in grain microstructure and modify the stress-vs.-depth profile.

As a proof-of-concept experiment, Recipe LayerStack in Table 4.2 consists of four 85-minute depositions of Recipe DOE2-5. To ensure grain growth interruption from layer to layer, the vacuum was broken in-between the depositions by opening the furnace door. The disadvantage of this approach is that the temperature has to re-stabilize and temperature overshoot occurs during the stabilization. As a result, more processing time is required and hence the thermal budget is larger. With a more sophisticated LPCVD reactor, it should be possible to simply flow O<sub>2</sub> in-between depositions to avoid the need to open the door, so that the furnace temperature can remain stable throughout the film deposition process and therefore process throughput would not be affected significantly.

The stress distribution within the layered film and the cross sectional TEM image are shown in Figure 4.22. The stress profile of the layered film also consists of four regions, each very similar to the stress profile for the bottom quarter of the film shown in Figure 4.16(e) for recipe DOE2-5. Every layer within the film is very similar to the bottom quarter of the film shown in Figure 4.16(e). Overall, the stress distribution with the multiple-layered film is more uniform as compared to a single-layered film, so that

the absolute value of the strain gradient is smaller. Due to unintentional heating during temperature stabilization, the earlier deposited layers were annealed so that their amorphous regions are partially crystallized, resulting in a downward curvature (negative strain gradient) of the released cantilever beam. This fine-grained layered-stack film ends up with a strain gradient of  $-1.2 \times 10^{-4} \mu\text{m}^{-1}$ . Finer grains and more uniform stress distribution can be achieved with more layers. To avoid having a negative strain gradient, a fully crystallized film should be used because of its better thermal stability.

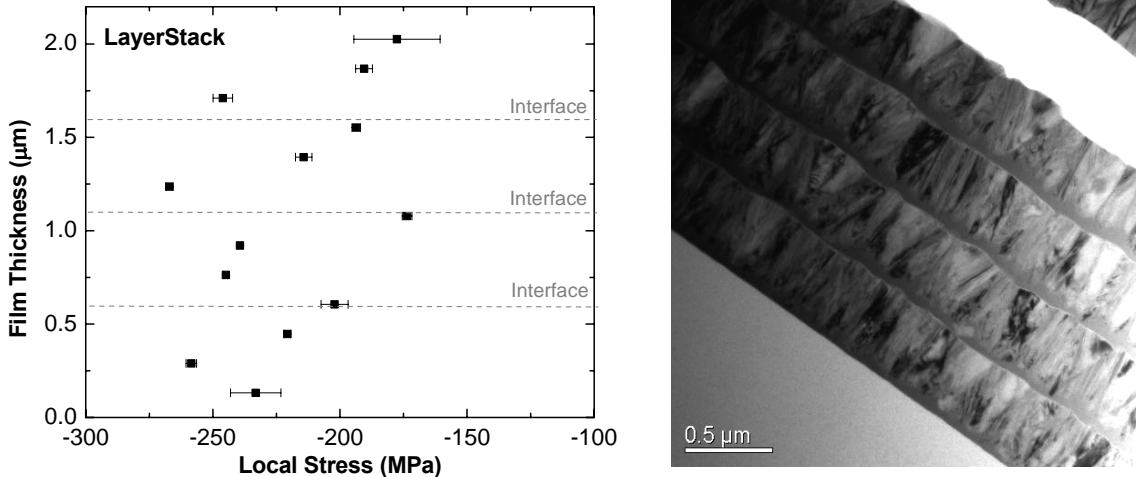


**Figure 4.22** Stress profile and cross sectional TEM image for Recipe LayerStack

#### 4.9 Seeding layer experiments

Previous TEM images show that the SiGe film starts out amorphous at the oxide interface for deposition temperature lower than 440 °C with Si<sub>2</sub>H<sub>6</sub> seeding. For low strain gradient film, the thickness variation of this amorphous region causes a uniformity problem. This section discusses methods to minimize the amorphous region and its effects on strain gradient.

In the interest of lowering the thermal budget, a 410°C deposition temperature is being studied here. All of the previous experiments show that films deposited at 410°C have an amorphous starting layer, but eventually crystallize. In the earliest stage of film formation, the nuclei are spaced far apart. Before they can diffuse on the surface to find low energy crystal lattice sites, they are pinned to the substrate by subsequently absorbed atoms (adatoms). Eventually, these adatoms form clusters serving as crystal seeds and subsequently adatoms can attach to crystal seeds, resulting in their growth. To initialize the crystallization earlier in the deposition, a lower deposition-rate seeding layer could be used.

A quick test on this crystallization hypothesis was done with a low gas flow rate and low pressure at 410°C (SiGeSeed-t1 listed in Table 4.2). In this recipe, low pressure and low SiH<sub>4</sub> and GeH<sub>4</sub> flow rates are used to reduce the deposition rate. BCl<sub>3</sub> flow rate stays high to enhance crystallization. At low deposition rates, gas molecules have more time to settle down at low energy crystal lattice sites on the wafer surface before the next gas molecules are adsorbed. The cross sectional TEM image is shown in Figure 4.23. Fully crystallized films are achieved at the oxide interface at 410°C with ~60% germanium content.

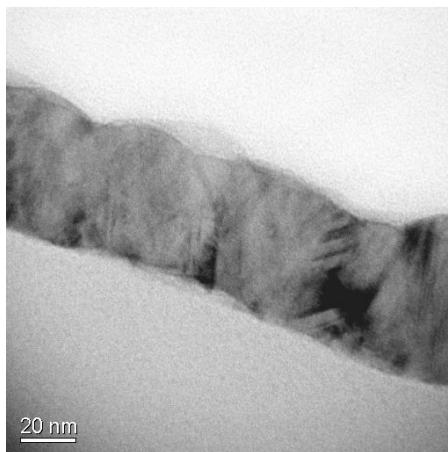


**Figure 4.23** Cross sectional TEM image for film deposited with recipe SiGeSeed-t1

The above recipe (SiGeSeed-t1) is used as the seeding layer for deposition SiGeSeed-1 (listed in Table 4.2). After the thin crystallized seeding layer deposition, the most optimal recipe from DOE2 was used for the main deposition. The vacuum was not broken between the seeding layer and the main deposition. The process pressure and gas flow rates are ramped up immediately in the process recipe. This recipe was intended to grow a columnar microstructure without an amorphous region at the oxide interface.

The stress profile and cross sectional TEM image of recipe SiGeSeed-1 is shown in Figure 4.24. The film is indeed fully crystallized, but the texture is conical rather than columnar. The initial low pressure and low gas flow rates seeding recipe enhances crystalline seeding due to the resultant low deposition rate and high boron concentration. Fine crystal grains formed during the initial stage of film deposition compete for lateral growth, resulting in a conical grain structure and high strain gradient. Since there is variation in grain size through the film thickness, there is also variation in the stress distribution. At the bottom of the film where the randomly oriented grains compete to

grow, higher compressive stress is developed. This film has high strain gradient. During the grain growth, grains oriented with the fastest growing plane survive and the film consists of conical structures.

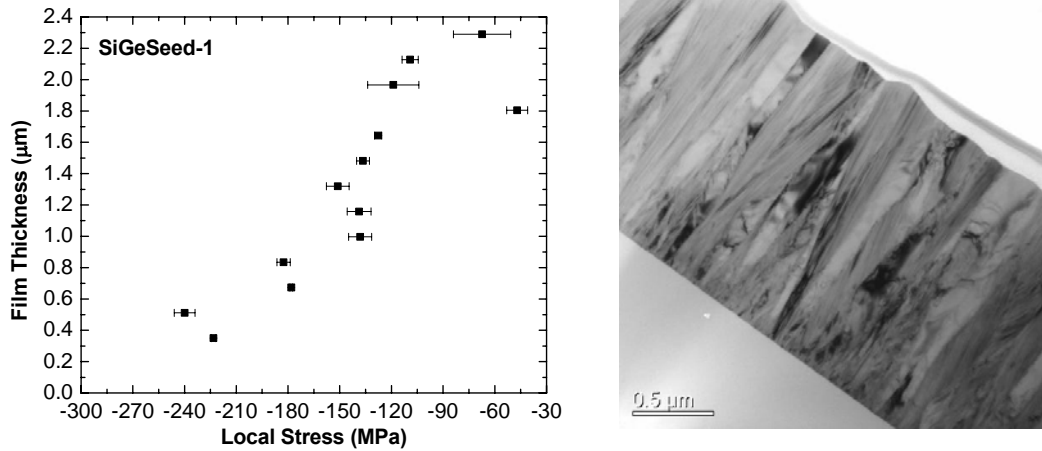


**Figure 4.24** Stress profile and cross sectional TEM image for recipe SiGeSeed-1

The above experiment shows that fine grain seeding results in conical microstructures with high strain gradient. In order to achieve film with low strain gradient and good uniformity, the amorphous region should be suppressed while keeping a columnar texture. The 2<sup>nd</sup> DOE shows that films deposited at 350 mTorr have thinner and more uniform amorphous regions, with sparse crystal seeding. The next seeding experiment SiGeSeed-2 combines recipes DOE2-5 and DOE2-2. Recipe DOE2-5 was used for the initial 20 minute seeding and recipe DOE2-2 was used for the main deposition. The process pressure jumps from 350 mTorr to 600 mTorr after the seeding layer without breaking vacuum. This recipe was designed to deposit a film with a very

thin amorphous region and columnar crystal structures. The deposition time targeted 2  $\mu\text{m}$  film thickness.

The results of the SiGeSeed-2 deposition are listed in Table 4.2. The stress profile and the cross sectional TEM image are shown in Figure 4.25. As expected, this film has a uniform stress distribution. The texture is columnar, with an initial amorphous region of about 0.1  $\mu\text{m}$  in thickness. The defect density within each grain is low.

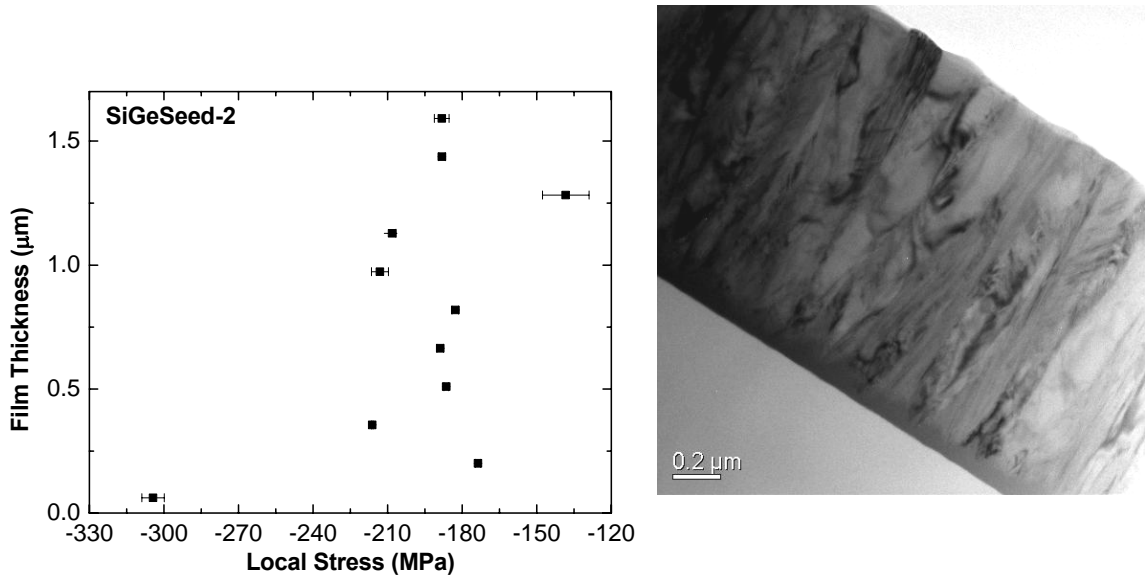


**Figure 4.25** Stress profile and cross sectional TEM image for recipe SiGeSeed-2

Columnar microstructure is a characteristic feature for films with low strain gradient. The film deposited by recipe SiGeSeed-2 has a low strain gradient and the strain gradient uniformity is significantly better than other film with similar thicknesses as shown in Figure 4.26. Comparing the TEM images for SiGeSeed-2 with those of recipes DOE2-1, DOE2-2 and DOE2-3 in Figure 4.16, the main difference is in the amorphous region. Films deposited by recipe SiGeSeed-2 have thinner and more uniform amorphous

regions. For the recipes in DOE2, the variations in amorphous region results in large variations in strain gradient.

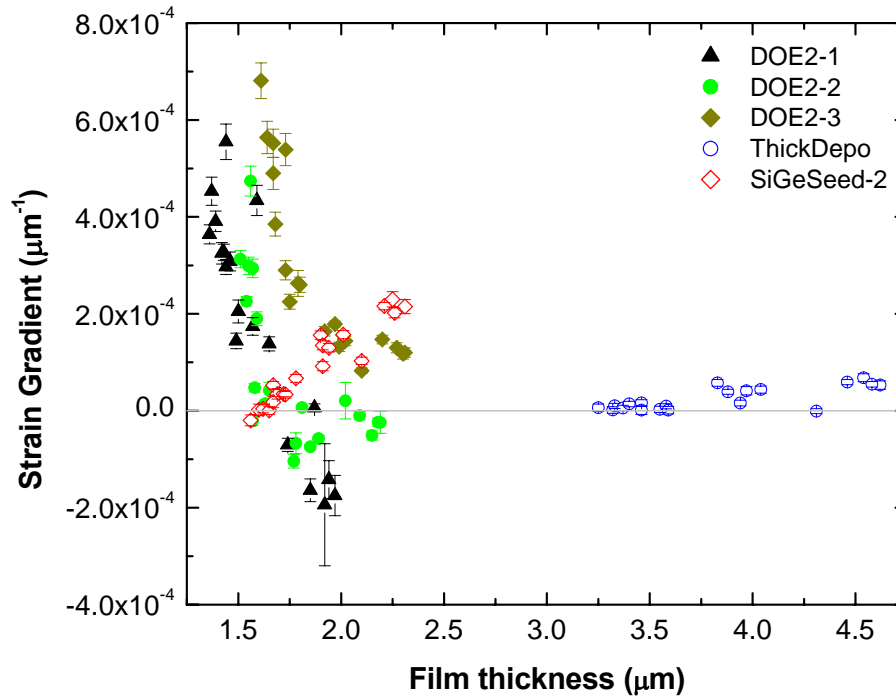


**Figure 4.26** Strain gradient vs. film thickness for various recipes

#### 4.10 Structure properties study

The previous sections provided a large amount of information on deposition conditions, microstructures and the resulting strain gradient in the film. This section reviews all the experiments and presents the correlation between the strain gradient and film microstructure as well as the effects of film deposition conditions on film microstructure [4.15].

#### 4.10.1 Strain gradient and film microstructure

Grains within boron-doped poly-SiGe films generally have vertical orientation, with either conical or columnar shape. Films with low strain gradient are highlighted in light yellow in Table 4.2. A few TEM images are presented again in Figure 4.27 and Figure 4.28 for comparison. Films with a strain gradient larger than  $4.5 \times 10^{-4} \mu\text{m}^{-1}$  generally have conical grain structure with many twins and other defects (Figure 4.27); in contrast, films with positive strain gradient less than  $1 \times 10^{-5} \mu\text{m}^{-1}$  (Figure 4.28) generally have columnar grain structures with few defects within a single grain.

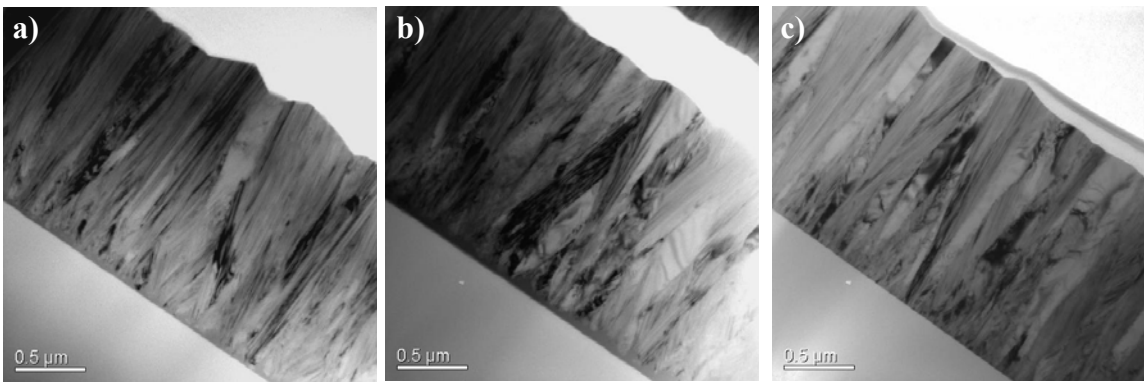


**Figure 4.27** X-TEM images of as-deposited poly-SiGe films with strain gradient  $>4.5 \times 10^{-4} \mu\text{m}^{-1}$ , deposited with: a) Recipe Ramp-ref; b) Recipe DOE2-5; c) Recipe SiGeSeed-1. (ref. Table 4.2.)

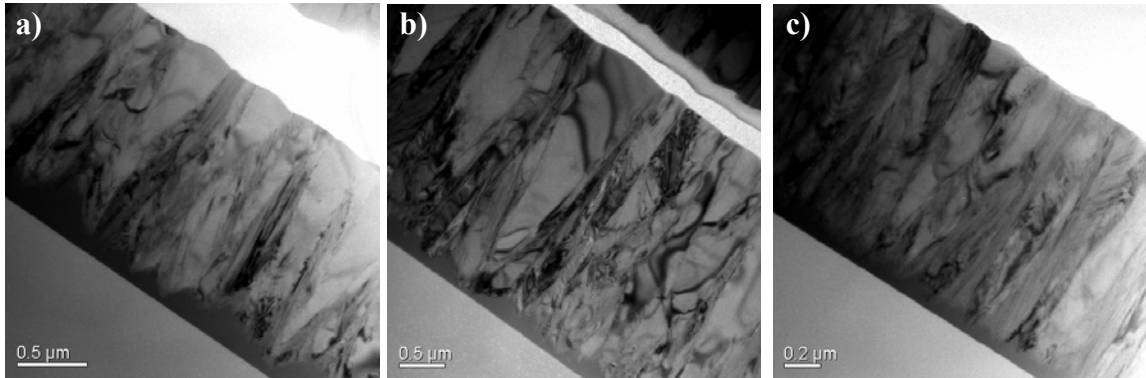


**Figure 4.28** X-TEM images of as-deposited poly-SiGe films with positive strain gradient  $<1 \times 10^{-5} \mu\text{m}^{-1}$ , deposited with: a) Recipe DOE2-2; b) Recipe Thick-depo; c) Recipe SiGeSeed-2. (ref. Table 4.2)

The strain gradient, which can also be interpreted as the stress-*vs.*-depth distribution, is strongly correlated with the film microstructure [4.16]. Films that have a large strain gradient usually start out with fine grains during the initial stage of deposition. As the deposition proceeds, these fine grains grow vertically and compete with each other for lateral growth. Defects are formed during the competition, and the surviving grains develop into conical structures. As a result, the compressive stress is larger in the lower portion of the deposited film as compared to the upper portion, as shown in Figure 4.29(a). This positive stress gradient causes the film to bend upward upon release.

Films that have a low strain gradient start out as an amorphous layer with sparse crystalline seeds. This structure results in large grain size because of the large spacing between the seeds ( $>100$  nm spacing), which reduces lateral grain growth competition and hence results in fewer defects within the grains. To achieve the lowest strain gradient,

the spacing between seeds should match the final lateral grain size, in the range of 100 nm to 200 nm. In such a case, the residual stress remains approximately uniform throughout the film thickness, as shown in Figure 4.29(b). The thin amorphous layer at the bottom of the film has slightly higher compressive stress than the crystalline upper portion of the film, which results in a small positive strain gradient. The stress of the thin amorphous region is difficult to measure accurately for the stress-*vs.*-depth profile due to the cumulative effect of etching non-uniformity, which leads to a significant uncertainty in the residual thickness as it is thinned down to the amorphous region.

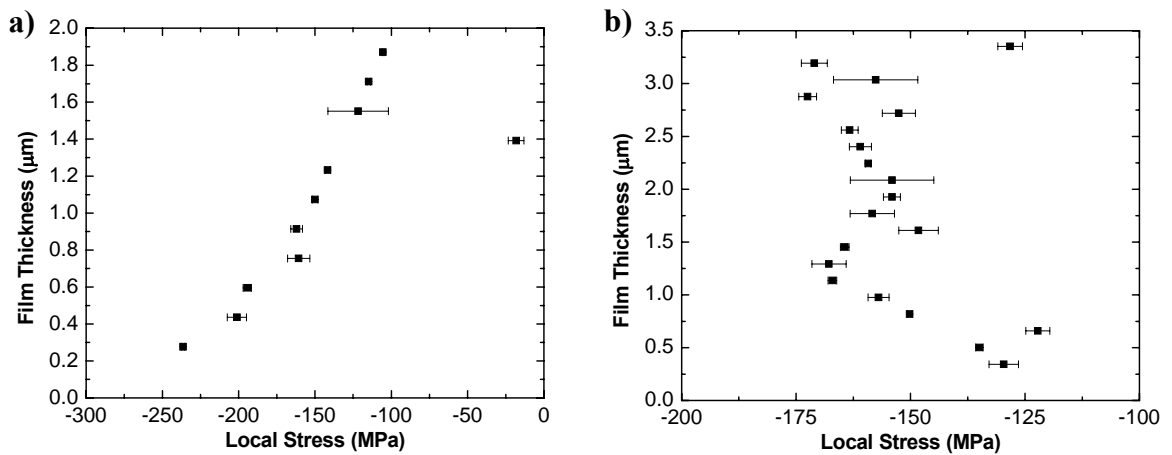


**Figure 4.29** Stress-*vs.*-depth profiles: a) film with large strain gradient, shown in Figure 2.27(b); b) film with small strain gradient, shown in Figure 4.28(b)

To further understand grain growth competition, the grain orientations for all samples shown in Figure 4.27 and 4.28 were analyzed with conventional XRD. The measurement gives an average of crystal orientation of the entire film thickness. Data are shown in Figure 4.30. Since the XRD equipment is not dedicated to thin film

measurement, the silicon substrate gives a strong  $\langle 400 \rangle$  signal at  $69^\circ$ . It should be noted that the absence of dual peaks indicates that the SiGe alloy is homogeneous.

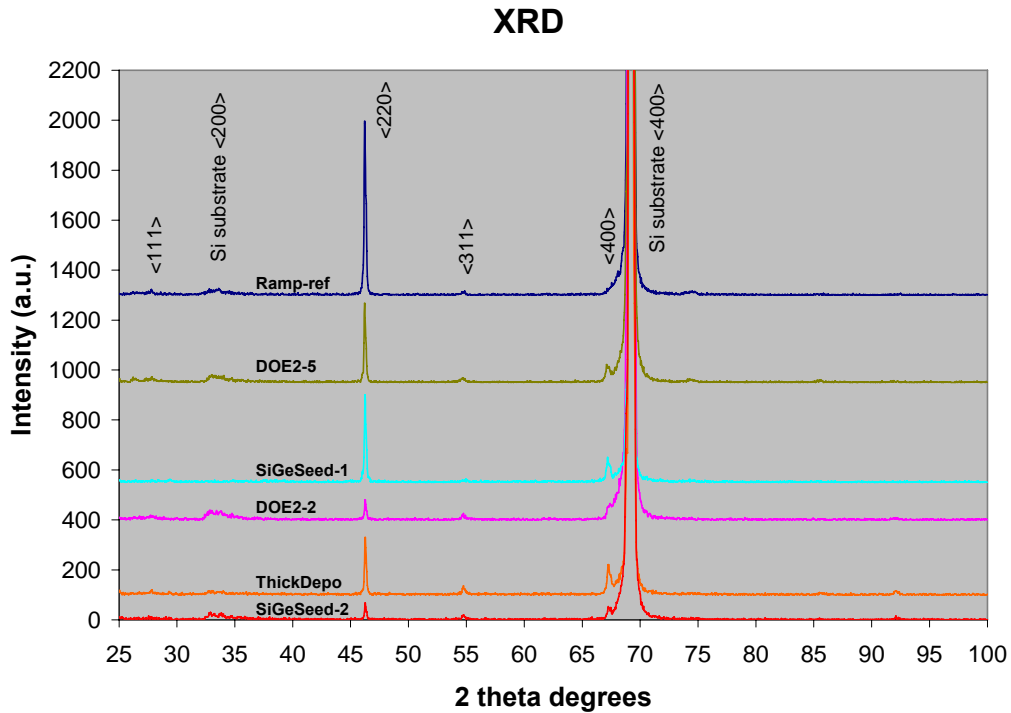


**Figure 4.30** XRD data for films shown in Figure 4.27 and Figure 4.28

The big picture is that samples with large stress gradient have strong  $\langle 220 \rangle$  orientation and samples with small stress gradient have less preference in grain orientations. Since the oxide substrate is amorphous, grains should start with random orientations. For the low strain gradient films without much grain growth competition, the final grain orientation is also random. For high strain gradient films with grain growth competition, orientation  $\langle 220 \rangle$  is favored.

There is also a correlation between the pronounced  $\langle 220 \rangle$  texture and grains with high density twinning defects in the high strain gradient films. The  $\langle 220 \rangle$  direction is the only crystal direction which contain two  $\{111\}$  planes that are the twin-planes. In a

<220>-oriented grain there are two different potential twin planes parallel to the growth direction. This means that twins once formed stay in the grain: *i.e.* they extend in the newly formed part of the grain during growth. Also multiple twinning can take place.

#### 4.10.2 Film Microstructure and Deposition Conditions

The film microstructure is determined by its deposition conditions. The effects of deposition temperature, deposition pressure, boron doping level, film thickness, seeding layer, and multiple-layered deposition are summarized in this section.

Deposition Temperature. Comparing the films shown in Figure 4.27(a) (Recipe Ramp-ref) and Figure 4.28(a) (Recipe DOE2-2), the only difference in processing condition is the deposition temperature. A higher deposition temperature results in a thinner amorphous region at the oxide interface and finer initial grains. Although the volume of the highly compressive amorphous region is suppressed, grain-size evolution during deposition is a more significant factor, resulting in a larger strain gradient.

Deposition Pressure. Deposition pressure is the only variable for the films shown in Figure 4.27(b) (Recipe DOE2-5) and Figure 4.28(a) (Recipe DOE2-2). In both cases, the films start out as an amorphous layer with sparse crystalline seeds. Since the deposition rate decreases as the process pressure goes down, adatoms have a better chance to form clusters and crystal seeds at low pressure. As a result, crystal seeds form earlier. For a fixed deposition temperature, a lower deposition rate also results in more lateral diffusion for the adatoms and hence more lateral grain growth. Thus, the grains are more conical in shape; thus films deposited at lower pressure have larger strain gradient.

Boron Doping Level. Experiments in DOE1 indicated that boron doping enhances crystallinity for films deposited near to the amorphous-to-crystalline transition temperature, i.e. if the initial amorphous region is minimal, the strain gradient can be reduced by increasing the boron doping concentration. Higher doping levels are explored in DOE2. Figure 4.31 shows the relationship between strain gradient and resistivity. X-TEM images are also shown for selected cases. The thickness of the amorphous region at the lower oxide interface remains approximately constant as the boron doping level exceeds a certain threshold, beyond which the strain gradient in the film is determined by other factors, such as grain size and defect density.

Film Thickness. The films shown in Figure 4.28(a) (Recipe DOE2-2) and Figure 4.28(b) (Recipe ThickDepo) have significantly different thicknesses. Since the boron concentration is not a significant factor at high doping levels, deposition time is the main difference between these two films. In both cases, the thickness of the amorphous region is similar, but the thicker film has taller columnar grains. Thus, a larger portion of the thicker film consists of columnar crystalline structures.

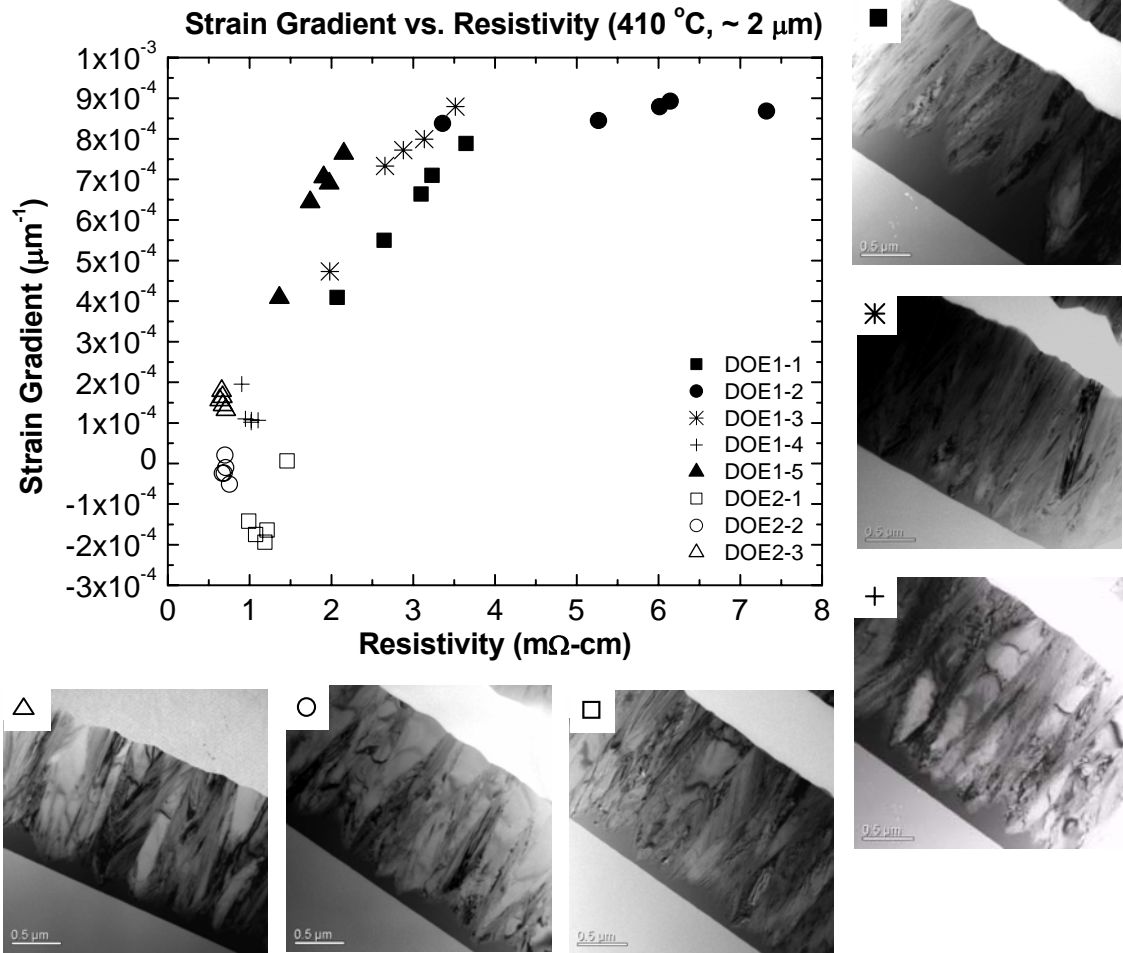


**Figure 4.31** Relationship between strain gradient and resistivity, and film microstructure for films deposited near to the amorphous-to-polycrystalline transition temperature.

Seeding Layer. The films shown in Figure 4.27(c) (Recipe SiGeSeed-1), Figure 4.28(a) (Recipe DOE2-2) and Figure 4.28(c) (Recipe SiGeSeed-2) were deposited using similar main deposition conditions but different seeding layers. It should be noted that vacuum was not broken between the seeding and the main deposition steps, so that grain growth was not interrupted.

The low pressure and low gas flow rates used for SiGe seed-layer deposition in Recipe SiGeSeed-1 enhance crystal seeding due to the resultant low deposition rate and high boron concentration. Fine crystal grains formed during the initial stage of film deposition compete for lateral growth, resulting in a conical grain structure and high strain gradient as shown in Figure 4.27(c).

As discussed above, lower deposition pressure enhances initial crystal seeding as well as lateral grain growth. Recipe SiGeSeed-2 combines a low pressure deposited SiGe seed layer with a high pressure deposited main layer. The resulting film (Figure 4.28(c)) has a thinner amorphous layer (compared to the film shown in Figure 4.28(a) and columnar grains.

Multiple-layered film deposition. Section 4.8 described the generation of fine-grained poly-SiGe by multiple layer deposition. Grain growth can be interrupted by breaking the vacuum between depositions. The grain size and the stress distribution can be controlled by the number of deposition steps. Since the partially amorphous layer generated by Recipe DOE2-5 was used for each of the depositions, the final film ended up with a negative strain gradient due to *in-situ* annealing of the earlier deposited amorphous regions. A fully crystallized film such as the one generated by recipe SiGeSeed-1 has better thermal stability and therefore it should be used for each layer deposition to avoid having a negative strain gradient for the multiple-layered film deposition.

### **4.10.3 Uniformity**

Since a LPCVD system is a batch reactor, cross-wafer and cross-load uniformities are important manufacturing considerations. The film thickness, resistivity, and average

residual stress are fairly uniform for all of the deposition recipes studied in this work. The strain gradient, however, is very sensitive to deposition process variations. Achieving low strain gradient with good uniformity is a major challenge for high volume manufacturing of poly-SiGe inertial sensors. Within the limitations of a horizontal LPCVD system in an academic laboratory, we are able to study the sensitivity of strain gradient to deposition process variations.

Figure 4.32 presents the stress-gradient variation data for all deposition runs yielding films with absolute strain gradient  $\leq 1 \times 10^{-4} \mu\text{m}^{-1}$ . For each run, the strain gradient data was collected from four wafers across the load, and five locations on each wafer. For each location on a wafer, more than ten measurements of cantilever beam tip deflection were used to determine the strain gradient. The variation represents the range of these measurements for the same location.

At first glance, it would seem that larger variation is seen for negative strain gradient as compared with positive strain gradient. However, this is due to limitations in measurement accuracy rather than process uniformity issues, because there is not much room for the cantilever beams to bend downward so that only the very short beams could be measured. Also, tip deflection is difficult to measure for a curled-down beam.

Films with low strain gradient always have a thin amorphous region and large columnar grains. The amorphous region contributes a small positive strain gradient due to its higher compressive stress as compared to the crystalline region of the film. Although the amorphous region is necessary to ensure proper crystal seeding to form columnar grains, variations in the thickness of this region result in variations in strain gradient.

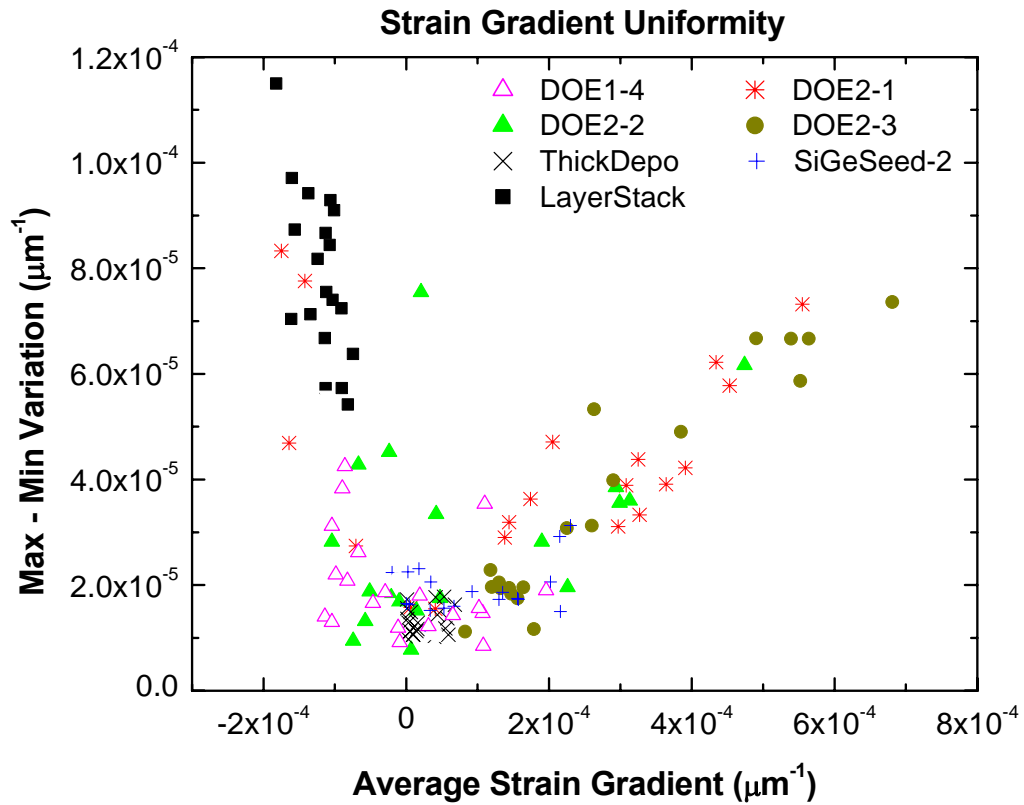


**Figure 4.32** Variation in strain gradient vs. the average strain gradient.

A simple approach to minimize the effect of the lower amorphous region is to grow a thicker columnar crystalline layer. As shown in Figure 4.32, Recipe ThickDepo yields the best results for strain gradient and uniformity, due to its large film thickness. The average film thickness is  $3.8 \mu\text{m}$  for Recipe ThickDepo whereas it is approximately  $2 \mu\text{m}$  for the other recipes. Among the  $2 \mu\text{m}$  deposition recipes, Recipe SiGeSeed-2 achieves the best strain gradient and uniformity. In this case, the additional low pressure deposited SiGe seed layer makes the initial amorphous layer thinner and more uniform, which significantly improves the uniformity of the strain gradient. Increasing the volume ratio of the crystalline region to the amorphous region is the key for improving stress-

gradient uniformity for single-layered columnar films. The combined use of the low pressure SiGe seed layer and a long deposition time should further improve the results.

Recipe LayerStack, the multiple-layer deposition process, was intended to yield a film with lower and more uniform strain gradient. Indeed, the strain gradient is improved as compared to Recipe DOE2-5. Unfortunately, the negative curvature results in a large measurement error, so that it is not possible to confirm that uniformity is improved.

#### 4.11 Summary

The deposition of *in-situ*-boron-doped poly-SiGe films has been investigated with the design-of-experiments technique. At a CMOS compatible deposition temperature of 410°C, films with low resistivity and low wet-etch rate in heated H<sub>2</sub>O<sub>2</sub> solution can be achieved with a reasonable deposition rate. The films with 60% germanium content generally have compressive residual stress so that careful design is required to prevent buckling of released clamped-clamped beams.

Strain gradients in LPCVD poly-SiGe films have been studied extensively using cantilever-beam tip deflection measurements, stress-vs.-depth profiling, and microstructure analysis using cross-sectional TEM. Films with strain gradients meeting the specification of  $1 \times 10^{-5} \mu\text{m}^{-1}$  for inertial sensor applications always have a thin initially deposited amorphous layer and thick columnar grains. The uniformity of strain gradient across a wafer and across a wafer load can be improved with a thinner amorphous region and thicker crystalline region. Alternately, uniformity can also be improved with a multiple-layered deposition process.

In our academic research laboratory, the as-deposited poly-SiGe films can achieve strain gradient below  $7 \times 10^{-5} \mu\text{m}^{-1}$  across a load of twenty-five 150mm-diameter wafers, with less than  $1.6 \times 10^{-5} \mu\text{m}^{-1}$  variation within a single wafer for certain slots within the load and a best case of only  $1.1 \times 10^{-6} \mu\text{m}^{-1}$ . This result is for  $\sim 3.8 \mu\text{m}$ -thick films deposited at  $410^\circ\text{C}$  for 8 hours, which meets the thermal process budget constraint imposed by CMOS electronics [4.17]. With tighter process control within a production environment, the strain gradient and its uniformity can be further improved.

## References

- [4.1] P. A. Krulevitch, "Micromechanical Investigations of Silicon and Ni-Ti-Cu Thin Films", Ph.D. Thesis, University of California, Berkeley (1994)
- [4.2] W. L. Bragg, "The diffraction of short electromagnetic waves by a crystal", *Proceedings of the Cambridge Philosophical Society*, **17**, pp. 43-57 (1912)
- [4.3] Dismukes, J.P., L. Ekstrom, E.F. Steigmeier, I. Kudman and D.S. Beers, "Thermal and Electrical Properties of Heavily Doped Ge-Si Alloys up to 1300°K", *J. Appl. Phys.* **35**, 1964, 2899. (b)
- [4.4] K. Nunan, G. Ready, P. Garone, G. Sturdy and J. Sledziewski, "Developing a Manufacturable Process for the Deposition of Thick Polysilicon Films for Micro Machined Devices", *Proceedings of IEEE/SEMI Advanced Semiconductor Manufacturing Conference*, pp. 357-366 (2000)
- [4.5] S. D. Senturia, *Microsystem Design*, Kluwer Academic Publishers, pp. 201-238 (2001)
- [4.6] C. W. Low, T.-J. King Liu and R. T. Howe, "Characterization of polycrystalline silicon-germanium film deposition for modularly integrated MEMS applications," *IEEE/ASME Journal of Micro-electromechanical Systems*, vol. 16, no.1, pp.68-77, Feb. 2007
- [4.7] B. L. Bircumshaw, M. L. Wasilik, E. B. Kim, Y. R. Su, H. Takeuchi, C. W. Low, A. P. Pisano, T.-J. King and R. T. Howe, "Hydrogen Peroxide Etching and Stability of P-type Poly-SiGe Films," *17<sup>th</sup> IEEE Micro Electro Mechanical Systems Conference (MEMS-04)*, Maastricht, The Netherlands, Jan. 25-29, 2004, pp. 514-519
- [4.8] D. C. Montgomery, *Introduction to Statistical Quality Control*, 4<sup>th</sup> edition, John Wiley & Sons, Inc., pp. 571-672, 2001

- [4.9] T. Van der Donck, J. Proost, C. Rusu, K. Baert, C. Van Hoof, J.-P. Celis and A. Witvrouw, "Effect of deposition parameters on the stress gradient of CVD and PECVD poly-SiGe for MEMS applications," in *Proc. of the SPIE Conference*, San Jose, CA, USA, Jan. 28-29, 2004, pp. 8-18
- [4.10] Molfese, A. Mehta and A. Witvrouw, "Determination of stress profile and optimization of stress gradient in PECVD poly-SiGe films," *Sensors and Actuators A*, vol. 118, pp. 313-321, 2005
- [4.11] S. Sedky, A. Witvrouw, A. Saerens, P. V. Houtte, J. Poortmans and K. Baert, "Effect of *In Situ* Boron Doping on Properties of Silicon Germanium Films Deposited by Chemical Vapor Deposition at 400 °C", *Journal of Materials Research*, Vol. 16, No. 9, pp. 2607-2612 (2001)
- [4.12] D. Mirfenderski, M. Ferrari and A. Der Kiureghian, "Analysis of microfabricated textured multicrystalline beams. I. Homogenization approach," in *Proc. Smart Materials Fabrication and Materials for Micro-Electro-Mechanical Systems*, Mater. Res. Soc, Pittsburgh, PA, 1992, pp. 91-96
- [4.13] D. Mirfenderski, A. Der Kiureghian and M. Ferrari, "Analysis of microfabricated textured multicrystalline beams. II. Probabilistic approach," in *Proc. Smart Materials Fabrication and Materials for Micro-Electro-Mechanical Systems*, Mater. Res. Soc, Pittsburgh, PA, 1992, pp. 97-101
- [4.14] S.-M. Sun, S. L. Girshick and M. R. Zachariah, "The role of total pressure in gas-phase nucleation: A diffusion effect," *Journal of Chemical Physics*, vol. 118, no. 2, pp. 736-745
- [4.15] C. W. Low, T.-J. King Liu and R. T. Howe, "Study of poly-SiGe structural

properties for modularly integrated MEMS,” in *Proc. Electrochem. Soc. SiGe and Ge: Materials, Process, Devices Symp.* Cancun, Mexico, Nov. 3, 2006

[4.16] C. V. Thompson, “Structure evolution during processing of polycrystalline films,” *Journal of Annu. Rev. of Mater. Sci.*, vol. 30, pp. 159-190, 2000

[4.17] H. Takeuchi, A. Wu, X. Sun, R. T. Howe and T. –J. King, “Thermal budget limits of quarter-micron foundry CMOS for post-processing MEMS devices,” *IEEE Trans. Electron Devices*, vol. 52, pp. 2081-2086, 2005

## **Chapter 5: Post-Deposition Processing of Poly-SiGe Films**

Various post-deposition processes have been studied to look into the effects of post-processing on mechanical properties of poly-SiGe structural films and the performance of the underlying CMOS electronics. The goal of post processing is to improve the poly-SiGe film structural properties while keeping a low thermal budget for the CMOS electronics. Annealing is widely used in poly-Si and poly-SiGe structural films to lower the resistivity, stress, strain gradient and improve quality factor [5.1] – [5.4]. The changes in structural properties of poly-SiGe have been studied with a large variety of annealing methods, including furnace annealing, rapid thermal annealing, flash lamp annealing and excimer laser annealing. This chapter also discusses ion implantation as an alternative for modifying the mechanical properties of the poly-SiGe film without increasing the thermal budget. Finally, the results of an investigation into the CMOS thermal budget allowance will be presented.

### **5.1 Furnace annealing**

As discussed in Chapter 4, LPCVD poly-SiGe films with low strain gradient always have a thin amorphous region at the lower oxide interface. Post-deposition annealing in a nitrogen ambient can be used to crystallize this amorphous region. An atmospheric pressure furnace was used to anneal a few unpatterned wafers from deposition ThickDepo (ref. Table 4.2). The nitrogen flow rate was set to 3000 sccm during the annealing to prevent oxidation. Annealing temperature and time are the variables in the recipe. In the annealing furnace, the temperature has to stabilize before

loading the wafers. It takes about 5 minutes to reach temperature set point again after loading. Once the annealing is done, the process temperature ramps down immediately and the furnace door opens. A minimum annealing time of 30 minutes was used to minimize the error in thermal budgets.

Various annealing times and temperatures were explored for this film, as listed in Table 5.1. In all cases, the annealing temperature was higher than the deposition temperature (410°C). We can see that there is no significant change in resistivity, but the average residual stress is reduced and the strain gradient becomes more negative. Annealing at 600°C is not compatible with advanced CMOS devices [5.5], but this high-temperature annealing magnifies the result for this study. The strain gradient of the as-deposited film is on the order of  $1 \times 10^{-5} \mu\text{m}^{-1}$ . Recipes FA-b and FA-c result in negative curvature of the released cantilever beams.

**TABLE 5.1** Summary of post-deposition furnace annealing (FA).

Recipe	Temp. (°C)	Time (min.)	Resistivity (mΩ-cm)	Stress (MPa)	Strain Gradient ( $\mu\text{m}^{-1}$ )
As-deposited	NA	NA	0.6	-150	$4.7 \times 10^{-5}$
FA-a	430	30	0.6	-147	$2.7 \times 10^{-5}$
FA-b	430	180	0.6	-144	$-1.52 \times 10^{-4}$
FA-c	600	30	0.6	-115	$-4.4 \times 10^{-4}$

The stress profile and cross-sectional TEM analyses of the as-deposited and annealed films are shown in Figure 5.1-4. Crystallization of the lower amorphous portion can be clearly seen for the 600°C-annealed film (Figure 5.4) as compared to the as-deposited film (Figure 5.1). In contrast, a change in the film microstructure is not readily apparent for the 430°C-annealed films. In all cases, no apparent changes are observed for the upper crystalline portion of the film.

Comparing the stress profile in Figure 5.4 against the one in Figure 5.1, the stress distribution within the upper crystalline portion remains the same, whereas the stress within the lower portion changes dramatically from compressive to tensile after the 600°C annealing, resulting in the large negative shift in the strain gradient. This is consistent with the cross-sectional TEM analyses of the film microstructure. The amorphous region of the as-deposited film is not densely packed. Upon high-temperature annealing, voids and defects are removed, resulting in tensile stress in this region. The crystallization of the amorphous region makes the average stress less compressive and changes the strain gradient towards the negative direction. The resistivity of the film does not change significantly. The boron concentration in the film is about  $1 \times 10^{21} \text{ cm}^{-3}$ . Probably there is no additional dopant activated by the annealing. Also the amorphous region in the as-deposited film is relatively thin compared to the film thickness and it does not reduce the overall resistivity significantly after crystallization.

The stress distribution does not show a significant change after 30 minutes of annealing at 430°C (FA-a) compared to the as-deposited film, consistent with the cross-sectional TEM analyses of the film microstructure. The reduced variability in the stress distribution as compared to that of the unannealed film can be attributed to differences in measurement accuracy and position of the wafer within the furnace. Although not clearly visible, a small part of amorphous region got crystallized by the low temperature annealing, and this contributes to a small change in strain gradient. With longer annealing time, the change is more significant.

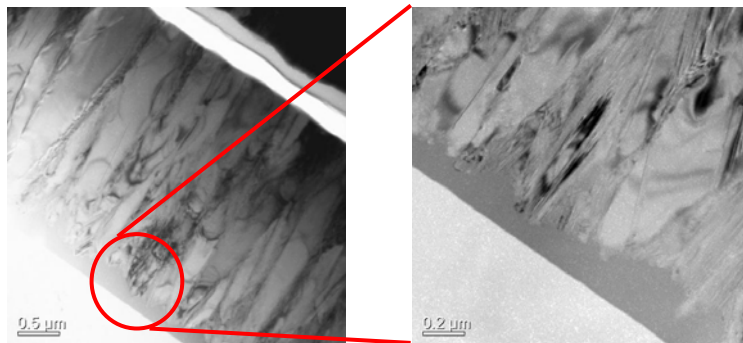
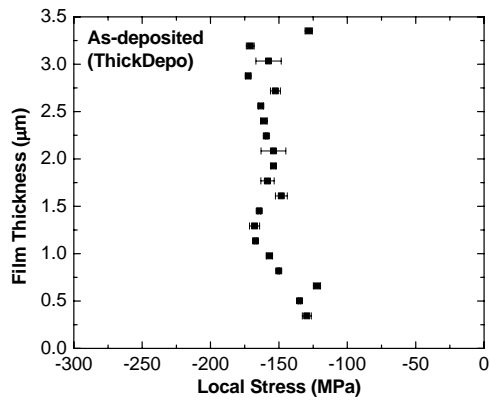


**Figure 5.1** Stress profile and cross-sectional TEM image for the as-deposited film (film deposited by Recipe ThickDepo)

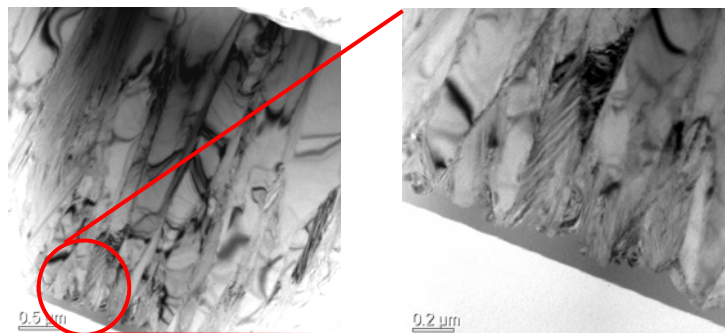
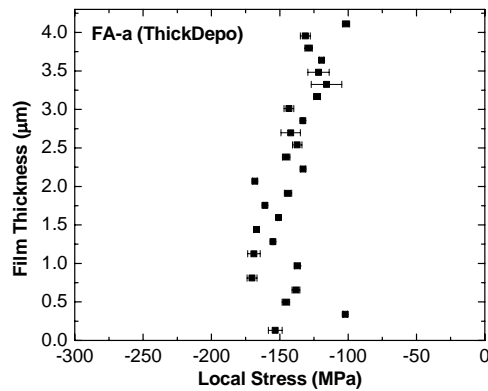


**Figure 5.2** Stress profile and cross-sectional TEM image for FA-a (film deposited by Recipe ThickDepo)

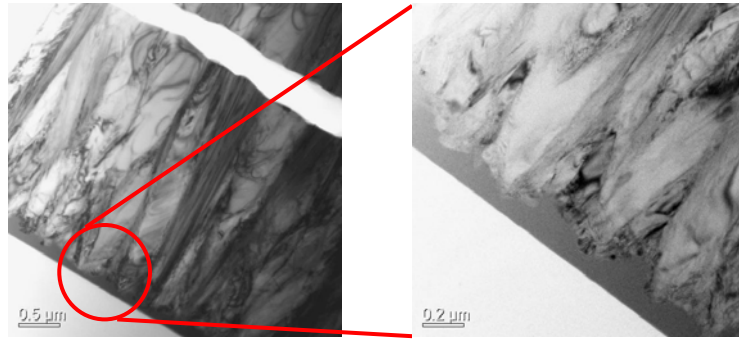


**Figure 5.3** Cross-sectional TEM image for FA-b (film deposited by Recipe ThickDepo)

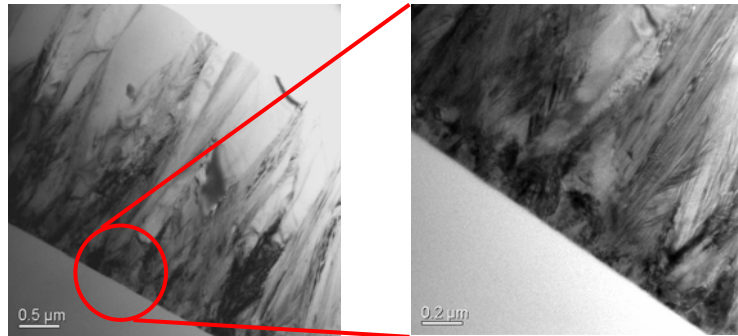
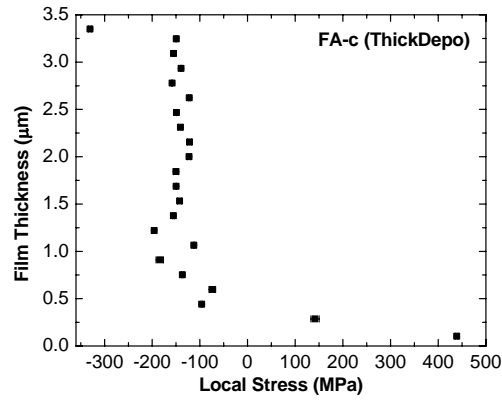


**Figure 5.4** Stress profile and cross-sectional TEM image for FA-c (film deposited by Recipe ThickDepo)

Furnace annealing at elevated temperature (higher than the deposition temperature) causes the amorphous layer to crystallize and thereby changes the strain

gradient in the negative direction. Thus, caution is advised when post-processing poly-SiGe films at temperatures higher than the deposition temperature for a long period of time.

## **5.2 Rapid thermal annealing**

The rapid thermal annealing (RTA) tool is a single wafer system using lamp illumination for rapidly heating the wafer. The temperature of the wafer can be ramped up in a few seconds. The process temperature of the RTA tool is controlled by a thermocouple with a feedback system. With appropriate setting, the wafer temperature can stabilize to the set point in a few seconds. A water cooling system is attached to the process chamber so that the wafer temperature can be dropped down by hundreds of degree Celsius in a few seconds after heating.

Wafers from Recipe ThickDepo (ref. Table 4.2) were also used for the RTA study. The annealing temperatures were chosen to be 410°C, 430°C, 470°C, 510°C and 550°C. The recipe was adjusted so that the temperature does not overshoot, but it takes 10 seconds to reach the set point. One minute of annealing time was used in each recipe. Nitrogen flow was used during the annealing so that the film does not oxidize.

The results of the annealing are listed in Table 5.2 for comparison. There is no significant change in resistivity, but the changes in stress and strain gradient are dramatic. It is interesting that the results of all RTA runs are very similar to those of the furnace annealing at 600°C for 30 minutes (listed in Table 5.2). The film was deposited at 410°C for hours and annealing at 410°C for 1 minute should not change the properties of the

film. This observation suggested that the temperature the film experienced during the RTA section might be a lot higher than the set point.

**TABLE 5.2** Summary of post-deposition rapid thermal annealing (RTA).

Recipe	Temp. (°C)	Time (min.)	Resistivity (mΩ-cm)	Stress (MPa)	Strain Gradient ( $\mu\text{m}^{-1}$ )
As-deposited	NA	NA	0.6	-150	$4.7 \times 10^{-5}$
RTA-a	410	1	0.6	-112	$-4.6 \times 10^{-4}$
RTA-b	430	1	0.6	-110	$-3.3 \times 10^{-4}$
RTA-c	470	1	0.5	-118	$-3.5 \times 10^{-4}$
RTA-d	510	1	0.5	-102	$-3.6 \times 10^{-4}$
RTA-e	550	1	0.6	-115	$-4.4 \times 10^{-4}$

Stress profile and TEM analysis for the as-deposited film, recipe RTA-b and RTA-e are shown in Figure 5.1, Figure 5.5 and Figure 5.6, respectively. Both of the RTA conditions fully crystallized the bottom amorphous regions of the films and the stress of those regions become less compressive. The stress profile and the microstructures of the RTAed films are very similar to those of the 600°C furnace annealed film (shown in Figure 5.4). Comparing RTA and furnace annealing at 430°C, furnace annealing for longer time does not create visible change in the amorphous region, as shown in Figures 5.2 and 5.3 in the previous section. This observation suggests that there is a temperature discrepancy between the RTA chamber and the annealing furnace. The annealing furnace has similar a temperature control as the poly-SiGe deposition furnace; therefore, the annealing temperature and the deposition temperature should be consistent.

The results of this RTA experiments are not very helpful for understanding how a reduced thermal budget would change the properties of the film, because of the uncertainty in annealing temperatures. It is confirmed again that crystallization of the initially amorphous region creates a dramatic change in the residual stress and this affects the strain gradient of the entire film significantly.

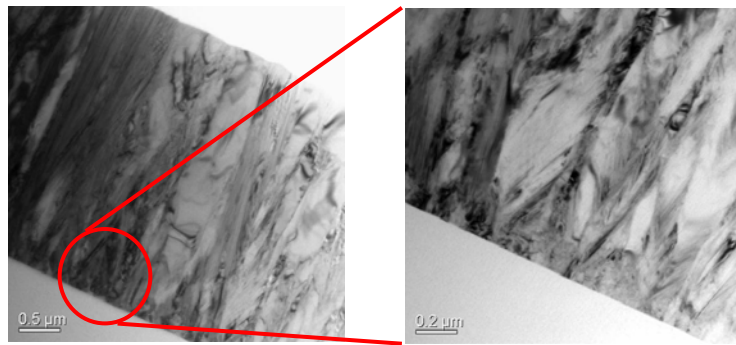
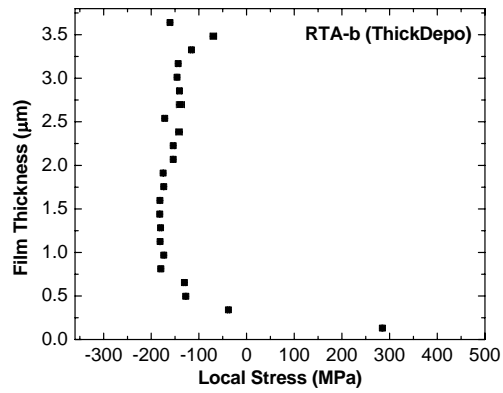


**Figure 5.5** Stress profile and cross-sectional TEM image for RTA-b (film deposited by Recipe ThickDepo)

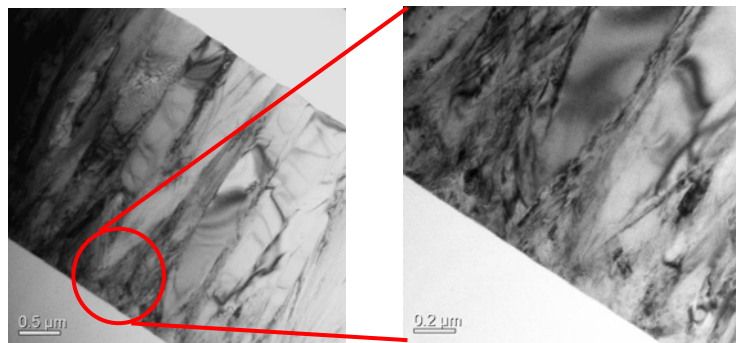


**Figure 5.6** Cross-sectional TEM image for RTA-e (film deposited by Recipe ThickDepo)

### 5.3 Flash lamp annealing

Flash lamp annealing (FLA) is an advanced rapid thermal annealing process that allows the wafer to be held at process temperature for just a few milliseconds and then to be cooled down rapidly. Flash lamp annealing has been investigated in the IC industry for ultra-shallow junction formation [5.6] - [5.8]. The effect of flash lamp annealing on poly-SiGe film was studied with the support of Mattson Technology, the manufacturer of the FLA tool.

Flash lamp annealing of a few SiGe samples was done in a demo tool at Mattson Technology. The temperature distribution across the substrate is close to a Gaussian distribution over the sample area, but the sample holder makes the edge of the sample slightly hotter. In this experiment, the samples were preheated to an intermediate temperature of 220°C. A capacitor bank is discharged through the heating lamp to achieve the additional temperature jump on the top side of the sample. The duration of the annealing is on the order of 1 ms. The temperature jump could be measured by the additional increase in backside temperature. The backside temperature can be measured by a radiometer if it is above 760°C. The annealing temperatures for the poly-SiGe films were chosen to be at 500°C, 600°C and 700°C. In this case, the temperature cannot be measured by the radiometer, so is roughly predicted by the lamp power.

Poly-SiGe films from depositions DOE1-3 and DOE1-13 (ref. Table 4.2) were used in this experiment. The two depositions recipes have different process temperature but identical process pressure and gas flow rates. The results of the annealing are listed in Tables 5.3a and 5.3b. The sample size for the demo tool is restricted to 12 mm by 12 mm. After the annealing, the lithography, etch and release steps were done at die level. In this

case, the average residual stress cannot be measured with the change in wafer curvature. The strain gauge test structure defined by the mask did not survive after the release. Therefore the average residual stress is not available for these annealed films. We can see that for both DOE1-3 and DOE1-13 films, flash lamp annealing does not change the resistivity significantly. Also, only the 700°C annealing changes the strain gradient towards the negative direction.

**TABLE 5.3a** Summary of post-deposition flash lamp annealing (FLA) for deposition DOE1-3.

Recipe	Temp. (°C)	Time (ms.)	Resistivity (mΩ-cm)	Stress (MPa)	Strain Gradient (μm <sup>-1</sup> )
As-deposited	NA	NA	2.6	-168	$5.8 \times 10^{-4}$
FLA-a	500	1	2.8	NA	$5.9 \times 10^{-4}$
FLA-b	600	1	2.3	NA	$5.8 \times 10^{-4}$
FLA-c	700	1	2.3	NA	$-2.92 \times 10^{-5}$

**TABLE 5.3b** Summary of post-deposition flash lamp annealing (FLA) for deposition DOE1-13.

Recipe	Temp. (°C)	Time (ms.)	Resistivity (mΩ-cm)	Stress (MPa)	Strain Gradient (μm <sup>-1</sup> )
As-deposited	NA	NA	6.1	-100	$3.8 \times 10^{-4}$
FLA-d	500	1	6.8	NA	$3.8 \times 10^{-4}$
FLA-e	600	1	5.4	NA	$3.2 \times 10^{-4}$
FLA-f	700	1	5.0	NA	$5.8 \times 10^{-5}$

The textures of the films before and after annealing are compared by TEM analysis. For reference, the stress profiles and the TEM images for the as-deposited films are shown in Figures 5.7 and 5.10. Both DOE1-3 and DOE1-13 depositions result in conical textures with amorphous starting layers and the compressive stress gradually decreases along the film thickness. Since DOE1-13 is a higher temperature deposition, the amorphous region is thinner.

Comparing Figure 5.7 with Figure 5.8, we can see that flash lamp annealing at 600°C of the DOE1-3 film does not change the microstructure so that the strain gradient of the film remains the same. Figure 5.9 shows the film after 700°C FLA and the bottom amorphous region is completely crystallized. Similar to furnace annealing and RTA

discussed in previous sections, this crystallization of the bottom amorphous layer changes the local stress from compressive to tensile. A negative bending moment is generated at the bottom of the film by the crystallization and the strain gradient changes towards the negative direction. Figure 5.11 shows similar results with the DOE1-13 film annealed at 700°C. Since the as-deposited amorphous region for deposition DOE1-13 is thinner, the negative bending moment generated by the crystallization is also smaller. As a result, the change in strain gradient after the annealing is less significant compared to the DOE1-3 film.

It should be noted that the crystallized region at the bottom of the FLA-ed film looks different from the furnace annealed film (Figure 5.4) or RTA-ed film (Figure 5.6). The FLA results in fine grained polycrystalline structures that are distinguishable from the as-deposited crystalline structures, whereas the furnace annealing or the RTA “extends” the grain growth from the original crystalline structures. In all cases, the surface roughness remains the same after the annealing. This indicates that the flash lamp annealing does not involve melting or re-solidification.

The flash lamp annealing changes the stress and the strain gradient in a similar fashion as the furnace annealing and the rapid thermal annealing, by crystallizing the amorphous region at the bottom of the SiGe film. Since the duration of the heat pulse is in the millisecond range, crystallization does not occur for temperatures below 700°C. The effects of the flash lamp annealing on the underlying CMOS electronics will be studied in a later section.

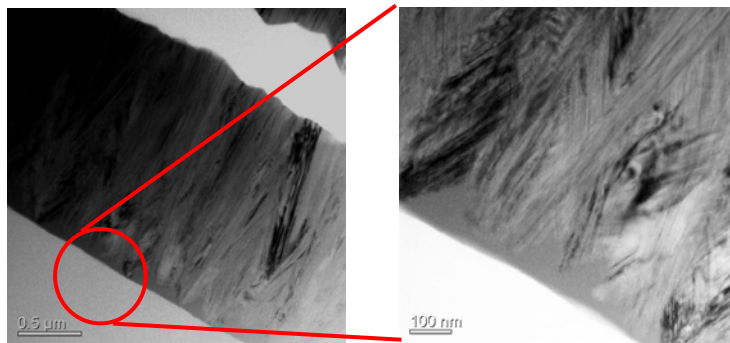
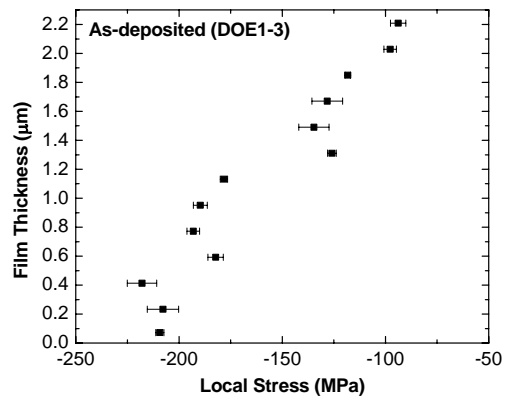


**Figure 5.7** Stress profile and cross-sectional TEM image for the as-deposited film (film deposited by Recipe DOE1-3)

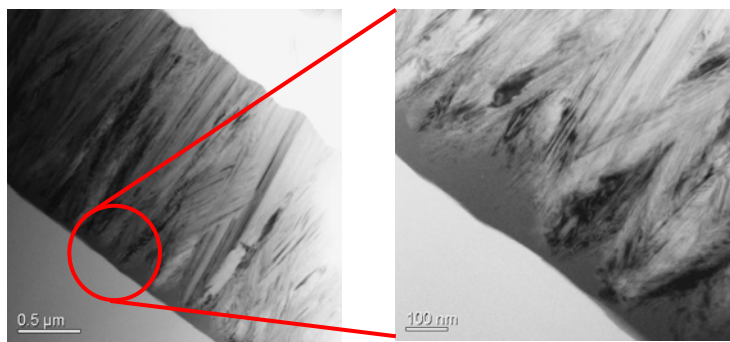


**Figure 5.8** Cross-sectional TEM image for FLA-b (film deposited by Recipe DOE1-3)

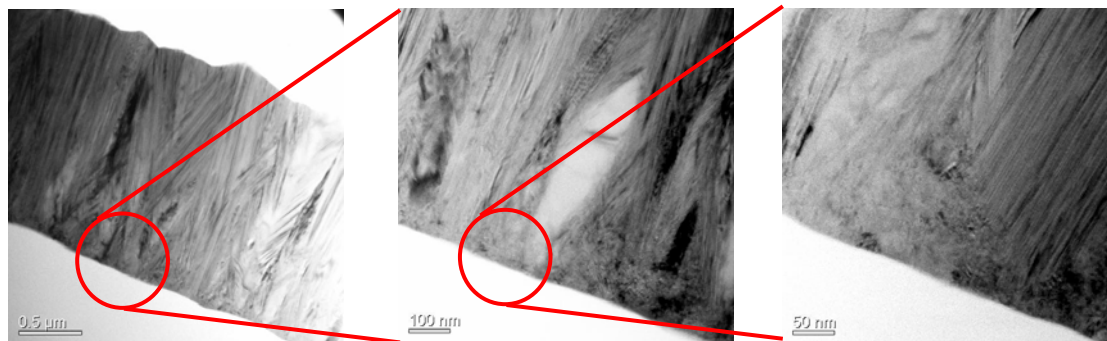


**Figure 5.9** Cross-sectional TEM image for FLA-c (film deposited by Recipe DOE1-3)

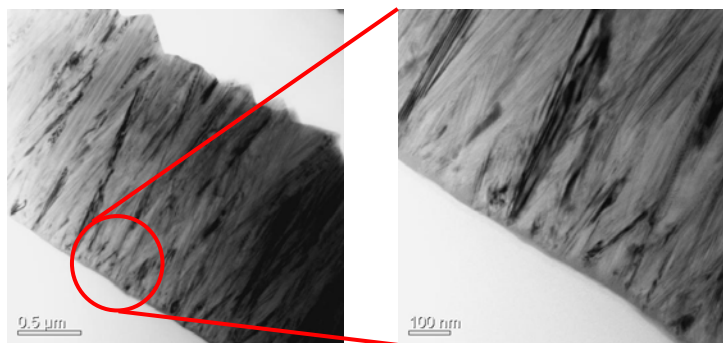
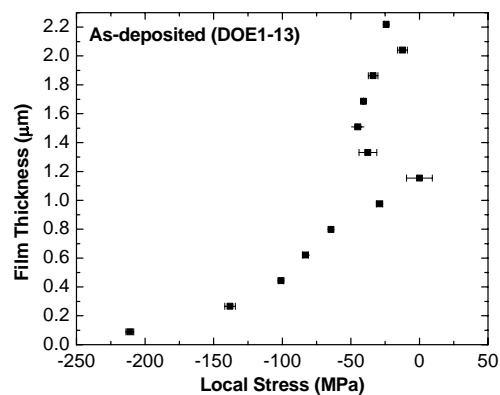


**Figure 5.10** Stress profile and cross-sectional TEM image for the as-deposited film (film deposited by Recipe DOE1-13)

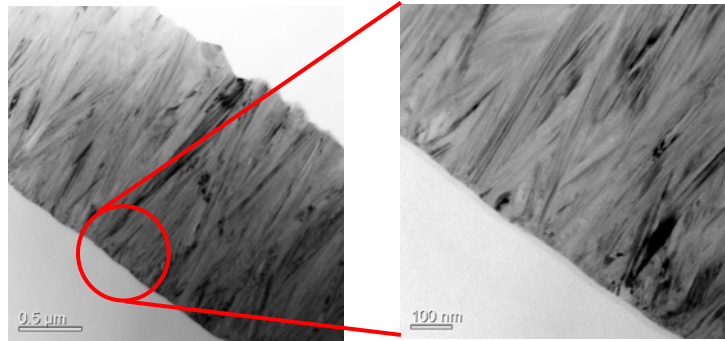


**Figure 5.11** Cross-sectional TEM image for FLA-f (film deposited by Recipe DOE1-13)

#### **5.4 Excimer laser annealing**

The excimer lasers are commonly used in material processing research due to its high energy density. They can be used as energy sources for surface annealing or material ablation. Excimer laser annealing (ELA) of poly-SiGe had been previously studied by other researchers [5.9] – [5.11] and the author [5.12]. Pulsed-laser annealing can be used to tune the stress and the strain gradient of the poly-SiGe film. The laser energy locally heats up the SiGe film, and therefore the thermal budget seen by the underlying CMOS is not increased. This section briefly reviews the work done by the author for a Master’s project [5.12].

Excimer is short for “excited dimmer”. The laser used in the experiments has KrF as the gaseous lasing media, excited by means of electrical discharge. The diatomic molecule KrF has very short lifetime and dissociates to release the energy through ultraviolet photons at the wavelength of 248 nm. The laser excitation is pulsed with a duration time of 38 ns. The laser beam output has a fluence range of 200 – 800 mJ/cm<sup>2</sup>.

This fluence level allows the radiation to penetrate the top most portion of the poly-SiGe film, down to a depth of  $\sim 0.3 \mu\text{m}$ .

The laser energy melts the top region of the film, and the melted region re-solidifies upon cooling. This melting and re-solidification process densifies the affected region and results in tensile stress locally. Most of the single layer as-deposited poly-SiGe films have compressive stress with a positive stress profile (positive strain gradient). After the excimer laser annealing, the strain gradient of the film will be worsened by the tensile stress on the top region of the film. However, if excimer laser annealing is applied to a film with negative strain gradient, the strain gradient of the annealed film will change in the positive direction toward zero.

The results of the excimer annealing study are summarized in Table 5.4. A bi-layer deposition recipe was chosen to generate a film with negative strain gradient with the stress tuning technique [5.13]. The bottom layer was deposited at higher temperature with higher germanium content compared to the top layer. After the ELA, the resistivity of the film remains the same, whereas the residual stress and the strain gradient change in the positive direction. The texture of the as-deposited and ELA-ed films can be compared with the cross-sectional TEM images shown in Figures 5.12 and 5.13.

**TABLE 5.4** Summary of post-deposition excimer laser annealing (ELA).

Recipe	Energy (mJ/cm <sup>2</sup> )	Resistivity (m $\Omega$ -cm)	Stress (MPa)	Strain Gradient ( $\mu\text{m}^{-1}$ )
As-deposited	NA	1.4	-7	$-1.23 \times 10^{-4}$
ELA-a	200	1.4	7	$-2.05 \times 10^{-5}$
ELA-b	400	1.4	40	$5.90 \times 10^{-4}$
ELA-c	600	1.4	72	$1.07 \times 10^{-3}$

The melted depth is about 250 nm for 600 mJ/cm<sup>2</sup> fluence. The tensile stress of this melted thin region is a few hundreds of MPa and creates a large positive bending

moment, therefore the strain gradient changes significantly after annealing. Since the melting and re-solidification involves reflow, the surface roughness of the film decreases after the annealing.

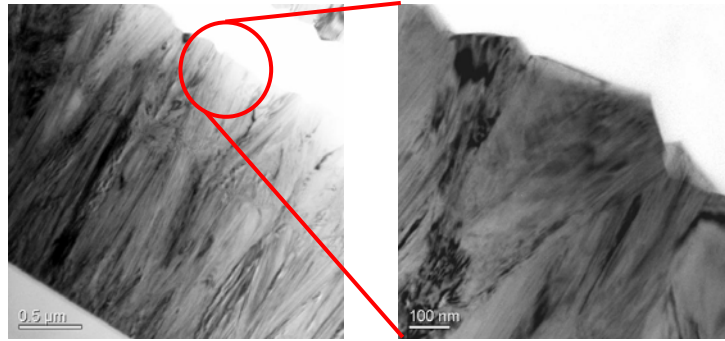


**Figure 5.12** Cross-sectional TEM image for the as-deposited film in the ELA experiment

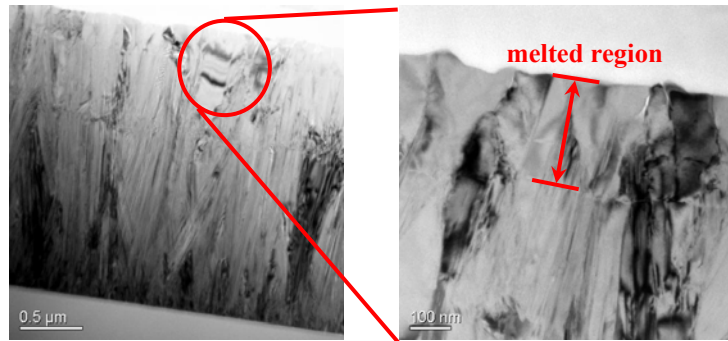


**Figure 5.13** Cross-sectional TEM image for ELA-c

Excimer laser annealing has the lowest thermal budget of all the annealing method discussed above, because the heating is limited to the top region of the poly-SiGe film and the underlying CMOS won't be affected. However, the mechanical properties of the poly-SiGe film are very sensitive to the laser energy and achieving low strain gradient with good uniformity is very difficult.

## 5.5 Argon implantation

Ion implantation and machining have each been used to modify the stress in thin films [5.14], [5.15]. Argon implantation is a low-cost and high-throughput process that is readily available in the IC industry. Therefore, the effect of argon implantation (AI) on the strain gradient was studied in this work, for different doses and acceleration energies. Multiple-layered poly-SiGe films deposited by Recipe LayerStack (ref. Table 4.2) were used in this study. The results are summarized in Table 5.5.

**TABLE 5.5** Summary of post-deposition argon implantation (AI) for deposition LayerStack.

Recipe	Energy (keV)	Dose (cm <sup>-2</sup> )	Resistivity (mΩ-cm)	Stress (MPa)	Strain Gradient (μm <sup>-1</sup> )
As-deposited	NA	NA	3.1	-229	-1.17 × 10 <sup>-4</sup>
AI-a	30	1 × 10 <sup>14</sup>	4.7	-201	-4.97 × 10 <sup>-5</sup>
AI-b	65	1 × 10 <sup>14</sup>	5.9	-198	1.25 × 10 <sup>-5</sup>
AI-c	100	1 × 10 <sup>14</sup>	5.7	-189	1.32 × 10 <sup>-4</sup>
AI-d	100	1 × 10 <sup>13</sup>	3.4	-207	-1.97 × 10 <sup>-4</sup>
AI-e	100	1 × 10 <sup>12</sup>	3.1	-203	-1.44 × 10 <sup>-4</sup>
AI-f	180	1 × 10 <sup>16</sup>	1.9	-162	6.25 × 10 <sup>-4</sup>

As an extreme case, Figures 5.14 and 5.15 show the stress profiles and cross-sectional-TEM for the as-deposited film and a film implanted with  $1 \times 10^{16} \text{ cm}^{-2} \text{ Ar}^+$  at 180 keV. The implantation amorphizes the top portion ( $\sim 0.3 \text{ μm}$ ) via damage to the crystalline structure, and thereby relieves the compressive stress within this portion of the film. The implant also causes a small drift of the stress in the position direction in the middle region of the film compared to Figure 5b. Though not apparent from the X-TEM image, some argon ions penetrate the film beyond the amorphized region, which may possibly account for the small amount of stress relaxation in the middle region of the film. Overall, the stress profile after argon implantation has a positive slope (increasing from the bottom of the film to the top of the film) and results in a strain gradient of  $6.25 \times 10^{-4} \text{ μm}^{-1}$ , whereas the as-deposited film has a strain gradient of  $-1.2 \times 10^{-4} \text{ μm}^{-1}$ .

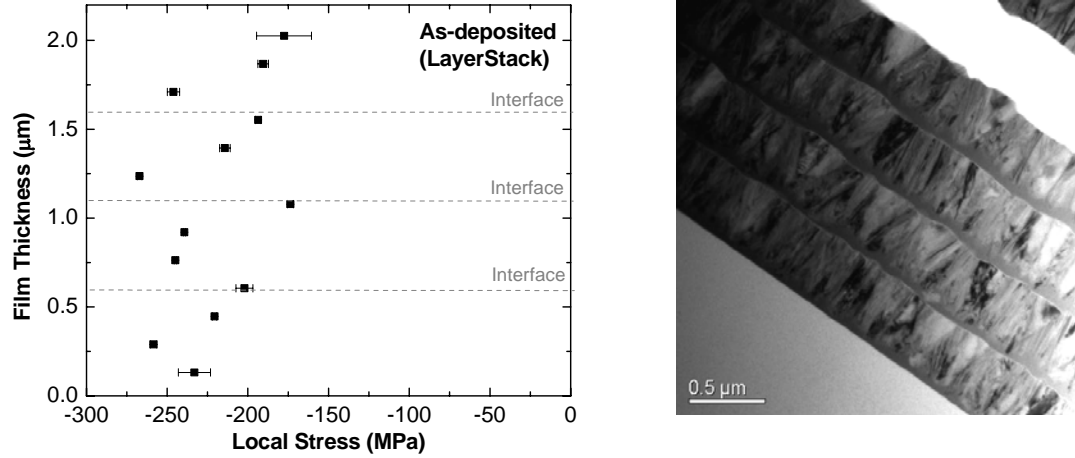


**Figure 5.14** Stress profile and cross-sectional TEM image for the as-deposited film (film deposited by Recipe LayerStack)

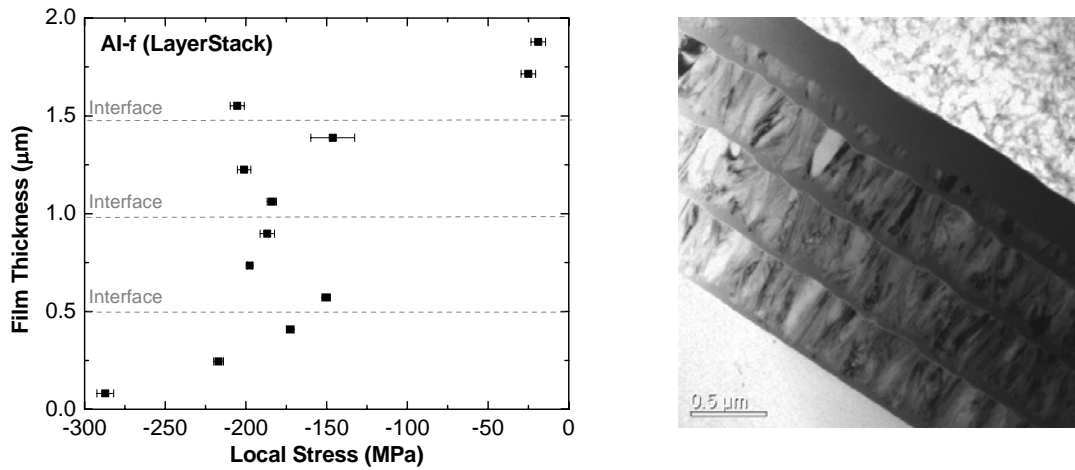


**Figure 5.15** Stress profile and cross-sectional TEM image for AI-f (film deposited by Recipe LayerStack)

The amorphization thickness and the stress distribution within the film can be modified with the implant dose and acceleration energy. Thus the strain gradient can be tuned by ion implantation. Figure 5.16 shows the relationship between the strain gradient and the argon implantation conditions. X-TEM images are inserted next to most of the data points, and clearly show the upper amorphized region created by the implantation. For a given dose, higher acceleration energy results in thicker amorphized region. Amorphization does not occur for dose  $\leq 1 \times 10^{13} \text{ cm}^{-2}$  at 100 keV. The lowest strain gradient is achieved with  $1 \times 10^{14} \text{ cm}^{-2}$  dose and 65 keV acceleration energy.

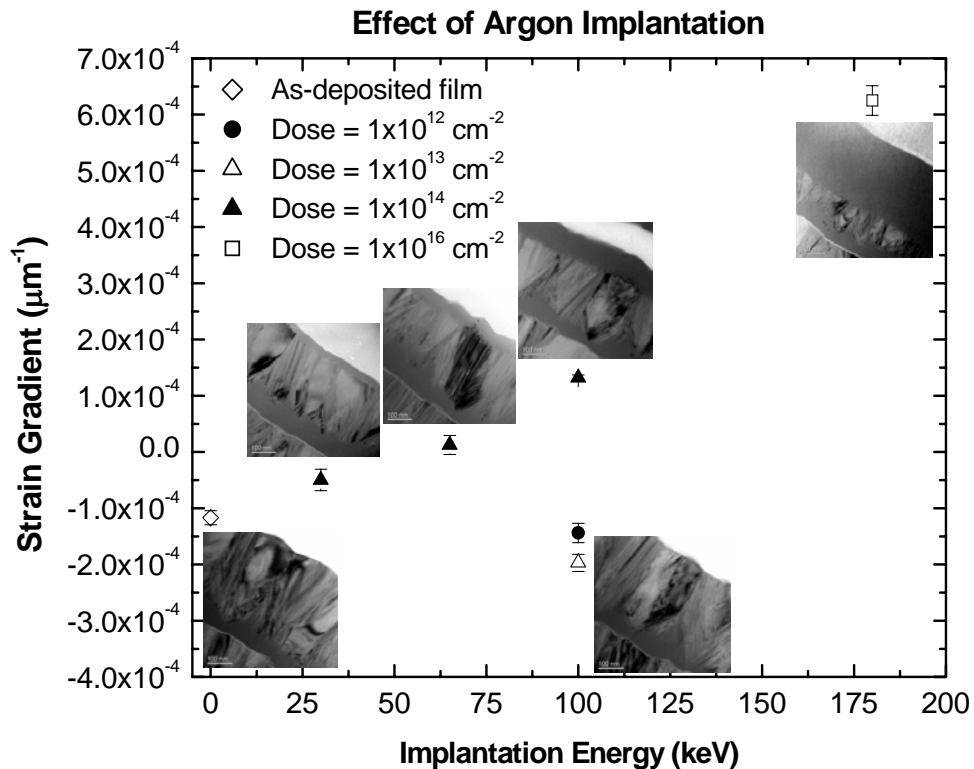


**Figure 5.16** Correlation of strain gradient with post-deposition argon implantation conditions.

It should be noted that the implanted film remains electrically conductive (resistivity  $< 10 \text{ m}\Omega\text{-cm}$ ) even though the upper portion is amorphous. However, the resistivity is lower for the case with maximum dose and energy and this is not well-understood. No increase in wet-etch rate in heated  $\text{H}_2\text{O}_2$  solution is seen for the implanted film.

Among all the post-processing methods discussed above, ion implantation is the lowest thermal budget method. It also has the advantage being a standard low-cost and high throughput process in IC manufacturing and has well controlled process uniformity and repeatability.

## **5.6 CMOS thermal budget limitations**

Integration of SiGe MEMS on CMOS had been demonstrated before. Franke *et al.* first demonstrated SiGe MEMS resonators on  $3 \text{ }\mu\text{m}$  gate-length CMOS circuitry made in the UC Berkeley Microfabrication Laboratory [5.3]. Witvrouw *et al.* demonstrated a SiGe MEMS gyroscope over  $0.35 \text{ }\mu\text{m}$  foundry CMOS circuitry [5.16]. Takeuchi *et al.* studied the thermal budget limits of  $0.25 \text{ }\mu\text{m}$  foundry CMOS circuitry by rapid thermal annealing and furnace annealing [5.5]. In this work,  $0.13 \text{ }\mu\text{m}$  and  $0.25 \text{ }\mu\text{m}$  foundry CMOS are studied with the thermal budget generated by the actual MEMS film depositions.

### **5.6.1 Processing of the MEMS layers**

Since there were a limited amount of  $0.13 \text{ }\mu\text{m}$  and  $0.25 \text{ }\mu\text{m}$  foundry CMOS chips provided by collaborators, the CMOS thermal budget test were done at the die level. As

shown in Figure 5.17, a thin layer of pure germanium was first deposited as the passivation for the sacrificial release. Then 2  $\mu\text{m}$  of oxide was deposited as the sacrificial layer. Lastly, 2  $\mu\text{m}$  of SiGe structure layer was deposited. The thermal history the CMOS chips experience for the depositions includes:

Ge deposition – 3 hr 30 min. at 350°C

Oxide deposition – 4 hr 30 min. at 400°C

SiGe deposition – 5 hr 45 min. at 410°C

There is temperature fluctuation of  $\pm 20^\circ\text{C}$  during stabilization for each deposition. The CMOS chips were split into three groups. Some had no further thermal processing, some were flashed lamp annealed at 700°C for 1 ms and some were rapid thermal annealed at 430 °C for 1 minute.

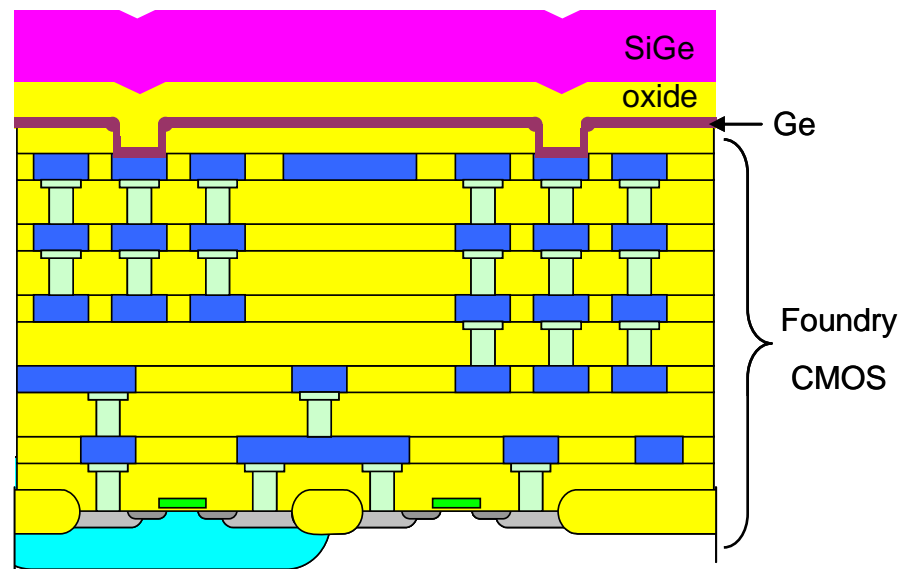


**Figure 5.17** Schematic of MEMS layers processing on foundry CMOS

In order to do electrical measurement of CMOS after the MEMS processing, the MEMS films need to be stripped off to re-expose the metal bond pads for probing. The SiGe film was stripped off using a reactive ion etch at 60°C. The oxide sacrificial layer was removed in HF solution (50 ml 49% HF + 200 ml DI water) at room temperature for 10 minutes. The germanium layer was removed in 30% H<sub>2</sub>O<sub>2</sub> solution at 80°C for 5 minutes.

### **5.6.2 Metal contact damage**

During the film removal steps, metal contact damage is observed. Figure 5.18 shows the conditions of the metal contact along the film removal steps. Since pre-measurement was done on the CMOS electronics, there are probe marks left on the metal contacts. The residue around the bond pads become visible after the removal of the SiGe film. By the end of the film removal processes, the residual is clearer and there is almost no metal left on the contact.

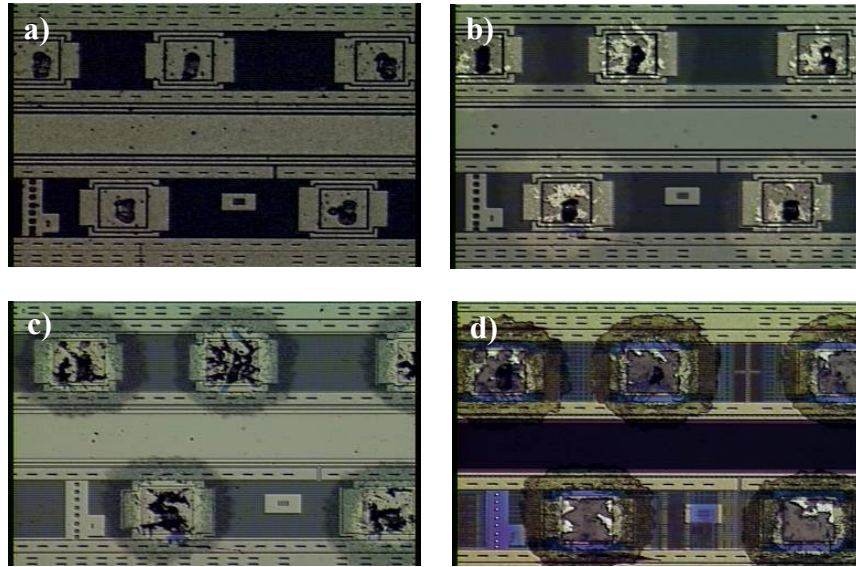


**Figure 5.18** CMOS metal contacts: a) after all depositions; b) after SiGe film removal; c) after oxide film removal; d) after Ge film removal

The chips with no further thermal processing after the depositions and the ones with furnace annealing or flash-lamp annealing have similar metal contact damage. The chips that went through the rapid thermal annealing have more damage, as shown in Figure 5.19. Film delamination happened right after the RTA step. The MEMS layers and the CMOS passivation peeled off and the metal contacts were exposed. The metal contacts were completely damaged during the film removal processes.

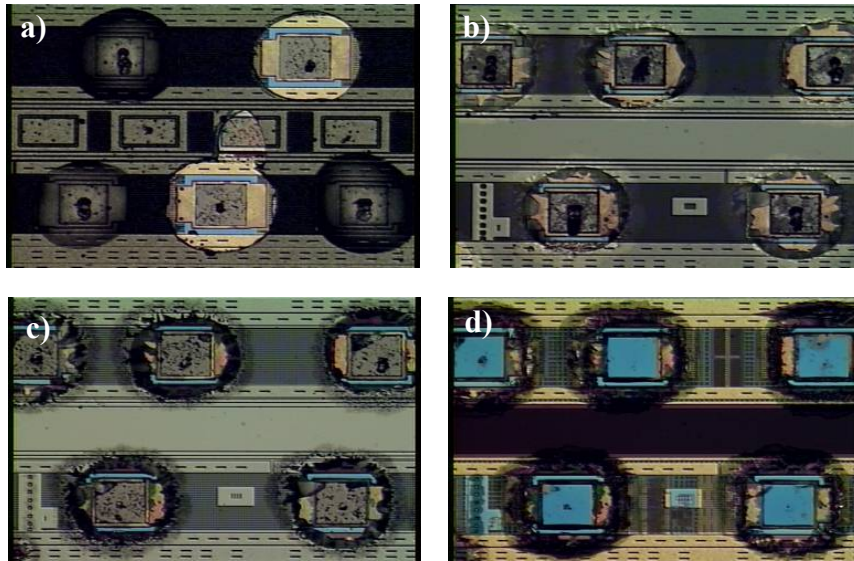


**Figure 5.19** CMOS metal contacts: a) after all depositions and rapid thermal annealed at 430°C; b) after SiGe film removal; c) after oxide film removal; d) after Ge film removal

In order to understand the origin of the metal contact damage, etch experiments were done on CMOS chips with no film deposited on them. Figure 5.20(a) shows that the peroxide etch does not attach the metal layer. Figure 5.20(b) shows that the HF etch attaches the metal, but does not create the residual damage around the bond pads as seen before. Therefore the bond pad damage shown in Figures 5.18 and 5.19 is not caused by HF attack through the germanium passivation.

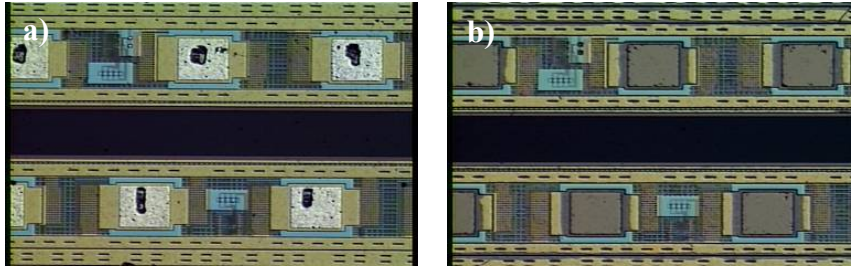


**Figure 5.20** CMOS metal contacts: a) without depositions and etched in 30% H<sub>2</sub>O<sub>2</sub> solution at 80°C for 5 minutes; b) without depositions and etched in HF solution (50 ml 49% HF + 200 ml DI water) at room temperature for 10 minutes

The damage of the metal contact is likely due to Al and Ge reaction. The eutectic point of Al-Ge is at 420°C [5.17]. During temperature stabilization for the LTO and SiGe depositions, the temperature can easily exceed 420°C. Aluminum diffuses into the germanium layer. After the film removal, the Al-Ge residue becomes visible around the metal contact. A thin layer of TiN should be used between aluminum and the germanium layers. TiN is being used as diffusion barrier for Si and Al, also SiGe and Al. In addition, TiN can be removed using H<sub>2</sub>O<sub>2</sub> solution [5.18].

### 5.6.3 Film delamination after RTA

Figure 5.19(a) shows that the film delaminates after the 430 °C RTA. However, no delamination is observed with furnace annealing or flash lamp annealing. Previous experiments show that RTA has a more dramatic effect on mechanical properties compared to long furnace annealing at the same temperature. It is believed that the actual

RTA temperature is higher than specified. The poor adhesion is likely due to the change in stress after the RTA.

As described in Figure 5.17, Ge, SiO<sub>2</sub> and SiGe layers are deposited on foundry CMOS chips sequentially. The stress of individual film after each thermal process is summarized in Table 5.6. For these measurements, thermal budget of the sequential depositions is generated by furnace annealing at comparable temperature and duration. The germanium layer has the most significant stress change since the sequential depositions and annealing step are at higher temperatures compared to its deposition temperature.

**TABLE 5.6** Stress of individual thin film after each thermal process step

Thin Film	Stress after Ge dep.	Stress after oxide dep.	Stress after SiGe dep.	Stress after RTA
Ge	-220 MPa	NA	-144 MPa	5 MPa
SiO <sub>2</sub>	NA	-46 MPa	-30 MPa	-31 MPa
SiGe	NA	NA	-215 MPa	-137 MPa

RTA experiments were also done with different thin film stacks to check their adhesion. The results are listed in Table 5.7. The single or double-layer films show no delamination after the RTA, whereas the SiGe, SiO<sub>2</sub> and Ge tri-layer stack delaminates on either silicon substrate or CMOS chips due to the larger mismatch in stress.

**TABLE 5.7** Adhesion of various thin film stacks after RTA at 430 °C for 1 minute

Film stack	Delamination
Ge on Si substrate	No
SiO <sub>2</sub> on Si substrate	No
Ge and SiO <sub>2</sub> on Si substrate	No
SiGe and SiO <sub>2</sub> on Si substrate	No
SiGe, SiO <sub>2</sub> and Ge on Si substrate	Yes
SiGe, SiO <sub>2</sub> and Ge on CMOS chips	Yes

#### **5.6.4 Electrical measurements**

Electrical measurements on the same device were made before and after the process and compared. Transistors, Kelvin test structures for via resistance and metal resistance were measured for the 0.13  $\mu\text{m}$  technology. Previous results show that the an increase in via resistance limits the thermal budget for 0.25  $\mu\text{m}$  CMOS technology [5.5]. In this study, none of the 0.25  $\mu\text{m}$  via structures were measurable before the processing. Only the transistor was tested for the 0.25  $\mu\text{m}$  technology. The CMOS test results are summarized in Table 5.8. Due to the metal contact damage, post-process measurement is affected by the contact resistance significantly, especially for the 2-terminal devices. Isolating the failure caused by the thermal process metal contact damage is difficult.

**Table 5.8** CMOS test summary

Process	Technology	Chip ID	Device	Survive?	Failure analysis
Depositions FLA @ 700 °C for 1 ms Film removals	0.13 μm	MOS1	NMOS	Yes	
			PMOS	Yes	
		MOS2	NMOS	Yes/No	Large gate leakage
			PMOS	No	Punch through
		Kel1	via1	Yes	
			via2	Yes	
			via3	Yes	
			via4	No	Damaged metal line
			via5	Yes	
			via6	No	Damaged metal line
			via7	No	Damaged metal line
		Kel2	via1	Yes	
			via2	Yes	
			via3	No	Damaged metal line
			via4	No	Damaged metal line
			via5	No	Damaged metal line
			via6	No	Damaged metal line
		Met1	m1	Yes	
			m2	Yes	
			m3	Yes	
			m4	Yes	
			m5	No	Bad contact
			m6	Yes	
			m7	Yes	
			m8	Yes	
		Met2	m1	No	Bad contact
			m2	No	Bad contact
			m3	No	Bad contact
	m4		No	Bad contact	
	m5		No	Bad contact	
	m6		No	Bad contact	
	m7		No	Bad contact	
m8	No		Bad contact		
0.25 μm	Die1	NMOS	Yes		
		PMOS	Yes		
	Die2	NMOS	Yes		
		PMOS	Yes		
	Die3	NMOS	No		
		PMOS	Yes		
Depositions RTA @ 430 °C for 1 min Film removals	0.13 μm	MOS3	NMOS	No	No gate control
			PMOS	Yes	
		Kel3	via1	Yes	
			via2	Yes	
			via3	No	Damaged metal line
			via4	Yes	
			via5	No	Damaged metal line
			via6	No	Damaged metal line
		Met3	via7	No	Damaged metal line
			m1	No	Bad contact
			m2	No	Bad contact
			m3	No	Bad contact
			m4	No	Bad contact
			m5	No	Bad contact
	m6		No	Bad contact	
	m7		No	Bad contact	
	m8	No	Bad contact		
	0.25 μm	Die4	NMOS	No	
			PMOS	No	

Depositions Film removals	0.13 $\mu\text{m}$	MOS4	NMOS	Yes	
			PMOS	Yes	
		Kel4	via1	Yes	
			via2	Yes	
			via3	Yes	
			via4	Yes	
			via5	No	Damaged metal line
			via6	No	Damaged metal line
			via7	No	Damaged metal line
		Met4	m1	Yes	
			m2	Yes	
			m3	Yes	
			m4	Yes	
			m5	No	Bad contact
	m6		No	Bad contact	
	m7		No	Bad contact	
	m8		No	Bad contact	
	0.25 $\mu\text{m}$	Die5	NMOS	Yes	
PMOS			Yes		

In summary, the group of samples that did not go through additional annealing has the best survival rate. Most of the devices could not survive rapid thermal annealing. Film delamination after the RTA exposes the devices to the HF solution during the sacrificial oxide removal. Also, the actual temperature of the RTA tool is believed to be higher than the set point as discussed in section 5.2. The performance of the flash lamp annealing group falls in-between that of the unannealed devices and the RTA-ed devices.

The performance of the surviving 0.13  $\mu\text{m}$  technology transistors is plotted in Figure 5.21. The threshold voltage, on-current, off-current, sub-threshold swing and transconductance of the NMOS devices increase after the process. The threshold voltage of the PMOS devices becomes more negative and the on-current, off-current and sub-threshold swing decrease. The change in transconductance is inconsistent. The NMOS performance does not degrade as much as the PMOS. For the PMOS, the  $I_{\text{on}}$  change is smaller compared to the change in  $V_t$ , but the  $I_{\text{off}}$  change is consistent with the change in  $V_t$ . The degradation in PMOS performance is a bigger concern.

The performance of the Kelvin via and metal electromigration structures for 0.13  $\mu\text{m}$  technology are plotted in Figure 5.22 and Figure 5.23. Resistance increases for all devices after processing. Most of the dead devices have visible broken metal lines due to the film removal process. There are also many devices not measurable due to contact damage.

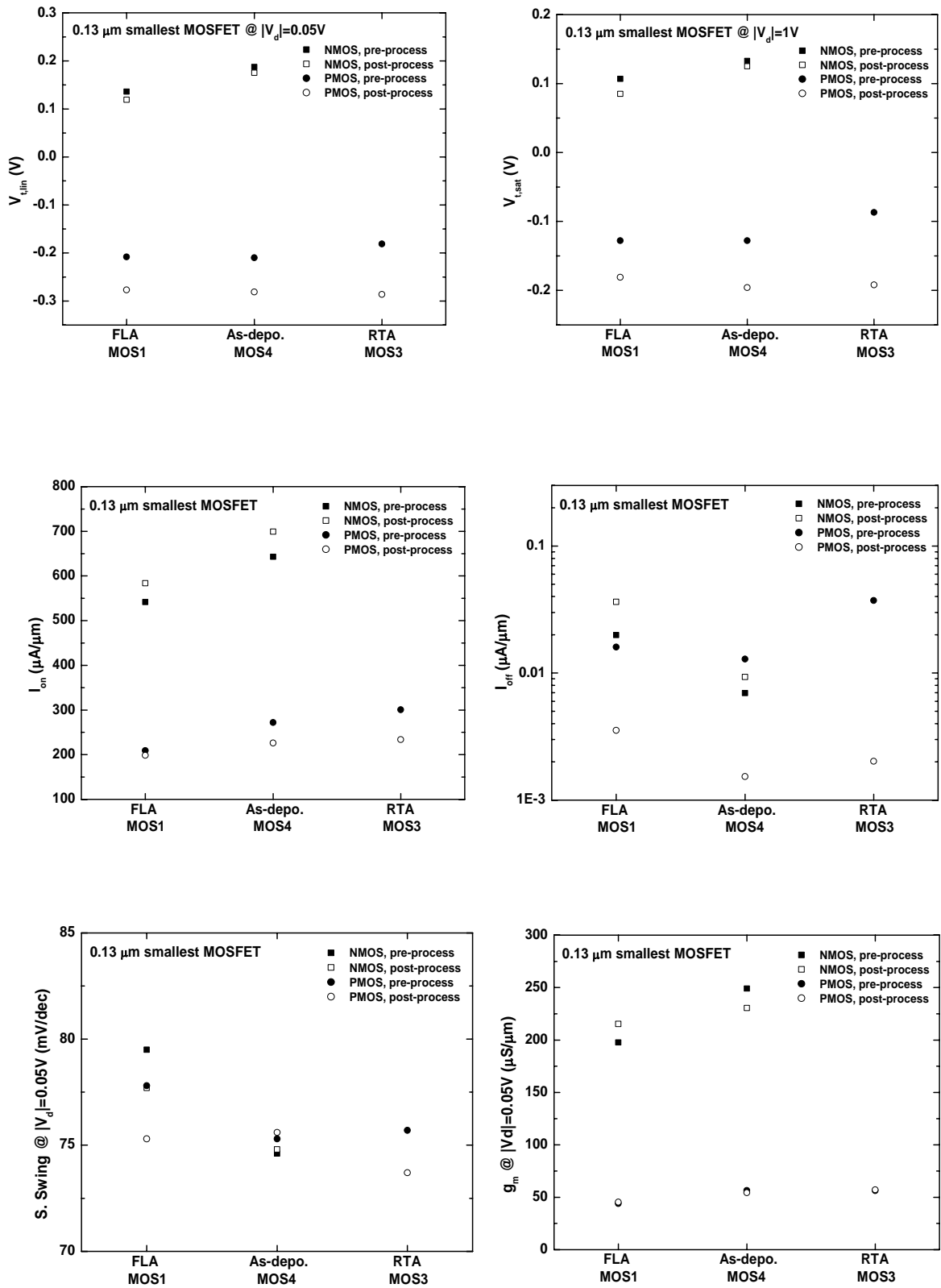
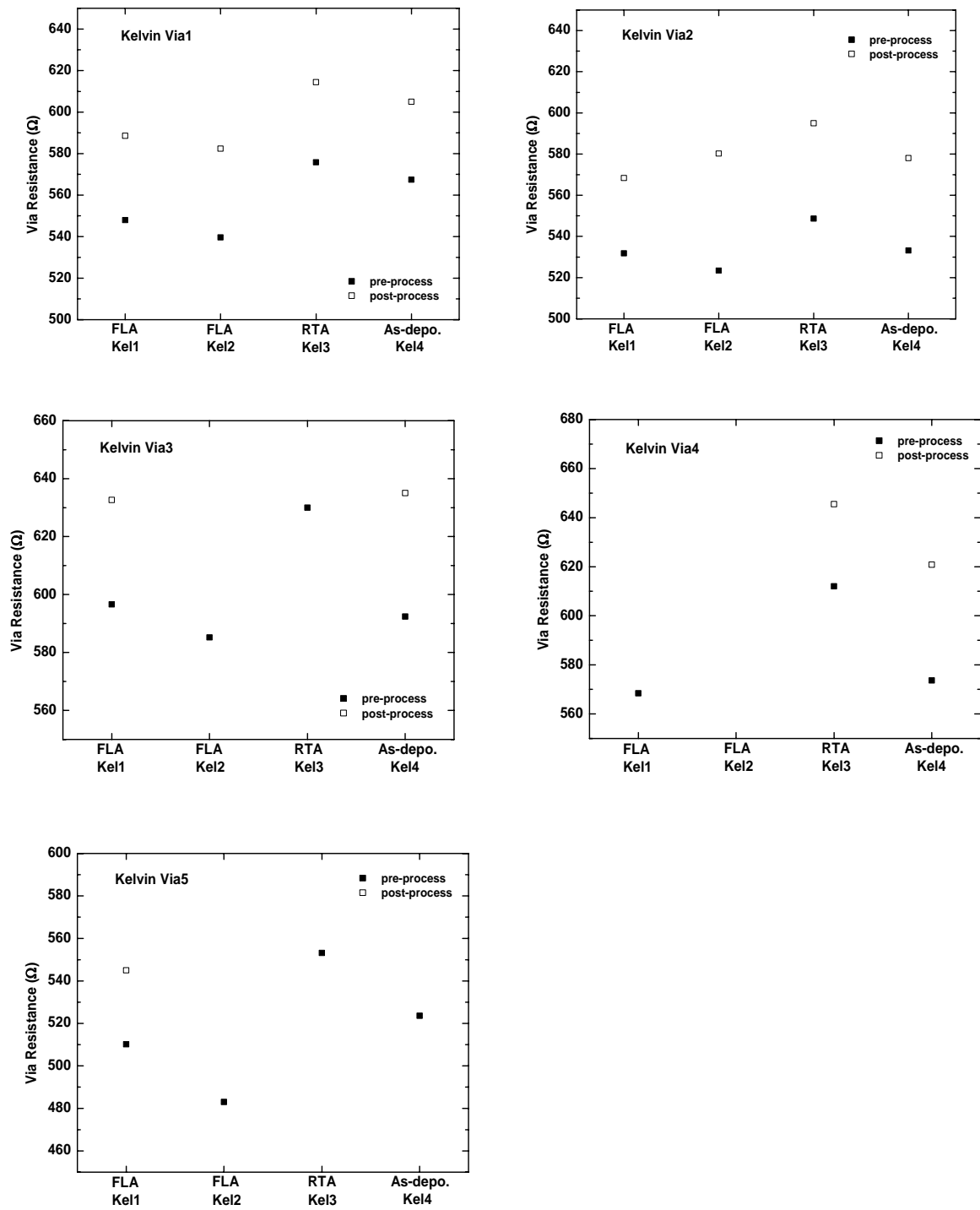
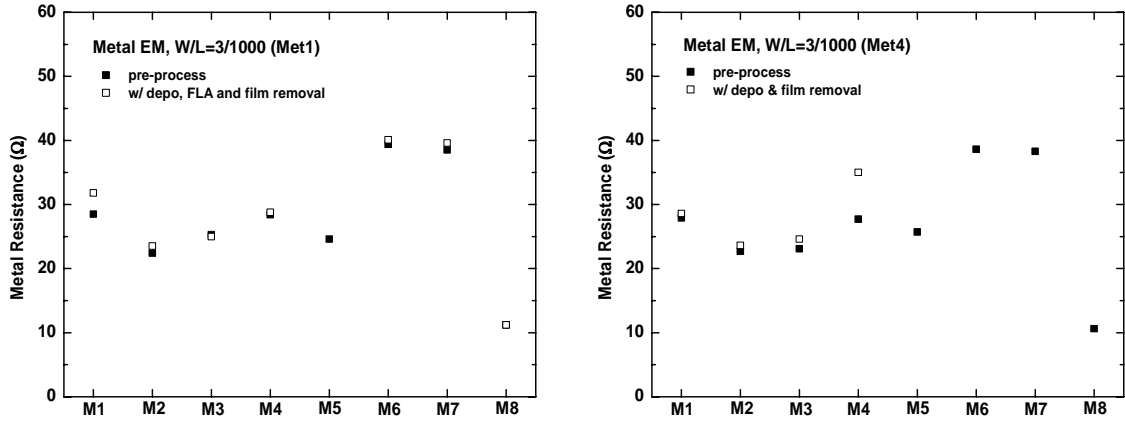


Figure 5.21 0.13 μm technology transistor performance before and after post-processing.



**Figure 5.22** 0.13  $\mu\text{m}$  technology Kelvin via resistance before and after post-processing.



**Figure 5.23** 0.13  $\mu\text{m}$  technology metal electromigration test structure resistance before and after post-processing

The performance of the 0.25  $\mu\text{m}$  technology transistors are plotted in Figure 5.24. The threshold voltage of the NMOS moves in the negative direction. The threshold voltage of PMOS moves in the positive direction. The relative change is less than 3%. The on-current change doesn't show the same trend for all annealing conditions. The off-current increases after annealing, which is consistent with the threshold voltage shift.

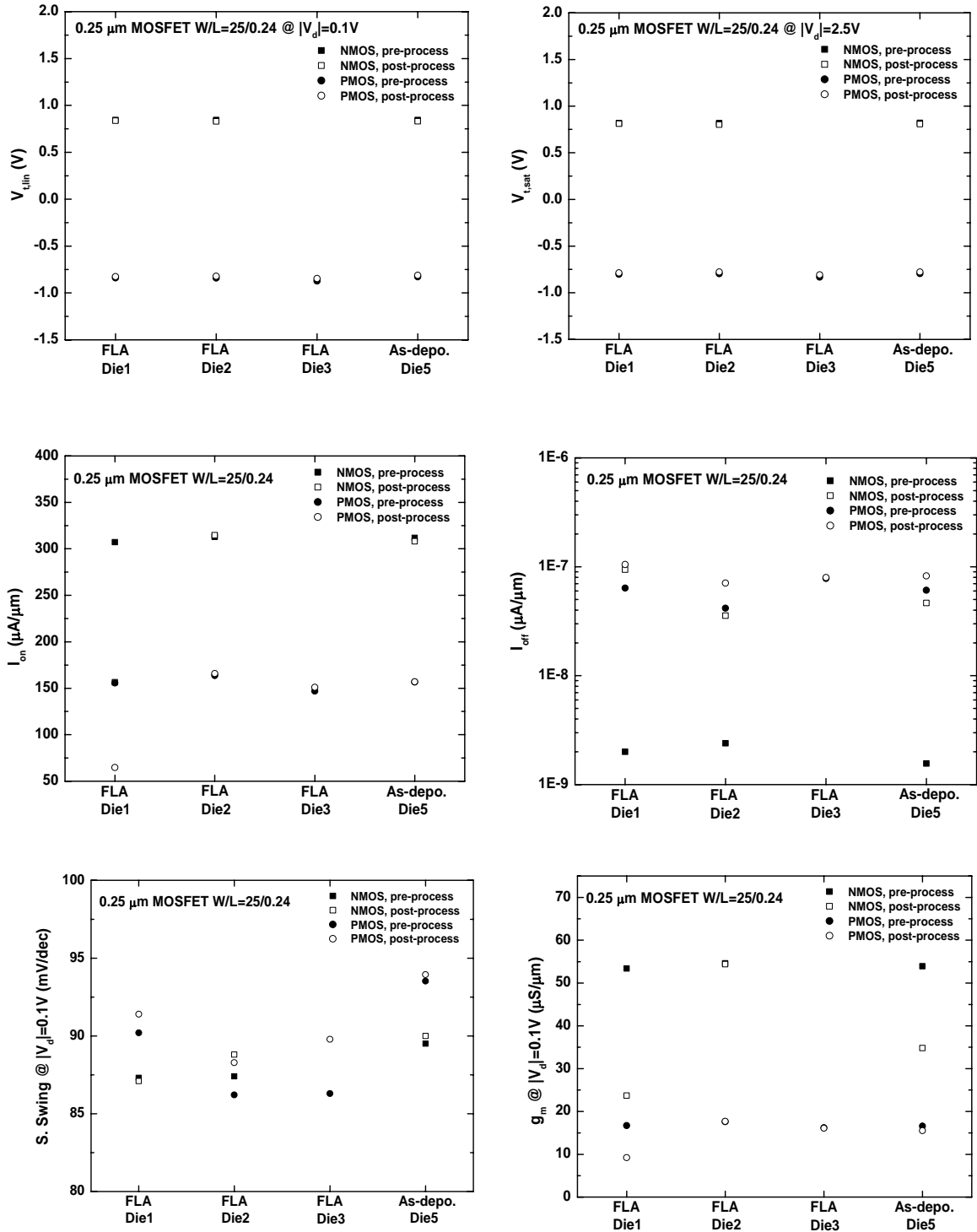


Figure 5.24 0.25 μm technology transistor performance before and after post-processing.

## 5.7 Summary

A variety of post-deposition processes are discussed in this chapter. Annealing the poly-SiGe film at elevated temperature can crystallize the bottom amorphous region. The top polycrystalline region can be melted and re-crystallized with an excimer laser. High dose and high energy argon ion implantation can be used to amorphize the top crystalline region. All of these post-processes can alter the film mechanical properties. With the appropriate combination of deposition and post-processing, the desired film properties can be achieved. However, the as-deposited film can also have the desired mechanical properties, as described in Chapter 4. Post-deposition processing of poly-SiGe is not recommended for tuning the mechanical properties, because of additional sources of variability. Also, caution is advised for back-end processes such as anti-stiction coating and encapsulation at elevated temperature.

The CMOS thermal budget limit study with the film depositions and removals was inconclusive. Without a Ti/TiN barrier layer, inter-diffusion between the aluminum and the germanium passivation layer damages most of the electrical contacts. Thus, the cause of the apparent degradation in device performance cannot be definitively attributed to the thermal post-processing. Another experiment conducted with equivalent thermal budget furnace annealing is needed to eliminate apparent degradation due to metal contact damage. A full process with film depositions and removals can then be repeated with the Ti/TiN barrier layer deposited first.

## References

- [5.1] P. A. Krulevitch, "Micromechanical investigations of silicon and Ni-Ti-Cu thin films," Ph.D. Thesis, Dept. of ME, University of California at Berkeley (1994)
- [5.2] K. Nunan, G. Ready, P. Garone, G. Sturdy and J. Sledziewski, "Developing a manufacturable process for the deposition of thick polysilicon films for micro machined devices," in *Proceedings of IEEE/SEMI Advanced Semiconductor Manufacturing Conference*, pp. 357-366 (2000)
- [5.3] A. E. Franke, Ph.D. thesis, "Polycrystalline silicon-germanium films for integrated Microsystems," Ph.D. Thesis, Dept. of EECS, University of California at Berkeley, 2000
- [5.4] S. A. Bhawe, B. L. Bircumshaw, W. Z. Low, Y.-S. Kim, A. P. Pisano, T.-J. King and R. T. Howe, "Poly-SiGe: A high-Q structural material for integrated RF MEMS," in *Proc. Solid-State Sensors and Actuators Workshop*, Hilton Head Island, SC, 2002, pp. 34-37
- [5.5] H. Takeuchi, A. Wu, X. Sun, R. T. Howe and T. -J. King, "Thermal budget limits of quarter-micron foundry CMOS for post-processing MEMS devices," *IEEE Trans. Electron Devices*, vol. 52, pp. 2081-2086, 2005
- [5.6] T. Gebel, M. Voelskow, W. Skorupa, G. Mannino, V. Privitera, F. Priolo, E. napolitani and A. Carnera, "Flash lamp annealing with millisecond pulses for ultra-shallow boron profiles in silicon," *Nuclear Instruments and Methods in Physics Research Section B: Beam Interactions with Materials and Atoms*, vol. 186, issue 1-4, pp. 287-291, 2002
- [5.7] H. Wirth, D. Panknin, W. Skorupa and E. Niemann, "Efficient p-type doping of 6H-

- SiC: Flash-lamp annealing after aluminum implantation,” *Applied Physics Letters*, 74, issue 7, pp. 979-981 (1999)
- [5.8] T. Ito, K. Suguro, T. Itani, K. Nishinohara, K. Matsuo and T. Saito, “Improvement of threshold voltage roll-off by ultra-shallow junction formed by flash lamp annealing,” *Proceedings of 2003 Symposium on VLSI Technology*, pp. 53-54, 2003
- [5.9] S. Sedky, J. Schroeder, T. Sands, R. T. Howe, T. -J. King, “Pulse Laser Annealing of Silicon Germanium Films”, *Material Research Society Symposium Proceedings*, 741, J4.1.2-6, p. 61-66, 2002
- [5.10] S. Sedky, R. T. Howe, and T.-J. King, “Pulse laser Annealing, a low thermal budget technique for eliminating stress gradient in poly-SiGe MEMS structures”, *Journal of Microelectromechanical Systems*, vol. 13(4), pp. 669-675, 2004
- [5.11] S. Sedky, M. Gromova, T. Van der Donck, J.-P. Celis and A. Witvrouw, “Characterization of KrF excimer laser annealed PECVD Si<sub>x</sub>Ge<sub>1-x</sub> for MEMS post-processing,” *Sensors and Actuators A*, vol. 127, pp. 316-323, 2006
- [5.12] C. W. Low, M.S. report, “Excimer laser annealing of silicon germanium for MEMS applications,” Dept. of EECS, University of California at Berkeley, 2004
- [5.13] B. C.-Y. Lin, T.-J. King and R. T. Howe, “Optimization of poly-SiGe deposition processes for modular MEMS integration,” in *Proc. Materials Research Society Meeting, Symposium A*, Boston, MA, December 1-5, 2003, pp. A2.4.1-6
- [5.14] T. G. Bifano, H. T. Johnson, P. Bieden and R. Krishnamoorthy Mali, “Elimination of stress-induced curvature in thin-film structures”, *IEEE J. MEMS*, vol. 11, no. 5, pp. 592-597, 2002
- [5.15] W. Shi, H. Zhang, S. Wang, G. Zhang and Z. Li, “Modifying residual stress and

- stress gradient in LPCVD Si<sub>3</sub>N<sub>4</sub> film with ion implantation,” *13th International Conference on Solid-State Sensors, Actuators and Microsystems* pp. 824-827, 2005
- [5.16] A. Witvrouw, A. Mehta, A. Verbist, B. Du Bois, S. Van Aerde, J. Ramos-Martos, J. Ceballos, A. Ragel, J. M. Mora, M. A. Lagos, A. Arias, J. M. Hinojosa, J. Spengler, C. Leinenbach, T. Fuchs and S. Kronmüller, “Processing of MEMS gyroscopes on top of CMOS ICs,” in *Proc. 52nd IEEE International Solid-State Circuits Conference*, San Francisco, CA, February 6-10, 2005, pp. 88-89
- [5.17] B. Predel, Landolt-Bornstein, Group IV Physical Chemistry - *Phase Equilibria, Crystallographic and Thermodynamic Data of Binary Alloys, Volume 5 - Electronic Materials and Semiconductors*, Springer – Verlag, 1998
- [5.18] M.-A. N. Eyoum, PhD thesis, “Modularly integrated MEMS technology”, Dept. of EECS, University of California at Berkeley, 2006

## Chapter 6: Conclusion

### 6.1 Contributions of this work

The development of LPCVD poly-SiGe for MEMS applications started in UC Berkeley about a decade ago. A few generations of researchers have contributed to the fundamental understanding of the technology. As the technology has matured, interest for commercialization has grown. Most of the work done in this thesis is driven by industrial interests.

Reducing the thermal budget is an important consideration for post-CMOS integration. However, meeting both specifications for thermal budget and materials properties is challenging, especially for the strict strain gradient requirement for inertial sensor applications. There have been some efforts to improve strain gradient with post-deposition annealing. It is found that the post-deposition annealing adds extra variables to the process in addition to the extra thermal budget in most cases. Developing as-deposited films with the desired materials properties is preferred. Since temperature has an exponential effect on thermal budget, reducing the deposition temperature is an ongoing effort for poly-SiGe development. Table 6.1 summarizes the materials development of as-deposited LPCVD poly-SiGe films to date. The latest results of PECVD film are also listed for comparison. Stress balancing with multiple-layer depositions was used by Bhave [6.2], Lin [6.3] and Mehta [6.4] for strain gradient optimization. Comparing the results for LPCVD films, a recipe with the lowest thermal budget and the lowest strain gradient is developed in this thesis work. Comparing the best recipes for the LPCVD and the PECVD systems, the mechanical properties of the films

are comparable. Although the deposition rate of the best LPCVD recipe is an order of magnitude lower than that of the best PECVD recipe, a lower deposition temperature of 410°C was used in the LPCVD recipe. Microcrystalline SiGe deposited at 400°C or lower is under development using the PECVD system, but the desired materials properties have not been achieved yet [6.4]. Excimer laser annealing of PECVD SiGe deposited at 210°C is another low thermal budget approach for controlling mechanical properties [6.5]. Excimer laser annealing does not increase the thermal budget of the underlying CMOS since the thermal treatment is localized to the topmost MEMS layer. However, the excimer laser annealing step adds extra variables to the process. Also, compromise has to be made between electrical conductivity and strain gradient.

**TABLE 6.1** Summary of materials development of poly-SiGe (as-deposited films)

Method	Leading researcher	Date	Temp. (°C)	Time (min)	Thn. (µm)	Ge cont. (%)	Res. (mΩ-cm)	Stress (MPa)	Best strain gradient (µm <sup>-1</sup> )
LPCVD	Franke [6.1]	2000	450	180	3.1	67	1.8	10	$1.9 \times 10^{-4}$
LPCVD	Bhave [6.2]	2002	425		3	68/65/62			$1.8 \times 10^{-4}$
LPCVD	Lin [6.3]	2003	425		3.9	69/65	0.55	-36	$1.1 \times 10^{-5}$
LPCVD	Low	2006	410	480	3.5	60	0.65	-157	$1.1 \times 10^{-6}$
PECVD	Mehta [6.4]	2005	450	40	4	65/56	1.0	20	$3.5 \times 10^{-6}$

For the interest of high volume manufacturing, this thesis work furthers the understanding of the sensitivity of materials properties to process variations and improves the process stability with new process gases and hardware modifications. Having a stable and efficient dopant gas significantly reduces the maintenance effort and improves the process repeatability. *In-situ* control of the SiH<sub>4</sub> to GeH<sub>4</sub> gas flow ratio is also an important aspect of process monitoring.

In the interest of minimizing the strain gradient for inertial sensor applications, extensive materials analysis was performed to understand the correlations among the

deposition condition, the microstructure, and the mechanical properties. Boron-doped poly-SiGe films generally have vertically oriented grains, either conical or columnar in shape. Films with small strain gradient usually have columnar grain structure with low defect density. The uniformity of films deposited in a batch LPCVD reactor can be improved by increasing the deposited film thickness, using a proper seeding layer, and/or depositing the film in multiple layers.

## 6.2 Recommendations for future work

As the poly-SiGe MEMS technology is being transferred to industry, a more robust process is required for high volume manufacturing. Better equipment and tighter process control are necessary to generate high yield. Developing in-line measurement methods for film thickness and germanium content will be important for statistical process control.

For fundamental research, it would be interesting to study the process with the newly developed single-source silicon and germanium precursors  $\text{SiGe}_2\text{H}_8$  and  $\text{SiGeH}_6$ . These precursors have the potential of providing higher deposition rate and producing uniform germanium content film across a large batch.

While a deposition process that gives as-deposited low strain gradient film has been developed with large columnar microstructures, long term repeatability has not been proven. Fine-grained poly-Si films have been demonstrated with reproducibly low strain gradients. The grain size of poly-Si is control by *in-situ*  $\text{PH}_3$  or  $\text{O}_2$  doping [6.6]. Therefore, additional work can be done to investigate the feasibility of depositing fine-grained poly-SiGe films with average grain size approximately an order of magnitude

smaller than the film thickness, to achieve uniformly low strain gradient. Boron-doped poly-SiGe films always have conical or columnar microstructures. Phosphorus-doped poly-SiGe films can have fine-grained microstructures, but the deposition rate is retarded [6.1]. Carbon doping might provide another option to generate fine-grained microstructures. Carbon is commonly used in epi-SiGe for bandgap engineering and strain compensation, where  $\text{SiH}_3\text{CH}_3$  is the carbon precursor used in the CVD system. Carbon might be able to serve as an impurity to break up the grain formation and result in fine-grained microstructures.

## References

- [6.1] A. E. Franke, "Polycrystalline silicon-germanium films for integrated Microsystems", Ph.D. Thesis, Dept. of EECS, University of California at Berkeley, 2000
- [6.2] S. A. Bhave, B. L. Bircumshaw, W. Z. Low, Y.-S. Kim, A. P. Pisano, T.-J. King and R. T. Howe, "Poly-SiGe: a high-Q structural material for post-CMOS integrated RF MEMS," in *Proc. Solid-State Sensor, Actuator, and Microsystems Workshop*, Hilton Head Island, SC, 2003, pp. 34-37
- [6.3] B. C.-Y. Lin, T.-J. King and R. T. Howe, "Optimization of poly-SiGe deposition processes for modular MEMS integration," in *Proc. Materials Research Society Meeting, Symposium A*, Boston, MA, December 1-5, 2003, pp. A2.4.1-6
- [6.4] A. Mehta, M. Gromova, P. Czarnecki, K. Baert and A. Witvrouw, "Optimization of PECVD poly-SiGe layers for MEMS post-processing on top of CMOS," in *Proc. 13th International Conference on Solid-State Sensors, Actuators and Microsystems (Transducers 05)*, Seoul, Korea, June 5-9, 2005, pp. 1326-1329
- [6.5] S. S. Sedky, O. Mortagy and A. Witrouw, "Low thermal budget techniques for controlling stress in SiGe deposited at 210°C," in *Proc. Materials Research Society Meeting*, San Francisco, CA, January, 2006
- [6.6] K. Nunan, G. Ready, P. Garone, G. Sturdy and J. Sledziewski, "Developing a Manufacturable Process for the Deposition of Thick Polysilicon Films for Micro Machined Devices," *Proceedings of IEEE/SEMI Advanced Semiconductor Manufacturing Conference*, pp. 357-366, 2000

## **Appendix A: SAM Coating of Poly-SiGe for Stiction Reduction**

The large surface-to-volume ratio of MEMS devices makes them vulnerable to adhesion upon contact. The interfacial forces between surfaces include capillary, van der Waals, and electrostatic attractions. Capillary force causes stiction of the structure to the substrate during the sacrificial layer wet etch – so-called “release stiction”; van der Waals and electrostatic attraction cause surfaces permanently to adhere to each other during device operation – “in-use stiction”. Overcoming these interfacial forces is essential for the successful fabrication and operation of MEMS devices.

### **A.1 SAM overview**

Various techniques have been investigated to achieve low adhesion energy [A.1]. Surface modification using hydrophobic self-assembled monolayers (SAM) is one of the most successful strategies, as it addresses both release and in-use stictions. SAM coatings are conformal with dense and stable structures. In addition, the ability to tailor both the head and the tail groups of the constituent molecules gives a large variety of feasible coating materials.

Self-assembled monolayers (SAM) are molecular assemblies that are formed spontaneously by the immersion of the appropriate substrate into a solution of an active surfactant in an organic solvent. The molecule consists of three main parts. The first part is the head group, which chemisorbs at all of the surface sites, resulting in a close-packed monolayer. The second part is the alkyl chain, where van der Waals interactions between chains contribute further to the ordering of the monolayer. The third part is the terminal

group. For anti-stiction purposes, a methyl terminal group makes the surface hydrophobic.

Poly-Si has been a conventional MEMS material for more than a decade and various SAM coatings for poly-Si have been investigated [A.2 – A.6]. Poly-SiGe is a promising material for the modular integration of MEMS and CMOS, due to its low process thermal budget and its good electrical and mechanical properties [A.7]. Poly-SiGe MEMS processing shares many similarities with poly-Si processing; stiction is unfortunately also a problem with poly-SiGe. In this work, the feasibility of SAM coating on poly-SiGe is studied. OTS and 1-octadecene SAM were applied to poly-Si, poly-SiGe and poly-Ge surfaces for comparison. Effectiveness of the coating was measured by the water contact angle. N<sub>2</sub> ambient annealing was applied to SAM coated films for thermal stability study.

## **A.2 Experimental details**

Poly-Si, poly-SiGe and poly-Ge films used in this SAM study were deposited in conventional LPCVD reactors. The poly-SiGe film has approximately 68% germanium content. All films have surface roughness less than 3 nm rms so that topography does not affect the coating and the contact angle measurement significantly.

Alkyltrichlorosilane-based monolayer OTS [CH<sub>3</sub>(CH<sub>2</sub>)<sub>17</sub>SiCl<sub>3</sub>] and alkene-based monolayer 1-octadecene [CH<sub>3</sub>(CH<sub>2</sub>)<sub>15</sub>CH=CH<sub>2</sub>] were studied in this experiment. Both precursor molecules contain a straight 18-carbon chain and a hydrophobic CH<sub>3</sub> tail group. Both molecules bind to the substrate only at one end, but with different mechanisms. The chlorosilane molecules of the OTS react with water to form silanols, which then condense

to form siloxane polymers with the elimination of water [A.2]. The alkene-based SAM abandons the chlorosilane chemistry and adopts a free radical reaction of a primary alkene [1-octadecene,  $\text{CH}_3(\text{CH}_2)_{15}\text{CH}=\text{CH}_2$ ] to bind the precursor molecule to a hydrogen terminated silicon surface with a Si-C bond [A.4].

The coating procedure of OTS and 1-octadecene are listed in Tables A.1 and A.2. A hexadecane and carbon tetrachloride mixture with 6:4 volume ratio was used as the OTS solvent. The OTS concentration was approximately 1mM. The 1-octadecene solution was prepared with 10% volume of 1-octadecene with 90% volume of hexadecane as the solvent. All chemicals used in the SAM coating process were standard solvent grade except hexadecane and chloroform were anhydrous (Aldrich Chemical Co.).

**TABLE A.1** OTS coating procedure

<b>Purpose</b>	<b>Procedure</b>	<b>Duration</b>
Cleaning	Acetone rinse	5 min.
	IPA rinse	5 min.
	DI wafer rinse	5 min.
	UVO light*	5 min.
Oxidation	HF etch	5 min.
	UVO light*	5 min.
SAM coating	IPA rinse	5 min.
	OTS mixture	60 min.
Cleaning	IPA rinse	5 min.
	DI water rinse	5 min.

\* Poly-SiGe and poly-Ge films did not get the UVO light treatment since their oxides form readily in air.

**TABLE A.2** 1-octadecene coating procedure

<b>Purpose</b>	<b>Procedure</b>	<b>Duration</b>
Cleaning	Acetone rinse	5 min.
	IPA rinse	5 min.
	DI wafer rinse	5 min.
H termination	HF rinse and dry	5 min.
SAM coating	IPA rinse	5 min.
	1-octadecene mixture @ 180°C with N <sub>2</sub> purge	30 min.
	Petroleum ether rinse	5 min.
Cleaning	IPA rinse	5 min.
	DI water rinse	5 min.

The thermal stability of the coatings in N<sub>2</sub> ambient was tested using a rapid thermal annealing system. Temperature was ramped up to the set point from room temperature in 30 sec, the set temperature stayed constant for 5 minutes and then slowly cooled down to room temperature in about an hour.

The effectiveness of the SAM coatings and thermal stability were evaluated with static water contact angle measurement. Data were taken with DI water (resistivity > 18 MΩ) according to the sessile droplet method. Droplet size was approximately 4 μl.

### **A.3 Results and discussion**

#### **A.3.1 Film characterization**

Water contact angle data given in Figure A.1 and Table A.3 confirms that well-packed monolayers are formed on all poly-Si, poly-SiGe and poly-Ge surfaces. Data for uncoated samples are also listed for reference. Samples exposed to ambient humidity for 5 days show similar water contact angles, which indicates the SAM coatings do not degrade in ambient at room temperature.

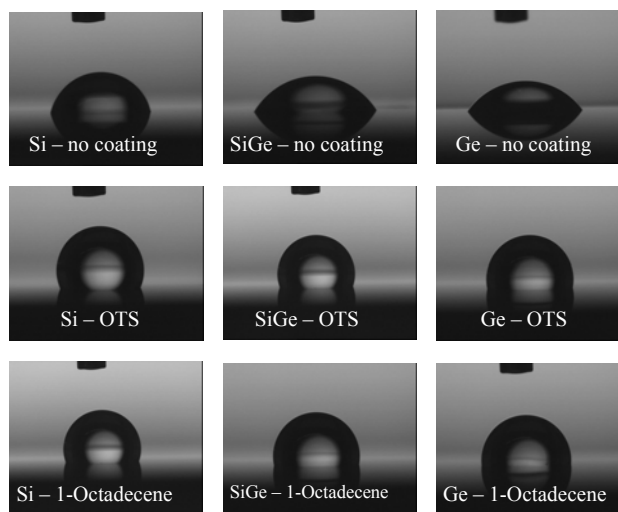


**Figure A.1** Images of water droplet on various surfaces

**TABLE A.3** Water contact angle data for poly-Si, poly-SiGe and poly-Ge surfaces

Coating	Poly-Si	Poly-SiGe	Poly-Ge
None	71.3°	60.5°	54.7°
OTS	116.4°	114.3°	112.3°
1-octadecene	108.8°	100.9°	93.5°

The contact angle data indicate that all surfaces become hydrophobic after the SAM coating. However, having large water contact angle is not sufficient to show that the head group of SAM is chemically bonded to the substrate.

The data show that the contact angle decreases with germanium content for both SAM coatings. In the case of OTS on oxidized poly-Si, absorption takes place through the hydrolysis of the Si-Cl bonds to form Si-OH groups; the OH groups interact with OH groups on the oxidized surface, forming Si-O-Si bonds to the substrate through condensation reaction. Si-O-Si bonds are also form between adjacent head groups, creating a cross-linked network at the surface [A.2]. If a similar reaction happens on oxidized poly-SiGe or poly-Ge surfaces with the formation of Si-O-Si and/or Ge-O-Ge

bonding networks, the larger cell dimension of germanium would reduce the packing density of OTS molecules, resulting in smaller water contact angles.

For the case of 1-octadecene on poly-Si, the SAM molecule bonds directly to the hydrogen terminated silicon [A.4]. By analogy with this reaction, one would expect that hydrogen terminated germanium surfaces would be required for the bonding to form at the substrate. It is well known that germanium surfaces are less stable compared to Si surfaces and that a native germanium oxide layer forms readily in air [A.8]. It has been observed that an HF dip makes poly-Si hydrophobic, whereas poly-SiGe and poly-Ge remain hydrophilic. Therefore, it is unclear that if 1-octadecene are chemically bonded to germanium. It has been reported that 1-octadecene could coat substrates other than hydrogen terminated silicon without chemical bonding and still result in large water contact angles [A.4].

### **A.3.2 Thermal stability**

Thermal stability of the SAM coatings has been investigated in N<sub>2</sub> ambient since most MEMS packaging processes contain steps at elevated temperatures. The resulting water contact angle data of the films after heating are summarized in Figure A.2 and Figure A.3. We found that OTS coating survives to higher temperatures, consistent with results reported on poly-Si surface [A.2, A.4, A.9, and A.10].

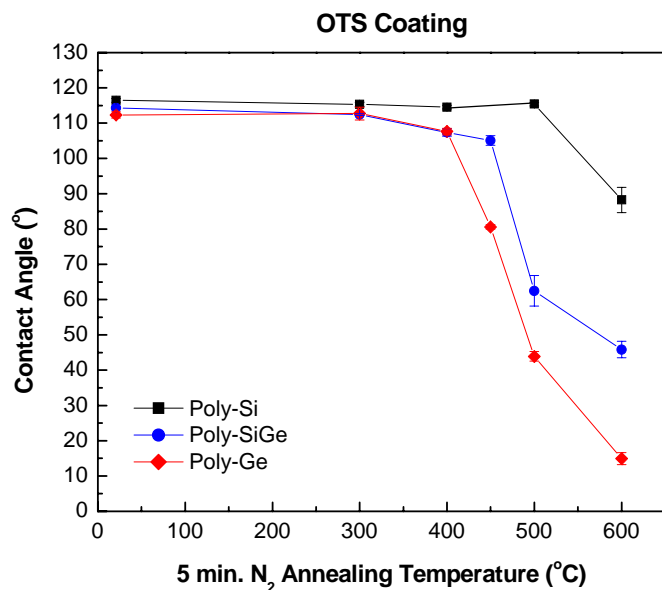


**Figure A.2** Water contact angle measurements on OTS SAM-coated Si, SiGe and Ge to assess thermal stability in N<sub>2</sub> ambient.

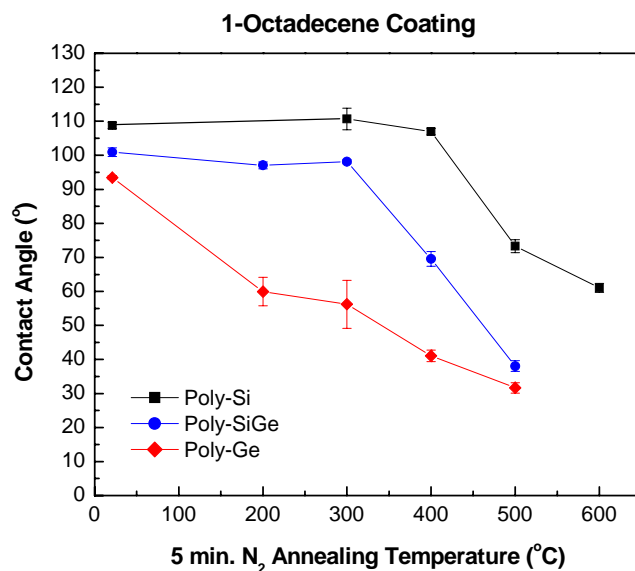


**Figure A.3** Water contact angle measurements on 1-octadecene SAM-coated Si, SiGe and Ge to assess thermal stability in N<sub>2</sub> ambient.

There are three possibilities for the OTS decomposition mechanism: cleavage of the Si-O or Ge-O head group bond, cleavage of the Si-C bond, and cleavage of the C-C bond. Thermal stability of OTS coating on oxidized silicon surface has been well-studied with high resolution electron energy loss (HREEL) spectrum [A.9]. HREEL spectrum shows that the siloxane head groups remain on the surface until about 827°C. Si-C modes are hard to detect due to the presence of the Si-O-Si symmetric stretch. If Si-C bond cleavage were occurring to a significant extent, the entire chain would be desorbed completely. Gradually decrease in water contact angle upon heating suggests that the decomposition of OTS coated Si surface begin with the cleavage of C-C bonds at 467°C. As a result of the C-C bond cleavage, a shorter alkyl radical is left on the surface and reactions with molecular hydrogen in the ambient yield CH<sub>3</sub> group at the tail. Although the chain length has been significantly reduced, the monolayer is still reasonably well-ordered at a temperature slightly higher than the C-C bond cleavage point.

If OTS coatings on poly-SiGe or poly-Ge are analogous, we would expect them to have similar thermal stability as poly-Si. However, the data show that thermal stability decreases with increased germanium content. Since germanium oxide is known to be unstable at elevated temperature [A.8], the Ge-O bond cleavage might happen before the C-C bond cleavage.

The desorption mechanism of 1-octadecene monolayer on silicon surface is very different from OTS [A.10]. HREEL spectrum shows the presence of Si-H groups following annealing to 377 °C. This suggests the desorption of the alkyl monolayers occurs through  $\beta$ -hydride elimination. At higher temperatures, the entire chain decomposed with SiC vibrational modes evident.

From Figure A.3, we can see the SAM coating on poly-SiGe follows the trend of poly-Si, but break down starts at a lower temperature. On the other hand, poly-Ge breaks down at a significantly lower temperature compared to poly-Si. As discussed before, the germanium oxide could not be eliminated before the 1-octadecene coating. The head group of the SAM might not be able to bond to the germanium surface with the Ge-C bond. Upon heating, the SAM molecules become disordered due to the lack of chemical bonding at the head group. For the case of coating on poly-SiGe, there should exist some Si-C bonds. However, the packing density of the monolayer should be lower compared to that of poly-Si surface, which results in smaller water contact angle and worse thermal stability.

#### **A.4 Summary**

Water contact angle measurement shows that self-assembled monolayer coatings on unpatterned poly-SiGe surfaces have hydrophobic properties and reasonable thermal stability. The existence of germanium oxide at the surface degrades the packing density and thermal stability of the SAM coating. Comparing OTS and 1-octadecene coatings, OTS monolayer gives higher water contact angle and better thermal stability on poly-SiGe surface. Due to the existence of germanium oxide at the poly-SiGe surface, alkyltrichlorosilane-based monolayer is believed to be a better coating material for poly-SiGe than alkene-based monolayer.

Further experiments should be done with cantilever beam array to characterize the release and in-use stiction of the SAM-coated poly-SiGe surfaces. HREEL spectroscopy

should also be used to further study the correlation between the germanium content and the desorption mechanism.

## References

- [A.1] R. Maboudian, R. T. Howe, "Critical review: Adhesion in surface micromechanical structures," *J. Vac. Sci. Technol. B* vol. 15(1), pp. 1-19, 1997
- [A.2] U. Srinivasan, M. R. Houston, R. T. Howe, and R. Maboudian, "Alkyltrichlorosilane-based self-assembled monolayer films for stiction reduction in silicon micromachines," *J. MEMS*, vol. 7(2), pp. 252-260, 1998
- [A.3] B. H. Kim, T. D. Chung, C. H. Oh and K. Chun, "A new organic modifier for anti-stiction," *J. MEMS*, vol. 10(1), pp. 33-40, 2001
- [A.4] W. R. Ashurst, C. Yau, C. Cararo, C. Lee, G. J. Kluth, R. T. Howe, R. Maboudian, "Alkene based monolayer films as anti-stiction coatings for polysilicon MEMS," *Sensors and Actuators A*, vol. 91(3), pp. 239-248, 2001
- [A.5] T. M. Mayer, M. P. de Boer, N. D. Shinn, P. J. Clews, and T. A. Michalske, "Chemical vapor deposition of fluoroalkylsilane monolayer films for adhesion control in microelectromechanical systems," *J. Vac. Sci. Technol. B*, vol. 18(5), pp. 2433-2440, 2000
- [A.6] W. R. Ashurst, C. Carraro, R. Maboudian and W. Frey, "Wafer level anti-stiction coatings for MEMS," *Sensors and Actuators A*, vol. 104(3), pp. 213-221, 2003
- [A.7] A. E. Franke, J. M. Heck, T. -J King, and R. T. Howe, "Polycrystalline silicon germanium films for integrated Microsystems," *J. MEMS*, vol. 12, pp. 160-171, 2003
- [A.8] K. Prabhakaran, F. Maeda, Y. Watanabe, and T. Ogino, "Thermal decomposition pathway of Ge and Si oxides: observation of a distinct difference," *Thin Solid Films*, vol. 369, pp. 289-292, 2000

- [A.9] G. J. Kluth, M. M. Sung, and R. Maboudian, "Thermal behavior of alkylsiloxane self-assembled monolayers on the oxidized Si(100) surface", *Langmuir*, vol. 13, pp. 3775-3780, 1997
- [A.10] M. M. Sung, G. J. Kluth, R. W. Yauw, and R. Maboudian, "Thermal behavior of alkyl Monolayers on silicon surfaces," *Langmuir*, vol. 13, pp. 6164-6168, 1997

## **Appendix B: Stress Stability of LPCVD Poly-SiGe and SiO<sub>2</sub> Films**

Reliability specifications typically require MEMS structural layers to have long-term material stability. In past research, results from the analysis of wafer curvature over time appeared to indicate that poly-SiGe films experience a stress drift in humid environments [B.1]. This observation created a major challenge to the plausibility of poly-SiGe MEMS technology. In order to understand the stress-drift phenomenon, multi-layer thin film stress is modeled [B.2] with the same methodology used to derive the Stoney Equation [B.3]. Results show that the residual stress of poly-SiGe films is, in fact, stable in ambient conditions. The apparent residual stress drift of the poly-SiGe films reported in Ref. [B.1] was caused by the unstable low temperature LPCVD oxide on the backside of the wafers.

### **B.1 Experimental details**

The average residual stresses of various thin films were determined with wafer curvature measurements before and after thin film deposition using a Tencor FLX-2320. Long term average residual stress monitoring was done with various layer stacks as shown in Figure B.1. Poly-Si, poly-SiGe, and poly-Ge, as well as various oxides, were deposited and removed from single crystal silicon (SCS) wafers under different conditions as summarized in Table B.1. Initial wafer curvature measurements were taken from the bare Si wafer for the single layer stacks (Figure B.1a & Figure B.1b), and from the oxidized wafer before poly-Si, poly-SiGe or poly-Ge deposition for the bi-layer stacks (Figure B.1c).

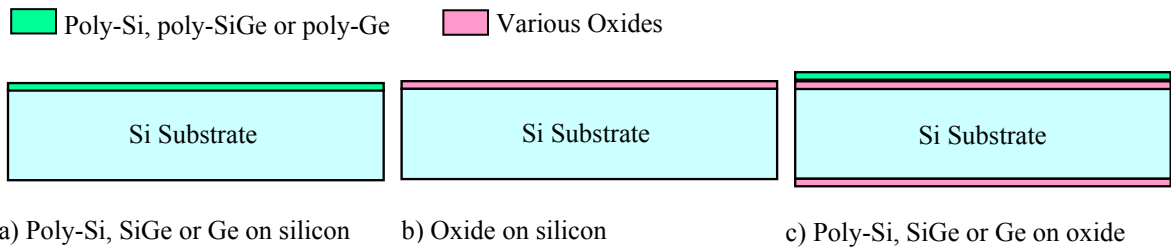


**Figure B.1** Layer stacks for stress monitoring

**TABLE B.1** Deposition and removal conditions of the various thin films

Film	Deposition method	Removal method
Poly-Si (0.6 $\mu\text{m}$ )	LPCVD @ 620°C	RIE @ 60°C
Poly-SiGe (0.2 – 1 $\mu\text{m}$ )	LPCVD @ 400 – 450°C	RIE @ 60°C
Poly-Ge (0.4 $\mu\text{m}$ )	LPCVD @ 350°C	RIE @ 60°C
Dry thermal oxide (1200 Å)	Thermally growth @ 1050°C	HF solution @ 21°C
Wet thermal oxide (1600 Å)	Thermally growth @ 1050°C	HF solution @ 21°C
LPCVD oxide (2 $\mu\text{m}$ )	LPCVD @ 450°C	HF solution @ 21°C
PECVD oxide (0.5 $\mu\text{m}$ )	LPCVD @ 390°C	NA (single side deposition)

## B.2 Results and discussions

Wafers used in Ref. [B.1] to monitor the stress stability had a poly-SiGe film deposited on top of a 2  $\mu\text{m}$  LPCVD oxide, as shown in Figure B.1c. This layer stack is commonly used in MEMS: the thick oxide serves as a sacrificial layer and the poly-SiGe serves as the structural layer. For comparison purposes, the results reported in Ref. [B.1] have been reproduced in this work, as plotted in Figure B.2. The measured stresses of poly-SiGe and poly-Ge on LPCVD oxide become more tensile over time, but all poly-Si, poly-SiGe and poly-Ge films on thermal oxide or SCS are stable. These results indicate a problem with the LPCVD oxide. It should also be noted that poly-Si films on LPCVD oxide are more stable than poly-SiGe and poly-Ge films on the same oxide. This is because, during the poly-Si deposition, the LPCVD oxide is annealed at 620 °C.

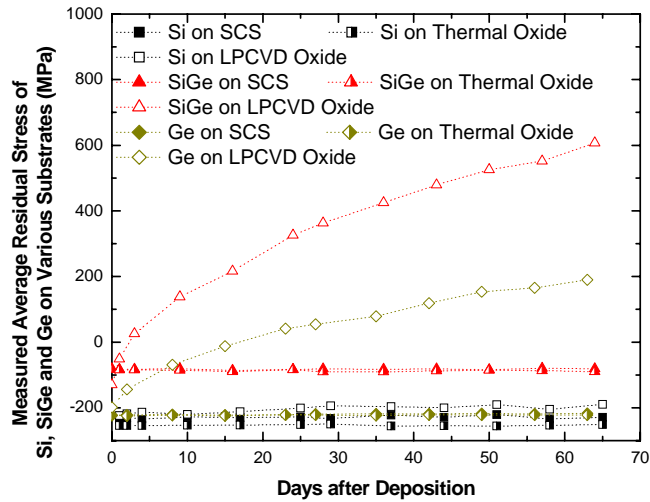


**Figure B.2** Stress stability of poly-Si, SiGe and Ge on various substrates.

Further experimentation was done with the poly-SiGe on LPCVD oxide wafers (Figure B.3). If the backside poly-SiGe films of two similar wafers are removed at different times, the drift profiles and absolute stresses of the wafers are nearly identical, with an offset in the x-axis. When the backside poly-SiGe and LPCVD oxide films are both removed, the stresses of the topside poly-SiGe and LPCVD oxide films become stable. This suggests that the stress drift reported in Ref. [B.1] is due solely to the instability of the LPCVD oxide film exposed to the ambient on the backside of the wafer.

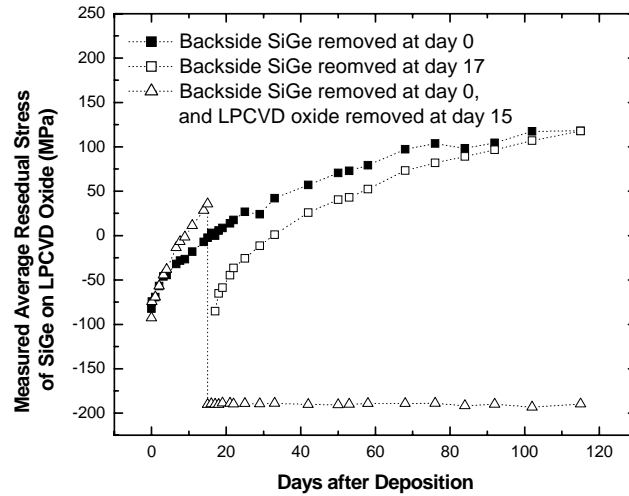


**Figure B.3** Stress stability of poly-SiGe on LPCVD oxide

Low-temperature (450°C) LPCVD oxide films are known to be porous and of poor quality [B.4]. In this investigation, different experiments were done with LPCVD oxide wafers to characterize its stability (Figure B.4). The residual stress of the as-deposited LPCVD oxide wafer becomes more compressive over time. The “drift” rate slows over time. The backside oxide removal date does not affect the measurement. Putting the LPCVD oxide films in a desiccated environment slows down the stress drift. Annealing the films at 615°C for five hours results in a tensile film that becomes more compressive more slowly than unannealed films. The above facts suggest that the absorption of ambient water into the LPCVD oxide films is the major cause of the observed stress drift. As water is absorbed, the films become more compressive. The 615°C N<sub>2</sub> annealing appears to densify the oxide and decreases the diffusion constant. It is also shown in Figure B.4 that if a wafer is annealed 136 days after deposition in N<sub>2</sub> at 425°C for an hour, the resultant stress was approximately that of a fresh oxide film. The

stress drift of this 425 °C annealed wafer is faster than a monitor wafer with the backside also etched on day 136. Since the 425°C anneal is lower than the deposition temperature of 450°C, it is unlikely that the anneal rearranges or densifies the oxide molecules; rather, the anneal most likely drives out the absorbed water. Ultimately, the stress drift of the 425°C annealed wafer is faster than that of the control wafer on day 136 due to a larger moisture gradient.

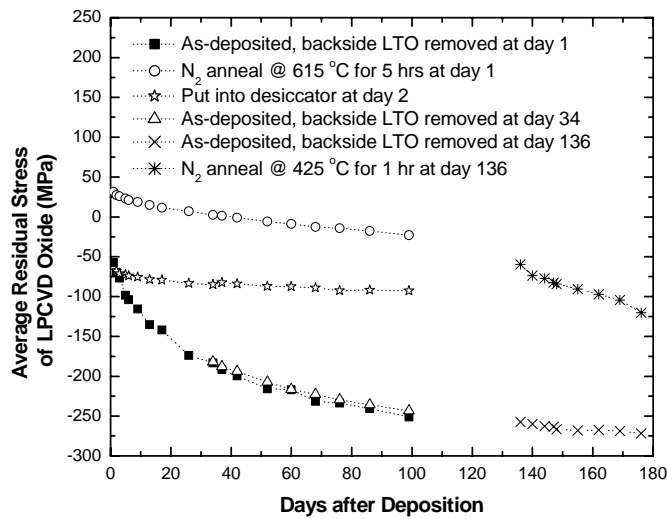


**Figure B.4** Stress stability of LPCVD oxide

Returning to the data for poly-SiGe on LPCVD oxide wafers in Figure B.3, as the backside oxide films became more compressive, the poly-SiGe film appeared to become more tensile. Data in Figure B.3 also indicates that poly-SiGe is an effective barrier to moisture. The backside LPCVD oxide did not drift until it was exposed to the ambient after the poly-SiGe layer was removed. Finally, the stress of the frontside LPCVD oxide did not drift under the poly-SiGe cap.

Figure B.5 shows the stress stability of different oxide films. The stress of the 450°C LPCVD oxide becomes more compressive while the stresses of the 1050°C dry and wet thermal oxides are nearly stable. The stresses of TEOS-based PECVD oxides deposited at 390°C also become more compressive, but at a much higher rate than the LPCVD oxide films. Also, the TEOS-based PECVD oxide films begin to saturate within 30 days of being exposed to the ambient. Their remarkably high stress drift rate is expected since TEOS-based oxides are generally more porous [B.5] and the diffusion constant of water is much higher. In contrast, silane-based PECVD oxide films were found to have better stress stability in humid environments (data not presented here).

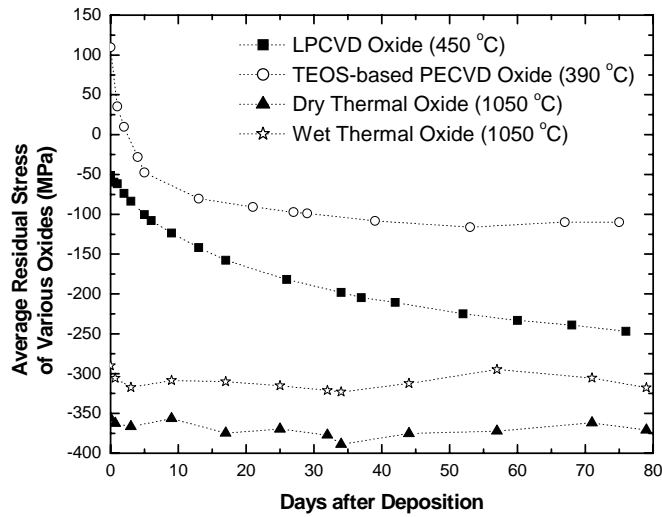


**Figure B.5** Stress stability of various oxides

### B.3 Modeling thin film stress

We can now turn to the stress analysis of  $n$  thin films on the frontside and  $m$  thin films on the backside of a single-crystal substrate wafer. In this case, the thin films experience nearly ideal biaxial stress, or plane stress. Moreover, the residual stresses in

the films are uniform over the wafer, not varying with direction or position. We shall assume that the thin films are linear, isotropic materials. This is reasonable for amorphous and poly-crystalline materials. The single-crystal substrate, on the other hand, is anisotropic. However, proper choice of the Young's modulus will minimize the error introduced by this assumption [B.6].

To proceed, we assume that there exists a neutral axis in the substrate whose position is unaffected by the existence of the films. Further, it is assumed that the deflections are small and the shear forces are negligible. Finally, we shall assume the residual stress in the thin films is small compared to the substrate stiffness, allowing us to neglect the contraction/extension of the wafer caused by the thin films. The material and geometric constants of the substrate and thin films are listed in Table B.2. Figure B.6 illustrates the setup for two frontside and two backside films.

**TABLE B.2** Material and geometric constants

	Substrate	Film f1	...	Film fn	Film b1	...	Film bm
Young's Modulus	$E_s$	$E_{f1}$	...	$E_{fn}$	$E_{b1}$	...	$E_{bm}$
Thickness	H	$h_{f1}$	...	$h_{fn}$	$h_{b1}$	...	$h_{bm}$
Residual Stress	$\sigma_s = 0$	$\sigma_{f1}$	...	$\sigma_{fn}$	$\sigma_{b1}$	...	$\sigma_{bm}$

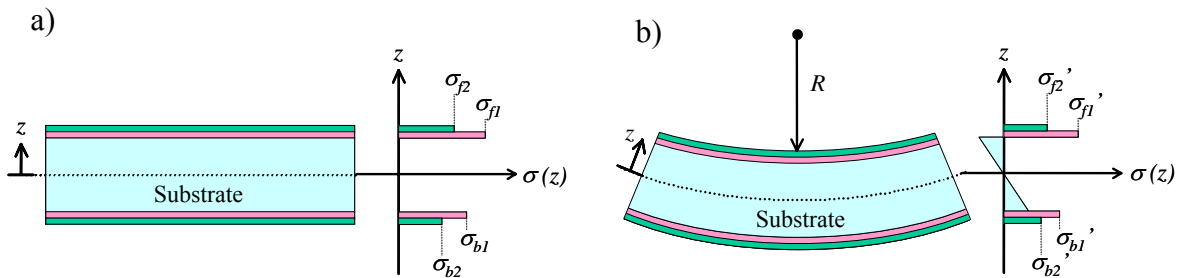


**Figure B.6** Cross-sectional views of a substrate with thin films on both sides for  $n = 2$  and  $m = 2$ : a) before release; b) after release.

For uniform, constant biaxial stress, the constitutive relation relating stress,  $\sigma$ , to strain,  $\varepsilon$ , is:

$$\sigma = \frac{E}{1-\nu} \varepsilon = E' \varepsilon \quad (\text{B.1})$$

where  $E'$  and  $\nu$  are the biaxial elastic modulus and Poisson's ratio of the material, respectively. Conceptually, we imagine the wafer clamped so that, despite the thin film residual stresses, there is no deflection of the wafer or stress-relaxation of the thin-films. This is the "Before Release" state. Next, we imagine the wafer released from its clamps and deforming to an equilibrium state: the "After Release" state.

The system is in static equilibrium after release. Therefore, the net moment per unit length of the system after release,  $M_{ar}$ , must equal the net moment before release,  $M_{br}$ . Before release, the moments are due only to the thin films:

$$M_{br} = \sum_{i=1}^n \int_{-H/2}^{H/2+F(i)} \sigma_{fi} z dz - \sum_{j=1}^m \int_{-H/2-B(j)}^{-H/2} \sigma_{bj} z dz \quad F(i) = \sum_{i=1}^n h_{fi}, \quad B(j) = \sum_{j=1}^m h_{bj}$$

$$M_{br} \approx \frac{H}{2} \left[ \sum_{i=1}^n \sigma_{fi} h_{fi} - \sum_{j=1}^m \sigma_{bj} h_{bj} \right] \quad (\text{B.2})$$

After release, the substrate develops a balancing moment via pure bending,  $M_{ar}$ :

$$M_{ar} = \int_{-H/2}^{H/2} \sigma_s' z dz = \int_{-H/2}^{H/2} E_s' \frac{z^2}{R} dz = \frac{E_s'}{12R} H^3 \quad (\text{B.3})$$

where  $R$  is the radius of curvature of the wafer. Recall that, for static equilibrium after release, we require  $M_{ar} = M_{br}$ . Hence, equating (B.2) and (B.3):

$$\frac{1}{6} \left( \frac{E_s'}{R} \right) H^2 = \sum_{i=1}^n \sigma_{fi} h_{fi} - \sum_{j=1}^m \sigma_{bj} h_{bj} \quad (\text{B.4})$$

The Tencor FLX-2320 measures the change in the radius of curvature of a substrate caused by the stress of a thin film. The stress of the thin film is calculated with a simplified version of Eq. (B.4):

$$\sigma_{measured} = \frac{1}{6} \left( \frac{E_s'}{R} \right) \frac{H^2}{h_f} = \sigma_f \quad (\text{B.5})$$

which is appropriate for single layer thin films as shown in Fig. 1a & b.

For the bi-layer stacks shown in Fig. 1c, Eq. (4) can be simplified to:

$$\sigma_{measured} = \frac{1}{6} \left( \frac{E_s'}{R} \right) \frac{H^2}{h_{SiGe}} = \sigma_{SiGe} + \sigma_{ox(f)} \frac{h_{ox(f)}}{h_{SiGe}} - \sigma_{ox(b)} \frac{h_{ox(b)}}{h_{SiGe}} \quad (\text{B.6})$$

If the stresses of the frontside oxide and the backside oxides are cancelled out, Eq. (B.6) would be equivalent to Eq. (B.5) and the measured stress would be the true SiGe film stress. However, the backside oxide absorbs moisture and becomes more compressive; whereas the stress of the frontside oxide is constant under the SiGe cap. Therefore, the measured stress is not the true stress of SiGe film once the backside oxide starts to absorb moisture. An apparent stress drift of the SiGe film is observed and qualitative agreement with the oxide stress change is found.

#### **B.4 Summary**

The average residual stresses of poly-Si, poly-SiGe, poly-Ge, and thermal oxide are stable in ambient conditions. Poly-SiGe remains a promising material for modular MEMS integration. LPCVD and TEOS-based PECVD oxides absorb moisture and become more compressive in a humid environment. Due to their high deposition rates, LPCVD and PECVD oxides are often used as MEMS sacrificial layers. However, the

stress drift in sacrificial materials is not anticipated to affect the mechanical properties of the MEMS structure layers since they are eventually removed.

## References

- [B.1] B. L. Bircumshaw, M. L. Wasilik, E. B. Kim, Y. R. Su, H. Takeuchi, C. W. Low, A. P. Pisano, T.-J. King and R. T. Howe, "Hydrogen peroxide etching and stability of p-type poly-SiGe films," *17<sup>th</sup> IEEE Micro Electro Mechanical Systems Conference (MEMS-04)*, Maastricht, The Netherlands, Jan. 25-29, 2004, pp. 514-519
- [B.2] C. W. Low, B. L. Bircumshaw, T. Dorofeeva, G. Solomon, T.-J. King and R. T. Howe, "Stress stability of poly-SiGe and various oxide films in humid environments", *Proceedings of Stability of Thin Films and Nanostructures Symposium*, Materials Research Society, Boston, MA, Nov. 29 – Dec. 3, 2004
- [B.3] G. Stoney, "The tension of metallic films deposited by electrolysis", *Proc. Roy. Soc London*, vol. A82, pp. 172, 1909
- [B.4] M. Madou, *Fundamentals of Microfabrication*, 2<sup>nd</sup> ed, CRC Press, p. 302, 2002
- [B.5] K. Kwok E. Yieh, S. Robles and B. C. Nguyen, "Surface related phenomena in integrated PECVD/Ozone-TEOS SACVD processes for sub-half micro gap fill: electrostatic effects", *J. Electrochem. Soc.*, vol. 141(8), pp. 2172-2177, 1994
- [B.6] S. D. Senturia, *Microsystem Design*, Kluwer Academic Publishers, pp. 201-238, 2001

## **Appendix C: Tystar20 Logbook**

The process logbook was created to monitor the LPCVD reactor (Tystar20) and sustain the process. This logbook is a more comprehensive summary of the reactor than the Microlab wand system record, as it includes the process conditions, fault reports, and maintenance comments. Users are required to enter pre-deposition standby conditions, deposition recipe, and process comments in the Wand system. Standby information including temperature, process pressure (PRCPR), N2dope flow rate, and injector pressure, are recorded at the standby mode to track the injector condition. Deposition information includes temperature, pressure, gas flow rates, and deposition time. Users can also enter observations in the comment log. When there is a problem with the reactor, users enter a fault report in the Wand system and equipment staff will diagnose the problem and enter a maintenance comment. Failure analysis, design improvement and new process qualification have been studied based on the historical information of the reactor recorded in the logbook.

It should be noted that process conditions entered by users are sometimes incomplete and contradictory. Some of the process conditions can be retrieved in the furnace condition recording computer inside the Microlab. However, the computer does not have a record of the injector pressure, and the injector condition has to be monitored manually.

User	Date	Standby conditions				Deposition conditions										Comments
		Standby Temp. (°C)	Standby Press (Torr)	Standby PRCPR (mTorr)	Standby N2DOPE (mTorr)	Inj. Press. (Torr)	Time (min)	Temp (°C)	SH4 (secm)	E2H6 (secm)	BCB (secm)	GeH4 (secm)	Press (mTorr)			
Webdy	12/5/2002	<b>New injector</b>				3.9	670	425	100	60		60	400	Uniform +2.5%, 10 Ohm/sq		
christop	12/6/2002	6.46	102			4	270	425	100	60		400	uniform			
christop	12/6/2002					3.~	60	450	100	60		600	Low R, uniform			
msyoum	12/11/2002					3.~	60	450	100	60		600	Low R, uniform			
msyoum	12/13/2002					3.~	60	450	100	60		600				
christop	12/16/2002					4.6	240	425	100	60		400	uniform			
Christop	12/17/2002	6.7														
Webdy	12/18/2002	<b>New injector</b>				3.5	30	425	100	60		400	coat			
Christop	12/18/2002															
Christop	12/19/2002	7.53				3.77	67	425	100	60		300				
Blake lin	1/6/2003						159	425	100	60		600				
Blake lin	1/7/2003	7.38					134	425	100	60		300				
Blake lin	1/8/2003	6.68	101		89.5		201	425	100	60		300				
blake lin	1/10/2003	7.08	101		89.5		53	425	100	60		600				
Suy	1/16/2003	7.26	102		89.3		90	450	100	60		600				
Wlow	1/16/2003						150	400	100	60		800	uniform			
Wlow	1/17/2003						30	450	85	80		600	Not uniform, more than 100% resistance variation			
Webdy	1/17/2003	<b>GeH4 tank changed.</b>				6.29	30	450	85	80		90				
Tabeuchi	1/21/2003															
Webdy	1/22/2003															
Wlow	1/22/2003						150	400	100	60		800	uniform			
Wlow	1/22/2003						30	450	85	80		600	Bottom part of wafer has 40% less resistivity			
Msyoum	1/22/2003						4.4	450	100	60		600				
bob	1/24/2003															
Webdy	1/27/2003															
Chelley2	1/28/2003															
Msyoum	2/2/2003															
Msyoum	2/2/2003															
msyoum	2/2/2003															
Webdy	2/4/2003															
Jimmymc	2/5/2003															
Yanzw	2/6/2003															
Blake lin	2/6/2003	6.~	101		89.3		150	400	100	60		600	Calibration from 300-500C Good amorphous film			

Blake lin	2/7/2003	6.83	101	89.3	3.95	210	380	100	60	30	600	Good amorphous film
Blake lin	2/9/2003	7.08	101	89.5	4.22	210	390	100	60	30	600	Good amorphous film
Wlow	2/11/2003	7.35	101	89.5	4.54	150	400	100	60	50	800	Very uniform film, 1% R variation across wafer/lot
Wlow	2/12/2003	8.06	102 (after)	89.3	4.64-	120	425	100	60	60	800	Uniform looking, 1.5% R variation
Me youn	2/13/2003	11.2(?)			5.3		490	100	100	100	600	
Blake lin	2/19/2003	7.82	101	89.4	4.81	150	395	100	60	30	600	No standby between runs
Blake lin	2/19/2003	N/A	N/A	N/A	1.50	150	395	100	60	30	600	
Blake lin	2/21/2003	8.23	101	89.5	5.22	150	425	100	60	70	400	No standby between runs.
Blake lin	2/21/2003	N/A	N/A	N/A	5.46	53	425	100	60	58	600	New generic recipe, process aborted during depc. Ge
Me youn	2/22/2003	8.7			60	60	490	60	60	60	600	tank empty.
Webdy	2/24/2003											
Me youn	2/24/2003				5.9	60	490	100	60	60	600	Film is uniform, but resistivity is very high
Equvry	2/25/2003	8.93	101	89.2	0.2	300	425	0	0	0	400	Annealing run
Wlow	2/26/2003											
Webdy	2/27/2003											
Suy	2/27/2003				3.~	410	425	100	20	70	400	B2H6 tank pressure down to 4.5 psi
Me youn	2/28/2003				N/A	35	375	0	0	120	600	First wafer is fine, and second is not uniform. Event out of standby recipe!
bob	3/3/2003											
Webdy	3/4/2003											
Equvry	3/5/2003	6.35	101	89.4	0.2	300	400	0	0	0	400	The rmal annealing
Wlow	3/6/2003	350.1	6.35	101	89.3	6.89	400	100	60	25	800	Same recipe as before, wafers changes from amorphous
Me youn	3/6/2003	350	6.9		3.99	50	325	100	60	60	600	
suy	3/7/2003	350	6.53	101	89.3	4.09	490	100	60	58	600	Adjusted boat position. Load boat: 15.5 in. Center boat: 24 in. Pump boat: 32.875 in to the back of the door
Wlow	3/7/2003	372.5	101	89.3	1.50	150	400	100	60	25	800	Injector pressure gauge got turned off
Webdy	3/10/2003											
Me youn	3/8/2003				89	30	400	0	60	180	300	
Zaiyu	3/11/2003											
Zaiyu	3/12/2003				0.4	4.8		100, 650m	60, 650m	48, 650m	400, 650m	
Suy	3/13/2003	350	7.87	101	89.8	5.29	490	100	60	58	600	
Zaiyu	3/14/2003				5.78	60		100	60	25	400	
Zaiyu	3/16/2003				3.6	100		100	20	25		
Zaiyu	3/18/2003											
Webdy	3/18/2003											
Suy	3/18/2003											
Webdy	4/3/2003											

1<sup>st</sup> time: process stopped because SiH4 low (actually not true) 2<sup>nd</sup> time: stopped at DTEQ. Cannot run without recipe

Quartz tube is broken, did not do a run

Replaced quartz tube and liner (enabled 176 hr, 53 hr of depc). Installed new TC sheath and split TC cover. Base pressure 12 m.T. Rate of rise 1.5 mT/min cold. Have turned on the firing circuit. After reaching operating temp, base pressure is 7 m.T, and rate of rise is 6 mT/min.



Blake lin	5/20/2003																		No standby between runs.
Lingang	5/21/2003	330	7.46	101	90	50	425	100	60	58	600								Expected thickness 2 um
Equerry	5/23/2003		7.7	102	90	120	330	0	60	200	300								Can't record standby parameters.
Lingang	5/28/2003		7.7	101	89	290	425	100	60	65	400								Nucleation 5 min
Equerry	5/29/2003						330	0	60	200	300								The pump will be replaced.
Equerry	6/5/2003		8.32	102	89.9	120	330	0	60	200	300								
Webdy	6/11/2003	The IE80 mechanical pump has frozen. Protocols from Edwards for rotating the pump did not free the rotor. The pump will be replaced. Replace mechanical pump. Pumped down to base pressure of 11 mT, rate of rise is 12 mT/min.																	
Jimmyzmc	6/13/2003																		
Jimmyzmc	6/16/2003					4.8	330	0	60	200	300								Furnace stated at idle mode, no standby info.
Ma youn	6/16/2003		8.46	112	89.4		425	100	60	70	400								
Blake lin	6/17/2003	330				330	425	100	60	58	600								No standby between runs.
Blake lin	6/17/2003	444	11.52	101	90	6.54	400	100	60	35	800								Ge tank empty, process aborted.
Meznil	6/17/2003	Replaces Ge tank.																	
Blake lin	6/18/2003	The 6" boat has lots of particles.																	
Webdy	6/20/2003	New injector																	
who	6/20/2003	Ran the standby recipe for Si2H6 coating, and found the furnace in special hold mode. Checked history, the process failed the leak check.																	
who	6/20/2003	Lysatzel has been taken out of "special hold" and returned to service.																	
Ma youn	6/23/2003	Found furnace in idle mode, no standby info. Quartz tube broken																	
Webdy	6/30/2003	Change quartz tube. (enabled 277 hr, \$3 hr of delay)																	
who	7/2/2003	Cannot run recipe. Error message "MPS/TCU I/O error or manual mode prevents run".																	
Webdy	7/2/2003	Found 460 #2 in manual. Placed it into auto. Started standby recipe.																	
Wlow	7/2/2003	441.2	7.75	112	89.8	60	450	100	60	58	600								Excellent uniformity
Wlow	7/3/2003	347.6	7.25	112	89.3	4.40-4.50	280	425	100	60	400								Very uniform
Wlow	7/6/2003	330.3	7.63	112	89	4.55	150	400	100	60	800								No standby between runs. Cloudy wafer, resistivity not uniform.
Wlow	7/6/2003					4.71	150	400	100	60	800								
Wlow	7/6/2003					5.6	30	450	85	80	600								No standby between runs. Resistivity has 10% variation across wafer, and 40% variation across load
Wlow	7/7/2003	330	8.07	112	89.3	4.85-4.91	150	400	100	60	800								Resistivity not uniform, varies in 4 orders of magnitude.
Wlow	7/7/2003					5.00-5.07	150	400	100	60	800								No standby between runs. 10% variation in resistivity.
Wlow	7/7/2003					5.20-5.23	150	400	100	60	800								No standby between runs. Resistivity 100x higher than expect. 100% variation across wafer.
Ningc	7/8/2003						450												Film is cloudy
Ma youn	7/8/2003					5.3-5.8	240	425	100	60	400								No standby info between runs. Film has uniform resistivity. Process aborted during AFBG.
Wlow	7/9/2003	348	9.5	112	89.3														Furnace monitoring, didn't do a run. Request injector change.
Webdy	7/11/2003	Get standby film. New injector																	

Wlow	7/13/2003	352.2	7.02	112	89.2	30	450	85	80	90	600	Forgot to check injector pressure during de po. Resistivity 4X higher than expect. 20% variation across wafer. No standby between runs. Film has excellent uniformity in R. 2% variation across wafer and load.
Wlow	7/13/2003					4.39-4.41	400	100	60	40	800	
Wlow	7/13/2003					4.38-4.44	400	100	60	40	400	No standby between runs. 10% R variation across wafer. 40% across load.
Wlow	7/14/2003	348.2	7.31	112	89.3	4.41-4.54	400	100	60	25	800	Film is cloudy. R varies in orders of magnitude.
Wlow	7/14/2003					4.55-4.61	400	100	60	25	800	No standby between runs. Film is cloudy.
Wlow	7/16/2003	349.5	7.49	112	89.4	4.62-4.68	400	100	60	50	800	Good film. 5% variation of R.
Sblim	7/17/2003	347.8	7.63	112	89	240	350	0	0	200	300	Cloudy film
sblim	7/18/2003	344.8	7.63	112	89.4	240	350	200	0	200	300	Good film
Wlow	7/18/2003	445.5	8.43	114	89.2	4.73	400	100	60	50	800	Good film. 5% variation in R.
equary	7/20/2003		7.87	112	89.6	120	350		60	200	300	Nucleation 400C, 300mT, Si2H6 200, 5 min, Expect 2 um film
Equary	7/23/2003											Abort. Ge tank empty
Webby	7/23/2003											Excellent film
Wlow	7/24/2003	351.9	8.01	112	89.6	5.01	400	100	60	50	800	No standby between runs. Excellent film.
Wlow	7/24/2003					5.10-5.26	400	100	60	50	800	Nucleation 350C, SiH4 200, 300 mT, 5 min. Abort during nucleation step.
Msyoum	7/25/2003	430	9.4		90	120	350		60	200	300	No standby info. Nucleation 350C, SiH4 200, 300 mT, 5 min
msyoum	7/25/2003					4.8	350		60	200	300	
Jimmyzac	7/26/2003	Modify recipe and now users can deposit polysilicon in tystar20. Phosphine is the dopand gas.										
Ben	7/26/2003											No standby info. "buffer queue error" during backfills of boat in Jimmy thought computer crashed.
Ben	7/28/2003						500					No standby info. Abort after 6 hr of de po. Jimmy found SiH4 out of tolerance.
Ben	7/29/2003						500					Jimmy restarted the process and let it run for the remaining time. 7 hr total.
Ben	7/30/2003						615			0	375	No standby info. Abort after 45 min of de po. Failed 3 times after about 20 mins etch due to low phosphine flow. The film looks metallic as expected.
Jimmyzac	7/30/2003	Tried to restart Ben's process. The process aborted due to PH3 low alarm after 1.5-20 mins de po. Move recipe to wait step. Will check PH3 line. Tystar20 is down for doped poly process.										
Webby	7/30/2003	B2H6 tank changed.										
Webby	7/30/2003	Replaced quartz cover for the lifting fork.										
sblim	7/31/2003						450	100	60	58	600	8.96

Equerry	7/31/2003					1.20	350	0	60	200	300	Event out of standby, nucleation, 400C, 300mT, Si2H6 200, 5 min, expect 2um film, film looks beautiful			
Equerry	8/3/2003	9.24	112	89.6		1.40	425	100	60	60	400	nucleation, 400C, 300mT, Si2H6 200, 10 min, expect 2um film, film looks beautiful			
Equerry	8/4/2003	9.3	111	89.6	6.09		425	100	60	60	400	nucleation, 400C, 300mT, Si2H6 200, 10 min, film looks a bit cloudy. This run has very different Ge content with the previous.			
bob	8/6/2003											Tested GeH4 MFC. 0-200: 25 sccm = 58 mT, 50 sccm = 90 mT, 100 sccm = 140 mT. 0-50: 25 sccm = 61 mT, 50 sccm = 94 mT.			
Prof. King	8/6/2003											Standard SiGe process is down due to phosphorus out-diffusion by the doped poly process. Dope poly process should be shut off.			
jimmyzac	8/6/2003											get rid of poly-Si recipe			
Webby	8/11/2003											New injector			
wlow	8/11/2003	435	7.44	114	89.7	4.33-4.38	90	100	60	58	600	Standard MEMS exchange recipe for monitoring the furnace. Eight wafers were placed at the two ends (skipping the first slot) of both 4" boats. Resistivity is pretty much uniform. 20% variation across wafer. 5% variation across metal boat to the load side of the non-metal boat. The pump side of the non-metal boat has significantly low R <sub>s</sub> half of other wafers!			
bob	8/12/2003											There is a ~5% discrepancy between the 0-50 and 0-200 sccm Germans MFC at 50 sccm. A freely calibrated 0-200 sccm MFC has been procured and will be installed to fix this			
webby	8/13/2003											Changed GeH4HI MFC. Flowed GeH4 into lo and hi MFCs. GeH4LO 2.5sccm=56mTorr, 50sccm=83mTorr, 100sccm=130mTorr.			
tsuruichi	8/15/2003											recipe aborted due to GeH4HI leak			
bob	8/19/2003											The recipe switch for delivery of dopant gases to the gas ring and injector is not working. Dopant can only be delivered to the injector. Jimm has traced the failure to one of the pressure valves that switch gas delivery.			
webby	8/20/2003											Changed GeH4HI MFC. Flowed GeH4 into lo and hi MFCs. GeH4LO 2.5sccm=61mTorr, 50sccm=94mTorr, GeH4HI 2.5sccm=61mTorr, 50sccm=90mTorr, 100sccm=144mTorr.			
Webby	8/20/2003											Changed out nitrogen on injector line. PH3 now flows.			
equerry	8/21/2003					7.21	112	89.8	4.26	280	425	100	60	400	nucleation, 400C, 300mT, Si2H6 200, 10 min, expect 2.2 um
Webby	9/5/2003														Changed quartzware (not broken, enabled 213 hr, 66 hr of depo), new tube new cantilever sheaths and gas ring. Reinstalled rear piping, TC, heat baffles and boats. Lowest base pressure is 22 mT. Rate of rise is 35 mT/min.
Webby	9/8/2003														Base pressure is at 11 mT and rate of rise at 15 mT/min cold. Have turned on the firing circuits.
Webby	9/8/2003														Pump is making noise. It has been checked out and filled with DI water and oil. Base pressure and rate of rise are good. Tystar20 needs dummy wafers and a coating run.
Webby	9/9/2003														Performing dimmense maintenance.
Webby	9/10/2003														Maintenance: Coating run has been completed. Calibration has been completed at 400, 450, 500 C.
equerry	9/10/2003					4.22	60	350	0	60	200	300	nucleation, 400C, 300mT, Si2H6 200, 5 min		
ebkim	9/11/2003	330	7.99	107	89.8	4.65	60	425	100	60	60	400	The 2 wafers placed on the load side of the load boat (1 dummy in) were a little cloudy and there was a dark spot (unclouded on the lower quadrant closest to me as		
rudolf	9/12/2003					4.71	60	425	100	60	60	400	nucleation, 400C, 300mT, Si2H6 200, 5 min		

swy	9/15/2003	330	7.72	110	89.7	0.16	60	42.5	100	0	60	400	film looked real bad, parts for the wafer are very dull, only the center looks shiny, perhaps reaction was really bad	
Ms youm	9/16/2003					4.8	90	42.5	100	60	60	600	bilayer	
Ms youm	9/16/2003					1.20	330	0	60	180	300	300	bilayer	
Ms youm	9/16/2003					90	42.5	100	60	60	600	600	bilayer	
Ms youm	9/17/2003	330	10.9	89.9		5.14	90	42.5	100	60	60	600	Nucleation 400C, 300mT, Si2H6 100, 20 min. The center boat cover has a ~1" long piece broken off.	
Ms youm	9/17/2003					1.20	330	0	60	180	300	600	nucleation, 400C, 300 mT, Si2H6 200, 5 min.	
swy	9/18/2003	330	8.24	111	90.2	0.03	60	42.5	100	0	60	300	nucleation, 400C, 300 mT, Si2H6 200, 5 min.	
Webdy	9/19/2003	Injector pressure near 9. New injector												
wlw	9/21/2003	330	6.06	111	90.1	3.65	330	400	100	60	50	800	nucleation, 400C, 300 mT, Si2H6 200, 5 min. There is a ring at the bottom of wafers closer to the pump.	
Webdy	9/22/2003	Replaces boros boat cover.												
Webdy	9/22/2003	Ge H4 tank change.												
wlw	9/22/2003	330	6.17	110	89.9	3.74-3.91	440	400	100	60	50	800	undoped SiGe with N2Dope flow if 60 through the injector.	
ebkim	9/23/2003	390	6.64	111	89.6	5.52	30	42.5	100	0	60	400	nucleation, 450 C, 300 mT, Si2H6 200, 1 min. Didn't realize there is no input for Si2H6 in depo. Ended up Bilayer de position. Nucleation, 400C, 300mT, Si2H6 200, 5 min. Three wafers are at the center boat. The one at the load end is fine. The ones in the middle and at the pump end have rings at the bottom again. Injector flow issue.	
chanyj	9/24/2003	330	6.88	112	89.6	0.05	270	450	0	0	300	300	was not able to run the process.	
wlw	9/24/2003	449	7.06	112	89.6	3.97-4.01	130	400	100	60	50	800	The injector was cleared out about a week ago, and there appear to be problems already. Perhaps the injector cleaning/replacement process is not working properly.	
wlw	9/24/2003					4.03-4.08	130	400	100	60	45	800	nucleation, 350 C, 300 mT, Si2H6 100, 10 mins. Film is nice and uniform.	
msreport	9/25/2003	Germane and diamane usage will no longer be logged manually at the end of your runs. The usage will be determined from flow sensors automatically.												
ebko	9/25/2003	Please flow 60 sccm of N2Dope when running undoped poly-SiGe process so that the injector doesn't get clogged. Jimmy wrote up a new recipe especially for this purpose with a variable flow rate input for N2Dope: UDS\GFA.020												
boimb	9/25/2003	The injector was cleared out about a week ago, and there appear to be problems already. Perhaps the injector cleaning/replacement process is not working properly.												
Ms youm	9/25/2003	330	6.5	0	89.6	0.02	120	350	0	0	180	300	nucleation, 400 C, 300 mT, Si2H6 200, 5 mins. Film is nice and uniform.	
ebkim	9/26/2003	Please flow 60 sccm of N2Dope when running undoped poly-SiGe process so that the injector doesn't get clogged. Jimmy wrote up a new recipe especially for this purpose with a variable flow rate input for N2Dope: UDS\GFA.020												
Ms youm	9/26/2003	347	6.67	111	89.9	3.6	120	330	0	60	180	300	nucleation, 350 C, 300 mT, Si2H6 100, 10 mins. Film is nice and uniform.	
yann	9/26/2003	445	6.69	111	89.9	0.02	360	375	0	0	180	300	nucleation, 400 C, 300 mT, Si2H6 200, 5 mins. Film is nice and uniform.	
Ms youm	9/27/2003	330	6.46	112	89.9	3.45	90	42.5	100	60	60	600	nucleation, 425 C, 400 mT, Si2H6 100, 10 mins. Film is nice and uniform.	
Blsblm	9/27/2003					4.75	483	42.5	100	60	65	400	No standby info. Bilayer run.	
Blsblm	9/27/2003					4.8	28	42.5	100	60	58	600	Continue depo. No nucleation. Film looks fine.	
yann	9/28/2003	330	7.72	112	90.2	0.03	300	375	0	0	180	300		
Webdy	9/29/2003	Replaces injector due to the ring at the bottom of the wafer.												
Webdy	9/30/2003	Replaces GeH4 tank.												



ebbm	10/22/2003	330	6.84	123	89.6	5.84	70	425	110	0	60	425	Use UDSIGEA recipe. 60 secm of N2dbye flow through injector
Equv	10/22/2003					3.84	12	350	0	60	200	300	no standby info
who	10/22/2003					4.17	90	400	100	60	40	800	No standby info. Nucleation 400C, S2H6 200, 300 mT, 10 min
gubal	10/23/2003	330				5.51	60	353.4	0	0	181	300	resistivity of C3 is nice and uniform. 8.8 ohm/eq
ebno	10/28/2003	330	6.83	123	89.9	70	425	90	0	0	70	400	resistivity of C8 is not uniform. top 8.8 ohm/eq, bottom 23.6 ohm/eq
Webry	11/3/2003												resistivity of C13 is worse. top 1.1 ohm/eq, bottom 6.23 ohm/eq
sey	11/6/2003	330	6.77	122	89.7	4.08	120	400	0	60	90	600	nucleation 400C, 20 min, 600 m Torr, 100 S2H6. Center boat cover was missing, borrowed from Hyslar19.
Webry	11/7/2003												
Ms youm	11/7/2003					4.25	90	425	100	60	60	400	tailerz
Ms youm	11/7/2003					4.38	90	425	100	60	60	400	
Ms youm	11/7/2003												
Webry	11/10/2003												
Ms youm	11/13/2003	330	7.11	122	89.9	3.73	30	425	100	40	60	400	Nucleation 425C, S2H6 100, 400 mT, 15 min.
Ms youm	11/14/2003	330	7.19	122	90	3.17	90	425	100	45	60	400	Nucleation 425C, S2H6 100, 400 mT, 15 min.
Ms youm	11/14/2003					3.87	90	425	100	45	60	400	no standby info
Ms youm	11/14/2003					3.92	90	425	100	45	60	400	no standby info
Ms youm	11/15/2003	330	7.36	122	89.7	0.003	120	350	0	0	170	300	Nucleation 425C, S2H6 100, 400 mT, 15 min.
Ms youm	11/15/2003					3.8	90	425	100	45	60	400	no standby info
Ms youm	11/15/2003					1.59	40	425	125	10	35	400	Nucleation 425C, S2H6 100, 400 mT, 15 min.
Ms youm	11/20/2003	330	7.61	121	89.9	2.05	40	425	120	15	40	400	no standby info
Ms youm	11/20/2003					2.036	40	425	120	20	40	400	no standby info
Ms youm	11/21/2003					2.36	40	425	110	25	40	400	Nucleation 425C, S2H6 100, 400 mT, 15 min.
who	12/2/2003	346.2	7.7	122	89.9	0.1	60	425	100	0	55	400	Nucleation 425C, S2H6 100, 400 mT, 15 min.
who	12/2/2003	356	7.86	122	89.7	0.1	80	425	100	0	42	400	Nucleation 425C, S2H6 100, 300 mT, 10 min.
who	12/2/2003	454.5	8.59	123	90.1	0.1	100	425	100	0	30	400	Nucleation 425C, S2H6 100, 300 mT, 10 min.
chanyj	12/3/2003	330	7.8	120	90	6.22	180	450	180	0	0	300	amorphous Si
Ms youm	12/8/2003	330	7.65	121	90.2	2.45	110	425	115	20	45	400	Nucleation 425C, S2H6 100, 400 mT, 10 min.
Ms youm	12/8/2003					3.65	240	350	0	45	170	300	no standby info
chanyj	12/9/2003	330	7.74	118	90	7.46	180	450	150	20	0	300	amorphous Si
chanyj	12/9/2003	330	7.74	118	90	7.8	270	450	149	19.7	0	300	amorphous Si

Ms youm	12/11/2003	330	8.76	118	90.2		100	425	115	15	45	400	Nucleation 425C, S12H6 100, 400 mT, 10 min.	
Ms youm	12/11/2003					5.29	120	425	110	60	45	400	Nucleation 425C, S12H6 100, 400 mT, 10 min.	
Ms youm	12/12/2003					3.29	40	425	100	15	45	400	no standby info	
Ms youm	12/12/2003						120	425	115	15	45	400	Nucleation 425C, S12H6 100, 400 mT, 10 min.	
Ms youm	12/13/2003	330	8.68	122	92.3	3.39	30	330	0	30	170	300	Nucleation 330C, S12H6 100, 300 mT, 15 min.	
Ms youm	12/13/2003					2.18	30	330	0	0	170	300	Nucleation 330C, S12H6 100, 300 mT, 15 min.	
chenyj	12/15/2003	330	7.8	120	90	5.65	70	450	100	59.4	50.2	800	Nucleation 450C, S12H6 150, 300 mT, 2 min.	
Webdy	12/17/2003	New injector												
svy	12/18/2003	330	6.29	118	89.7	3.8th	90	450	100	58	60	600	Mo motor run.	
who w	12/19/2003	333.4	6.33	118	89	3.81	170	450	100	60	70	400	Nucleation 450C, S12H6 100, 300 mT, 10 min. Bi-layer	
who w	12/19/2003						80	425	100	60	58	600		
chenyj	12/20/2003	330	6.6	118	90	3.73	60	450	110	50	40	850	Nucleation 450C, S12H6 150, 300 mT, 2 min.	
bob	12/22/2003	GeH4 tank change.												
who w	12/23/2003	349.2	6.64	118	89.7	3.99-4.05	130	400	100	60	50	800	Nucleation 400C, S12H6 100, 300 mT, 15 min. Bi-layer.	
who w	12/23/2003					4.10-4.16	120	400	100	60	37	800		
chenyj	12/27/2003	330	6.73	117	89.6	4	90	450	100	60	50	800	Nucleation 450C, S12H6 150, 300 mT, 2 min.	
who w	12/27/2003					4.22-4.29	130	425	100	60	50	800	No standby info. Nucleation 425C, S12H6 100, 300 mT,	
who w	12/27/2003					4.33-4.38	120	425	100	60	25	800	15 min. Bi-layer.	
chenyj	12/30/2003	330	7.23	118	89.9	0.43	180	400	105	0	45	800	Nucleation 400C, S12H6 100, 300 mT, 20 min. Didn't get GeH4 changed	
Jimmygmc	12/30/2003	Check GeH4 flow manually. OK.												
who w	12/30/2003	346	7.29	2	0	4.5-4.54	140	450	100	60	70	400	Nucleation 450C, S12H6 100, 300 mT, 10 min. Bi-layer. 1st layer depo was set to be 150 min, but recipe absorbed at 140 min. Standby info effected by Jimmy's	
who w	1/1/2004	346.5	7.53	118	89.9	4.8-4.86	140	450	100	60	70	400	Nucleation 450C, S12H6 100, 300 mT, 10 min. Bi-layer.	
who w	1/1/2004					4.8-4.92	120	425	100	60	50	600		
who w	1/4/2004	349.4	7.75	118	89.7	4.77-4.9	130	425	100	60	58	400	Nucleation 425C, S12H6 100, 300 mT, 15 min. Saw "power fail" alarm and cleared. Cantilever cracked when door opens. Wafer boat got stuck inside the tube.	
who w	1/4/2004					4.77-4.91	130	400	100	60	35	800		
Webdy	1/5/2004	Adjusted cantilever section. Closed lysnar20. Tysnar20 is ready for wafer removal.												
Jimmygmc	1/6/2004	Checked "Power fail" error. There might be a power glitch for the building. If it was less than 3 sec, the process will resume.												
Webdy	1/7/2004	Standby injector pressure 8.1. Replaced injector.												
chenyj	1/7/2004	330	6.88	120	90	0.35	190	410	105	0	45	800	Nucleation 400C, S12H6 100, 300 mT, 20 min. Didn't get GeH4 changed again.	
svy	1/12/2004	330	7.02	121	90	4.45	90	450	100	60	58	600	Mo motor run.	
Ms youm	1/12/2004					4.32	120	425	115	60	45	400	No standby info. Nucleation 425C, S12H6 100, 400 mT, 10 min.	
who w	1/13/2004	352.1	7.23	118	89.9	4.37-4.45	130	425	100	60	55	400	Nucleation 425C, S12H6 100, 300 mT, 15 min. Bi-layer. "Power fail" happened a few times, always after 1	
who w	1/13/2004					4.48-4.55	180	400	100	60	40	800	layer. "Power fail" happened a few times, always after 1	
Webdy	1/13/2004	Checked connectors on back of CPU board and they were tight. Probably what is happening is that the keyboard when pressed is giving a bounce on a certain key combination making the CPU think it had a power fail.												



wlw	2/24/2004	350.3	off	0	0	NA	60	400	100	16.5	60	400	Si2H6 nucleation 400C, Si2H6 100, 300 mT, 15 min. Ge nucleation: 350C, GeH4 100, BCl3 16.5, 300 mT.
jinmayznc	2/26/2004	Perform clean maintenance after MicroLab power failure last night.											
Wahdy	3/3/2004	Remove front injector and bagged it. Install clean rear injector on tystar20.											
bob	3/4/2004	Yijian reported heavy film produce by tystar19, could not produce good result with the same recipe. B2H6 cylinder is 8 months old and ~100 psi. It began at 1800 psi. We know there is some decay of B2H6 and a recently replaced quartz injector in tystar19 clogged prematurely. B2H6 tank will be changed every 6 months.											
Wahdy	3/5/2004	Replaces B2H6 tank.											
swy	3/9/2004	350	9.61	283	89.4	1.89	210	425	11.5	1.5	45	400	Nucleation 400 C, Si2H6 100, 400 mT, 15 min. Sheet resistance from 4ppm: I=0.453mA, V=1.15-3. From the SEM, film thickness is 1.15 um (too thick), and surface is quite rough.
chenyj	3/11/2004	350	9.58	284	89.3	2.06	180	400	10.5	20	45	400	Nucleation 425 C, Si2H6 100, 300 mT, 15 min. BCl3 run. Some particles on wafers.
wlw	3/12/2004	There are lots of particles in the furnace after the power failure on Feb. 25, 2004. Cannot do anything to the tube. The best we can do is to clear all the dummies. After restoring the B2H6 process with a newly clear injector, injector pressure is found to be very high (9.5 Torr), PRCPR is also high (283 mTorr). This is because the standby recipe got changed during the BCl3 experiment. There is 200 sccm of N2BKFL during standby in addition to 90 sccm of N2DOPE. Jimmy will get rid of the N2BKFL and this problem can be cleaned.											
wlw	3/12/2004	352	9.84	288	90	NA	10	450	200	18	60	800	Nucleation 450C, Si2H6 200, 800 mT, 60 min. Switch to open boat for BCl3 depo. This is a coating run.
wlw	3/12/2004	NA	NA	NA	NA	NA	180	425	20	16.5	12	400	Nucleation 425 C, Si2H6 100, 300 mT, 15 min. BCl3 run. Some particles on wafers.
wlw	3/12/2004	This is a follow up of the particle problem. The dummy wafers were coated with a layer of particles. I trashed all of them. The deposition after the dummy change still has particles, at least 20 particles per wafer are visible. The particles are caused by the power failure a few weeks ago. The furnace had been used after that. However, since most people use caged boat configuration, they don't see significant amount of particles on wafers. I am using open boat for BCl3 doping, and it is a big problem. There should be more particles on the wall. The boats (caged and open), cantilevers, heat baffles should be cleaned as soon as possible. The injector might also need a change. I will do two more not so critical runs to collect more particles to the dummy wafers tomorrow.											
wlw	3/12/2004	NA	NA	NA	NA	NA	60	425	100	2	60	400	Nucleation 425 C, Si2H6 100, 300 mT, 15 min. BCl3 run. Some particles on wafers. Forgot to record standby info.
wlw	3/13/2004	NA	NA	NA	NA	NA	60	425	100	16.5	60	400	Nucleation 350 C, Si2H6 150, 300 mT, 20 min. Ge nucleation 100 GeH4, 16.5 BCl3, 300 mT, 10 min. BCl3 run. Some particles on wafers. Forgot to record standby info.
wlw	3/13/2004	450	10.47	289	89.6	NA	60	425	100	6.5	60	400	Nucleation 425 C, Si2H6 100, 300 mT, 15 min. BCl3 run. Switch back to caged boat after depo.
chenyj	3/13/2004	350	9.82	291	89.3	2.08	1.5	410	10.5	0	45	400	Nucleation 410 C, Si2H6 100, 400 mT, 10 min.
najenn	3/16/2004	Clean dummy wafers, wipe off cantilevers and wall.											
ebblin	3/16/2004	9.94											
chenyj	3/17/2004	350	9.98	286	89.5	2.18	60	450	100	60	58	600	Minor run.
chenyj	3/17/2004	Before I started my process, I saw the dummy wafers (6" boats) are covered by particles. But the surface of my wafer after deposition seems ok.											
jinmayznc	3/18/2004	Particles will be fixed in the film. The user observe no particles on his film, the problem is clear for now. Will monitor the tube regularly.											
jinmayznc	3/18/2004	Turn off N2BKFL at standby.											
chenyj	3/18/2004	350	7.15	121	89.3	0.07	120	410	110	0	40	400	Nucleation 410C, Si2H6 100, 400 mT, 10 min.
jinmayznc	3/18/2004	Test GeH4 and B2H6.											
chenyj	3/23/2004	350	7.21	118	89.5								

chenyi	3/24/2004	330	7.22	118	89.5	4.36	180	415	110	60	40	400	Nucleation 415, S12H6 100, 400 mT, 10 min.
chenyi	3/24/2004	330	7.22	118	89.5	4.36	180	415	110	60	40	400	Nucleation 450, S12H6 200, 800 mT, 20 min. Coating after switching to open boat
wlw	3/25/2004	349.8	7.44	117	89.4	NA	1	450	100	0	0	800	Nucleation 425C, S12H6 100, 300 mT, 15 min. BC13 test.
wlw	3/25/2004	NA	NA	NA	NA	NA	180	425	100	16.5	60	400	Nucleation 410C, S12H6 100, 400 mT, 10 min.
Webster	3/29/2004	GeH4 tank change. 7 psi can barely finish a deposition with 60 secm GeH4 for 3 hr.											
chenyi	3/29/2004	330	7.45	118	89.5	4.38	120	410	110	55	40	400	Nucleation 415C, S12H6 100, 400 mT, 10 min.
chenyi	3/29/2004	330	7.45	118	89.5	3.12	120	415	110	30	40	400	Nucleation 420C, S12H6 100, 400 mT, 10 min.
chenyi	3/30/2004	330	7.65	121	89.6	2.04	120	420	110	1.5	40	400	Process aborted at NTEQ. Nucleation 420C, S12H6 100, 400 mT, 10 min.
chenyi	3/31/2004	330	7.65	121	89.6	NA	120	420	110	5	40	400	
chenyi	3/31/2004	Pressure too high and process aborted at NTEQ.											
bob	3/31/2004	The B2H6 supply to tystar20 will be pumped to vacuum to temporarily while we service the pre-diborane valve on tystar19. Tystar20 remains up and useable without E2H6. This work should be completed by noon today and diborane restored.											
Webster	4/1/2004	Tystar20 is being used to pump out the diborane gas line for tystar19.											
chenyi	4/3/2004	330	7.75	121	89.5	3.5	120	420	110	5	40	400	Nucleation 420C, S12H6 100, 400 mT, 10 min.
chenyi	4/4/2004	330	7.81	118	89.5	NA	150	325	0	0	80	400	Nucleation 400C, S12H6 100, 400 mT, 20 min.
chenyi	4/5/2004	330	7.82	118	89.4	NA	150	420	100	3	40	400	Nucleation 420C, S12H6 100, 400 mT, 10 min.
chenyi	4/6/2004	330	7.82	118	89.4	0.05	30	325	0	0	80	400	Nucleation 400C, S12H6 100, 400 mT, 4 min.
chenyi	4/6/2004	330	7.82	118	89.4	0.4	120	420	110	1	40	400	Nucleation 420C, S12H6 100, 400 mT, 10 min.
chenyi	4/7/2004	330	7.81	118	89.4	NA	120	425	115	5	35	400	Nucleation 425C, S12H6 100, 400 mT, 7 min.
chenyi	4/7/2004	330	7.83	118	89.4	NA	120	430	120	0	30	400	Nucleation 430C, S12H6 100, 400 mT, 5 min.
chenyi	4/7/2004	330	7.82	118	89.4	1.03	120	430	120	5	30	400	Nucleation 430C, S12H6 100, 400 mT, 7 min.
Me young	4/7/2004	Report particle problem.											
wlw	4/9/2004	330	7.92	121	90	4.5	90	330	0	60	170	300	Nucleation 330C, S12H6 100, 300 mT, 15 min.
wlw	4/12/2004	NA	NA	NA	NA	NA	120	425	100	16.5	60	400	Nucleation 425C, S12H6 100, 300 mT, 15 min.
wlw	4/12/2004	Building power failed for 20 minutes.											
wlw	4/12/2004	NA	NA	NA	NA	NA	90	425	80	16.5	48	400	Thick coating run was done before depo to recover from power failure. Nucleation 425C, S12H6 100, 300 mT, 15 min.
wlw	4/13/2004	333.9	8.06	118	89.9	NA	60	400	100	16.5	60	400	Si seed 450C, S12H6 100, 300 mT, 15 min; Ge nuc 330C, GeH4 100, 300 mT, 16.5 BC13, 300 mT
wlw	4/13/2004	336.5	7.97	118	89.7	NA	120	425	50	16.5	30	400	Nucleation 425C, S12H6 100, 300 mT, 15 min.
wlw	4/14/2004	346.6	8.02	118	90.1	NA	60	425	100	16.5	60	400	Si seed 450C, S12H6 100, 300 mT, 15 min; Ge nuc 330C, GeH4 100, 300 mT, 16.5 BC13, 300 mT
wlw	4/14/2004	443	8.87	121	89.7	NA	60	350	0	16.5	100	400	Nucleation 450C, S12H6 100, 300 mT, 15 min.
wlw	4/14/2004	No particle in all of my wafers from the deposition during the past few days.											
my2	4/15/2004	430	8.65	121	90.1	5.23	60	450	100	60	58	600	Nucleation 450C, S12H6 100, 400 mT, 10 min. Lots of particles in 6" diamines.
my2	4/15/2004	Report particle problem.											
wlw	4/16/2004	Particle problems are likely caused by the dirty injector. Request injector change.											
Webster	4/16/2004	Injector changed due to particle problem.											

sw2	4/19/2004	330	7.01	121	90	4.37	30	450	100	60	58	600	check particle problem
sw2	4/20/2004	330	7.06	121	90	4.23	60	425	100	60	70	400	Nucleation 425C, S2H6 100, 400 mT, 10 min
Equerry	4/22/2004	NA	7.83	NA	NA	NA	1.2	350	0	60	180	300	Nucleation 350C, S2H6 200, 300 mT, 1 min
Equerry	4/23/2004	330	NA	NA	NA	NA	1.2	330	0	60	180	300	Nucleation 330C, S2H6 10, 300 mT, 1 min
chenyj	4/24/2004	330	7.2	121	89.9	0.12	120	420	110	0	40	400	Nucleation 420C, S2H6 100, 400 mT, 10 min. Process aborted.
Jimmyzac	4/26/2004	Previous process was aborted due to SiH4 out of tolerance. Restart the process with no problem. Will monitor MFC.											
bob	4/26/2004	Clean dummy wafers.											
sw2	4/27/2004	330	7.16	121	89.9	4.3	38	425	100	60	70	400	Nucleation 425C, S2H6 100, 400 mT, 10 min.
wlw	4/28/2004	447.3	7.91	122	89.9	4.3	60	425	100	60	60	400	Nucleation 425C, S2H6 100, 300 mT, 15 min.
bob	4/30/2004	The BC33 cylinder has been changed to 1%. With a setpoint of 20 psi, the cylinder pressure is 7.30 psi.											
wlw	4/30/2004	333.5	7.28	121	90.1	NA	60	425	100	60	60	400	Dummy run for BC33 line clean out. Nucleation 425C, S2H6 100, 300 mT, 15 min.
wlw	4/30/2004	NA	NA	NA	NA	NA	60	425	100	60	60	400	Nucleation 425C, S2H6 100, 300 mT, 15 min.
wlw	4/30/2004	NA	NA	NA	NA	NA	60	425	100	60	60	400	Nucleation 425C, S2H6 100, 300 mT, 15 min.
wlw	4/30/2004	NA	NA	NA	NA	NA	60	425	100	60	60	400	Nucleation 425C, S2H6 100, 300 mT, 15 min.
wlw	4/30/2004	350.5	7.33	121	89.9	NA	60	425	100	60	60	400	Nucleation 425C, S2H6 100, 300 mT, 15 min.
wlw	5/1/2004	NA	NA	NA	NA	4.52	60	450	100	60	60	400	Nucleation 450C, S2H6 100, 300 mT, 15 min.
wlw	5/1/2004	NA	NA	NA	NA	4.36	60	400	100	60	60	400	Nucleation 400C, S2H6 100, 300 mT, 15 min.
chenyj	5/2/2004	330	7.45	121	90	NA	120	420	110	0	40	400	Nucleation 420C, S2H6 100, 400 mT, 10 min.
Equerry	5/10/2004	NA	7.35	NA	NA	4.04	120	350	0	60	180	300	Nucleation 350C, S2H6 200, 300 mT, 5 min.
chenyj	5/12/2004	330	7.41	121	90	NA	25	420	110	0	40	400	Nucleation 420C, S2H6 100, 400 mT, 10 min.
chenyj	5/13/2004	330	7.45	121	90	NA	120	420	110	10	40	400	Nucleation 420C, S2H6 100, 400 mT, 10 min.
chenyj	5/15/2004	330	7.51	121	90	1.97	120	430	120	15	30	400	Nucleation 430C, S2H6 100, 400 mT, 10 min.
chenyj	5/15/2004	330	7.54	121	90	NA	15	430	120	10	30	400	Nucleation 430C, S2H6 100, 400 mT, 7 min.
Equerry	5/17/2004	NA	7.51	NA	NA	4.74	200	350	0	60	180	300	Nucleation 350C, S2H6 100, 300 mT, 1 min.
Webdy	5/18/2004	GeH4 tank change.											
yanw	5/18/2004	330	7.61	111	90.1	NA	80	420	110	0	40	400	Did not run the process
chenyj	5/20/2004	330	7.6	121	90	NA	80	420	110	0	40	400	Nucleation 420C, S2H6 100, 400 mT, 10 min.
chenyj	5/20/2004	330	7.65	121	90	NA	1.5	420	110	0	40	400	Nucleation 420C, S2H6 100, 400 mT, 10 min.
Webdy	5/21/2004	SiH4 tank change.											
chenyj	5/22/2004	330	7.65	121	90	NA	90	325	0	0	80	400	Nucleation 400C, S2H6 100, 400 mT, 10 min.
chenyj	5/22/2004	330	7.65	121	90	NA	1.5	420	110	0	40	400	Nucleation 420C, S2H6 100, 400 mT, 10 min.
Webdy	6/2/2004	Front flange has been locked up from the gas flange to allow front injection.											
wlw	6/2/2004	NA	NA	NA	NA	NA	20	425	100	16.5	60	400	Nucleation 425C, S2H6 100, 300 mT, 2 min. Switch to open boat, install front injector. Coating run.
wlw	6/2/2004	448.8	8.81	118	89.9	NA	60	425	100	16.5	60	400	Nucleation 425C, S2H6 100, 300 mT, 15 min. Front injector test.
wlw	6/4/2004	Jon Goldman equipment has not been recording data for all ben5 furnaces since mid-May. Rebooting the computer does not work. Recipe cannot be loaded from computer to furnace.											
webdy	6/9/2004	Jon Goldman computer is fixed by computer support group via windows 2000.											
webdy	6/10/2004	Gasring switching function does not work.											

Webster	6/14/2004	Gaining now switches back and forth. Removed capped front injector port and installed ultrorr adapter.	7.89	121	89.9	4.7	40	42.5	100	60	70	400	Nucleation 425C, S12H6 100, 400 mT, 10 min.
sw2	6/14/2004	Recipe not injector change for long depo.											
sw2	6/15/2004	Injector changed.	7.11	117	89.9	4.37	123	42.5	100	60	40	400	Nucleation 400C, S12H6 200, 400 mT, 5 min.
Equerry	6/16/2004		7.47	121	90	0.18	15	420	110	0	40	400	Nucleation 420C, S12H6 100, 400 mT, 10 min.
chenyi	6/16/2004		7.47	121	90	0.18	90	32.5	0	0	80	400	Nucleation 400C, S12H6 100, 400 mT, 20 min.
chenyi	6/17/2004		7.45	121	90	0.34	15	420	110	0	40	400	Nucleation 420C, S12H6 100, 400 mT, 20 min.
chenyi	6/17/2004		7.24	117	89.9	0.19	60	42.5	100	16.5	60	400	Nucleation 425C, S12H6 100, 300 mT, 15 min. Front injector test. No difference with gas ring.
wlow	6/19/2004												
chenyi	6/19/2004	Found standby process was aborted, could not find reason from process history.											
jimmyzmc	6/22/2004	Suspected that the standby recipe was corrupted. Deleted the recipe and download from DCS30 PC. Ran the recipe and it finished without problem.											
blakeim	6/23/2004		7.26	117	89.9	4.98	483/60	42.5	100	60	65/58	400/6100	No nucleation layer. Bi-layer run. Didn't break vacuum in between.
sw2	6/23/2004	Tried to run the coating part of the standby recipe last night, came in this morning and found the process is aborted. Checked process history, it seems PRCPFR was high and triggered the abort sequence.											
Webster	6/25/2004	Ran standby recipe with no problem. Process pressure and rate of rise are good. Base pressure is good.	8	117	89.9	5.11	270	42.5	100	60	70	400	Nucleation 425C, 400 mT, S12H6 100, 10 min.
sw2	6/25/2004		7.8	121	90	NA	120	420	110	1.5	40	400	Nucleation 420C, 400 mT, S12H6 100, 10 min.
chenyi	6/26/2004												
Webster	7/2/2004	Injector changed.	7.23	121	90	NA	32	350	0	60	180	300	Nucleation 350C, 300 mT, S12H6 200, 1 min.
Equerry	7/3/2004		7.92	121	90	0.37	360	NA	NA	NA	NA	600	Nucleation 375C, 400 mT, S12H6 100, 8 min.
yanw	7/4/2004												
wlow	7/5/2004	Found lysar20 in ABPG mode. DH shows after 2 minutes of standby coating, process was aborted with error "IFPRCPFR NE". After 2 minutes into ABR.T, step went to ABPG with message "PRCPFR OK". Furnace was at N2BKFL=199, PRCPFR=231, Temp=450, injector pressure=8.71. Exited out of abort mode and reloaded the recipe. Same thing happened.											
jimmyzmc	7/6/2004	Found that the process aborted due to PRCPFR too high. The initial N2VAC shooted up which caused the problem. Adjusted the pid constants for pressure control on MFS460. Tried the recipe twice and the pressure stabilized within one minute.											
Equerry	7/6/2004		7.78	121	89.9	4.44	300	42.5	100	60	40	400	Nucleation 400C, 400 mT, S12H6 200, 5 min.
Equerry	7/7/2004		7.65	118	90.1	NA	5	300	0	60	180	300	No nucleation
Equerry	7/9/2004		7.66	119	89.9	NA	5	300	0	60	180	300	No nucleation
chenyi	7/9/2004		NA	121	90	NA	120	420	110	1.5	40	400	Nucleation 420C, 400 mT, S12H6 100, 10 min.
wlow	7/11/2004		7.73	118	89.9	3.36	60	42.5	100	16.5	60	400	Nucleation 425C, 300 mT, S12H6 100, 15 min. Left rear injector test.
wlow	7/11/2004	Got a change of \$113490.13 for S12H6. Only used 100 secm S12H6 for 15 minutes.											
voros	7/13/2004	RUMS software was rebooted and checked by Tim D. Changes are OK now.											
Equerry	7/12/2004		NA	NA	NA	NA	300	42.5	100	60	40	400	Nucleation 400C, 400 mT, S12H6 200, 5 min. Found furnace in abort mode. Had to run standby recipe twice to get the coating step. Usual problem, computer gauges pressure too high and abort the recipe.
chenyi	7/16/2004		NA	NA	90	NA	120	410	110	40	40	400	Nucleation 410C, S12H6 100, 400 mT, 10 min.
chenyi	7/17/2004		8.33	121	90	NA	105	420	110	30	40	400	Nucleation 420C, S12H6 100, 400 mT, 10 min.
Webster	7/20/2004	GeH4 tank change.											

Webtry	7/20/2004	Injector pressure 8.5. Injector changed.	7.15	118	89.9	4.05	30	350	0	60	180	300	No nucleation.	
Equerry	7/20/2004	366	NA	121	90	NA	8	420	100	0	40	400	Nucleation 420C, S2H6 100, 400 mT, 10 min.	
chanyj	7/20/2004	330	NA	120	90	NA	9	325	0	0	80	400	Nucleation 400C, S2H6 100, 400 mT, 15 min.	
chanyj	7/21/2004	330	7.87	120	90	NA	9	420	110	0	40	400	Nucleation 420C, S2H6 100, 400 mT, 10 min.	
Equerry	7/23/2004	349	7.22	121	90	NA	30	350	0	60	180	300	No nucleation.	
chanyj	7/24/2004	350	NA	121	90	1.95	120	420	110	1.5	40	400	Nucleation 420C, S2H6 100, 400 mT, 10 min.	
bbablm	7/26/2004	330	7.26	121	90	NA	27	400	100	60	40	300	No nucleation. GeH4 charge did not show up.	
Equerry	7/28/2004	330	7.28	121	89.6	4.12	12	350	0	60	180	400	No nucleation.	
chanyj	7/31/2004	330	7.33	121	90	2	90	420	110	1.5	40	400	Nucleation 420C, S2H6 100, 400 mT, 10 min.	
Equerry	8/1/2004	330	7.33	118	90	NA	20	350	0	30	180	300	No nucleation.	
Equerry	8/3/2004	330	7.43	118	89.9	NA	60	350	0	30	180	300	Nucleation 350C, S2H6 200, 300 mT, 5 min.	
bbablm	8/4/2004	330	7.39	118	89.8	5.03/5.13	483/45	425/425	100/100	60/60	65/53	400/600	No nucleation. Bilayer process.	
Equerry	8/4/2004	330	8.14	118	89.7	0.06	20	350	0	0	180	300	Nucleation 350C, S2H6 200, 300 mT, 5 min.	
chanyj	8/6/2004	330	NA	120	90	0.2	60	420	112	0	37	400	Nucleation 420C, S2H6 100, 400 mT, 10 min.	
chanyj	8/6/2004	330	NA	121	90	NA	90	420	112	0	37	300	Nucleation 420C, S2H6 100, 400 mT, 10 min.	
Equerry	8/9/2004	330	8.15	121	89.9	5.27	130	425	100	60	40	400	Nucleation 400C, S2H6 200, 400 mT, 5 min.	
chanyj	8/9/2004	330	NA	121	90	NA	60	420	112	0	37	400	Nucleation 420C, S2H6 100, 400 mT, 10 min.	
Webtry	8/9/2004	Injector pressure 8.5. Injector changed.												
Equerry	8/10/2004	390	7.79	121	89.7	4.61	130	425	100	60	40	400	Nucleation 400C, S2H6 200, 400 mT, 5 min.	
Equerry	8/11/2004	349	7.53	121	89.9	NA	45	350	0	60	180	300	Nucleation 350C, S2H6 100, 300 mT, 1 min.	
Equerry	8/12/2004	330	7.63	121	90	4.73	300	425	100	60	40	400	Nucleation 400C, S2H6 200, 400 mT, 5 min.	
Equerry	8/14/2004	351	8.04	121	89.9	NA	5	300	0	60	180	300	No nucleation.	
Equerry	8/14/2004	330	8.04	118	89.9	5.04	300	425	100	60	40	400	Nucleation 400C, S2H6 200, 400 mT, 5 min.	
wfo w	8/16/2004	Verify that the front injector is leaky. Plugged up the front injector port with a rod, pumped out the line, and then flow N2 to build up some pressure. The pressure dropped immediately to zero once the N2 flow was turned off.												
chanyj	8/16/2004	330	8.6	121	90	NA	120	420	110	1.5	40	400	Nucleation 420C, S2H6 100, 400 mT, 10 min.	
chanyj	8/17/2004	330	8.6	121	90	NA	180	325	0	0	80	400	Nucleation 400C, S2H6 100, 400 mT, 20 min.	
chanyj	8/17/2004	330	8.6	121	90	4.3	130	420	110	40	40	400	Nucleation 420C, S2H6 100, 400 mT, 10 min.	
Webtry	8/19/2004	Injector pressure 8.63. Injector changed.												
bob	8/19/2004	The manifold was inspected and cleaned.												
Webtry	8/19/2004	Tytar20 front injector for the dopant line has been capped off. Tytar20 line that went to the front injector now has been hooked up to the right rear injector. This will allow switching of the one injector or the other when the gas ring is on. As hooked up at present the left injector can only be read by manually switching it.												
ebblm	8/19/2004	347.1	7.51	117	89.6	NA	20	425	100	60	70	400	Nucleation 425C, S2H6 100, 300 mT, 10 min.	
wfo w	8/19/2004	NA	NA	NA	NA	NA	60	425	100	3.6	60	400	Nucleation 425C, S2H6 100, 300 mT, 15 min. No standby info. Test right rear injector.	
chanyj	8/19/2004	NA	NA	NA	NA	NA	90	420	110	30	40	400	NA	
wfo w	8/20/2004	NA	NA	NA	NA	NA	60	425	100	16.5	60	400	Nucleation 425C, S2H6 100, 300 mT, 15 min. No standby info. Test right rear injector.	
wfo w	8/20/2004	NA	NA	NA	NA	NA	60	350	0	16.5	100	300	Nucleation 450C, S2H6 100, 300 mT, 15 min. No standby info. Test right rear injector.	
chanyj	8/20/2004	330	NA	121	90	0.22	180	325	0	0	80	400	Nucleation 400C, S2H6 100, 400 mT, 20 min.	
ebblm	8/25/2004	351.7	7.71	118	89.9	NA	25	425	100	60	70	400	Nucleation 425C, S2H6 100, 300 mT, 10 min.	



wlw	10/1/2004	330	7.78	118	89.6	NA	60	42.5	140	12	60	600	Nucleation 42.5C, S2H6 100, 300 mT, 10 min. 6" wafers only, open boats 28" from door.
chanvj	10/2/2004	330	NA	121	90	NA	1.20	420	110	0	40	300	No nucleation.
chanvj	10/2/2004	330	NA	121	90	0.09	45	32.5	0	0	80	300	No nucleation.
chanvj	10/3/2004	330	NA	121	90	NA	1.20	420	110	0	40	300	No nucleation.
vidya	10/4/2004		7.95	117	89.5								
Equerry	10/5/2004						1.30	42.5	100	60	40	400	Nucleation 400C, S2H6 200, 400 mT, 5 min.
Ms yuam	10/5/2004					0.21	2.30	42.5	100	18	60	400	Nucleation 42.5C, S2H6 100, 400 mT, 1.5 min.
Equerry	10/7/2004												
Equerry	10/7/2004	330	8.17	118	89.2	4.72	72	330	0	60	180	300	No nucleation.
chanvj	10/10/2004												
Computer frozen while entering recipe. Communication lost with the furnace, alarm in the back. Problem solve later.													
The boat-in/out step in software seemed to be messed up. Some times when I pressed "event" after I loaded my wafers, the boat entered only half-way and then came out automatically with "boatout" showing on the CRT screen. Today the boat stopped movement before the door is closed, both manual and auto modes did not make door close successfully. Finally I used my hands to push the boat in.													
chanvj	10/10/2004	330	8.16	121	90	NA	10	420	110	0	40	300	Nucleation 400C, S2H6 100, 300 mT, 3 min.
chanvj	10/10/2004	330	8.16	121	90	NA	90	32.5	0	0	80	300	Nucleation 400 C, S2H6 100, 300 mT, 3 min.
chanvj	10/10/2004	330	8.16	121	90	NA	1.5	420	110	0	40	300	Nucleation 400C, S2H6 100, 300 mT, 3 min.
robotek	10/11/2004												
The drive pulley was loosed on the shaft. It has been tightened.													
bob	10/11/2004												
GeB4 tank changed.													
Equerry	10/11/2004	330	9.11			4.38	300	42.5	100	60	40	400	Nucleation 400C, S2H6 200, 400 mT, 5 min.
blake lin.2	10/11/2004	450					1.65	42.5	11.5	40	60	400	No nucleation.
bob	10/12/2004												
Injector pressure 8.82. B 2H6 injector changed.													
Equerry	10/12/2004	330	7.73	118	89.2		7	300	0	60	180	300	No nucleation.
Equerry	10/13/2004	330	7.73	118	89.3		300	42.5	100	60	40	400	Nucleation 400C, S2H6 200, 400 mT, 5 min.
Equerry	10/14/2004	330					1.20	42.5	100	60	40	400	Nucleation 400C, S2H6 200, 400 mT, 5 min.
chanvj	10/16/2004	330	8.89	121	90	4.89	1.20	420	110	50	40	300	Nucleation 400C, S2H6 100, 300 mT, 3 min.
chanvj	10/20/2004	330	9.19	121	90		60	430	110	0	40	400	Nucleation 400C, S2H6 100, B2H6 100, 400 mT, 3 min.
blake lin.2	10/21/2004	330	9.12	117	89.3	0.5	90	400	100	0	20	800	Nucleation 400C, S2H6 100, 400 mT, 3 min.
blake lin.2	10/22/2004	330	9.13	118	89.4	0.5	1.20	400	100	0	35	800	Nucleation 400C, S2H6 100, 400 mT, 3 min. Took 1 hr 45 min to stabilize to 400 C.
blake lin.2	10/24/2004	330	9.1	117	89.5	0.18	0	0	0	0	0	0	Nucleation 400C, S2H6 100, 400 mT, 2 hr.
blake lin.2	10/25/2004	330	9.11	118	89.6	0.49	0	0	0	0	0	0	Nucleation 400C, S2H6 200, 800 mT, 4 hr.
blake lin.2	10/28/2004	330	9.02	117	89.2	0.49	1.30	410	150	0	10	800	No nucleation.
blake lin.2	10/29/2004	330	9.11	118	89.6	0.49	300	410	150	0	10	800	No nucleation.
Found furnace running standby recipe, bec 2 step. Set temp is 430 C, but center temp is only 289 C, stuck at this step for more than a day. Changed set temp to 300 C, and put furnace on hot.													
wlw	10/30/2004												
Reset tu, firing package and fcs10. Temp started to respond. Ran the standby recipe without problem. Done tu calibration.													
jinmyang	11/2/2004												
Communication failure with DCS30. No monitoring.													
Equerry	11/3/2004												
Turned off DCS30 and restarted. Went into the tu calibration program and disconnected the communication. DCS30 is recording furnace info now.													
Equerry	11/3/2004	330	9.05	118	89.6	45	330	0	60	180	300	300	No nucleation.
Ms yuam	11/3/2004						2.40	400	100	18	45	300	Nucleation 42.5C, S2H6 100, 400 mT, 1.5 min.
Equerry	11/5/2004	330	9.1	119	89.8	1.30	42.5	100	60	40	400	400	No nucleation.
wlw	11/8/2004												
S2H6 ran out. Standby recipe aborted at coat step.													

Performing injector maintenance. (BC13 injector is changed by error). Maintenance notes from bob (09-nov-2004 14:12:48) :													
The SS injector on tystar20 has been changed. The installed injector was first measured with a capillary gauge to assure the orifices were open at to specification. The 0-100 torr injector pressure gauge was zeroed (added +25 torr to zero). The following pressure correlations were measured (logged B2H6 injector reading):													
NZDOPE scdm	Injector Pressure/torr (Temp 450C)												
10	3.1												
20	4.5												
40	6.67												
60	8.36												
80	9.84												
100	11.17												
To assure the injectors meet spec. I am ordering additional, new injectors and have ordered a set of carbide drills to match the orifices. tystar20 is in standby and ready for use.													
blake lin 2	11/9/2004	330	10.31	118	89.3	7.58	485/35	425/425	100/100	60/60	6.5/58	400/600	Bi-layer deposition. No nucleation. Deposition injector pressure taken at 2nd layer.
Maintenance notes from bob (10-nov-2004 15:19:27) : (BC13 injector is changed by error again) The injector installed 11/09 was removed and inspected. There is no doubt it is 100% open -- unobstructed and the orifices are sized correctly. A spare injector, freshly drilled and with an open bome was installed. The following NZDOPE pressures were recorded (logged B2H6 injector reading):													
NZDOPE scdm	Pressure	Temp = 350C											
bob	11/10/2004	20	5.9										
		40	7.57										
		60	9.44										
		80	11.06										
		100	12.5										
Performing injector maintenance. Maintenance notes from bob (10-nov-2004 17:17:08) :													
It is likely I have entered and been changing the wrong injector. I have changed the other injector and here are the results:													
NZDOPE scdm	nbtrr	temp	350C										
bob	11/10/2004	20	3.22										
		40	4.76										
		60	6.00										
		80	7.88										
		100	8.03										
eliso	11/12/2004	347.8	7.45	118	89.4	4.77	1.90	42.5	100	60	40	400	No nucleation.
Equvey	11/13/2004			5	392	42.5	100	60	40	400	400	400	SiCevato recipe. No nucleation.
wbw	11/13/2004	347.5	8.34	117	89.5								Injector monitor. No de position.
Equvey	11/16/2004	351	8.33	117	89.2	5	300	0	60	180	300	300	No nucleation.
Equvey	11/17/2004	330	8.34	121	89.5	392	42.5	100	60	40	400	400	No nucleation.
linan	11/18/2004												
bob	11/19/2004												
bob	11/19/2004												
wbw	11/19/2004												

Install quartz injector for BC13 line.  
New quartz injector stand by conditions: temp=350, pvcpr=118 n2dope=89.6, injt pressure=7.6



chenyj	12/1/2004	330	9.11	121	90		120	420	110	50	40	300	Nucleation 400C, S2H6 100, 300 mTorr, 2 min.	
eliso	12/1/2004	330	7.8 (?)			5.52	90	330	0	60	180	300	No nucleation	
eliso	12/1/2004	Process doesn't seem to progress. It is in SHLD step.												
bob	12/3/2004	There is an issue with stable disilane delivery. The mass flow controller is suspect and will be replaced on Monday. In the meantime, L20 is in use; however, disilane delivery may be a problem.												
eliso	12/3/2004	330	8.4 (?)			5.21	130	400	100	60	40	400	No nucleation.	
wlw	12/5/2004	349.1	9.89	118	89.6								B2H6 injector monitor. No deposition.	
bob	12/6/2004	The disilane MFC has been changed. The new MFC was tested in normal mode. It seems to work well.												
blablm2	12/6/2004	330	9.95	117	89.5	NA	27	400	100	60	40	800	No nucleation.	
igroback	12/7/2004	Injector pressure 10 Torr at 330C. B2H6 injector changed.												
Equerry	12/7/2004	330	7.4	117	89.3	4.62	130	435	100	60	40	400	Nucleation 400C, S2H6 200, 400 mT, 5 min.	
blablm2	12/10/2004	330	7.71	121	89.7	8340.244.1160100730		425	00/11.310	60/40/40	6345/63	400	Trilayer depo. Nucleation 400C, S2H6 100, 400mT, 5 min.	
Equerry	12/10/2004	330	7.83	118	89.5	NA	38	330	0	60	180	300	No nucleation.	
Equerry	12/10/2004	B2H6 bottle depleted. Furnace went to SHLD step after 38 min. of deposition. I switch the furnace to PMFC to finish the recipe and put it back to standby.												
lman	12/15/2004	Plastic pump purge has been replaced with stainless steel.												
bob	12/16/2004	Install new quartz injector for BCl3 line. The previous quartz injector was somehow broken sitting on top of the pump cabinet.												
wlw	12/17/2004	347.1	7.68	quartz	117	89.3							No deposition. Quartz injector monitor.	
wlw	12/17/2004	345.6	7.73	117	89.5	0.5	60	440	150	60	50	600	Nucleation 410C, S2H6 100, 300 mT, 10 min.	
wlw	12/17/2004	406.7	8.24	117	89.3	0.5	60	410	130	18	70	600	Nucleation 440C, S2H6 100, 300 mT, 10 min.	
wlw	12/19/2004	345.6	7.71	117	89.5	0.5	300	425	140	18	60	600	Nucleation 425C, S2H6 100, 300 mT, 10 min.	
wlw	12/20/2004	337.9	7.82	117	89.5	0.5	420	410	150	18	70	600	Nucleation 410C, S2H6 100, 300 mT, 10 min.	
wlw	12/21/2004	344.7	7.73	117	89.3	0.5	45	330	0	12	100	300	Nucleation 330C, S2H6 100, 300 mT, 20 min.	
wlw	12/21/2004	452.2	8.53	117	89.5	0.46	237	440	150	6	50	600	Nucleation 440C, S2H6 100, 300 mT, 10 min.	
wlw	12/22/2004	351.1	7.74	117	89.4	0.43	230	410	130	18	70	600	Nucleation 410C, S2H6 100, 300 mT, 10 min.	
wlw	12/23/2004	330.9	7.7	117	89.4	0.4	263	440	150	18	50	600	Nucleation 440C, S2H6 100, 300 mT, 10 min.	
wlw	12/23/2004	430.7	8.34	117	89.5	0.39	290	425	150	12	50	600	Nucleation 425C, S2H6 100, 300 mT, 10 min.	
wlw	12/24/2004	330.2	7.72	117	89.4	0.41	133	440	130	6	70	600	Nucleation 440C, S2H6 100, 300 mT, 10 min. 9604 screen of GeH4 consumes 6.5 psi of the bottle.	
blablm2	12/27/2004	S2H6 has been added as a variable in recipe SiGeBC13, deposition step.												
wlw	12/27/2004	NA	NA	NA	NA	0.47	5	425	25	Si2H6	12	175	600	Nucleation 425C, S2H6 100, 300 mT, 10 min. Recipe check for Si2H6.
bob	12/28/2004	GeH4 tank change.												
wlw	12/28/2004	341.7	7.88	117	89.4	0.51	230	425	130	12	70	600	Nucleation 425C, S2H6 100, 300 mT, 10 min.	
wlw	12/28/2004	456.5	8.82	117	89.3	0.51	333	410	130	6	70	600	Nucleation 410C, S2H6 100, 300 mT, 10 min.	
wlw	12/29/2004	346.5	7.88	117	89.6	0.47	60	425	25	Si2H6	12	175	600	Nucleation 425C, S2H6 100, 300 mT, 10 min.
wlw	12/29/2004	NA	NA	NA	NA	0.25	287	330	0	12	100	300	Nucleation 330C, S2H6 100, 300 mT, 20 min.	
wlw	12/30/2004	353.7	7.89	117	89.3	0.51	318	410	140	12	60	600	Nucleation 410C, S2H6 100, 300 mT, 10 min.	
wlw	12/31/2004	353.6	7.96	117	89.4	0.51	218	440	140	12	60	600	Nucleation 440C, S2H6 100, 300 mT, 10 min.	

		Performing BC13 quartz injector monitor after 59 hours of BC13 doped de position.					
		N2DOPE (sec m)	Injector Pressure (torr)	Temp (deg C)	PRCPR (Torr)		
		10	2.29	363.5	22		
		20	3.37	363.3	39		
		30	4.23	363	54		
		40	4.95	362.7	67		
		50	5.59	362.1	78		
		60	6.2	361.3	89		
		70	6.72	360.6	98		
		80	7.24	359.5	110		
		90	7.71	358.5	117		
bob	1/5/2005	A new B2H6 cylinder is connected to tystar20. It is hard purging overnight and will be turned on 1/6 by 9 am. T20 will be up tomorrow.					
		The new B2H6 cylinder is installed. The quartz injector used by Carrie Low over the holidays has been removed. This quartz injector broke during removal due to mechanical forces.					
bob	1/6/2005	A dummy quartz stub has replaced it and the valve on the dummy line to this dummy injector has been closed. The B2H6 stainless injector was removed and replaced with a cleaned injector. The current injector pressure is: 90 secm N2dope - 7.03 Torr.					
jimmymac	1/18/2005	Found the standby recipe at special hold step. Check the history and found the reason was pressure high. Check the pump and found it is off. Equip staff please check the pump. If it is OK, please restart the pump. Tystar20 is do wa.					
		Restarted the pump. Ready for use.					
mcsail	1/18/2005	330	7.4	119	89.9	340	425
equvay	1/19/2005	350	7.87	120	90	110	420
chenyj	1/20/2005	330	7.43	120	90	120	325
chenyj	1/23/2005	330	7.23	118	89.2	5	300
Equvay	1/23/2005	330	7.8	121	90	110	420
chenyj	1/26/2005	330	6.9	101	89		
bob	2/3/2005	Marie requested to install a new quartz injector for the BC13 line.					
Ms youm	2/3/2005	330	6.9	101	89		
jimmymac	2/3/2005	Found that tystar1 & t2 flow SIH4 without problem, but both tystar19 and 20 could not flow SIH4. Traced the gas line and could not find any valve closed. The recipe is set to wait. Lab member can unload her wafers. Tystar20 is down for any process that uses SIH4. Equip staff please double check the gas lines.					
whw	2/3/2005	Standby recipe aborted due to S2E6 flow error.					
bob	2/4/2005	There is a definite problem with SIH4 flow on t20. At 2000 secm flow. The supply was exhausted in ~ 3 minutes. Tystar19 was tested and could still flow SIH4. We will replace the SIH4 mt6 for tystar20 later this afternoon and see if this is a fix. Tystar20 remains down and will hopefully be up by the end of today.					
bob	2/4/2005	A new SIH4 mt6 was installed on t20. There is an issue with the SIH4 flow. We cannot complete repairs today and need to take the SIH4 circuit offline on Monday to make further checks. t20 is down and locked for the weekend.					
bob	2/4/2005	There seems to be something amiss with the 460. A new mt6 does not work under the control of the 460 but does work perfectly under control of a test electronics package.					
grcback	2/7/2005	Substituting a new cable from 460 to s14 mt6 results in still wrong, but different behavior.					
bob	2/8/2005	The tystar20 SIH4 flow issue has been traced to the delivery line. We will open the line for inspection in the morning.					
bob	2/9/2005	The flow issue with t20 has been located and fixed. Tomorrow, (2/10/05) I will check the GeH4 and SIH4 mt6's for flow values. If all is well the tube should be back available by the afternoon.					
bob	2/10/2005	Found the gas ring line booted up to the front injector port. Clogged port caused gas flow problem. The SIH4 and GeH4 0-200 mscf were removed and the calibration measured and recorded. Both are correct. Previous SIH4 flows were likely 75% of set values. Carrie Low will compare previous runs to compare results. Carrie is also looking into ways to monitor flow and ratios for SIH4 and GeH4.					

	Perform MFC test with N2 flow meter.													
	MFC	Electronic input	N2 output (sccm)	correction factor	conversion (sccm)									
who	2/10/2005	SIH4 200 (before)	100 %	250	0.6	150								
		SIH4 200 (before)	50%	125	0.6	75								
		SIH4 200 (now)	100%	320	0.6	192								
		SIH4 200 (now)	50%	155	0.6	93								
		GeH4 200 (now)	100%	330	0.57	188.1								
		GeH4 200 (now)	50%	160	0.57	91.2								
		GeH4 200 (new spare)	100%	345	0.57	196.65								
		GeH4 200 (new spare)	50%	165	0.57	94.05								
who	2/10/2005	Standby recipe aborted twice with error message "IF PRCPR_NE". Jon Goldman is not collecting data and I cannot find out what went wrong.												
Jimmygac	2/11/2005	Reboot DCS30 PC. Will monitor the pressure.												
who	2/11/2005	A follow up on the standby recipe abort problem: I was watching the furnace when the process aborted 2 minutes into the Si2H6 coating step. The pressure could not be achieved and N2vec kept changing values to adjust the pump. It always got too high or too low. Also tested the PRCPR at manual mode. Flow 100 sccm N2dope, no other gas. PRCPR cannot be settled at 300 or 400 mTorr in 5 minutes. After 10 minutes, it could reach the set point. If the PRCPR setpoint is 600 mTorr, it could be achieved faster. Some problem with the PRCPR and N2vec feedback control?												
Jimmygac	2/11/2005	Adjusted the pressure control constant offset 0, reset 2, delay 0. The pressure control can reach 300 and 900 mTorr in a minute.												
elicio	2/11/2005	348	9.2	118	90	4.51	1.50	425	100	60	20	400	Nucleation 400C, Si2H6 200, 5 min.	
chenyj	2/13/2005	330		120	90	1.20	1.20	325	0	0	80	300	Nucleation 400C, Si2H6 100, 3 min.	
													Nucleation 410 C, Si2H6 100, 300 mT, 10 min. Film color not uniform. Some dots as big as 5 mm in diameter that have different color at the lower right corner of each wafer.	
blabala	2/14/2005	330	8.13	112	89.9	NA	660	410	150	18	50	600	No nucleation.	
Equy	2/15/2005	330	8.11	112	89.2	5.65	340	425	100	60	40	400	Nucleation 400 C, Si2H6 100, 3 min.	
chenyj	2/17/2005	330	8.96	120	90	NA	110	420	110	35	40	300	Nucleation 375C, 300 mT, Si2H6 100, 15 min.	
who	2/20/2005	356.6	9.18	112	89.9	0.53	60	375	25 Si2H6	0	12	175	Uniform but high R film.	
who	2/20/2005	456.5	10.16	112	89.9	0.57	70	425	0	0	0	600	Furnace anneal. Flow 100 sccm N2.	
who	2/21/2005	353.3	9.17	112	89.9	0.53	60	440	130	0	18	70	Nucleation 440 C, 300 mTorr, Si2H6 100, 10 min. Repeat DOE-15 to identify SIH4 MFC problem.	
who	2/21/2005	454.5	10.15	112	89.2	0.54	60	400	25 Si2H6	0	12	175	Nucleation 400 C, 300 mT, Si2H6 100, 12 min. Cloudy film, large R variation.	
who	2/22/2005	346	9.13	112	89.9	0.57	60	440	150	0	6	50	Nucleation 440 C, 300 mT, Si2H6 100, 10 min. Repeat DOE-11 to identify SIH4 MFC problem.	
who	2/22/2005	458.1	10.2	112	89.9	0.28	60	400	15 Si2H6	0	18	185	Nucleation 400 C, 300 mT, Si2H6 100, 12 min. Uniform film, high R.	
who	2/22/2005	457.2	10.19	112	89.9	0.27	60	425	15 Si2H6	0	18	185	Nucleation 425 C, 300 mT, Si2H6 100, 10 min. Uniform film, low R. Pressure varied from 250-350 mTorr.	
who	2/22/2005	Pressure varied from 250-350 mTorr in the previous depo. Lower limit of the pressure is reached for the particular gas flow. Need to adjust PIN setting with Jimmy.												
who	2/23/2005	343.4	9.14	112	89.9	0.3	60	425	25 Si2H6	0	18	175	350	Nucleation 425 C, 300 mT, Si2H6 100, 10 min. Cloudy film.
who	2/23/2005	GeH4 tank pressure reaches a hard zero. 6 psi barely covers a 1-hr depo with 175 sccm.												

pprobask	2/24/2005	GeH4 tank changed.												
pprobask	2/24/2005	Tested pump throughput with N2. The corresponding flow and pressure: 100-121, 200-211, 300-418, 1000-712, 1500-978, 2000-1236.												
wlw	2/24/2005	356	9.19	112	89.9	0.3	60	425	15 Si2H6	0	18	150	350/300	Nucleation 425 C, 300 mT, Si2H6 100, 10 min. Pressure cannot be stabilized at 300 mTorr. Manually change setpoint to 330 mTorr.
bob	2/24/2005	Jimmy will adjust the FIN setting to find the right Px value for the pressure feedback.												
blablin2	2/24/2005	350	9.15	111	89.9	NA	115	425	130	12	70	600	600	Nucleation 425 C, 300 mT, 100 Si2H6, 10 min. Process absorbed after 1 hr 6 min into depo. History shows SiH4 flow problem.
bob	2/25/2005	SiH4 delivery pressure to T20 is 23 psi - normal. Manually tested gas flow and no problem can be found at this time. Will monitor. With the agreement of lab members, the following modifications have been made to tystar20: 1) the injector line formerly used for B2H6 has been routed to the quartz injector. 2) the SS injector has been removed and the tubulation plugged off on the tube. 3) the valve used for dopant -> gas ring has been capped at the rear gas shelf and no longer in use. The He/BC13 1% is now the only boron source for tystar20 (B2H6 remains available for tystar19). The mfc used for He/BC13 remains a 0-20 sccm. The configuration file for the FCS10 remains as before as does the definition table on the rear MFS2 (460 controller). To be done at a future date: 1) Change He/BC13 1% mfc from 0-20 sccm to 0-50 sccm. 2) Change the dilution mfc from 0-100 sccm to 0-200 sccm. 3) Add series mfm for insitu radioflow checks of SiH4, Si2H6, GeH4. 4) Update FCS10 config so it is up to date. 5) Update the MFS2 (460 controller) definition table. 6) Update recipes												
bob	2/28/2005													
wlw	3/1/2005	Did normal gas flow test to verify the injector pressure gauge connection. The injector pressure gauge is now reading the BC13 quartz injector pressure. Should choose "gas ring off" option to flow BC13, opposite to before.												
wlw	3/1/2005	The furnace got into a strange "STBY" mode, cannot get it back to normal with several attempts. Checked the tube configurations, it was ok. Found all the recipes were corrupted. Down loaded b2outb, sigstmc, and sigelb3 into the fcs10. Tried to download more recipes, but the fcs10 alarmed for power failure, and all the recipes previously downloaded corrupted. Tried again, and everything repeated. Now there are only the above 3 recipes in the fcs10. Suspected that the rear of fcs10 is not working right. Some ran may be malfunction which limited the number of recipes. Tystar20 is running standby recipe now. The temperature reverts to 350C. Equipment staff should contact Tystar for further diagnosis.												
jimmynyc	3/1/2005	The backup battery voltages were tested on 1/7-20. T20 showed 3.74 volts, a bit lower than the rest which were slightly over 4 volts. A call is in to Tystar asking if this might account for recipe corruption. New batteries will be sought in any case.												
pprobask	3/2/2005	Jimmy has successfully reloaded four recipes and T20 is operational. The symptoms observed are believed to be faulty RAM and the folks at Tystar have agreed to send a set of replacement chips which will be installed upon arrival. For now T20 is up and running.												
pprobask	3/3/2005	350	6.23	112	89.9	2.18	115	425	130	12	70	600	600	Nucleation 425 C, 300 mT, 100 Si2H6, 10 min.
blablin2	3/4/2005	350	6.21	112	89.9	0.57	180	410	130	0	70	600	600	Nucleation 410 C, 300 mT, 100 Si2H6, 10 min.
blablin2	3/6/2005	When I opened the furnace to load my wafers, I realized that the tube was broken. There were lots of the broken pieces everywhere inside the furnace. I left the tube on BT00B recipe.												
Me yorum	3/7/2005	Found that the quartz liner was broken. The tube is still holding vacuum. The leak rate is 3mltorr/min. Wait for the equip staff to change it. Tystar20 is down.												
jimmynyc	3/11/2005	Changed the liner, along with new TC sheath, injector and can flapper cover.												
pprobask	3/22/2005	Did thermal calibration. The tube failed leak check when running standby recipe.												
jimmynyc	4/1/2005	Changed quartz tube, re-used other quartzware from last time. Leak rate 2 mT/min. (231 hr of depo)												
pprobask	4/5/2005	Thermal calibration 300-450 C.												

who	4/7/2005	Jon Goldman is not recording data. "TCU communication error" on screen.												
jimmyzac	4/8/2005	Reset the TCU. DCS30 is recording data again.												
flaw (?)	4/7/2005	330	6.2	112	112 (?)	6.2 (?)	60	410	150	9 (?)	18	50	600	Nucleation 410 C, 300 mT, 100 Si2H6, 2 min.
blakein	4/8/2005	330	6.08	112	89.9	NA	30	425	130		12	70	600	Nucleation 425 C, 300 mT, 100 Si2H6, 10 min.
blakein	4/9/2005	330	6.12	112	89.9	2.02/NA	115/386	425/410	130/130	12 and 6	70/70	600/600	600	Nucleation 425/410 C, 300 mT, 100 Si2H6, 10 min. 4 run bi-layer.
who	4/10/2005	353.6	6.14	112	89.9	2.06	60	425	140		12	60	600	Nucleation 425 C, 300 mT, 100 Si2H6, 10 min. DOE recipe 8, redo test run for MFC calibration.
who	4/10/2005	451.5	6.65	115	89.9	2.57	60	440	103		18	70	600	Nucleation 440 C, 300 mT, 100 Si2H6, 10 min. DOE recipe 15 with adjusted SiH4 flow for MFC cal.
jimmyzac	4/11/2005						10	400	0		0	180	300	Nucleation 400 C, 300 mT, Si2H6 100, 10 min.
who	4/12/2005	351.4	6.1	112	89.9	1.42	60	440	119		6	50	600	Nucleation 440 C, 300 mT, 100 Si2H6, 10 min. DOE recipe 11 with adjusted SiH4 flow for MFC cal.
jimmyzac	4/13/2005	330					6	400	0		0	180	300	Nucleation 400 C, 300 mT, Si2H6 100, 10 min.
Msyoum	4/19/2005	330	6.02	112	89.9		10	440	150		12	50	600	Nucleation 440 C, 300 mT, Si2H6 100, 10 min.
jimmyzac	4/22/2005	330					16	400	0		0	180	300	Nucleation 400 C, 300 mT, Si2H6 100, 60 min. 2 eir runs, 1kA undoped Ge
Msyoum	4/23/2005	330	6.16	112	89.9		5	425	140		12	60	600	Nucleation 425 C, 300 mT, Si2H6 100, 1 min. Recipe aborted since gas ring was set to on (cannot flow)
Msyoum	4/23/2005					2.13	140	425	140		12	60	600	Nucleation 425 C, 300 mT, Si2H6 100, 10 min.
Equerry	5/2/2005		6.2				125	425	115		20	55	600	Nucleation 425 C, 300 mT, Si2H6 100, 10 min.
Equerry	5/3/2005	330	6.43				125	425	115		20	55	600	Nucleation 425 C, 300 mT, Si2H6 100, 10 min.
Equerry	5/14/2005						72	350	0		12	100	300	No nucleation.
Equerry	5/15/2005	330	6.25				80	350	0		12	100	300	No nucleation.
blakein2	5/16/2005	330	6.25	112	89.9		20+10	350	0		12	180	300	No nucleation.
equerry	5/17/2005	330					285	425	0		20	50	600	Nucleation 425 C, 300 mT, Si2H6 100, 10 min.
equerry	5/17/2005	330					30	350	0		12	100	300	No nucleation.
bob	5/18/2005	Tystarbank5 shutdown because of a brief power outage, ~12 noon. The bank has been restarted, the pumps turned on and the standby recipes loaded. The tystar20 MFS-1 (460 controller) is giving an error: FLOWCTRL ID. I have not seen this error before. We cannot reset it. I have a call into Tystar for guidance on a fix. Tystar20 is down until this problem is cleared.												
jimmyzac	5/18/2005	Talked to Tystar engineer and obtained flow ID. Checked the ID with MFS-460 dip switches. Found one switch was set wrong. Reset the dip switch and the problem went away.												
equerry	5/20/2005	330	6.2	118			24	350	0		12	100	300	No nucleation.
equerry	5/20/2005	330					12	350	0		12	100	300	No nucleation.
equerry	5/21/2005	330	6.2	118	89.9		470	425	120		20	50	600	Nucleation 425 C, 300 mT, Si2H6 100, 10 min.
bob	5/23/2005	GeH4 bottle changed.												
blakein2	5/24/2005	330	6.26	112	89.5	2.82/NA	485/35	425/425	110/110	20/20	70/60	400/600	400	No nucleation. Bi-layer process.
Msyoum	5/28/2005	330	6.28	112	89.9	2.02	100	425	130		10	70	600	Nucleation 425 C, 300 mT, Si2H6 100, 10 min.
equerry	6/7/2005	330	6.1	118			60	425	115		20	55	600	Nucleation 425 C, 300 mT, Si2H6 100, 10 min.
equerry	6/8/2005	330	6.2	119			2	350	0		12	100	300	No nucleation.
equerry	6/8/2005	330					16	350	0		12	100	300	No nucleation.
equerry	6/9/2005	330					410	425	120		20	50	600	Nucleation 425 C, 300 mT, Si2H6 100, 10 min.
Msyoum	6/11/2005	330	6.27	112	89.5	2.74	660	410	120		18	50	600	Nucleation 410 C, 300 mT, Si2H6 100, 2 min.

The SiGe film on my wafers turned out to be very hazy and non-uniform. I am not sure why is this, I am trying to identify if this is due to a furnace problem or a process issue. The sheet resistance of the film was pretty low.

I had 5 patterned wafers and 2 SiO2 test wafers distributed throughout boat 6 boats. Patterned wafers were more hazy than non patterned wafers. This indicates that maybe it's due to a pre-furnace cleaning process. I used SVC14 and DI-water since I had SiGe films underneath. I am still trying to find the best wet cleaning process prior to the furnace.

330	6.27	112	89.5	1.40	42.5	140	12	60	600	Nucleation 300 C, 300 mT, Si2H6 100, 10 min.
330	6.2	118	89.2	20	330	0	12	100	300	No nucleation
330				1.20	42.5	120	20	50	600	Nucleation 42.5 C, 300 mT, Si2H6 100, 10 min.
330	6.31	112		2.78	25	410	18	30	600	Nucleation 410 C, 300 mT, Si2H6 100, 5 min. Process aborted.

I found the furnace aborted after 2.5 min of deposition. When checking the history to find out the problem, the ABORT step says Pressure High. My wafers are still in the furnace.

Tystar20 has been reset and Marie will remove her wafers. Jimmy Chang needs to review the history file for this tube to learn why the recipe aborted. Marie requests a monitor run once Tystar20 is back up and running.

found that the process ended after the nucleation step. Si2H6 flowed 5 minutes and pressures stayed at 300 mtorr. after that the process gas flow the reason could be that the furnace was disabled. re-run the process with the process parameter. process went thru nucleation and 5 minutes into deposition without problem. pressure control was within 1 minute to the set point could not repeat the problem. in the future, please do not remove wafers or run any other recipe. it will delete all the alarm info in the first 0. tystar 20 is up for use.

The keyboard for tystar20 has been replaced. Tystar20 is ready to use.

Performing GeH4 maintenance. The LOW GeH4 was tested at several flows. It seems to be working correctly.

330	6.35	115	89.5	2.25	360	42.5	105	12	70	600	Nucleation 42.5 C, 300 mT, Si2H6 100, 5 min.
				1.20	410	125	12	50	600	600	Continuous runs. Nucleation 410 C, 300 mT, Si2H6 100, 3 min.
				2.23	100	410	11.5	12	60	600	Continuous runs. Nucleation 410 C, 300 mT, Si2H6 100, 3 min.
				2.23	80	410	10.5	12	70	600	Continuous runs. Nucleation 410 C, 300 mT, Si2H6 100, 3 min.

Tystar20 is showing Si/Ge recipes. The process pressure and gas control has been checked and does not seem to be the issue. t20 is enabled in my name pending review by Jimmy Chang.

				2.2	170	410	12.5	12	50	600	No nucleation.
				2.2	130	410	10.5	12	70	600	No nucleation.

Tystar20 is operating correctly and Marie has completed her run. we do not know why two previous run attempts aborted but it is likely the shutoff of the toxic gases for the addition of an mfn may have been the cause. Tystar20 is up.

330	6.26	115	89.5	2.2	240	410	13.5	12	40	600	No nucleation
						410	130	12	45	600	Recipe aborted

Marie's recipe was aborted 5 minutes into deposition.

Her recipe: SiH4=130, GeH4=45, BC13=12, 410 deg C, 600 mTorr

Recent computer shows SiH4 and BC13 flow were fine. GeH4 flow was 45 sccm, but setpoint was 0. PRCPR was 138 mTorr, but setpoint was 0. N2V AC was 0, didn't respond for pressure control.

Test gas flow manually. SiH4, BC13, PRCPR and N2V AC all respond to input value. But GeH4(high) cannot flow. Jimmy found there was not compress air signal sent to the GeH4 valve.

jimmyzac	10/31/2005	found that a valve in the gas cabinet was turned off. turned on the valve and the gas flow without problem. equip staff please turn on the valve after finishing jobs. tystar20 is up for use.											
msyoum	11/1/2005	330	6:26	115	89.5	2.22	210	410	130	12	45	600	No nucleation
msyoum	11/1/2005	330	6:3	115	89.5	2.2	360	425	105	12	70	600	Nucleation 425 C, 300 mT, Si2H6 100, 5 min.
msyoum	11/1/2005					2.22	210	410	130	12	45	600	No nucleation.
Henry Haidneder of Tyetar Co. is here to change the definition table and update the furnaces.													
MFM loop is hooked up.													
When GasLink = on, all gases (dopant and precursor) can run through the MFM loop for MFC calibration.													
BCB MFC has been updated from 20 to 50 sccm full range.													
Remove GeH4(lo), PH3 and B2H6 channels. EXPINJ and EXPGR are available for new dopant and precursor.													
Modify PIN setting for temperature control.													
GeH4 tank is empty. N2 is running overnight through the BCB line after the MFC change. Temperature calibration is in progress.													
Temperature calibration did not finish. Edit standby and deposition recipe. Add a 5-min leak monitor step to recipes.													
GeH4 bottle changed. BCB is back on.													
who	11/8/2005	436	6:33	115	87								Leak monitor - door open right before.
who	11/9/2005	356	6:41	115	87								Leak monitor - door open right before.
who	11/9/2005	Run MFC monitor manually.											
who	11/9/2005					NA	10	430	140	30	60	600	Leak monitor - door kept close for a few hours. Check recipe. Nucleation 430 C, 300 mT, Si2H6 100, 5 min.
who	11/9/2005	Data record in DCS30 do not match the definition table. N2Dope is off by 10x, PH3, GeH4(low), GeH4(high) are still there. N2MFM, BCL3, GeH4, etc do not show properly.											
jimmyzac	11/10/2005	Start temperature calibration for the range of 300 - 450 C.											
jimmyzac	11/14/2005	Temperature cannot stabilize at 300 C over the weekend. Restart calibration for the range of 350 - 400 C.											
jimmyzac	11/16/2005	End zones temperature are off by a few degrees. Center zones temperature are good to 0.5 deg C.											
who	11/16/2005	Change configuration in DCS30. Now gas channels show up properly.											
who	11/16/2005	Run MFC monitor manually.											
msyoum	11/17/2005					2.1	120	425	105	12	70	600	Nucleation 425 C, 300 mT, Si2H6 100, 2 min.
msyoum	11/18/2005	330	6:27	115	87	2.1	240	425	105	12	70	600	Nucleation 425 C, 300 mT, Si2H6 100, 10 min.
msyoum	11/18/2005					2.1	130	410	130	12	45	600	No nucleation.
who	11/21/2005	Run MFC monitor manually.											
who	11/21/2005	Some old dummy wafers have very thick deposition and stick on the quartz boats. Take all boats out and clean in Sitecher.											
who	11/21/2005	343.8	6:25	115	87		60	430	140	30	60	600	Nucleation 430 C, 300 mT, Si2H6 100, 10 min.
who	11/22/2005	Set up recipes: SIGENONU (deposition w/o nucleation), MULLA (12-layer deposition), MONYAR (MFC monitor for regular users)											
who	11/22/2005	While running standby recipe, "no auto" alarm in the back. Silence alarm and reset computer. Process seemed to proceed, but aborted after some time. Cannot display history on the screen.											
jimmyzac	11/23/2005	no auto alarm comes on when the FCS10 has power failure. if it is reset for long time, over a few seconds, the alarm will show up. since all the alarm messages were erased, could not know the cause. restart the coating (standby) recipe and if finished without problem, this problem is cleared for now.											
who	11/28/2005	349.9	6:22	115	87	2.30	430	140	30	60	600	600	Nucleation 430 C, 300 mT, Si2H6 100, 10 min.
who	11/29/2005	349.5	6:35	115	87	30*11	430	140-190	30	60	600	600	Nucleation 430 C, 300 mT, Si2H6 100, 10 min. SiH4 ramping experiment (+5 sccm per layer), 11 layer deposition.

who	11/30/2005	NA	NA	NA	30*11	430-380	140	30	60	600	Nucleation 430 C, 300 mT, Si2H6 100, 10 min. Temperature ramping experiment, (-5 deg C per layer), 11 layer deposition.
who	11/30/2005	Run MFC monitor manually.									
Ms youm	12/1/2005	330	6.9	115	80	425	105	12	70	600	Nucleation 425 C, 300 mT, Si2H6 100, 5 min.
Ms youm	12/1/2005	NA	NA	NA	60	410	130	12	45	600	No nucleation
who	12/2/2005	Modify BTOUTB recipe and set gas ring to off so that the MEM line is inactive for the 5000 sec. N2BKFL.									
who	12/8/2005	Run MFC monitor manually.									
who	12/10/2005	Center zone temperature off calibration. Set temperature is 450 C and actual temperature is ~160 C.									
jimmygmc	12/12/2005	Found that the TCU was locked up. Reset TCU all temperature read normal except the center zone. The center zone temp readout was fluctuating. There was a "B" symbol next to the temp readout. It indicated that the TIC was not working. Swapped the center zone 1/6 with other zone 1/6. Found that the 1/6 was working. It is suspected that the 1/6 block has a bad contact or we have a electronic problem. Tysar20 is down until equip staff fixed the 1/6 problem.									
who	12/15/2005	Created recipe MONCON for MFC monitor. There are three set values for each gas.									
postal	12/16/2005	Bad connections at both the TCU board and TC block. Connection re-establish and temperature now reading correctly from TC.									
who	12/16/2005	Start temperature calibration for the range of 300 - 450 C.									
who	12/17/2005	Started TCU calibration yesterday for 350-450 deg C. Found temp setpoint at 350 deg C and actual temp at 450 deg C (within 0.5 deg C). Temperature calibration should be done, but people said it started alarming since last night.									
who	12/17/2005	I disconnected the TCU section on the pull-down menu communication -> disconnect, then file -> exit. DCS30 gives error "TCU communication failure". The furnace is operational, but DCS30 cannot capture data.									
who	12/17/2005				60	410	150	30	50	1200	Nucleation 410 C, 300 mT, Si2H6 100, 10 min.
who	12/18/2005	The temperature stabilization for the standby recipe (450 deg C) takes forever. The temperature has to be good to within 1 deg C. The tolerance in the recipe is 5 deg C for the center zones and 10 deg C for end zones. This starts to happen after the TCU communication failure error. I ran a deposition recipe SiGeBC13 with set temperature 410 deg C. It can stabilize within an hour and the tolerance is correct.									
who	12/18/2005	Run MFC monitor with recipe MONCON.									
who	12/18/2005	350.5	6.31	116	60	410	150	30	50	900	Nucleation 410 C, 300 mT, Si2H6 100, 10 min.
jimmygmc	12/19/2005	Reset TCU. DCS30 now talking with Tysar20 and collecting data. the standby recipe was corrupted. the tolerance was set to default. Reload the recipe.									
who	12/19/2005	Standby recipe aborted 3 times. It always happened at the beginning of the Si2H6 coating step. I tested the Si2H6 flow manually and couldn't see any problem.									
who	12/20/2005	360	6.31	116	60	410	150	30	50	700	Nucleation 410 C, 300 mT, Si2H6 100, 10 min.
who	12/20/2005				60	410	140	30	60	600	Nucleation 410 C, 300 mT, Si2H6 100, 10 min.
jimmygmc	12/21/2005	Found that the reason for abort was N2DOPE instead of Si2H6. Ran the standby recipe twice with recipe and once manually, not problem with the process.									
who	12/21/2005	348	6.43	119	60	410	140	45	60	350	Nucleation 410 C, 300 mT, Si2H6 100, 10 min.
who	12/22/2005	449.7	6.97	119	230	410	140	30	60	600	Nucleation 410 C, 300 mT, Si2H6 100, 10 min.
Ms youm	12/22/2005	330	6.46	119	120	425	102	12	70	600	Nucleation 425 C, 300 mT, Si2H6 100, 5 min.
Ms youm	12/22/2005				100	410	130	12	45	600	No nucleation. Second layer of bi-layer.
who	12/22/2005	458.6	7.01	119	230	410	140	45	60	600	Nucleation 410 C, 300 mT, Si2H6 100, 10 min.
who	12/23/2005	Run MFC monitor with recipe MONCON.									
jimmygmc	12/23/2005	Tysar20 lost all the configuration when a lab member entering the recipe. Reset the FCS10 using cs command. Down load configuration file from DCS30. MFS460 #2 alarmed for BAD RAM. Reset it and the alarm cleared. Down load all the process recipes needed.									
who	12/23/2005	349.9	6.45	116	313	410	140	45	60	350	Nucleation 410 C, 300 mT, Si2H6 100, 10 min.
who	12/26/2005	350.2	6.49	121	230	410	140	15	60	600	Nucleation 410 C, 300 mT, Si2H6 100, 10 min.
who	12/27/2005	349	6.4	119	340	410	140	30	60	350	Nucleation 410 C, 300 mT, Si2H6 100, 10 min.
who	12/28/2005	351.7	6.55	119	360	410	140	15	60	350	Nucleation 410 C, 300 mT, Si2H6 100, 10 min.
who	12/28/2005	Run MFC monitor with recipe MONCON.									

1/10/2006 who w Run MFC monitor with recipe MONCON.  
I used the MONCON recipe to run weekly MFC monitor. The "gas ring" switch has a bad connection. The deposit gas went through the injector path rather than the MFM path. This was noticed with the reading on the injector pressure gauge and the MFM reading. The actual value of the gas ring follows the setpoint on the screen. I had to switch the "gas ring" on and off a few times in the RM page to get it to actually turn on.

1/10/2006 who w What was thought to be a simple bad connection turns out to likely be a malfunction in the electronics in the MFS-460. Currently in communication with Tyezar for help with trouble shooting mfs-460 I/O board components. Tyezar20 is down for now.

1/11/2006 postal swapped out MFS-460 I/O board with a replacement. MFS now correctly controls the gating solenoid. Malfunction most likely due to bad open collector transistor Q1 (2N6038) on the MFS-460 I/O board. Looking into replacing. Tyezar20 is up for use.

1/12/2006 who w Pressure jumps between 150 - 530 mTorr for the following recipe: 410 deg C, 47 sccm SiH4, 20 sccm GeH4, 35 sccm GaH4, 35 20 300 No nucleation. Pressure not stable

1/12/2006 who w 1/12/06, recipe SiGeNoNu.

1/13/2006 jimmygnc As a reference, 350 mTorr was fine in the past for 140 sccm SiH4, 60 sccm GeH4, 15-45 sccm BC13. Tyezar furnaces pressure control parameters are optimized for high gas flow (-200sccm trial) and high pressure (300 mtor and above). in order to run low gas flow (~100sccm trial) or low pressure, the control parameters needs to be changed again. will talk to the super user about the gas flows and slayw equip engineer how to adjust the parameters. Tyezar20 is still up for most of processes.

1/13/2006 jimmygnc adjusted the pressure control parameters according the tube use. new values are: rset 2.0, delay 0.5, offset 0.0 Super users test both high and low pressure deposition and ok with it. Tyezar20 is up

1/13/2006 who w	448	6.9	120	89	20	410	47	35	20	300	No nucleation.
1/13/2006 who w				15	430	47	35	20	20	300	No nucleation.

1/20/2006 who w Run MFC monitor with recipe MONCON.  
Start TCU calibration for 200-450 deg C.

1/25/2006 who w	348.6	6.36	120	89	15	350	0	12	100	300	No nucleation. Process aborted at the beginning of the deposition, because BC13 flow was higher than setpoint. Restarted the process manually and went OK.
1/26/2006 who w	349	6.31	120	89	8	300	0	6	50	300	No nucleation. 56 sccm of N2 flow during deposition.
1/26/2006 who w	451	6.86	120	89	15	350	0	0	100	300	No nucleation. 12 sccm of N2 flow during deposition.
1/26/2006 who w	449.7	6.83	120	89	8	300	0	0	50	300	No nucleation. 62 sccm of N2 flow during deposition.

1/30/2006 who w Run MFC monitor with recipe MONCON.  
Created recipe SiGeSeed. SiH4, GeH4, BC13, Si2H6, temperature and pressure are all variables in nucleation step. Main deposition follows nucleation immediately. Gas flow rates and pressure in the main deposition are variable, but temperature has to be the same as nucleation.

2/7/2006 who w	349.9	6.35	120	89	5	410	140	35	60	600	Nucleation 410 C, 300 mT, SiH4 47, GaH4 20, BC13 35, 5 min. Test SiGeSeed recipe.
2/7/2006 who w											Nucleation 410 C, 300 mT, SiH4 47, GaH4 20, BC13 35, 20 min.

2/9/2006 who w Activate BNTLK interlock for steps with toxic gas flow for all recipes. Increase safety factor for potential leak.

2/9/2006 who w	350.1	6.3	117	89	260	410	140	35	60	600	
----------------	-------	-----	-----	----	-----	-----	-----	----	----	-----	--

2/9/2006 who w Run MFC monitor with recipe MONCON.  
GeH4 bottle change. New pressure 137 psi.

2/20/2006 who w Run MFC monitor with recipe MONCON.



blablin2	4/12/2006	330	6.26	120	90	11.5	425	130	12	70	600	Nucleation 425 C, Si2H6 100, 300 mT, 10 min.
blablin2	4/12/2006	330	6.26	120	90	70	425	140	18	60	600	Nucleation 425 C, Si2H6 100, 300 mT, 10 min.
egamest	4/13/2006	330	6.24	120	89	1.5	450	100	0	0	600	No nucleation. Try to grow nanowire w/ Pt catalyst
egamest	4/13/2006	One of the 6" open boats is broken.										
psfal	4/14/06	Broken wafer boat replaced.										
maryamun	4/14/2006	442	6.7	120	89	1.80	440	130	18	70	600	Nucleation 440 C, Si2H6 100, 300 mT, 10 min.
blablin2	4/15/2006	352	6.3	117	89	1.80	410	130	12	70	600	Nucleation 410 C, Si2H6 100, 300 mT, 10 min.
wlw	4/20/2006	Run MFC monitor with recipe MONCON.										
egamest	4/21/2006	350.1	6.25	120	89	1.5	450	100 Si2H6	10	0	300	No nucleation. Try to grow nanowire w/ Pt catalyst. Also try to deposit poly-Si on Ag catalyst nanowire. (Ag removed)
egamest	4/26/2006	349.9	6.31	120	89	1.5	450	100 Si2H6	5	0	300	No nucleation.
wlw	4/27/2006	Tysnar20 started doing temperature stabilization for the standby coating since last night. The center zone has a "B" next to the actual temperature. All other zones are at ~400 C, where the setpoint is 450 C.										
jimmygac	4/28/2006	Tysnar20 started doing temperature stabilization for the standby coating since last night. The center zone has a "B" next to the actual temperature. All other zones are at ~400 C, where the setpoint is 450 C.										
psfal	5/1/2006	The "B" next to the temp reading means that the thermal couple in the tube is not working, the spike t/c is used as a backup instead since the spike t/c fluctuates more, it takes longer to stabilize the temp.										
wlw	5/1/2006	Tried resetting TCU, and FCS10, no effect										
blablin2	5/1/2006	Tried securing the t/c connection, no effect										
wlw	5/1/2006	equip staff please check the t/c and connections to find out that there is any open circuit.										
psfal	5/1/2006	Tysnar20 is usable, but it is better wait for the equip staff to fix the t/c.										
egamest	5/1/2006	Just like last time, this problem is caused by a faulty connection in the J1 connector coming out of the back of the TCU. Last time I was able to fix the bad connections using spare pins in the connector, but seeing as there are no more spare pins, I think it's the time to do a complete rebuild of the connector. This will be done when the Tysnar Tech comes up some time this week (possibly next week.) For now, the "B" is gone and Tysnar20 is available for use.										
egamest	5/5/2006	Run MFC monitor with recipe MONCON.										
psfal	5/9/2006	330	6.23	120	89	1.30	350	0	12	100	300	Nucleation 350 C, Si2H6 100, 300 mT, 20 min.
egamest	5/9/2006	Center zone thermocouple has bad connection. Temperature jumps from 35 deg C to 500 deg C. The heater is working hard to respond to the false temperature reading.										
psfal	5/9/2006	Unplugged unstable center T/C to force TCU to use the "back up" center T/C. Tysnar20 can be used in this state, temperature stabilization may take longer. This faulty T/C connection will be fixed permanently Tuesday.										
egamest	5/9/2006	350.1	6.28	120	89	90	450	100 Si2H6	10	0	300	No nucleation. Nanowire experiment.
psfal	5/9/2006	Henry Heithamer of Tysnar Co. fixed the TC problem.										
egamest	5/11/2006	330				72	350	0	12	100	300	No nucleation.
wlw	5/11/2006	Run MFC monitor with recipe MONCON.										
blablin2	5/14/2006	330	6.33	120	89	1.20	425	140	12	60	600	Nucleation 425 C, Si2H6 100, 300 mT, 10 min.
egamest	5/16/2006	330				300	410	140	45	60	600	Nucleation 410 C, Si2H6 100, 300 mT, 5 min.
jimmygac	5/18/2006	The center t/c showed "B" after the temp reading, it means the profile t/c is malfunction, either the t/c itself or the connection needs to be checked, the temp control is using the spike t/c outside the tube now. Tysnar20 is still usable.										
egamest	5/19/2006	Edi SiChNaNa recipe, add N2BKFL as a variable. Pressure can reach 2000 mTorr with 1500 sccm of N2BKFL for Erik Garnett's nanowire experiment.										
egamest	5/23/2006	353.3	6.24	120	89	90	450	100 Si2H6	5	0	300	No nucleation. Recipe aborted about 5 min short.
egamest	5/23/2006	Furnace aborted during post-deposition purge/pump step. Cannot unload wafers until problem is resolved. Wafers left in and furnace disabled.										
jimmygac	5/23/2006	Found that the deposition was not finished, the set time was 1:30:00, but it aborted about 5 minutes short, on the alarm history, the temp faults was the cause of abort, check on DCS30 computer, there were several spikes on the temp, monitor the status and found that the "B" showed up on Center and SC zones, this is an old problem that has not been fixed.										

